AN EXPERIMENTAL INVESTIGATION OF LOW TEMPERATURE PLASMA STERILIZATION, TREATMENT, AND POLYMERIZATION PROCESSES

A Dissertation
Presented to
the Faculty of the Graduate School
University of Missouri-Columbia

In Partial Fulfillment
of the Requirements for the Degree

Doctor of Philosophy

by

CHUN HUANG

Dr. Qingsong Yu, Dissertation Advisor

AUGUST 2006

The undersigned, appointed by the Dean of the Graduate School, have examined the dissertation entitled

AN EXPERIMENTAL INVESTIGATION OF LOW TEMPERATURE PLASMA STERILIZATION, TREATMENT, AND POLYMERIZATION PROCESSES

presented by

CHUN HUANG

a candidate for the degree of

Doctor of Philosophy

and hereby certify that in their opinion it is worthy of acceptance.

____
Dr. Qingsong Yu

____
Dr. Fu-Hung Hsieh

____
Dr. Stephen J. Lombardo

____
Dr. William A. Jacoby

____
Dr. Mark Haidekker

ACKNOWLEDGMENTS

I would like to express my sincere appreciation to my advisor, Dr. Qingsong Yu for his precious guidance, encouragement, patience, and support throughout my graduate studies. It is great honor to be the first student in Dr. Yu's research group. I have gained many benefits from his instructions and our discussions.

I would like to thank the members of my dissertation committee, Dr. Fu-Hung Hsieh, Dr. Stephen J. Lombardo, Dr. William A. Jacoby and Dr. Mark Haidekker for their helpful advices and assistances. Specially thanks to Dr. Fu-Hung Hsieh for his invaluable guidance and encouragement through my doctoral studies. I am also especially grateful to Dr. Hirotsugu K. Yasuda for introducing me to the surface science and plasma technology.

I represent my appreciation to Rita Preckshot and Stacy Bono for their assistance and a great source of conversation and humor throughout my graduate studies. I would also like to thank my colleagues and friends at the Surface Science and Plasma Technology Center, Mary Gilliam, Young Jo Kim, and Andrew Ritts for their friendships and encouragements.

And last but not least, I am extremely grateful to my mother, Tai-Jung, Chi, for her infinite love, patience and support in my life.

AN EXPERIMENTAL INVESTIGATION OF LOW TEMPERATURE PLASMA STERILIZATION, TREATMENT, AND POLYMERIZATION PROCESSES

Chun Huang

Dr. Qingsong Yu, Dissertation Advisor

ABSTRACT

This dissertation focuses on investigation of low temperature plasma processes occurring in non-thermoequilibrium glow discharges. Different types of glow discharges including atmospheric pressure direct current (DC) plasma, low-pressure DC plasma, and low-pressure radio frequency (RF) plasma are investigated with respect to their suitability for surface sterilization, modification, and polymerization. It was found that atmospheric pressure plasma is very effective in destruction of organisms and surface modification of conventional polymers. The bacteria cell destruction efficiency of atmospheric pressure plasma is highly dependent on the amount of oxygen in the gas mixture and the types of supporting media. The role of plasma polymerization and its relevance to aging phenomena encountered in gas detectors were investigated using low-pressure DC plasma systems. In DC plasma polymerization process, the majority of plasma

polymer deposition occurs on cathode surface, which is attributed to cathodic dissociation glow. Meanwhile, the negative ionization glow deposition also takes place and hence the plasma polymer deposition is also found on anode surface, which is related to the aging effects of gas detectors.

Research effort was also given to the study of RF plasma deposition of protective coating layer to polymeric materials. FTIR-ATR analysis characterized that plasma deposition of tetramethyldisiloxane (TMDSO) produced SiOx like hard films. Improved hardness and durable adhesion of the plasma deposited hard coatings were achieved on polymeric substrates.

TABLE OF CONTENTS

ACKNOWLEDGMENTS ii
ABSTRACT iii
LIST OF FIGURES ix
LIST OF TABLES xvii
CHAPTER 1 GENERAL INTRODUCTION 1
CHAPTER 2 LITERTURE REVIEW OF LOW TEMPEARTURE PLASMA 8
- 2.1. General Background 8
- 2.2. Plasma Sputtering 15
- 2.3. Plasma Surface Modification of Materials 17
- 2.4. Plasma Etching 21
- 2.5. Plasma Chemical Vapor Deposition and Plasma Polymerization 23
- 2.6. Plasma Sterilization 26
- 2.7. Reference 32

CHAPTER 3 THE GLOW CHARACTERISTICS OF DC BRUSH-SHAPE ATMOSPHERIC PRESSURE PLASMA 36
- 3.1. Introduction 36
- 3.2. Experimental procedures 42
  - 3.2.1. Experimental materials 42
  - 3.2.2. The low-temperature atmospheric pressure plasma brush 42
  - 3.2.3. Optical emission spectroscopy 44
- 3.3. Results and Discussion 45
- 3.4. Summary 68
- 3.5. Reference 70

CHAPTER 4 STERILIZATION USING A LOW-TEMPERATURE ATMOSPHERIC PLASMA BRUSH 72
- 4.1. Introduction 72
- 4.2. Experimental procedures 77
  - 4.2.1. Materials and organisms 77
  - 4.2.2. Low-temperature atmospheric plasma brush 77
  - 4.2.3. Experimental procedures 78
  - 4.2.4. Scanning electron microscopy 81
- 4.3. Results and Discussion 82
  - 4.3.1. Plasma sterilization effects on *Escherichia coli* and *Micrococcus luteus* 82

4.3.2. Effects of supporting medium 83
4.3.3. Effects of heat and gas blowing on cell reduction 85
4.3.4. Effects of argon plasma conditions 88
4.3.5. Effects of remote argon plasma exposure 90
4.3.6 Oxygen addition effects of *Escherichia coli* and *Micrococcus luteus* 92
4.3.7 Culture medium effects of *Escherichia coli* and *Micrococcus luteus* 94
4.3.8 DC power input effects of *Escherichia coli* and *Micrococcus luteus* 98
4.3.9 Remote Ar+O_2 mixture plasma exposure effects of *Escherichia coli* and *Micrococcus luteus* 98
4.3.10 Heat effects of *Escherichia coli* and *Micrococcus luteus* 100
4.3.11 SEM images of *Escherichia coli* and *Micrococcus luteus* under DC atmospheric pressure plasma brush treatment 102
4.4. Conclusion 107
4.5. Reference 110
CHAPTER 5 POLYMER SURFACE EFFECTS OF A COLD ATMOSPHERIC PLASMA BRUSH 112
5.1. Introduction 112
5.2. Experimental procedures 117
5.2.1. Experimental materials 117
5.2.2. Low-temperature atmospheric plasma brush 118
5.2.3. Experimental procedures 118
5.2.4. Static Contact Angle Measurement 119
5.2.5. Optical Emission Analysis 120
5.3. Results and Discussion 120
5.4. Summary 134
5.5. Reference 136
CHAPTER 6 A STUDY ON LUMINOUS GAS PHASES OF HYDROCARBON PLASMA POLYMERIZATION SYSTEMS 139
6.1. Introduction 139
6.2. Experimental procedures 141
6.2.1. Materials 141
6.2.2. Plasma polymerization system 142
6.2.3. Deposition Rate Measurement 146
6.2.4 Electrical Breakdown Measurement 147
6.3. Results and Discussion 147
6.3.1. Glow characteristics of DC hydrocarbon plasma polymerization systems

.... 147
6.3.2. Optical emission features of DC hydrocarbon plasma polymerization systems 150
6.3.3. Deposition features of DC hydrocarbon plasma polymerization systems 156
6.3.4. System characteristics of closed DC hydrocarbon plasma polymerization reactor 159
6.3.5. Electrical breakdown in DC plasma polymerization system 170
6.4. Conclusion 173
6.6. Reference 177
CHAPTER 7 THE ANALYSIS AGING PHENOMENA IN GAS DECTORS FROM DIRECT CURRENT PLASMA POLYMERIZATION INVESTIGATIONS 178
7.1. Introduction 178
7.2. Experimental setup 181
7.2.1 Materials 181
7.2.2. DC plasma polymerization reactor for deposition and electrical breakdown studies 181
7.2.3 Electrical Breakdown Measurement 183
7.2.4 Deposition Rate Measurements 183
7.3. Results and Discussion 184
7.3.1. Luminous gas phase of DC plasma polymer polymerization systems . 184
7.3.2. Electrical breakdown voltage analysis 192
7.3.3. DC plasma polymer deposition examination 201
7.4 Conclusion 207
7.5. Reference 209
CHAPTER 8 Deposition of Protective Coatings on Polycarbonate and Polymethylmethacrylate Substrates by Low Temperature Radio Frequency Plasma Process 210
8.1. Introduction 210
8.2. Experimental Procedures 212
8.2.1. Materials 212
8.2.2. RF Plasma Chemical Vapor Deposition 213
8.2.3. SiOx film Thickness Measurement 214
8.2.4. FTIR-ATR Measurement 214
8.2.5. UV-VIS transmission detection 215
8.2.6. Pencil Hardness Test Method 215

8.2.7. Tape Adhesion Test 216
2.8 Static Contact Angle Measurement..... 216
8.3. Results and Discussion 217
8.3.1. Uniformity of SiOx coating with different substrate sizes and plasma power inputs in RF plasma chemical vapor deposition 217
8.3.2. FTIR-ATR analysis of TMDSO plasma polymerized interlayer and SiOx coating properties..... 223
8.3.3. Plasma deposited protective coatings with different oxygen-TMDSO ratios on PC and PMMA substrates 225
8.3.4. Adhesion enhancement of plasma coated PMMA substrates 232
8.4. Summary and Future work..... 238
8.5. Reference 240
VITA 242

LIST OF FIGURES

Figure 3. 1. The configuration of the dielectric barrier discharge plasma [7,8] 38
Figure 3. 2. The configuration of the resistive barrier discharge plasma [7,10] 39
Figure 3. 3. The configuration of the RF atmospheric pressure plasma jet [7,10] 39
Figure 3. 4. The configuration of the microwave atmospheric pressure plasma jet [13] 40
Figure 3. 5. Schematic of the argon atmospheric pressure plasma brush reactor 43
Figure 3. 6. (a) Pictorial view of the atmospheric argon plasma brush on a fingertip 46
Figure 3. 7. The gas phase temperatures of the argon atmospheric pressure plasma brush 48
Figure 3. 8. Pictorial view from the luminous gas phase of atmospheric cold argon plasma brush 49
Figure 3. 9. The optical emission spectrum from APB with different view angles (a) face view (b) side view-cathode (c) side view-anode Conditions are 1500 sccm Ar, DC 15 Watt, 150g/mm, at 180sec. 51
Figure 3. 10. The relevance optical emission intensity from APB with different view angles (a) nitrogen 2nd positive band (b) argon and oxygen lines Conditions are 1500 sccm Ar, DC 15 Watt, 150g/mm, at 180sec. 55
Figure 3. 11. Optical emission intensity dependence of (a) nitrogen 2nd positive band (b) argon and oxygen lines on DC plasma power Conditions are 1500 sccm Ar, DC 7.5, 10.4, 15, and 19.5 Watt, 150g/mm, at 180sec. 56
Figure 3. 12. Optical emission intensity dependence of (a) nitrogen 2nd positive band (b) argon and oxygen lines on argon flow rate

Conditions are DC 15 Watt, 750, 1500, 2250, and 3000 sccm Ar,150g/mm, at 180sec. 58
Figure 3. 13. Optical emission intensity dependence of (a) nitrogen 2nd positive band (b) argon and oxygen lines on oxygen addition Conditions are DC 15 Watt, 1500 sccm Ar, 7.6%, 14.2%, and 18.9% oxygen addition 150g/mm, at 180sec. 61
Figure 3. 14. Optical emission intensity dependence of (a) nitrogen 2nd positive band (b) argon and oxygen lines on remote distance Conditions are DC 15 Watt, 1500 sccm Ar 150g/mm, at 180sec. 63
Figure 3. 15. Optical emission intensity dependence of (a) nitrogen 2nd positive band (b) argon and oxygen lines on remote distance Conditions are DC 15 Watt, 1500 sccm Ar 14.2% oxygen addition 150g/mm, at 180sec. 65
Figure 3. 16. The optical emission spectrum from APB intercalations with filter paper (a) pure argon (b) 7.6% oxygen (c) 14.2% oxygen (d) 18.9% oxygen Conditions are 1500 sccm Ar, DC 15Watt, 150g/mm, at 180sec. 66
Figure 3. 17. The optical emission spectrum from APB intercalations with aluminum panel (a) pure argon (b) 7.6% oxygen (c) 14.2% oxygen (d) 18.9% oxygen Conditions are 1500 sccm Ar, DC 15Watt, 150g/mm, at 180sec. 67
Figure 4. 1. Photographs of an argon atmospheric plasma brush touching a paper surface. Plasma conditions are 1500 sccm argon, 15 w DC power input………………………………… 79
Figure 4. 2. Temperature change of argon atmospheric plasmas with argon flow rate at different DC power input. 79
Figure 4. 3. Survival curves of *Escherichia coli* and *Micrococcus luteus* on filter paper medium after argon atmospheric plasma treatment with argon flow rate of 1500 sccm and DC power input of 15 W.... 83
Figure 4. 4. Survival curves of (a) *Escherichia coli* and (b) *Micrococcus luteus* in various supporting media after argon atmospheric plasma treatment with argon flow rate of 1500 sccm and DC power input of 15 W. 84
Figure 4. 5. Sterilization effects of (a) dry heat at 125℃ and (b) gas blowing at a 1500 sccm on *Escherichia coli* and *Micrococcus luteus* seeded on filter paper and nutrient broth. 87

Figure 4. 6. The surviving cell numbers of *Escherichia coli* and *Micrococcus luteus* on filter papers as a function of plasma parameters: (a) plasma power and (b) argon flow rate after 1 minute plasma treatment under condition, if not specified in the plots, of 1500 sccm argon and 15 W DC power input. 89
Figure 4. 7. Comparison of the survival curves of *Escherichia coli* and *Micrococcus luteus* on filter papers under direct plasma exposure and remote plasma exposure (2 mm away from the plasma glow). Argon atmospheric plasma conditions are 1500 sccm argon and 15 W DC power input. 91
Figure 4. 8. Survival curves of (A) *Escherichia coli* and (B) *Micrococcus luteus* on filter papers with different amount oxygen addition into argon atmospheric plasma treatment with argon flow rate of 1500 sccm and DC power input of 15 W. 93
Figure 4. 9. Comparison of survival numbers of *Escherichia coli* in various supporting media after argon atmospheric plasma and argon atmospheric plasma with oxygen addition (14.2 %) treatment. Atmospheric plasma condition: argon flow rate of 1500 sccm, oxygen flow rate of 250 sccm, and DC power input of 15 W........... 96
Figure 4. 10. Comparison of survival numbers of *Micrococcus luteus* in various supporting media after argon atmospheric plasma and argon atmospheric plasma with oxygen addition (14.2 %) treatment. Atmospheric plasma condition: argon flow rate of 1500 sccm, oxygen flow rate of 250 sccm, and DC power input of 15 W........... 97
Figure 4. 11. Comparison of survival curves of (A) *Escherichia coli* and (B) *Micrococcus luteus* on filter papers with different DC plasma power input under 1 minute argon atmospheric plasma and argon atmospheric plasma with oxygen addition (14.2 %) treatment with argon flow rate of 1500 sccm oxygen flow rate of 250 sccm and DC power input of 15 W.. 99
Figure 4. 12. Comparison of the survival curves of (A) *Escherichia coli* and (B) *Micrococcus luteus* on filter papers under direct plasma exposure and remote plasma exposure (2 mm away from the plasma glow). Argon atmospheric plasma and argon atmospheric plasma with oxygen addition (14.2 %) conditions: 1500 sccm argon, 250 sccm oxygen, and 15 W DC power input... 101

Figure 4. 13. Sterilization effects of dry heat at 125℃ and 165℃ on *Escherichia coli* and *Micrococcus luteus* seeded on filter paper.... 102

Figure 4. 14. Scanning electron micrographs of (A) Untreated *Escherichia coli* control (B) 5 min argon plasma treated *Escherichia coli* (C) 1 min argon plasma with 14.2% oxygen addition treated *Escherichia coli* under plasma condition 1500 sccm argon, 250 sccm, and 15 W DC power input 105

Figure 4. 15. Scanning electron micrographs of (A) Untreated *Micrococcus luteus* control (B) 5 min argon plasma treated *Micrococcus luteus* (C) 1 min argon plasma with 14.2% oxygen addition treated *Micrococcus luteus* under plasma condition 1500 sccm argon, 250 sccm, and 15 W DC power input 106

Figure 5. 1. Argon atmospheric plasma modification with argon flow rate of 1500 sccm and DC power input of 15 W. (a) polyethylene terephthalate (PET) (b) Nylon 6, 6 (PA 6,6) (c) silicon elastomer (SE) (d) polypropylene (PP) (e) low-density polyethylene (LDPE) ..122

Figure 5. 2. The optical emission spectrum from an argon atmospheric plasma brush. Conditions are 1500 sccm Ar, DC 15Watt, 150g/mm, at 180sec. 124

Figure 5. 3 Argon atmospheric plasma modification on polyethylene terephthalate (PET) with argon flow rate of 1500 sccm and DC power input of 15 W, Treatment Time: 10sec Distance: 0-6 mm (a) remote modification effect with distance (b) optical emission trend of major plasma species with remote distance........ 126

Figure 5. 4. Remote argon atmospheric plasma modification with argon flow rate of 1500 sccm and DC power input of 15 W. Remote Distance: 1mm (a) polyethylene terephthalate (PET) (b) Nylon 6, 6 (PA 6,6) (c) silicon elastomer (SE) (d) polypropylene (PP) (e) low-density polyethylene (LDPE)........ 128

Figure 5. 5. The static contact angles of argon atmospheric plasma treated polymers as a function of plasma power: (a) polyethylene terephthalate (PET) and (b) Nylon 6, 6 (PA 6,6) after 10 seconds plasma treatment time 130

Figure 5. 6 The static contact angles of argon atmospheric plasma treated polymers as a function of argon flow rate: (a) polyethylene terephthalate (PET) and (b) Nylon 6, 6 (PA 6,6) after 10 seconds

plasma treatment time 131
Figure 5. 7 .Aging effects with Direct Plasma Exposure and Remote Plasma Exposure. argon flow rate of 1500 sccm and DC power input of 15 W. 10sec (a) polyethylene terephthalate (PET) (b) Nylon 6, 6 (PA 6,6) (c) silicon elastomer (SE) (d) polypropylene (PP) (e) low-density polyethylene (LDPE) 133
Figure 6. 1. Pictorial view of DC glow discharge with different hydrocarbon monomers (a) methane (b)butane (c) ethane (d) ethylene (e) acetylene. Conditions are 1 sccm Flow System 50 mT, DC 5 Watt. 149
Figure 6. 2. The optical emission spectrum from cathode glow with different monomers (a) methane (b) ethane (c) n-butane (d) ethylene (e) acetylene Plasma Conditions are 1.48 sccm Flow System 69mT, DC 5Watt, 600g/mm, at 30sec. 152
Figure 6. 3. The optical emission spectrum from negative glow with different monomers (a) methane (b) ethane (c) n-butane (d) ethylene (e) acetylene Plasma Conditions are 1.48 sccm Flow System 69mT, DC 5Watt, 600g/mm, at 30sec. 153
Figure 6. 4. The CH /Hα emission intensity ratio in cathode glow from DC plasma polymerization of hydrocarbon monomers including methane (CH4), ethane (C2H6), n-butane (C4H10), ethylene (C2H4), and acetylene (C2H2). Plasma Conditions are 1.48 sccm Flow System 69mT, DC 5Watt, 600g/mm, at 30sec. 155
Figure 6. 5. Change of the luminous gas phase of DC ethane plasma polymerization with discharge time in the closed reactor system. Plasma Conditions: DC power 5W, 50mT ethane, Closed System. 160
Figure 6. 6. Change of the luminous gas phase of DC acetylene plasma polymerization with discharge time in the closed reactor system. Plasma Conditions: DC power 5W, 50mT acetylene Closed System. 162
Figure 6. 7. Time dependence of system pressure of hydrocarbon monomers including methane (CH_4), ethane (C_2H_6), n-butane (C_4H_{10}), ethylene (C_2H_4), and acetylene (C_2H_2) changed with discharge time in the closed DC plasma polymerization reactor system. Plasma Conditions are Closed System 50mT, DC 5Watt.. 163
Figure 6. 8. Time dependence of (a) thickness and refractive index (b) of

hydrocarbon monomers including methane (CH_4), ethane (C_2H_6), n-butane (C_4H_{10}), and ethylene (C_2H_4) changed with discharge time in the closed DC plasma polymerization reactor system. Plasma Conditions are Closed System 50mT, DC 5Watt. 165
Figure 6. 9. (a) The intensity of CH species (431nm) (b) The intensity of species H_α of the different H/C ratio in saturated hydrocarbon monomers changed with discharge time. including methane (CH_4), ethane (C_2H_6), and n-butane (C_4H_{10}) changed with discharge time in the closed DC plasma polymerization reactor system. Plasma Conditions are Closed System 50mT, DC 5Watt. 167
Figure 6. 10. (a) The intensity of CH species (431nm) (b) The intensity of species H_α of the different chemical structures hydrocarbon monomers including ethane (C_2H_6), ethylene (C_2H_4), and acetylene (C_2H_2) changed with time in the closed DC plasma polymerization reactor system. Plasma Conditions are Closed System 50mT, DC 5Watt. 169
Figure 6. 11. Electrical breakdown voltage in DC plasma polymerization of hydrocarbon monomers... 172
Figure 7. 1. Pictorial view of DC glow discharge of argon. Plasma Conditions: Input gas: 1 sccm argon, DC power 5 W, 50 mT Flow System ………………………………………………………..185
Figure 7. 2. The luminous gas phase of DC plasma polymerization. Plasma Conditions: Input gas: 1sccm methane, 1sccm methane+ 10sccm argon, DC power 5W, 50mT Flow System 187
Figure 7. 3. The luminous gas phase of DC plasma polymerization. Plasma Conditions: Input gas: 1sccm butane, 1sccm butane + 10sccm argon, DC power 5W, 50mT Flow System 188
Figure 7. 4. The luminous gas phase of DC plasma polymerization. Plasma Conditions: Input gas: 1sccm hexafluoropropene, 1sccm hexafluoropropene + 10sccm argon, DC power 5W, 50mT Flow System... 189
Figure 7. 5. The luminous gas phase of DC plasma polymerization. Plasma Conditions: Input gas: 1sccm hexafluoropropene oxide, 1sccm hexafluoropropene oxide + 10sccm argon, DC power 5W, 50mT Flow System 190
Figure 7. 6. Electrical breakdown voltage measurements for argon and

hydrocarbons, and their mixtures (a) methane (b) ethane (c) butane (d) ethylene Plasma Conditions: Input gas: 10sccm argon, 1sccm hydrocarbon monomer, 1sccm hydrocarbon monomer + 10sccm argon, DC power, Flow System 194
Figure 7. 7. Electrical breakdown voltage measurements for argon and fluorocarbons, and their mixtures (a) hexafluoropropylene (b) hexafluoropropylene oxide Plasma Conditions: Input gas: 10sccm argon, 1sccm fluorocarbon monomer, 1sccm fluorocarbon monomer + 10sccm argon, DC power, Flow System 195
Figure 7. 8. Electrical resistance of the broken-down gas phase measurement for argon methane and their mixtures (a) argon (b) methane (c) argon+ methane (10:1) Plasma Conditions: Input gas: 10sccm argon, 1sccm methane, 1sccm methane+ 10sccm argon, DC power current 5-20 mA, 280-920 V, Flow System.......................... 198
Figure 8. 1. The thickness profile of plasma deposited SiOx with different diagonal distances on different size substrates. The size of substrate: (a) 3x3 inch, (b) 7x7 inch, (c) 10x10 inch. Plasma Conditions: 1 sccm TMDSO, 10 sccm O_2, 30 mT, RF 40 W, 25 min. ………………..218
Figure 8. 2. The dependence of power density with deposition rate and refractive index Conditions: 1 sccm TMDSO, 10 sccm O_2, 30 mT, 25 min, the size of substrate: 3x3 inch, 7x7 inch, 10x10 inch 220
Figure 8. 3. The thickness profile of plasma deposited SiOx with different diagonal distances under different RF plasma power inputs. RF plasma power: (a) 10 W, (b) 20 W, (c) 40 W. Plasma Conditions: 1 sccm TMDSO, 10 sccm O2, 30 mT, 25 min, 10x10 inch substrate. 221
Figure 8. 4. The dependence of power density with deposition rate and refractive index Conditions: 1 sccm TMDSO, 10 sccm O_2, 30 mT, 25 min, RF plasma power:10 W, 20 W, 40 W 222
Figure 8. 5. FTIR-ATR spectra for plasma deposited coating (a) Plasma polymerized TMDSO coating (b) RF plasma deposited SiOx coating with different power input (c) RF plasma deposited SiOx coating with different TMDSO:O_2 ratio Plasma Conditions: 1 sccm TMDSO, 3,6,10 sccm O_2, 30 mT, 25 min, 10x10 inch substrate, RF plasma power:10 W, 20 W, 40 W. Thickness: 0.45 μm-0.8 μm. 224
Figure 8. 6. The average deposition rate and refractive index of SiOx

coatings with different O_2: TMDSO ratio monomer inputs on PC and PMMA substrates. Conditions: 1 sccm TMDSO, 10 sccm O_2, 30 mT, 25 min, 40 W 226
Figure 8. 7. UV-VIS transmission spectra of plasma deposited SiOx coatings with different O_2:TMDSO ratio monomer inputs on PC substrates. Plasma Conditions: 1 sccm TMDSO, 3,6,10 sccm O_2, 30 mT, 25 min, RF 40 W. Thickness: 0.66 μm-0.79 μm. 228
Figure 8. 8. The adhesion levels of wet tape tests from of SiOx coatings with different TMDSO:O_2 ratio monomer inputs on PC and PMMA substrates. Conditions: 1 sccm TMDSO, 10 sccm O_2, 30 mT, 25 min, 40 W 231
Figure 8. 9. The surface modification effects of PMMA from RF plasma pre-treatment with 1 sccm argon, 1sccm oxygen, 30mT, RF power input of 10 W, Treatment time: 10sec, 30sec, 60 sec 233

LIST OF TABLES

Table 3.1. Most Intense Emission Lines Observed in DC Brush-Shape Atmospheric Pressure Plasma…………………………………………..…..52
Table 5.1. Low-pressure plasma modification of conventional polymers…… ...115
Table 6.1. Deposition rates and the ratio of relevant deposition over total deposition on cathode and anode surfaces in DC plasma polymerization of hydrocarbon monomers.…………………………………………………...157
Table 7.1. Electrical resistivity measurements for argon, hydrocarbons, fluorocarbons, and their mixtures…………………………….……………………200
Table 7.2. Deposition rate on cathode and anode in DC plasma of hydrocarbon monomers, fluorocarbon monomers, and their mixtures with argon……..……..203
Table 8.1. Pencil hardness test for RF plasma deposited SiOx coatings on polycarbonate substrate.……….………………………………………….………..229
Table 8.2. Dry tape test for RF plasma deposited SiOx coatings on PC & PMMA substrates ………………...……………………… ……………………229
Table 8.3.Adhesion test results for RF plasma deposited SiOx coatings with various operational parameters of plasma chemical vapor deposition system …235

CHAPTER 1

GENERAL INTRODUCTION

The investigation of low-temperature plasma processing has been motivated and sparked by its many current and potential applications. Although many theoretical and computational studies have spearheaded in plasma physics to date, extensive experimental investigations in plasma chemistry will be crucial to the further progress of low-temperature plasma processing.

The objective of this dissertation is to conduct experimental researches that will allow study of low-temperature plasma process in several important applications. To achieve this, we investigated several low-temperature plasma techniques such as a brush-shape atmospheric pressure plasma source, low-pressure direct current (DC) plasma polymerization, and low-pressure radio frequency (RF) plasma deposition. Atmospheric pressure plasma brush was used to examine its sterilization and modification efficiencies of low-temperature plasma process without vacuum limitation required in traditional low-pressure plasma systems. Utilizing low-pressure DC plasma polymerization, the role of low energy molecular dissociation in plasma state was investigated in order to attain a clear picture of the plasma reaction mechanisms and possible origins of aging

phenomena in gas detectors. With RF plasma deposition, hard SiOx-like coatings were produced on polymeric substrates for improving their scratch-resistance in optical applications. The details of the research work are presented in chapters 3 through 8.

In chapter 3, we introduced an experimental apparatus of a new atmospheric pressure plasma brush system. The DC glow discharge was successfully generated at one atmospheric pressure with extremely low-power input. Depending on the gas flow rate and the DC power level, the glow discharge can be created and sustained in between the two planar electrodes inside the discharge chamber or blown out of the discharge chamber to form a low-temperature atmospheric pressure plasma brush. The brush-shape atmospheric pressure glow discharge can be ignited and sustained with argon inert gas. The brush-shape atmospheric pressure glow discharge is formed outside of the discharge chamber with typical dimensions of 15 to 20 mm in length, ~5 mm in width, and < 1.0 mm in thickness, which are adjustable by changing operational parameters. The temperature measurements using a thermocouple thermometer showed that the gas temperatures of the brush-shape atmospheric pressure plasma are close to room temperature when running with high gas flow rates. The photo-emission species in

brush-shape atmospheric pressure glow discharge was identified by optical emission spectroscopy (OES). It was found out that excited nitrogen (from air) and argon species dominated the OES spectrum of this brush-shape atmospheric pressure plasma. OES results from this study implied that, in brush-shape atmospheric pressure glow discharges, the plasma reactive species are also created by argon plasma/air interaction. The experimental results indicated that the brush-shape atmospheric pressure plasma possesses the distinct characteristics of low temperature plasmas.

In chapter 4, we use the atmospheric pressure plasma brush to inactivate the bacterial activities for surface sterilization and decontamination applications. Two bacteria including *Escherichia coli* and *Micrococcus luteus* seeded in various media were subjected to plasma treatment, and their survivability was examined. It was found that argon atmospheric plasma brush is very effective in destruction of the organisms. Improved bacterial inactivation efficiency was achieved with oxygen addition into the argon atmospheric plasma brush. The results showed that plasma treatment with O_2 addition induced a much faster cell reduction for both bacteria when compared to the Ar only plasma treatment under the similar conditions. The plasma treatment effects on the bacteria cell structures were also

examined using scanning electron microscopy (SEM), and cell structure damages due to the plasma exposure were observed on both bacteria. Consequently, the oxygen-based reactive species, such as O atoms present in the plasma were believed to play the dominant role for such bacterial deactivation. The bacteria cell destruction efficiency under DC glow discharge was also found to be highly dependent on the amount of O_2 in the gas mixture and the types of supporting media.

In chapter 5, the argon atmospheric pressure plasma brush was used for surface modification of conventional polymers. The surface properties of plasma-treated polymers were examined by static contact angle measurements. The influences of plasma conditions such as treatment time, DC plasma power, and Ar gas flow rate on the polymer surface properties were studied. The photoemission plasma species in the plasma brush was identified by optical emission spectroscopy. The aging effect of the treated polymer samples was investigated as well. Reduced water contact angle of the plasma-treated polymers indicated increased surface energy in comparison with untreated polymer surfaces. The emphasis of this study is placed on the importance of quick and consistent polymer surface modification by atmospheric pressure plasma process.

In Chapter 6, we investigated the luminous gas phases of low-pressure DC plasma polymerization systems. Plasma polymerization of hydrocarbon monomers including methane (CH_4), ethane (C_2H_6), n-butane (C_4H_{10}), ethylene (C_2H_4) and acetylene (C_2H_2) was carried out in DC glow discharges. The glow characteristics and the optical emission spectra of the plasma systems were investigated by optical photography and OES. It was found that cathode glow, which can be observed and designated, as molecular dissociation glow, is the characteristic glow of the plasma polymerization systems. It forms a strong contrast to the characteristic negative ionization glow of inert gas plasmas that do not polymerize. OES analysis of DC hydrocarbon plasma polymerization systems indicated that polymerizable species are mainly formed in the dissociation glow attached to the cathode surface rather than in the negative glow, which is some distance away from the cathode. To evaluate the correlation between the glow characterizations and the plasma polymerization features, the deposition distribution at both cathode and anode surfaces was studied. In DC hydrocarbon plasma polymerization systems, the majority of plasma polymer deposition occurs on cathode surface, which is attributed to molecular dissociation glow. Meanwhile, the negative ionization glow deposition also takes place, hence less plasma polymer deposition

is also found on anode surface.

In Chapter 7, we studied the plasma systems of argon and its mixtures with various hydrocarbons and fluorocarbons. This work was performed in DC glow discharges since the prospective cause of aging effects is considered to be plasma polymerization. The luminous gas phase and breakdown voltage for Ar and the above mixtures were investigated. To relate the electrical breakdown to the DC plasma polymerization, the deposition distribution at both the cathode and anode surfaces was studied. In DC plasma polymerization, the majority of the deposition occurs on cathode surface, which is attributed to cathodic polymerization. Meanwhile, negative glow polymerization also takes place and hence deposition is also found on anode surface, which is related to the classical anode aging effect in gas detectors. In this study, the ratio of relevant deposition over total plasma polymer deposition was examined and related to different plasma mixtures in DC plasma polymerization systems.

Finally, in Chapter 8, we studied RF plasma deposition using a tetramethyldisiloxane (TMDSO) and oxygen mixture to produce SiOx like hard coatings on polycarbonate (PC) and polymethylmethacrylates (PMMA) substrates. The plasma deposited hard coatings are transparent and hard. FTIR-ATR analysis

indicated that these plasma deposited coatings possess inorganic silicon dioxide features. Improved hardness and durable adhesion of these plasma coatings were achieved on PC substrates. However, the adhesion of the plasma coatings to PMMA substrate was less successful.

CHAPTER 2

LITERTURE REVIEW OF LOW TEMPEARTURE PLASMA

2.1. General Background

During the last three decades, low-temperature plasmas have made a remarkable impact on progressive technology and significantly improved the quality of semiconductor processes. This chapter gives an overview of the several important applications of low temperature plasma process. The emphasis of this paper is placed on the trend of research and development activities for low temperature plasma processes.

The plasma state exists in the universe or is created under the distinctive situations for definite purposes. The plasmas formed in nature, which cover a very large range of electron densities and gas temperatures, could be classified into two types:

•Thermodynamic equilibrium plasmas - Thermodynamic equilibrium plasmas (high temperature or hot plasmas) are only created in stars. The electron and gas temperatures of thermodynamic equilibrium plasmas are usually higher than 10^5 °K. They have no realistic significance because they do not be formed in the existing laboratory environments [1].

•Non-thermodynamic equilibrium plasmas - Non-thermodynamic equilibrium (low temperature or cold plasmas) are the focus of applications in the subsequent paragraphs. The low-temperature plasma technologies are formed in the low pressure system and widely applied in modern technology such as plasma sputtering, plasma etching, plasma modification, plasma chemical vapor deposition (PCVD), and plasma polymerization. As mentioned before, in low-pressure or nearly vacuum environment, thermodynamic equilibrium is not approached, even at a local scale, between the electrons and the heavy particles, and these plasmas are of the non- thermodynamic equilibrium type [1]. In the non-thermodynamic equilibrium plasmas the temperature of the electrons is much higher than that of the heavy particles. The electrons can reach temperatures of 10^4-10^5 °K (1-10 eV), while the gas phase temperature can be as low as room temperature [1]. The low temperature plasmas have been developed specifically and purposefully based on their non- thermodynamic equilibrium properties and their ability to cause physical and chemical reactions with the gas at relatively low temperatures. In the following sections, we will review and summarize in depth only the low temperature plasmas.

Low-temperature plasma is a partially ionized gas that contains electrons, positive and negative ions, neutral atoms, molecules, and photons [2]. In a plasma state, the densities of ions and electrons tend to be equal, thus the whole system remains electrically neutral. It is also defined as a quasi-neutral gas of charged and neutral particles exhibiting collective behavior [3]. Gases always collide with each other in plasma. Among gaseous phase collisions, collisions that involve electrons are the most frequent. If the electric field is applied, energy is transferred to electrons in the chamber. These energetic electrons will further encounter inelastic collisions with gas molecules to produce positive ions and secondary electrons in the cycle. Therefore, the electron impact ionization is the most important process to maintain the plasma state [4]. The essential energy to proceed with ionization is above 12 eV. In the plasma state, ionization is not the only event, a less energetic transfer to the bound electron would enable the electron to jump to a higher energy level in the atom with corresponding quantum absorption of energy. This energetic transfer process is known as excitation and, as ionization, can result from electron impact collision. Dissociation is the electrical process of breaking apart a molecule; it is usually favored over ionization because of the preponderance of low energy electrons in a plasma state. The energy required to produce dissociation is often

lower than 10 eV. Low-temperature plasma always consists of enough energy to cause ionization, excitation, and dissociation. It also causes recombination of ions and electrons to form neutral atoms or molecules and relaxation with excitation. Due to the relaxation of excited atoms or molecules, glow discharge is generated with low-temperature plasma. For this reason, low-temperature plasma is known as glow discharge.

The common types of low-temperature plasma are direct current, alternating current (AC, 50~60Hz), audio frequency (AF, <100kHz), radio frequency (RF, 13.56MHz), and microwave (2.45GHz) [1]. For many applications, the use of alternating current (AC, 50~60Hz) or radio frequency (RF, 13.56MHz) power supply is often favored because of the availability, versatility and feasibility of maintaining low-temperature plasma [5].

The direct-current (DC) plasma is characterized by its visual presence, several diffuse zones, and a constant potential difference between electrodes [6]. The characteristics of DC plasma are highly system dependent. System parameters, including pressure, distance between electrodes, and applied voltage play important roles in the general traits of DC plasma [7]. DC plasma requires two metal conductive electrodes inside a reactor. The disadvantage of the DC type is

that the electrodes are easily covered with the depositions of organic monomers [7]. Although DC plasma may be ignited, it will quickly extinguish as the electrons collect on the deposition as an insulator. Therefore, it is preferred to set electrodes outside the reactor to avoid contamination of the process. Nonetheless, the problem examined above can be overcome by alternating-current type glow discharge.

When an alternating-current type plasma (AC or AF) is applied, each electrode performs alternately as a cathode and an anode. At a sufficiently low frequency, the plasma will extinguish with inversing polarity due to the voltage drop below the breakdown voltage level, which is needed to sustain the glow discharge. At high frequency, the alternating cycles repeat rapidly. Because plasma can be fully established during each half-cycle of the applied field, the re-ignition energy of the glow discharge in each cycle is lowered by the presence of residual ionization from the previous cycle [8]. Therefore, plasma can be sustained with relatively lower applied voltage at high frequency rather than at low frequency.

The frequencies used in the high-frequency plasmas are in the range of radio transmission (13.56 MHz) called RF plasmas. Since 13.56 MHz is high frequency, the electrons gain energy through the oscillation in the field. The energy to plasma

can be supplied by the electromagnetic radiation with either capacitive or inductive coupling. The major advantages of the RF type plasma are that (1) RF plasma can be sustained with an external electrode as well as an internal electrode, (2) RF plasma can be ignited and maintained by either conductive or nonconductive electrodes, (3) RF plasma can be easily retained at lower pressure (1.3-66.5 Pascal or 1~50 mTorr) and lower voltage than in a DC plasma [9].

Microwave (MW) plasma is generated by power supplies at a frequency of 2.45 GHz [1]. The excitation of the microwave plasma is similar to the excitation with RF plasma, while differences may result from a wide range of frequencies. The magnitude of the electric field can vary with the reactor, which has dimensions of the same order of magnitude as the wavelength in microwave plasma. Since the collision frequency of electrons is closer to the microwave frequency, the power absorption is more effective in MW plasma than in RF plasma. Furthermore, microwave plasmas have been used mostly with high-density plasmas.

Low-temperature plasma, cold plasma, and non- thermodynamic equilibrium plasma are some of the coordinately used terms to define the same kind of glow discharge process. The low-temperature plasma processing is a critical technique

used in the production of advanced materials and in the production of present and future generations of microelectronics. The advantages of low-temperature plasma processing are also being discovered in diverse areas besides microelectronics. The other present and potential applications of low-temperature plasma process include modification of material surfaces for specific applications, sterilization of unfavorable microorganism for clinical use, and anticorrosion deposition on surfaces of industrial metals. The objective of low-temperature plasma process is to control the generation of ions, electrons, and free radicals on a surface to modify its property, either by depositing material on the surface (deposition) or removing material (etching or sputtering). Based on the kinds of monomer gases, low-temperature plasma can be sorted into three groups [2] (1) chemically non-reactive plasma (2) chemically reactive but non-polymer-forming plasma, and (3) chemically reactive and polymer-forming plasma.

The first groups, chemically non-reactive plasmas, are mostly monatomic inert gas such as argon and helium. These plasmas can ionize other molecules, modify the solid surface, or sputter materials but are not consumed by chemical reactions.

The second groups, chemically reactive but non-polymer-forming plasma, are

organic or inorganic molecular gases such as CF_4 and O_2. Though chemically reactive they will not polymerize in pure gas plasmas. Those plasmas can chemically etch the solid surface because of the formation of volatile gas compounds.

The third groups are comprised of chemically reactive and deposition-forming plasmas, which are organic gases or vapors such as methane and ethane. The interaction of deposition -forming plasmas with the solid surfaces causes the deposition of thin materials on the solid surfaces. This process of the deposition on the solid surface that is formed with the deposition-forming plasma is called plasma chemical vapor deposition or plasma polymerization.

2.2. Plasma Sputtering

Plasma sputtering is the reaction of atoms that would be ejected from the cathode surface when ions strike the cathode in the plasma system [1,10]. The sputtered atoms can deposit on the surface of a target or substrate material. The deposition rate of plasma sputtering on the substrate would rely on the amount of the ion energy and the ion generation on the target [11-13]. The plasma sputtering gas requires that the gas does not chemically react with the target or substrate, thus inert gases are used for sputtering process. Reactive plasma sputtering is widely

used in thin film deposition where it is beneficial to add chemically reactive gases to the inert gas in the sputter deposition of compound films [14-20]. This technique offers almost unlimited opportunities to produce thin films of unique compositions including thin films of oxides, nitrides, hydrides, carbides, silicides, sulfides, selenides, etc [21-24]. However, this great adaptability is accompanied by reproducibility problems when metastable thin films are being deposited. In these cases, the film stoichiometry will depend on the relative anion and cation fluxes, the former coming from the injected gas and the latter from the sputtering target [25-26]. Precise control of the relative anion and cation fluxes is hard to achieve.

Plasma sputter etching is the process that occurs when material is removed from a surface by sputter ejection [27]. The sputtering results from ion bombardments that move along electric field lines since electric field lines are always vertical to an equipotential surface, and then etch profiles are inherently perpendicular (anisotropic) [1,3,28]. It contrasts with the isotropic profiles observed with wet chemical etching. Plasma sputter etching can be carried out in a conventional sputtering system with a plasma glow discharge or with an externally generated ion beam. When using either a plasma or an ion beam source, there is the possibility of charge-exchange collisions occurring with neutral atoms in the

gas producing energetic neutrals which are not affected by the electric field lines and do not directly follow them to the target. In addition, the sputtered material from the target support could suffer collisions with the gas and be scattered back onto the substrate. This could lead to inaccurate results.

2.3. Plasma Surface Modification of Materials

In the recent years, there has been a giant growth in the use of low-temperature plasmas for the surface process to avoid the chemical waste problems related with wet processing. The effluent from plasma reactors which use chemically reactive gases might be toxic or corrosive and must be carefully processed, but the much smaller quantities compared to wet processing make this problem much less severe in plasma surface processing. Low-temperature plasma surface modification is the process that alters the physical and chemical characteristics of a surface of material without changing its bulk material properties [29]. It is becoming attractive and can be done on metals and alloys as well as ceramics and polymers. Some of the surface properties that can be modified by low-temperature plasma process include in hardness, adhesion, corrosion, fatigue, friction, oxidation, resistivity, toughness, and wear properties. The examples of low-temperature plasma surface modification processes are

plasma oxidation, plasma nitriding, and polymer surface modification.

The use of oxygen plasmas to deposit oxide films on metal or semiconductor surfaces is one of the oldest plasma-based surface processing techniques [11,30]. As is one of the cases for plasma chemical vapor deposition system, the major advantage of plasma oxidation is the ability to deposit oxide films at low temperatures or on surfaces that do not oxidize readily upon exposure to molecular oxygen. The applications of plasma oxidation are mostly in the oxidation of silicon, the oxidation of GaAs and InP, and in the growth of tunneling junctions on Nb, Pb, and related alloys [11]. These films are typically deposited under energetic ion bombardment conditions and relatively quickly attain a steady-state thickness, after which the oxide deposition rate and the removal rate by sputter etching are equal. The precise control of oxide deposition film thickness can be achieved by adjusting the plasma operational parameters such as power, pressure, gas composition, in that each set of parameters results in a different steady-state oxide thickness.

Plasma nitriding is greatly similar to plasma oxidation. The major difference is that whereas oxygen tends to become a negative ion reaching on metal or semiconductor surfaces, nitrogen does not [31]. For that reason, the film growth

by the negative ion motions to the film-substrate interface is not an important process in plasma nitriding. Plasma nitriding is typically performed as a relatively energetic positive ion bombardment process and can be expected to behave similarly to cathode oxidation. Therefore, nitrogen atoms as well as energetic and molecular nitrogen ions play an important role in the nitride film-deposition process. At low temperatures where thermal diffusion rates are very low, the nitride film thickness will be determined by the enhanced diffusion often associated with energetic ion bombardment of surfaces [11]. One of the most important commercial applications of plasma nitriding is the case-hardening of machine tools and other mechanical components [32]. In the microelectronics industry, there is attention in the plasma nitriding of semiconductor surfaces such as Si and GaAs.

The objective of this section is to show the feasibility and interest in polymer surface modification by low-temperature plasma techniques from results available in the literature. The main topics of low-temperature plasma polymer surface modification concern polymer surface energy change [29], and in particular mechanical properties [33], wetting properties [34], and low-temperature plasma processing of insulating materials [35,36]. The first and most immediate

application was the improvement of surface properties of polymers, such as fatigue property, wear life, and tribological properties [33,37,38]. In particular, the enhanced surface properties of polyamide after low-temperature plasma modification was attributed to ion bombardment induced cross-linking property [39], hence surface adhesion strength. The second and major application concerns the improvement of either wetting or hydrophobic [34] properties of polymers. Generally speaking, low-temperature plasma modification processing leads to impressive modifications of the wetting properties of polymers, but most studies have demonstrated that ion bombardment energy is the key factor for stability after treatment or for the treatment durability. The generally acknowledged plasma modification mechanisms are that the improved hydrophility is due to the formation of oxygen-containing hydrophilic functional groups, and that the high-energy ion bombardment produces deeper cross-linking of polymer chains, with the intention that the modified layers are more resistant to hydrophobic recovery with time [34, 40]. Many of low-temperature plasma surface modification researches are devoted to the polymer surface property, such as cross-linking, chain scission, creation of functional groups, and their relationship with the surface properties obtained after treatment.

2.4. Plasma Etching

The precise pattern transfer to a silicon wafer by etching process has become a vital technique for semiconductor fabricating whose critical feature dimensions is less than micro-or nano-scale. With plasma etching, it is possible to etch faster in the direction perpendicular to the surface of the material than parallel to the surface, resulting in anisotropic etching [1,3]. This permits finer features to be etched and more transistors and diodes could be placed on a microchip. Therefore, plasma etching becomes the mainstream in semiconductor fabricating processes and it is the key to produce smaller, faster, and cheaper microchips. Plasma etching is a chemical process involving reactive atoms and free radicals that react with the surface. It uses reactive gas to form reactive species and free radicals, which, upon reaction with surfaces, produce volatile products. The volatility of the reaction products is the critical necessity for this process to be successful. The plasma is needed for etching in at least three ways: (1) it produces the reactive species, usually Cl or F, which does the etching; (2) it prepares the suitable substrate surface so that the etching species can be more effective and (3) it provides the directionality that allows the etching to proceed in a straight line [11]. There are many configurations of plasma equipment that have been used for

plasma etching. In the beginning, the barrel configuration was used, most often to remove photoresist and other organic residues with oxygen glow discharges [1]. This apparatus is still used in certain non-lithographic applications where energetic ion bombardment is not required. Recently, the planar geometry has been the most popular approach in reactive-ion etching (RIE) and the triode setup of the device offers some distinct benefits, the most important of the advantages is the ability to control the ion bombardment energy and the plasma density independently [1,10,11]. The trend is to take this independent control of the plasma density and ion energy a step further and go toward equipment, where microwave discharges are most commonly used to generate the plasma and an RF-induced DC bias provides the ion acceleration to the surface. Reactive-ion etching (RIE) is defined as plasma etching with required simultaneous energetic ion bombardment of the processed surface. In fact, the most important reason that RIE has replaced wet chemical etching in semiconductor fabricating technology is the ability of RIE to achieve anisotropic etching. The materials such as silicon, silicon dioxide, silicon nitride, photo-resist, tungsten, and titanium used in micro fabrication readily lend themselves to plasma etching in that they form volatile compounds under proper conditions [11]. In addition to the applications in semiconductor fabricating

technology, the ability of RIE processing to reduce the large quantities of liquid chemicals needed for wet processing is a decisive improvement.

2.5. Plasma Chemical Vapor Deposition and Plasma Polymerization

Low temperature plasma processes are usually used to deposit materials on surfaces. Plasma chemical vapor deposition (PCVD) is the technique of forming solid deposition by initiating chemical reactions in plasma state [29]. Its major advantage over thermal chemical vapor deposition is the ability to deposit films at relatively low substrate temperatures [1,41]. Plasma chemical vapor deposition (PCVD) is especially useful for materials that might vaporize, flow, diffuse, or undergo a chemical reaction at the higher temperatures. In this method, gas or vapor are inputted into a relatively low power density plasma system. The gas molecules are dissociated by plasma, creating reactive radicals or atoms that condense on the substrate [29]. Usually, the substrates are heated to improve the film quality, but the substrate temperatures which are required are usually significantly lower than those required for thermal chemical vapor deposition [42]. As was the case for the previously discussed deposition methods, energetic ion bombardment of the growing film has a large influence on films deposited by plasma chemical vapor deposition, but again the mechanistic understanding is

missing.

In spite of the lack of mechanistic understanding of this process, plasma chemical vapor deposition has many applications in industry. One of the most important applications is the deposition of amorphous hydrogenated silicon films by the plasma decomposition of silane [1]. Another area in plasma chemical vapor deposition is widely used is in the final passivation of integrated circuits, which involves the deposition of silicon nitride (from silane and ammonia or nitrogen), silicon oxide (from silane and nitrous oxide), and silicon oxy-nitride (from silane, ammonia, and nitrous oxide) [43]. The other currently very popular area is the deposition of diamond films (from methane and excess hydrogen) [1].

Plasma polymerization is very similar to plasma chemical vapor deposition, the major difference being that in plasma chemical vapor deposition is concerned with depositing inorganic films, whereas in plasma polymerization the resulting film is an organic polymer [2,44]. Plasma polymerization is the formation of polymeric materials under the influence of plasma [2]. It is an atomic polymerization different from conventional polymerization [29]. Most of organic gases and vapors, even gases that cannot produce polymer by conventional polymerization methods such as methane, would produce polymeric material

(plasma polymers) in the glow discharge. In the system, polymeric materials are deposited on the solid surfaces forming ultra-thin solid films called plasma polymers. Plasma polymers have several advantageous properties such as being pinhole free, highly branched, and highly crossed linked [2]. Although they can form powdery and oily products in certain cases, the formation of such products can be prevented by controlling the system conditions and the reactor design. Due to the reaction, in which high energetic electrons break the chemical bond in plasma polymerization system, plasma polymers have no manifestly repeating units as conventional polymers. Therefore, it is hard to determine the properties of plasma polymers from used monomers in contrast to conventional polymerization which are linked together with a mere alternation of the chemical structure of monomer.

A noted example of plasma polymerization is the formation of a anti-corrosion protecting interlayer by introducing silicon carbon monomer gas into a low power density glow discharge. In recent research, the direct current (DC) glow discharge has an ideal method to coat a metallic substrate by plasma polymerization because the polymer nearly entirely deposits on the surface of cathode [45]. This is a promising field of DC plasma polymerization applied to

conducting materials, because plasma polymers mainly deposit on the substrate (used as the cathode) and efficiently perform plasma with the least contamination of the reactor. DC plasma polymerization supplied excellent corrosion protection for cold rolled steel [46] and aircraft aluminum alloys [47-49].

2.6. Plasma Sterilization

A novel sterilization method capable of more rapidly killing microorganisms and less damaging material is low-temperature plasma sterilization. The plasma sterilization is proceeding at low temperature without damaging polymeric materials [50] and it is safe as opposed to gaseous chemical sterilization (EtO sterilization) [51]. To perform the described process, plasma should be generated in a non-equilibrium state. The low-pressure plasma can be generated by radio frequency and microwave discharges. In low-pressure plasma generation, the mean free path of the plasma particles is extensive depended on the size of reactor chamber. The electron bombardment is the foremost process of low-pressure plasma state. However, the plasma enthalpy and UV radiation are not intense, and as a result, the duration of a vacuum process treatment must be large for it to be proficient (typically tens of minutes, and sometimes hours). The first report dealing with low-pressure plasma sterilization was published in 1968 [52] while

the first practical application was developed in 1972 [53]. It used halogen gas plasma and was proposed to sterilize contaminated surfaces. Usually, low -pressure plasma is used in combination with working gas familiar to the healthcare and medical applications such as hydrogen peroxide or paracetic acid vapor. Low pressure-plasma is effective against a broad range of bacteria and bacterial spores killing these microorganisms by generating oxygen, hydroxyl free radicals, and presumably other active species, although these killing mechanisms are still being studied [54].

Currently the marketed device based on low-pressure plasma sterilization is Sterrad® [55]. In Sterrad® system, the items to be sterilized are wrapped in plastic sterilization pouches and placed on trays inside a vacuum chamber; the trays are fully surrounded by the perforated electrode. *Bacillus stearothermophilus, Bacillus subtillis var. niger, Bacillus pumilus, Aspergillus niger, Escherichia coli, Staphylococcus aureus, Entercoccus faecalis, and Pseudomonas aeruginosa* were found to be efficiently killed by Sterrad® cycle consisting of 20 minutes of the diffusion with 2mg/liter hydrogen peroxide and 5 minutes of plasma at a power around 300 watts. Recently, more researchers studied low-pressure microwave plasma instead of Sterrad® system. J. Feichtinger et al. reported the fast spore

reduction of four orders of magnitude in the original concentration of *Bacillus subtilis* and *Aspergilus niger* in less than 1 second under low-pressure microwave plasma treatment [56]. The 1200 watts of Plamsodul® microwave power was applied at 100 sccm different working gases to create the plasma. From the experimental results, it was found that the faster spore inactivation occurred with ammonia and air as working gases as compared to argon.

Most generally, the three parameters responsible for the mechanisms of low-temperature plasma sterilization in killing microorganisms are (1) chemically reactive radicals, (2) charged particles, and (3) UV radiation. The efficiency of low-temperature plasma sterilization depends on the chemically reactive species of the plasma. There is the production of short-live chemically reactive radicals by electron impact dissociation of molecular gases and by ionized gases. Those radicals also occurred in the surface discharge inside the root of the micro-discharge close to the packaging material. After applying suitable discharge conditions, the ensemble of all micro discharges covers the whole packaging surface. In low-pressure plasma sterilization, Nagatsu et al. [57] and Lerouge et al. [58] experimentally showed that discharges containing oxygen have significant germinal effects.

The charged particles in non-equilibrium plasma are important if the microorganisms are lying on a surface, or suspended in a volume, and are crossed by the electrical current generating the plasma. The efficiency of this process observably depends on the current density and the electric field in the vicinity of the surface of microorganisms. Both factors determine the density flow and the degree of activation of the charged particles reaching the microorganism surface. This distinctive energy of the charged particles, as rule, is much higher than the binding energy of the organic molecules of the microorganism. Thus, these molecules are easily destroyed. Laroussi et al [59] reported that the outer membranes of *Escherichia coli* (gram-negative) were ruptured after 10-30 sec helium plasma exposure. UV radiation, which accompanies any plasma decay, is supposed to be an essential role of the plasma sterilization [60]. UV radiation induces the formation of thymine dimmers in the DNA to restrain the bacteria replication. Its efficiency of this process, obviously, depends on the irradiation intensity and is determined by the process of plasma generation and composition. Using low-pressure plasma sterilization, Feichtinger et al. reported the fast spore reduction of four orders of magnitude in the original concentration of *Bacillus subtilis* and *Aspergilus niger* in less than 1 second under low-pressure microwave

plasma treatment [56]. They used optical edge filters on the top of the samples to separate UV emitting lights. From experimental results, it was found that UV light emitted by the Plasmodul microwave plasma played the major role in spore reduction mechanism. The vacuum UV radiation at wavelength shorter than 200 nm was identified to be the most critical agent for killing Bacillus subtilis and Aspergillus niger. On the other hand, Lerouge et al. [61] found that vacuum ultraviolet (VUV) photons with wavelength ranging from 115 to 170 nm were ineffective to reduce the surviving spore density by less than the reduction of two orders of magnitude in 30 minutes. The feasible elucidation may be that UV radiation generated by plasma is not lethal enough to damage the microorganisms.

From the proceeding description, low-temperature plasma sterilization could be an alternative to conventional sterilizations. The studies on the sterilization by both low-pressure and atmospheric pressure plasma have been growing substantially and reached a stage of maturity. However, the research of low-temperature plasma sterilization has the complex issue, which is further burdened by a large number of experiment variables, is insufficiently definitive about the selected methodologies and experimental conditions. Certainly, more

tests and in-depth study of low-temperature sterilization are needed to elucidate the mechanism of low-temperature plasma sterilization.

2.7. Reference

1.A. Grill, *Cold Plasma in Materials Fabrication*, IEEE Press, New York, 1994.
2.H. Yasuda, *Plasma Polymerization*, Academic Press, Orlando, Florida, 1985.
3.B. Chapman, *Glow Discharge Process,* John Wiley& Sons, New York, 1980.
4.F. F. Chen, *Introduction to Plasma Physics*, Plenum Press, New York and London, 1974.
5.T. F. Wang, T. J. Lin, D. J. Yang, J. A. Antonelli, H. K. Yasuda, "*Corrosion protection of cold-rolled steel by low temperature plasma interface engineering I. Enhancement of E-coat adhesion."* Progress in Organic Coatings vol.28, no.4, pp.291-297, 1996
6.H.Suhr, *Applications of Non-equilbrium Plasmas to Organic Chemistry*, John & Sons, Inc, New York, 1974.
7.M. Mitchner, C. H. Kruger, *Partial Ionized Gases*, John Wiley & Sons, Inc, New York, 1973.
8.F.K. McTaggart, *Plasma Chemistry in electrical Discharge*, Elsevier Publishing Co., New York, 1967.
9.M.M. Shahin, In Reactions Under Plasma Conditions, vol. I, M. Venugopalan, Ed Wiley-Interscience, New York, 1971.
10.J. Leon. Shohet "*Plasma-aided manufacturing."* IEEE Trans. Plasma Sci., vol. 19, pp. 725-733, 1991.
11.J. W. Coburn "*Surface processing with partially ionized plasmas."* IEEE Trans. Plasma Sci., vol. 19, pp. 1048-1062, 1991.
12.J. J. Cuomo, R. J. Gambino, J. M. E. Harper, and J. D. Kuptsis, *"Origin and effects of negative ions in the sputtering of intermetallic compounds,"* IBM J. Res. Develop., vol. 21, no. 6, pp. 580-583, 1977.
13.G.K. Wehner, Y.H. Kim, D.H. Kim, and A.M. Goldman, *"Sputter deposition of YBazCu30;-,. films using a hemispherical target in a Hg vapor triode plasma,"* Appl. Phys. Lett., vol. 52, no. 14, pp. 1187-1189, 1988.
14.D. J. Ball, *"Plasma diagnostics and energy transport of a dc discharge used for sputtering,"* J . Appl. Phys., vol. 43, no. 7, pp. 3047-3057, 1972.
15.M. Nindi and D. Stulik, *"Cone formation and transformation on diamond microparticle contaminated silver surface: semidynamic studies,"* Vacuum, vol. 38, no. 12, pp. 1071-1077, 1988.
16.J.J. Hanak and J. P. Pellicane, *"Effect of secondary electrons and negative ions on sputtering of films,"* J. Vac. Sci. Technol., vol. 13, no. 1, pp. 406-409, 1976.

17.G.K. Wehner, Y.H. Kim, D.H. Kim, and A.M. Goldman, *"Sputter deposition of YBazCu30;-,. films using a hemispherical target in a Hg vapor triode plasma,"* Appl. Phys. Lett., vol. 52, no. 14, pp. 1187-1189, 1988.
18.D. J. Ball, *"Plasma diagnostics and energy transport of a dc discharge used for sputtering,"* J . Appl. Phys., vol. 43, no. 7, pp. 3047-3057, 1972.
20.J. A. Thornton, *"The microstructure of sputter-deposited coatings,"* J . Vac. Sci. Technol. A, vol. 4, no. 6, pp. 3059-3065, 1986.
21.J. E. Greene and **S.** A. Barnett, *"Ion-surface interactions during vapor phase crystal growth by sputtering, MBE, and plasma-enhanced CVD: applications to semiconductors,"* J. Vac. Sci. Technol., vol. 21, no. 2, pp. 285-302, 1982.
22.G. Betz and G. K. Wehner, *"Sputtering of multicomponent materials,"* in Topics in Applied Physics, vol. 52, pt. 11, R. Behrisch, Ed. Berlin: Springer-Verlag, , pp. 11 -90 1983.
23.H. F. Winters and E. Kay, *"Gas incorporation into sputtered films,''* J .Appl. Phys., vol. 38, no. 10, pp. 3928-3934, 1967.
24.J. L. Vossen, *"Control of film properties by RF sputtering techniques,"* J. Vac. Sci. Technol., vol. 8, no. 5 , pp. S12-S30, 1971.
25. H. F. Winters, D. L. Raimondi, and D. E. Horne, *"Proposed model for the composition of sputtered multicomponent films,"* J . Appl. Phys., vol. 40, no. 7, pp. 2996-3006, 1969.
26. J. A. Thornton, *"Influence of apparatus geometry and deposition conditions on the structure and topography of thick sputtered coatings,"* J . Vac. Sci. Technol., vol. 11, no. 4, pp. 666-670, 1974.
27.L. I. Maissel, C. L. Standley, and L. V. Gregor, *"Sputter-etching of heterogeneous surface,"* IBM J. Res. Develop., vol. 16, no. 1, pp. 67-70, 1972.
28.R.A. Gottscho and C.E. Gaebe, *"Negative ion kinetics in RF glow discharges,"* IEEE Trans. Plasma Sci., vol. PS-14, pp. 92-102, 1986.
29.H. Yasuda, *Luminous Chemical Vapor Deposition and Interface Engineering.* Marcel Dekker, New York ,2005.
30.S. Maniv and W. D. Westwood, *"Oxidation of an aluminum magnetron sputtering target in Ar/Oz mixtures,''* J . Appl. Phys., vol. 51, no. 1, pp. 718-725, 1980.
31.H. F. Winters and P. Sigmund, *"Sputtering of chemisorbed gas (nitrogen on tungsten) by low energy ions,"* J . Appl. Phys., vol. 45, no. 11, pp. 4760-4766, 1974.
32.M. Fukutomi, M. Kitajima, M. Okada, and R. Watanabe, *"Silicon nitride*

coatings on MO by RF reactive ion plating," J . Electrochem. Soc., vol. 124, no. 9, pp. 1420-1424, Sept. 1977.

33. H. Y. Kim, H. K. Yasuda, *"Improvement of fatigue properties of poly(methyl methacrylate) bone cement by means of plasma surface treatment of fillers."* Journal of Biomedical Materials Research vol. 48, no. 2, pp. 135-142, 1998
34. H. K. Yasuda "*Modification of polymer surfaces by plasma treatment and plasma polymerization."* Polymeric Materials Science and Engineering vol. 50, pp. 135-138, 1984
35. E. M. Charlson, E. J. Charlson, S. Burkett, H. K. Yasuda, *"Study of the contact electrification of polymers using contact and separation current."* IEEE Transactions on Electrical Insulation vol. 27, no. 6, pp. 1144-1157, 1992
36. Simon Lin, Syun-Ming Jang, Douglas Yu, "*Plasma treatment to improve barrier layer performance over porous low-k insulating dielectrics in semiconductor device."* U.S. Pat. Appl. Publ. 2006
37. C M Weikart, Y Matsuzawa, L Winterton, H K Yasuda *"Evaluation of plasma polymer-coated contact lenses by electrochemical impedance spectroscopy."* Journal of biomedical materials research vol. 54, no. 4, pp. 597-607, 2001
38. E. M. Charlson, E. J. Charlson, S. Burkett, H. K. Yasuda, *"Triboelectric properties of plasma polymers."* Journal of Applied Polymer Science: Applied Polymer Symposium pp. 109-136, 1990
39. Y.-S. Lin, H.-M. Liu, C.-L. Chen, "*Plasma surface modification of polyimide films by air glow discharge for copper metallization on microelectronic flex substrates."* Surface and Coatings Technology vol. 200, no. 12-13, pp. 3775-3785, 2006
40. d'Agostino, Riccardo. *"Process control and plasma modification of polymers."* Journal of Photopolymer Science and Technology vol. 18, no.2, pp. 245-249, 2005
41. T.J. Donahue and R. Reif, *"Silicon epitaxy at 650-800°C using low pressure chemical vapor deposition with and without plasma enhancement,"* J. Appl. Phys., vol. 57, no. 8, pp. 2757-2765, 1985.
42. R. Reif and W. Kern, *"Plasma-enhanced chemical vapor deposition,"* in Thin Film Processes II, J. L. Vossen and W. Kern, Eds. San Diego: Academic. 1991, pp. 525-564.
43. G. Lucovsky, D. V. Tsu, R. A. Rudder, and R. J. Markunas, *"Formation of inorganic films by remote plasma-enhanced chemical-vapor deposition,"* in Thin Film Processes II, J. L. Vossen and W. Kern, Eds. San Diego: Academic.

1991, 565-619.

44.J. F. Evans and G. W. Prohaska, *"Preparation of thin polymer films of predictable chemical functionality using plasma chemistry,"* Thin Solid Films, vol. 118, no. 2, pp. 171-180, 1984.

45.M. Miyama and H.K. Yasuda, J. Appl. Polym.Sci.vol.70, no.237,1998.

46.T.F. Wang, T.J. Lin, D. J. Yang, J.A. Antoneilli and H.K. Yasuda, Prog. Org. Coat vol.28, no.291 ,1996.

47.C.M. Reddy, Q.S. Yu, C.E. Moffitt, D.M. Wieliczka, R. Johnson, J.E. Deffeyes, and H. K. Yasuda, Corrosion (Houston) vol.56, no. 819 ,2000.

48.Q.S. Yu, C.M. Reddy, C.E. Moffitt, D.M. Wieliczka, R. Johnson, J.E. Deffeyes, and H. K. Yasuda, Corrosion (Houston) vol. 56, no.887 ,2000.

49.C.E. Moffitt, Q.S. Yu, C.M. Reddy, D.M. Wieliczka, R. Johnson, J.E. Deffeyes, and H.K. Yasuda, Corrosion (Houston) vol.56, no.1032 ,2000.

50.T. T. Chau, C. K. Kwan, B. Gregory, and M. Francisco, Biomaterials 17, 1996

51.N. Philps, B. Saoudi, M. C. Crevier, M. Moison, J. Barbeau, and J. Pelletier, "*The respective roles of UV photons and oxygen atoms in plasma sterilization at reduced gas pressure : the case of N2-O2 mixtures"* IEEE Trans. Plasma Sci. Vol. 30, 2002

52.Menashi, W.P. US Patent 3, 383,163., 1968

53.Ascham & Menashi, US Patent 3, 701,628,1972

54.R.B. Gadri, J.R. Roth, T.C. Montie, K. Kelly-Wintenberg, P.P. Tsai, D. J. Helfritch, P. Feldman, D. M. Sherman, F. Karakaya, Z. Chen, J. Surf. Coat. Technol. 131, 2002

55.P. T. Jacobs and S. M. Lin, " Disinfection, Sterilization and Preservation." ed. S. S. Block, Philadelphia, Lippincortt Willams & Wilkins, 2001

56.J. Feichitinger, A. Schulz, M. Walker, U. Schumacher, J. Surf. Coat. Technol. 174, 2003

57.M. Nagatsu, F. terashita, and Y. Koide, Jpn. J. Appl. Phys. 15, 2003

58.M. Laroussi, *"Nonthermal decontamination of biological media by atmospheric-pressure plasmas: review, analysis, and prospects"* IEEE Trans. Plasma Sci. 28, 2002

59.M. Laroussi, *"Biological decontamination by non-thermal plasmas"* IEEE Trans. Plasma Sci. 28, 2000

60.M. Moisan, J. Barbeau, and J. Pelletier, Le Vide (Science, Technique Applications) 299,15,2001

61.S. Lerouge, M.R. Wertheimer, and L.H. Yahia J. Plasma Polym,vol.5,no.1,2000

CHAPTER 3

THE GLOW CHARACTERISTICS OF DC BRUSH-SHAPE ATMOSPHERIC PRESSURE PLASMA

3.1. Introduction

Low temperature atmospheric pressure plasma process has recently received more attentions and exhibited great potential alternative of traditional low-pressure plasma process. Low temperature atmospheric pressure plasma does not require any vacuum systems and provides numerous applications such as sterilization, modification, and surface cleaning at low temperatures while operating open to the atmosphere. Several low temperature atmospheric pressure plasma sources have been developed since late 1980s [1-3]. In low temperature atmospheric pressure plasma state, the plasma is a continuous high-electron energy in which non-equilibrium can only be reached either in short pulses or in the presence of large gradients of electric field, concentration, and mass-flow velocity (for instance, in boundary layers) [3].

The developments of spatially uniform low temperature atmospheric pressure plasmas [4] are attractive by reason of their potential practical applications in the industrial fields [5]. One of the most studied non-equilibrium plasma at vacuum

pressures is the normal glow discharge [6]. Plasmas at higher pressures are generally unachievable owing to instabilities that cause a glow-to-arc transition [4]. As the pressure is increased the current density increases until attainment the threshold for the development of instabilities conducting to a transition to the arc phase and equilibrium plasma. This instability mainly contains two types: electronic instability and thermal instability. The electronic instability usually develops in the cathode fall regions with fluctuations of the electrical field. By using large ballasted resistors, the effect of these fluctuations could be minimized and eliminated, and as a result stable atmospheric glow discharges could be generated.

Several atmospheric pressure plasma sources including the dielectric barrier discharge, the resistive barrier discharge, and the atmosphere pressure plasma jet have been developed and reported [7]. The dielectric barrier discharge has two electrodes as shown in Fig. 3.1. A feature of the dielectric barrier discharge is that a dielectric material covers at least one of the electrodes, sometimes both. The dielectric is cardinal for the dielectric barrier discharge. Once ionization occurs at a location in the discharge gap the transported charge accumulates on the dielectric. The dielectric serves two functions: it limits the amount of charge transported by a

single micro-discharge, and distributes the micro-discharges over the entire electrode area. In most cases, the reduced field at breakdown corresponds to electron energies of about 1-10 eV. This is ideal energy range for excitation of atomic and molecular species and breaking of chemical bonds.

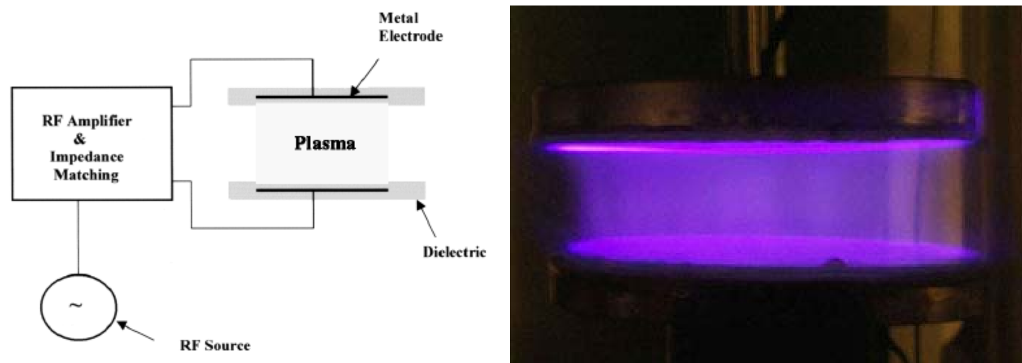

Figure 3. 1. The configuration of the dielectric barrier discharge plasma [7,8]

The notion of the resistive barrier discharge is based on the dielectric barrier discharge configuration as shown in Fig. 3.2. However, resistive barrier discharge used a highly resistive material in place of a dielectric material. The highly resistive material provides the proper function of distributed ballast that limits the discharge current and forbids arcing [8-9]. The benefit of resistive barrier discharge over dielectric barrier discharge is the prospect of using dc power supply to drive the discharge.

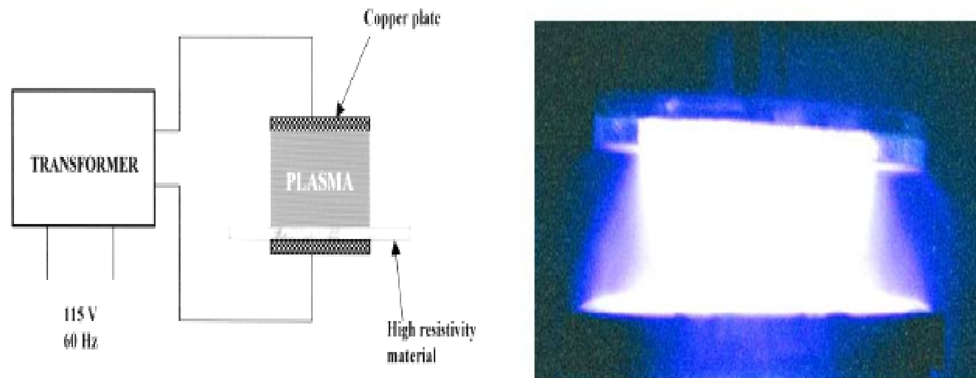

Figure 3. 2. The configuration of the resistive barrier discharge plasma [7,10]

The atmospheric pressure plasma jet can be generated by radio frequency and microwave discharges. The radio frequency atmospheric pressure plasma jet is a coactively coupled device consisting of two coaxial electrodes between which a gas flows at high flow rates as shown in Fig. 3.3. Radio frequency power at 13.56 MHz is applied to the center electrode accelerate free electrons and cause the gas to break down initiating a spatially uniform discharge [11].

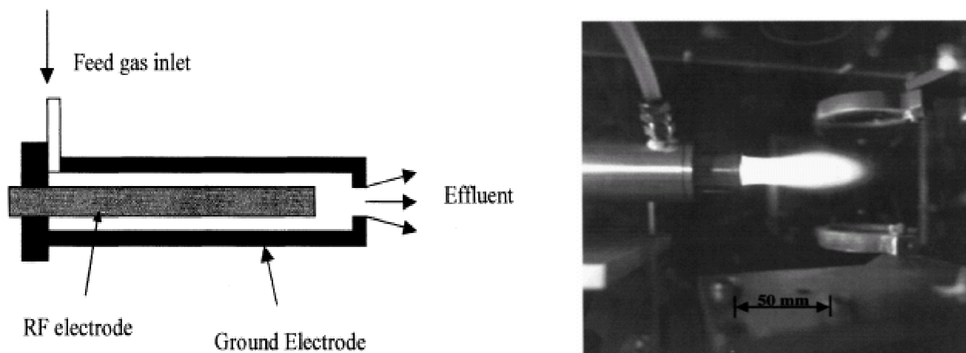

Figure 3. 3. The configuration of the RF atmospheric pressure plasma jet [7,10]

The waveguide-based microwave atmospheric pressure plasma jet is operated

without using electrode. The waveguide is used for increasing the electric field strength and minimizing the reflected wave. The plasma generated at the end of nozzle is produced by an interaction between the high electric field, which is generated by the microwave power, the waveguide aperture and the gas nozzle [12].

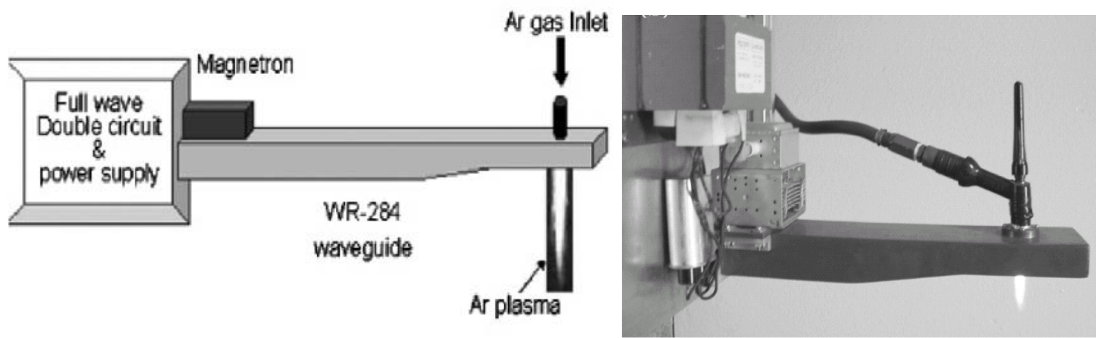

Figure 3. 4. The configuration of the microwave atmospheric pressure plasma jet [13]

Most of the atmospheric pressure plasmas described above has their native disadvantages. The electrode spacing of both dielectric barrier discharge and resistive barrier discharge restricts the size and the shape of the sample to be treated. The atmospheric pressure plasma jets are closed enough to thermal equilibrium to heat the neutral gas and active species to high temperatures; and their high power density can damage thin or sensitive item. These drawbacks have greatly restricted the atmospheric pressure plasma from practical applications.

To improve the deficiencies and limitations of those atmospheric pressure plasma techniques, the novel direct current (DC) atmospheric pressure glow discharge was successfully designed and developed [13,14]. Most of atmospheric pressure plasma processes commonly use inert gas-based glow discharges. The major cause attributes in relation to the simple ionization and bombardment characteristics. The brush-shape atmospheric pressure plasma is desired to sterilize/modify the surface of material. Therefore, further benefits may be possible in brush-shape atmospheric pressure plasma processes if the major reactive species reactions in plasma system can be understood.

There is a need for reliable and accurate continuous monitoring of reactive species worked in atmospheric pressure plasma processing. In the plasma, a large number of variables influence the whole system between physical and chemical process. Reliable and accurate plasma diagnostic techniques are presently being developed to provide real-time information in plasma system. In plasma state, the glow region is where most plasma reactions are involved; for this reason, the examination of the nature of glow becomes important to demonstrate the fundamental aspects of atmospheric pressure plasma. The method, which enables study of chemical and physical processes in plasma, is optical emission

spectroscopy (OES). Optical emission spectroscopy (OES), simple and non-invasive technique, was in advance used for investigation of many plasma processes [2]. OES collects the light emitted by the plasma through a viewport on the plasma reactor chamber and separates the light into its various spectral species. It can recognize the ions and radicals in the plasma by measuring the wavelengths and intensities of the emitted spectral lines. In this paper, the objective of this study is to examine the gas phase temperature, glow characteristics, and optical emission features of this novel brush shape atmospheric pressure plasma.

3.2. Experimental procedures

3.2.1. Experimental materials

Argon gas used to create the atmospheric pressure plasma brush was an industrial grade with 99.997% purity and purchased from General Store of University of Missouri-Columbia. Reactive gas used for atmospheric pressure plasma brush was an industrial grade oxygen (99.9% purity) purchased from General Store of University of Missouri-Columbia.

3.2.2. The low-temperature atmospheric pressure plasma brush

This plasma source contains discharge chamber with a proprietary design as shown in Fig. 3.5. The inert gas such as argon gas and helium gas passes through

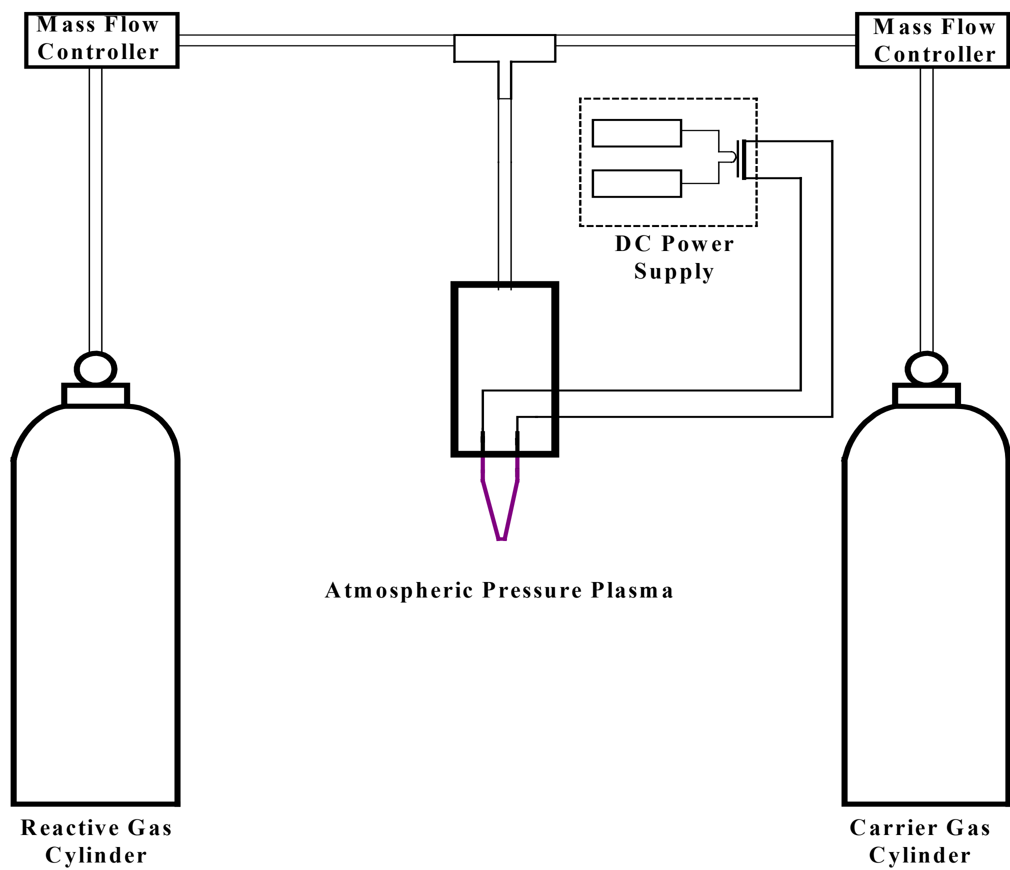

Figure 3. 5. Schematic of the argon atmospheric pressure plasma brush reactor

the discharge chamber at a flow rate controlled by a MKS mass flow controller (MKS Instruments Inc. Andover, MA, USA). An electrical field was applied to the two electrodes located inside the chamber to ignite a DC glow discharge by a DC power supply (Pd 1556C, Power Design Inc. New York, NY, USA). One of the two electrodes is connected with a ballasted resistor. The ballasted resistor is used to suppress the electrical field fluctuations in the cathodic region and also restrain the electrical current passing through the discharge to prevent glow-to-arc transition. The electrical voltage used to create DC atmospheric pressure plasma from several hundreds volts to several thousands volts with electrical current passing through the discharge on the order of milli-amperes. Consequently, the power input in generating and sustaining DC atmospheric pressure plasma is in the level of several watts or tens of watts. The low power input of DC atmospheric pressure plasma provides the unique advantage in the low power consumption. The gas phase temperatures of an atmospheric pressure plasma brush measured using a thermocouple thermometer (Fisherbrand Traceable Dual Channel Thermometer, Fisher Scientific, Houston, TX, USA)

3.2.3. Optical emission spectroscopy

The major plasma diagnostic apparatus of brush-shape atmospheric pressure

plasma is an optical emission spectroscopy. This equipment consists of both the instrumentation and spectrum analysis software, which was supplied by Princeton Instruments, Inc. The observable spectral range was 200-1050 nm. A 2m long fiber optic cable, coupled to a variable width (10–2000 ℳm) slit (typical width: 15 mm, with resolution: 0.3 nm), was mounted on a Jarrell–Ash Monospec 27 monochromator/spectrograph (crossed Czerny–Turner, 275 mm focal length, f/3.8) with a triple (150, 600, and 1200 grooves/mm) grating holder. A Princeton Instruments RY-1024 unintensified diode array detector is mounted at the Monospec 27 exit port, and is controlled by a Princeton Instruments ST120 OSMA detector controller that interfaces with a Dell computer.

3.3. Results and Discussion

Shown in Fig 3.6. is the low temperature and uniform exposure features of the atmospheric pressure plasma brush. When a proper electrical field is applied between the two electrodes, the argon atmospheric pressure glow discharge can be formed between the two electrodes inside the it’s gas compartment, or extend out of the discharge chamber through the outlet, as shown in Fig.3.6. In this study, the gas phase temperatures of the argon atmospheric pressure plasma brush maintained at different DC power levels of 10.4, 12.6, and 15.0 W were measured

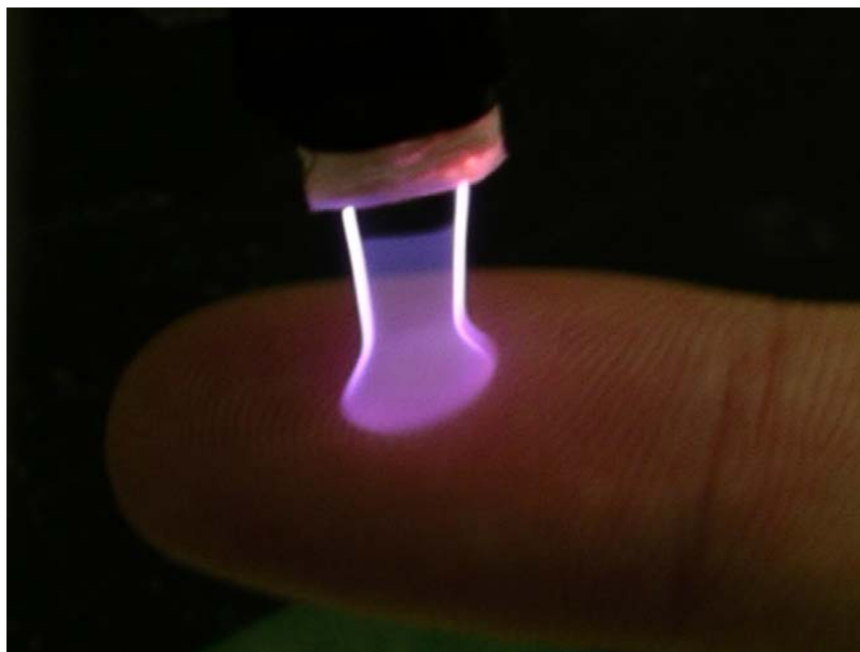

(a)

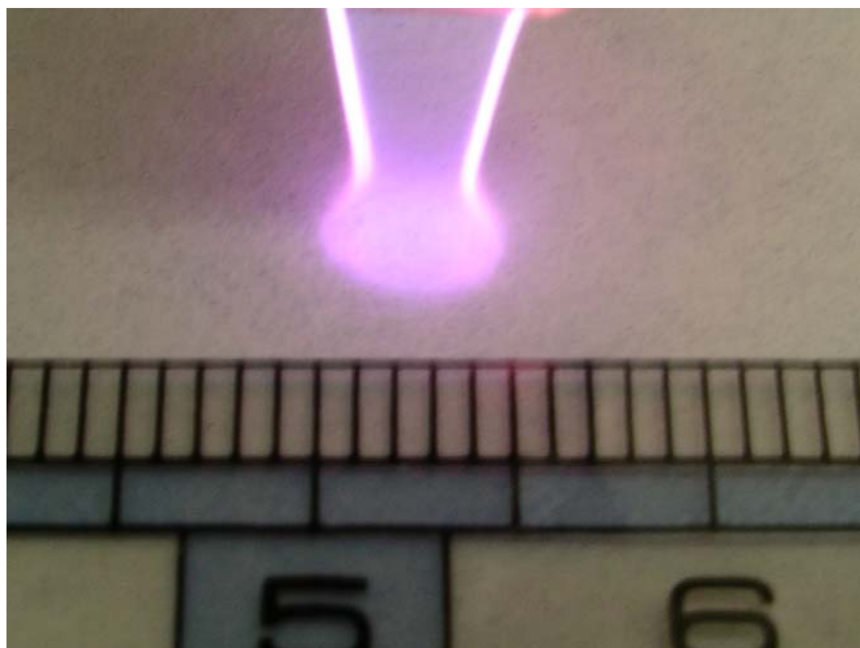

(b)

Figure 3. 6. (a) Pictorial view of the atmospheric argon plasma brush on a fingertip brush (b) Pictorial view of the uniform exposure from atmospheric argon plasma brush on a filter paper substrate

with a thermocouple thermometer as shown in Fig. 3.7. With the argon flow rate changing from 1000 to 3500 sccm; the gas phase temperature of the atmospheric pressure plasma brush is decreased from 160 ^{o}C to 40 ^{o}C, which evidently shows the low-temperature characteristic of this brush-shape atmospheric pressure glow discharge. Either the gas flow rate or direct current (DC) power can be used to sustain and control the glow region of argon atmospheric pressure plasma. The dimensions of the brush-shape argon atmospheric pressure glow discharge were determined by the gas flow rate or DC power input. Fig. 3.8. shows the change of luminous glow region from DC argon atmospheric pressure plasma brush with different gas flow rates /different DC power inputs. It is obviously noted that the luminous glow region of atmospheric pressure plasma brush were enhanced with the increasing of argon flow rate/ DC power input and the lengthening glow region was obtained at the higher argon flow rate/ DC power input. When the more argon gas molecules under the fast flow rate or more electrical energy from increasing DC power input were introduced into DC atmospheric pressure plasma brush, more gas collisions with electrons occurred, resulting in the energy transfer to photo-emitting plasma species. The effect on such an energy transfer was the

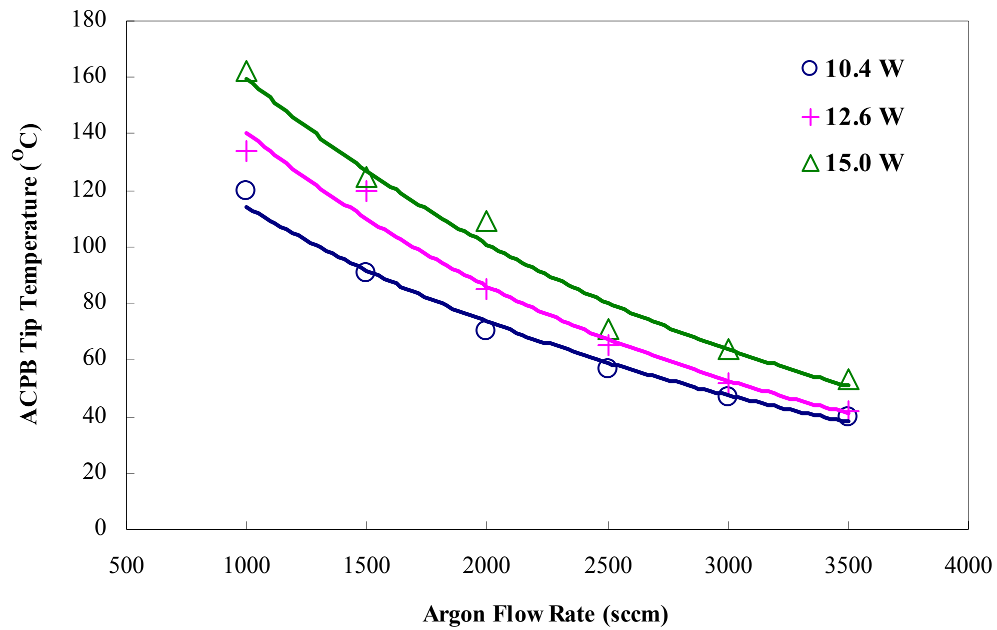

Figure 3. 7. The gas phase temperatures of the argon atmospheric pressure plasma brush

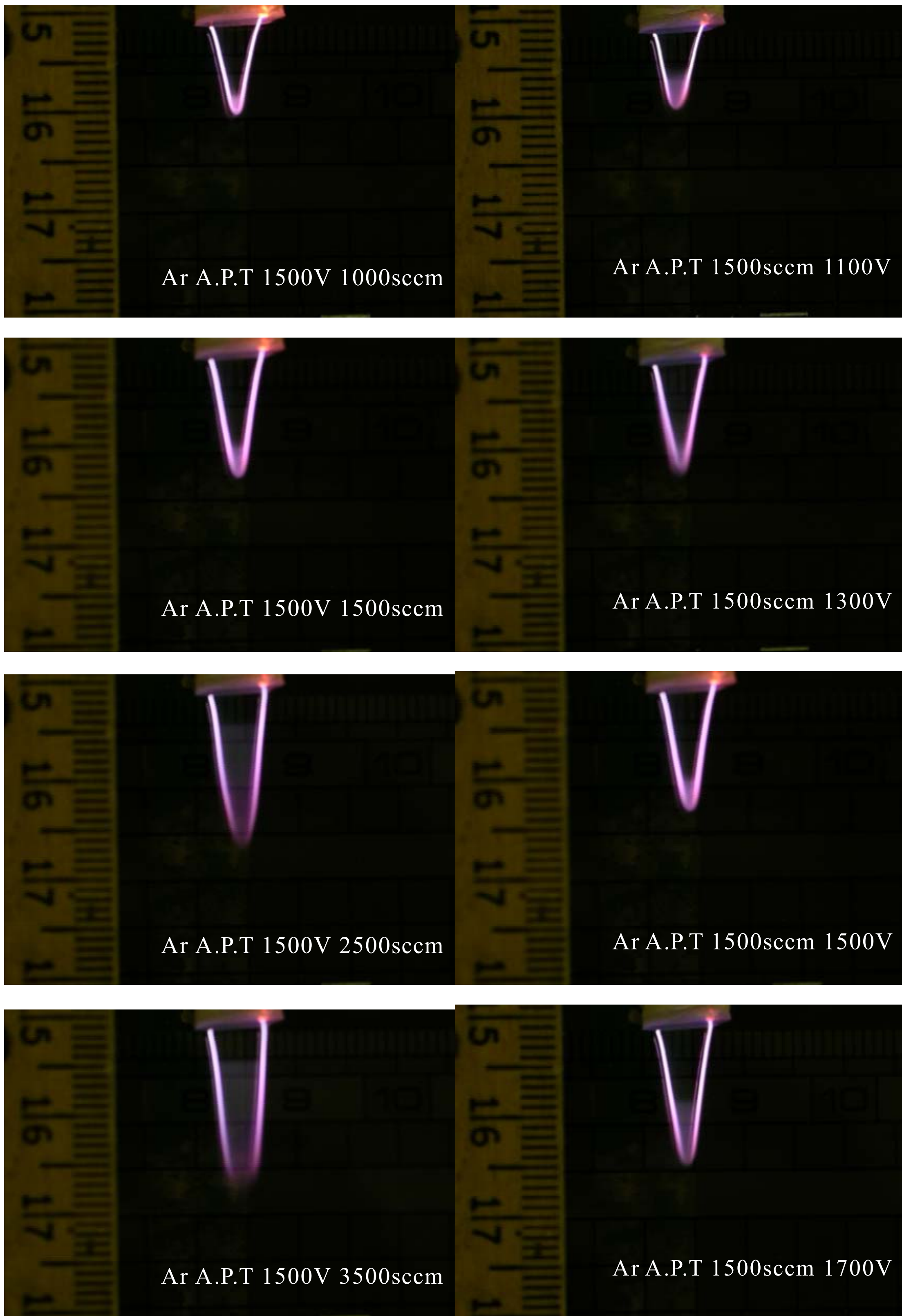

Figure 3. 8. Pictorial view from the luminous gas phase of atmospheric cold argon plasma brush

creation of the lengthening luminous glow region from the higher argon flow rate/ DC power input.

The emission spectra of argon atmospheric pressure plasmas have been recorded in the wavelength range from 200 to 1020 nm without adding any reactive gas. The typical emission spectra of argon atmospheric pressure plasmas from different viewpoints are shown in Fig. 3.9. The emissions of the argon atmospheric pressure plasma from different viewpoints correspond exclusively to excited argon and nitrogen species. Some typical emission lines from the major photoemission plasma reactive species of atmospheric pressure plasma are summarized in Table 3.1 First, the strong excited argon emission lines are observed at about 700-800 nm. This is the dominant features for argon atmospheric pressure plasma correspond to *4p—>4s* transitions, with no higher energy levels being clearly observed such as *5p—>4s*. Second, the strong emission of N_2 second positive system ($C^3\Pi_u$->$B^3\Pi_g$ transitions) were observed at about 300-400 nm, as well. Moreover, another optical emission of N_2 first positive line ($B^3\Pi_g$ ->$A^3\Sigma_u^+$ transitions) at 662.3 nm, which was one of the significant emissions in atmospheric pressure plasma, is also observed. Third, the emission line of the atomic oxygen at 777 nm is clearly evident in Fig. 3.9. As seen in

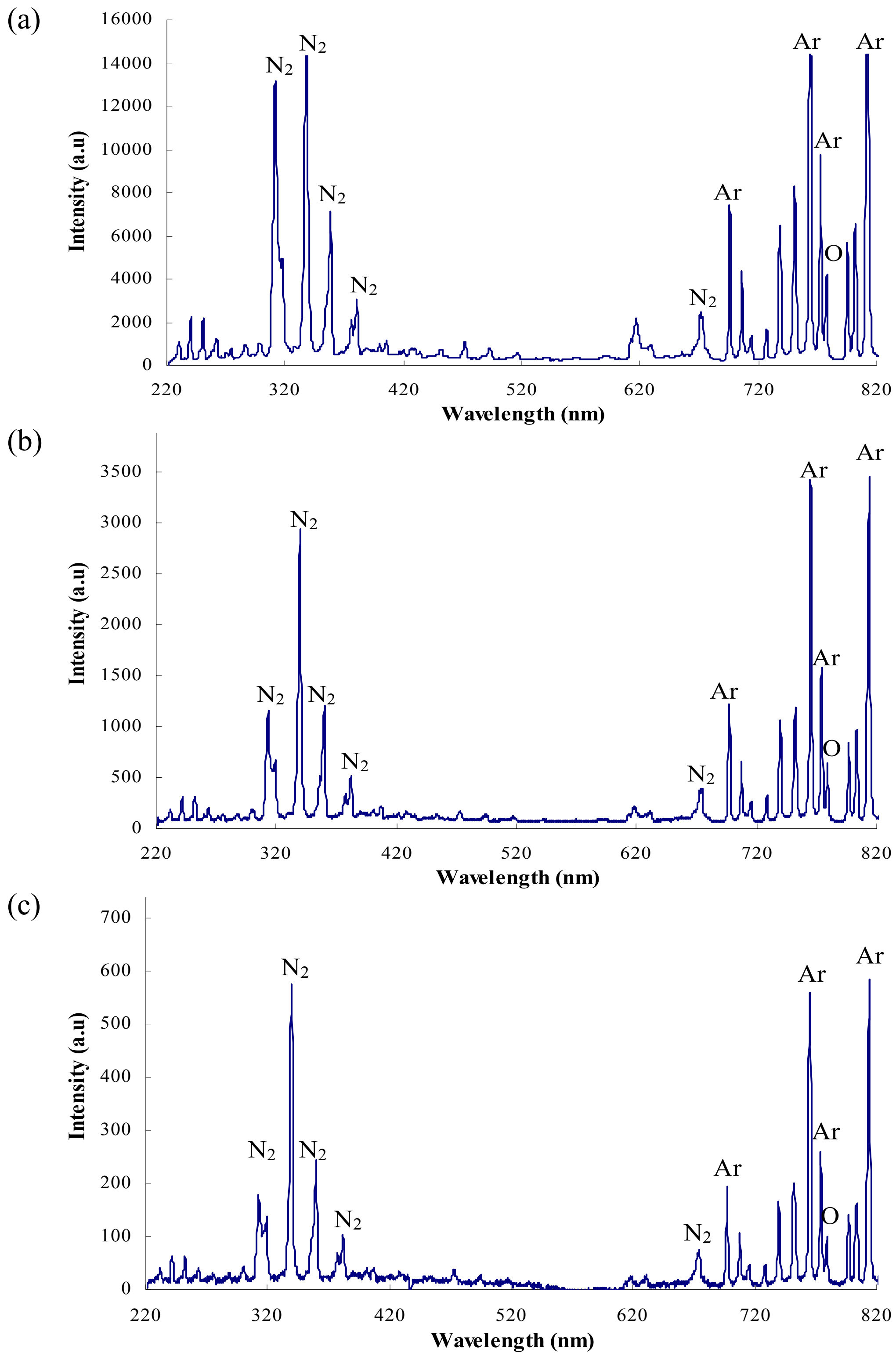

Figure 3. 9. The optical emission spectrum from APB with different view angles (a) face view (b) side view-cathode (c) side view-anode Conditions are 1500 sccm Ar, DC 15 Watt, 150g/mm, at 180sec.

Table 3.1. Most Intense Emission Lines Observed in DC Brush-Shape Atmospheric Pressure Plasma

Species	Emission Wavelength (nm)	Transition	Energy of emitting state above ground state E_B
Ar	696.5	$4p'[\frac{1}{2}] \rightarrow 4s[1\frac{1}{2}]^o$	13.33
	750.4	$4p'[\frac{1}{2}] \rightarrow 4s'[\frac{1}{2}]^o$	13.48
	763.5	$4p[1\frac{1}{2}] \rightarrow 4s[1\frac{1}{2}]^o$	13.17
	772.4	$4p'[\frac{1}{2}] \rightarrow 4s'[\frac{1}{2}]^o$	13.33
	794.8	$4p'[1\frac{1}{2}] \rightarrow 4s[\frac{1}{2}]^o$	13.28
	811.5	$4p[2\frac{1}{2}] \rightarrow 4s[1\frac{1}{2}]^o$	13.08
N_2	315.9	$C^3\Pi_u \rightarrow B^3\Pi g$	
	337.1	$C^3\Pi_u \rightarrow B^3\Pi g$	11.1
	357.7	$C^3\Pi_u \rightarrow B^3\Pi g$	
	380.5	$C^3\Pi_u \rightarrow B^3\Pi g$	
	662.3	$B^3\Pi_g \rightarrow A^3\Sigma_u{}^+$	7.4
O	777.2	$3p^5P \rightarrow 3s^5S^0$	10.7

Table 3.1, excited argon neutrals (E_B: 13 eV) have more than enough energy to excite either state of N_2 1st pos. (E_B: 7.4 eV) or N_2 2nd pos. (E_B: 11.1 eV). As a result, the excited argon species are recognized as the main energy sources that produce reactive species in atmospheric pressure plasma. Therefore, the electronic energy levels of argon neutrals/atoms should play a dominant role in active nitrogen excitation processes in the argon atmospheric pressure plasma.

The optical emission intensity of photo-emitting species in plasma state exhibits the number density of excited species. The change of optical emission intensity appears the concentration change from the plasma reactive species in the upper state energy level. From this aspect, the investigation of emission intensity change with different plasma conditions may provide some information about the influence of different plasma conditions on the concentration of the excited species in plasma system. For the face view angle of argon brush-shape atmospheric pressure plasma, most of the intense emission lines observed have been listed in Table 3.1. It should be noted that the excited species in argon atmospheric pressure plasma in the face view angle have much higher electron energy levels than those in argon atmospheric pressure plasma in the side view angles. As previously described, the feeble emission lines of an argon atmospheric

pressure plasma in the side view angles compared to argon emission spectrum in the face view angle are observed in Fig. 3.9. The optical emission intensity change of major species with different view angles, shown in Fig. 3.10, has the notable features. After comparison of argon atmospheric pressure plasma emission spectra from different view angles, several strong nitrogen, argon and oxygen peaks greatly decrease in cathode/anode view angles of argon atmospheric pressure plasma spectra, indicating there is a significant drop of the emission intensity once trace amounts of reactive species are introduced to argon brush-shape atmospheric pressure plasma.

In creation of atmospheric pressure plasmas, the energy input and gas flow not only affect the plasma density, but also the plasma temperature (Fig. 3.6). For the convenience with later discussion about OES analysis, the major intense emission lines would be plotted with different plasma conditions. The energy input effect by optical emission detection is shown in Fig. 3.11, as a function of plasma power. Due to the strong electric field, reactive species generation takes place either in the atmospheric pressure plasma chamber or in the gas phase with air in the downstream of atmospheric pressure plasma. As power increases from 7.5 W

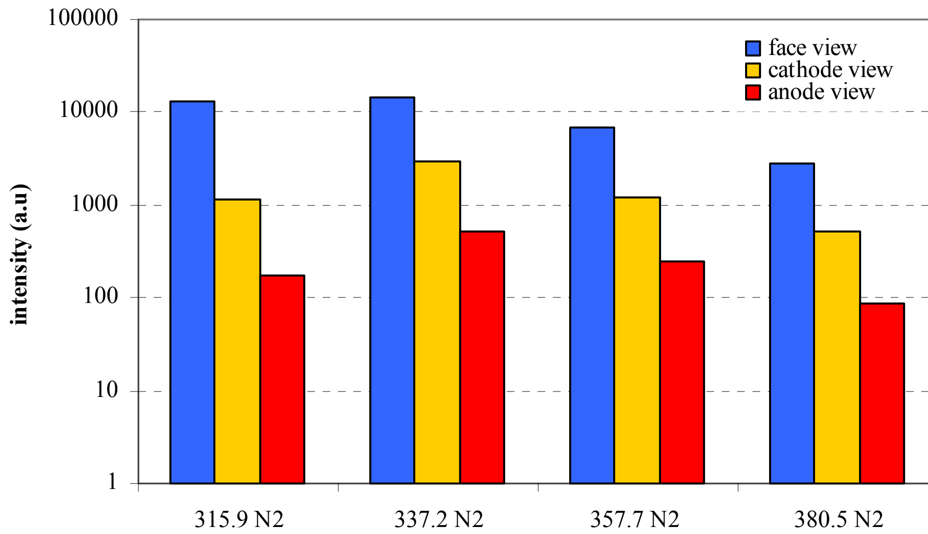

(a)

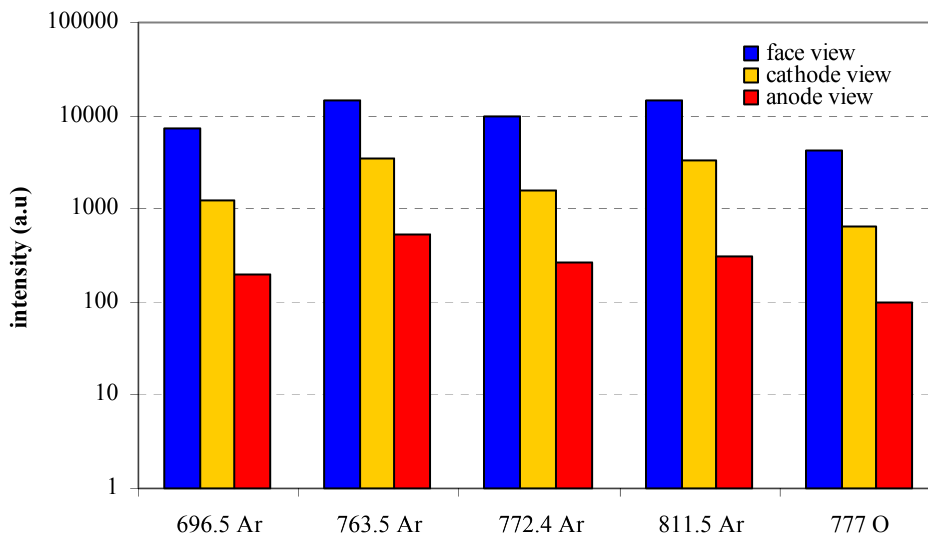

(b)

Figure 3. 10. The relevance optical emission intensity from APB with different view angles (a) nitrogen 2nd positive band (b) argon and oxygen lines Conditions are 1500 sccm Ar, DC 15 Watt, 150g/mm, at 180sec.

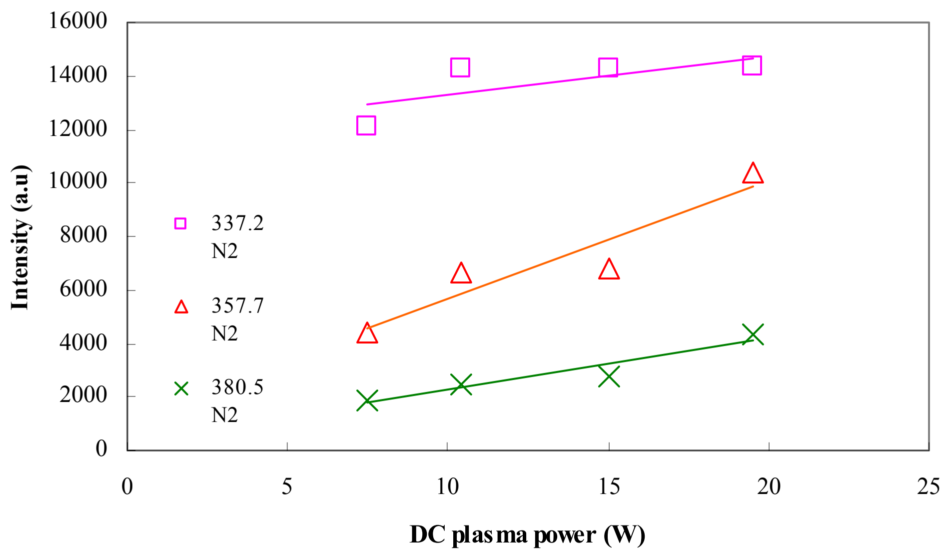

(a)

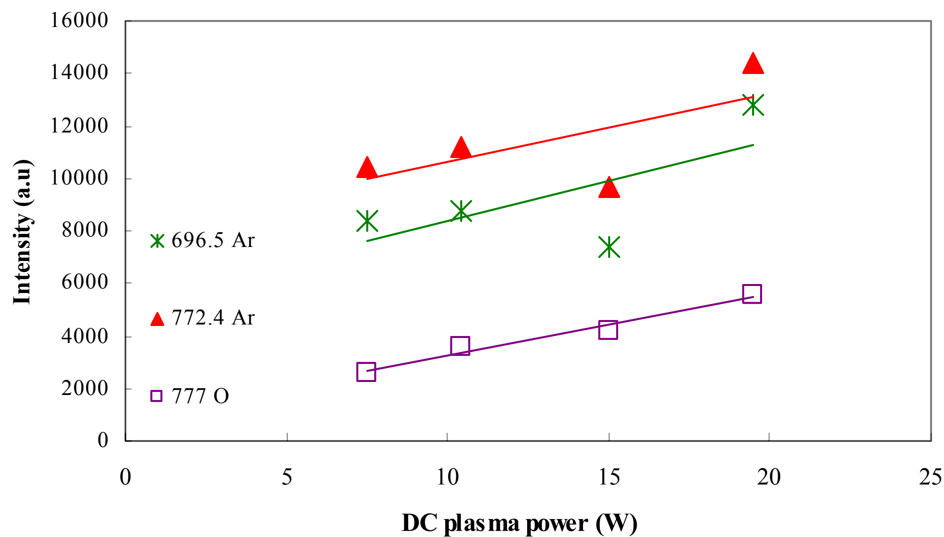

(b)

Figure 3. 11. Optical emission intensity dependence of (a) nitrogen 2nd positive band (b) argon and oxygen lines on DC plasma power Conditions are 1500 sccm Ar, DC 7.5, 10.4, 15, and 19.5 Watt, 150g/mm, at 180sec.

to 19.5 W, the major emission lines significantly increase due to an increase in the energy input as shown in Fig. 3.11. It is practical that the higher concentration of excited species can be attained with higher power input in the atmospheric pressure plasma system. The increased power input in the plasma contributes to improved excited Ar atoms by both direct electron-impact ionization and excitation of air, as well as through an increase in the metastable argon density and subsequent Ar*– air interactions. Higher power input could result in higher degree of ionization of the gas and thus increase the density of various plasma reactive species.

On the other hand, the increased argon flow rate can only improved the argon excitation as shown in Fig 3.12. According to the optical emission intensity dependence, the evolution of the N_2 second positive system ($C^3\Pi_u$->$B^3\Pi_g$ transitions) emission in the argon atmospheric pressure plasma can be therefore decreased or controlled by both increasing excited argon neutrals and argon ions. This finding with respect to argon gas flow rate may be explained by the fact that a higher flow rate could bring more unconsumed argon gas out of the atmospheric pressure plasma chamber and decrease the chance of electron collisions and electron/air interactions, therefore, resulting in decreasing emission lines of

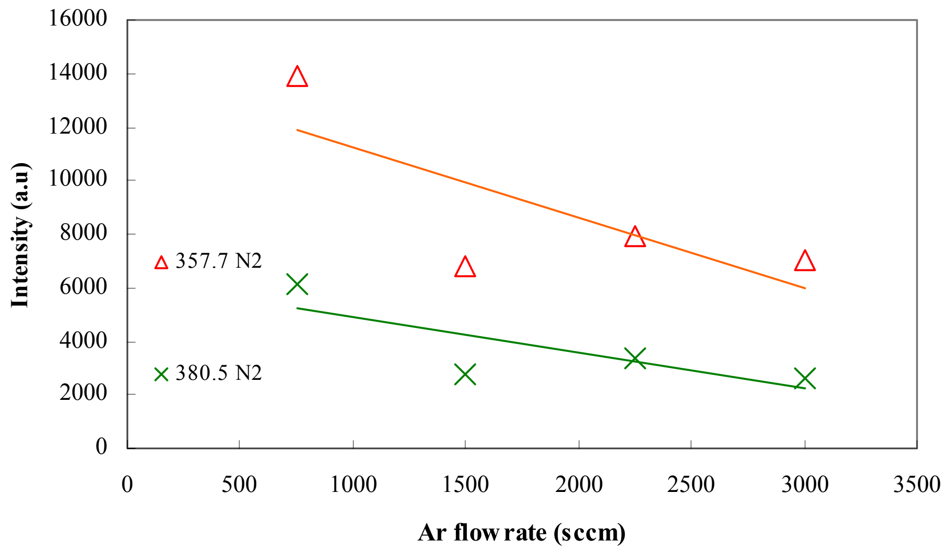

(a)

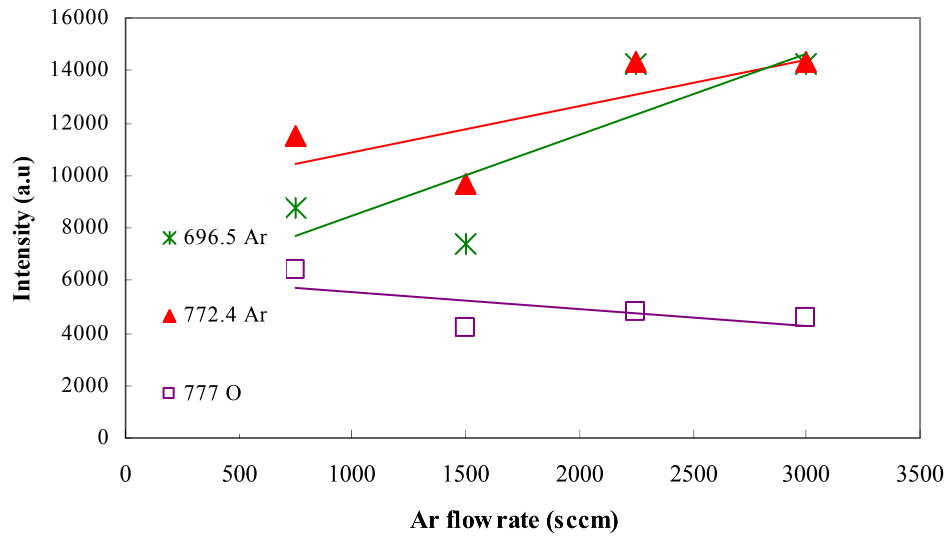

(b)

Figure 3. 12. Optical emission intensity dependence of (a) nitrogen 2nd positive band (b) argon and oxygen lines on argon flow rate Conditions are DC 15 Watt, 750, 1500, 2250, and 3000 sccm Ar,150g/mm, at 180sec.

nitrogen and oxygen.

Because reactive gases were added into brush-shape atmospheric pressure plasma at the site where electric field exists, the excitation transfer between active species of the carrier gases and reactive gases become dominant electron collisions. Upon addition of reactive gases to the brush-shape atmospheric pressure plasmas, the luminous gas phase of argon plasma without color change was highly quenched. When oxygen was added into argon atmospheric pressure plasma, the obvious quenching of nitrogen and argon emission of atmospheric pressure plasma was observed. The dominant features in the emission spectra are due to excited species corresponding to the relevant gases, with the decreasing emission intensities of major nitrogen or argon emission lines. The optical emission due to excited oxygen atoms at 777.2 nm (E_B: 10.7 eV) is observed for brush-shape atmospheric pressure plasma. When certain oxygen gas (18.2 %) was added to argon brush-shape atmospheric pressure plasma, the emission due to O at 777.2 nm greatly increased, which was not clearly observed in pure argon brush-shape atmospheric pressure plasma. In Fig. 3.13, several nitrogen and argon emission lines (337.2,358.9, 380.5, 696.5, 763.5, 772.4 and 811.5 nm) were chosen which are representative of all the nitrogen and emission bands, and one oxygen emission

line (777.2 nm) was chosen which is representative of all oxygen emission bands. It can be seen that, upon the addition of oxygen, all the activated nitrogen and argon species were quenched and exhibited the same decreasing tendencies with increasing oxygen addition percentage at range from 7.6-14.2 %. It was also noticed that the emission intensity of the oxygen emission line at 777.2 nm keeps increasing with increasing oxygen flow rate from 125-350 sccm, which shows that more activated oxygen species were produced.

For a given set of atmospheric pressure plasma conditions, the position of atmospheric pressure plasma could have a marginal effect on its working efficiency. In atmospheric plasmas, the plasma reactive species could lose its energy or reactivity in a very short time due to the much higher collision frequency among the plasma particles. The lifetime of the reactive plasma species in atmospheric plasmas is much shorter as compared to that in low-pressure plasmas. Fig. 3.14 shows optical emission intensity dependence of vertical distances away from atmospheric pressure plasma. At remote brush-shape atmospheric pressure plasma, the intensity of major emission lines decreased faster along away from brush-shape atmospheric pressure plasma as shown in Fig. 3.14. This can be easily understood due to the quicker consumption of excited

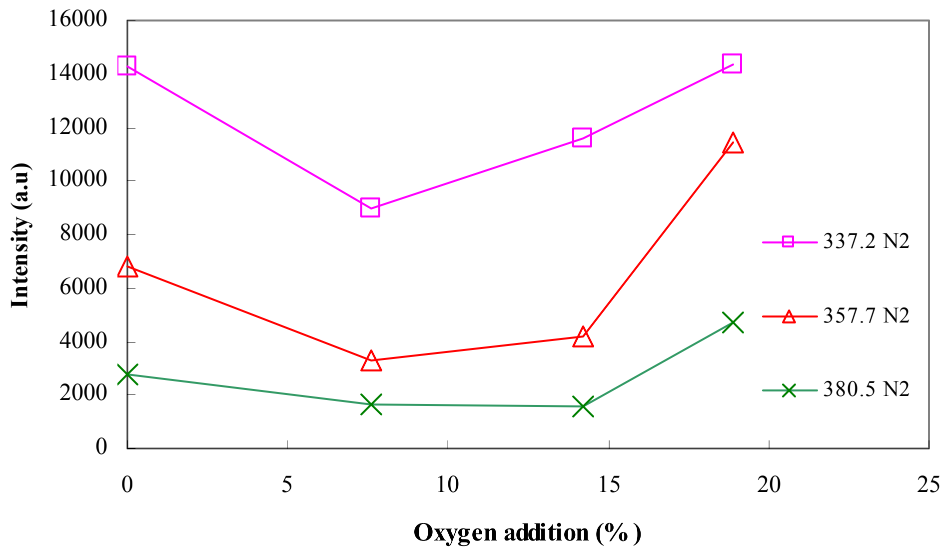

(a)

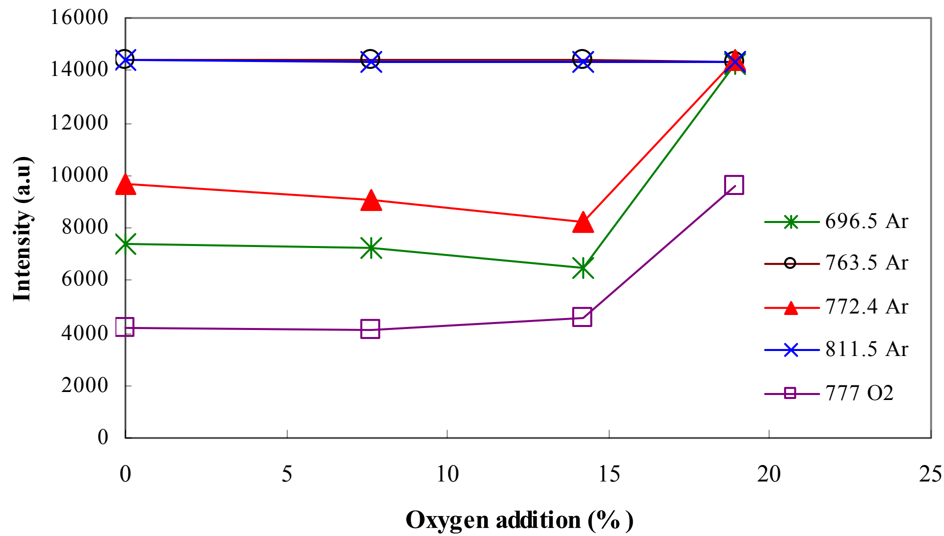

(b)

Figure 3. 13. Optical emission intensity dependence of (a) nitrogen 2nd positive band (b) argon and oxygen lines on oxygen addition Conditions are DC 15 Watt, 1500 sccm Ar, 7.6%, 14.2%, and 18.9% oxygen addition 150g/mm, at 180sec.

argon species at relatively longer distance. As discussed above, it can be concluded that, under the present operation conditions, the short lifetime of excited argon species are primarily responsible for the decreasing reactive species excitation in the remote brush-shape atmospheric pressure plasmas. Thus, it is obvious that the life times of excited argon species should play a dominant role in active nitrogen excitation processes in the brush-shape atmospheric pressure plasmas.

The optical emission spectra of oxygen addition (14.2 %) in argon remote brush-shape atmospheric pressure plasmas were also examined in the present work. The main optical emission intensity changes of oxygen addition (14.2 %) in argon remote brush-shape atmospheric pressure plasma with vertical distances away from glow discharge are shown in Fig 3.15. When vertical distance away from the glow was increasing, a strong decrease of all main emission lines was formed in the optical spectra. Comparison to the pure argon remote atmospheric pressure plasma in Fig. 3.14, the relevantly less emission intensities were observed. This indicates that the lifetime of the reactive species in remote $Ar+O_2$ (14.2 % addition) atmospheric pressure plasma are much shorter when compared to that in pure argon remote atmospheric pressure plasma. As a result, most of the plasma

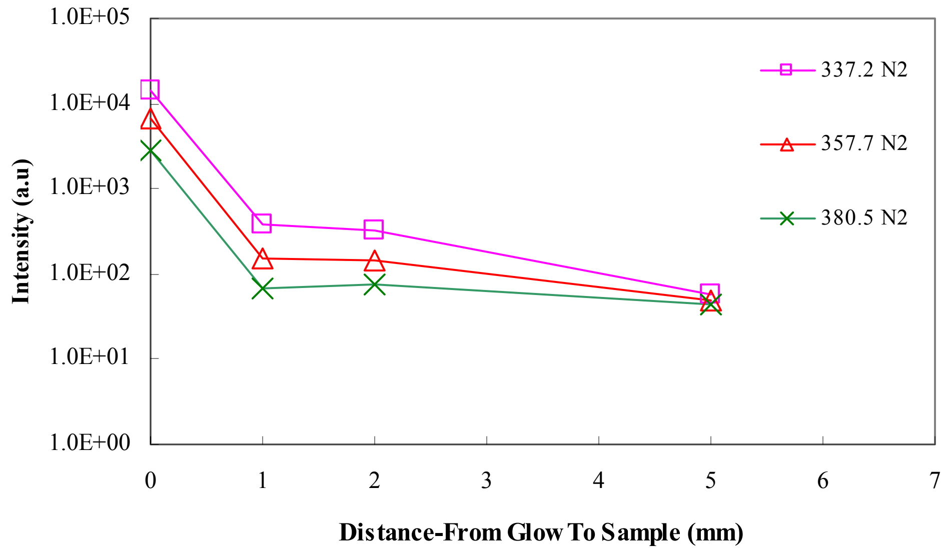

(a)

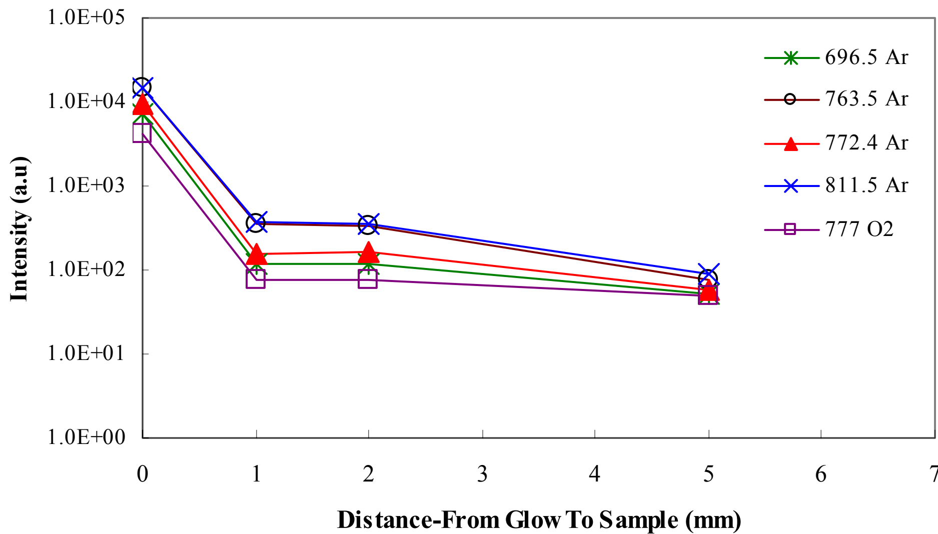

(b)

Figure 3. 14. Optical emission intensity dependence of (a) nitrogen 2nd positive band (b) argon and oxygen lines on remote distance Conditions are DC 15 Watt, 1500 sccm Ar 150g/mm, at 180sec.

species, except the argon metastables (long-life electronically-excited argon atoms) could lose their reactivity dramatically in a remote position (away from the glow). This finding (in Figs 3.14-15) also suggests that argon metastables in remote atmospheric plasmas are more effective than oxygen species in remote atmospheric plasmas.

The optical emission spectra of which atmospheric pressure plasma interacts with filter paper and aluminum substrates are presented in Fig. 3.16-17. From Fig. 3.16-17, it shows that the presence of optical emission species such as argon emission lines (696.5, 763.5, 772.4 and 811.5 nm), nitrogen emission lines (337.2, 358.9, 380.5 nm), and oxygen (the line at 777.2 nm) in the exposing area from atmospheric pressure plasma. The identified optical emission spectra are expected to elucidate the plasma -substrate surface interactions that may contribute to remove undesired components or increase the polarity on the substrate surface. However, the optical emission spectra in Fig. 3.16-17 showed no new photo-emitting plasma species appearance, suggesting that no fragments from the substrate surface are excited in the brush-shape atmospheric pressure plasma, for that reason, the potential plasma etching effect at the substrate surface is negligible for the brush-shape atmospheric pressure plasma process.

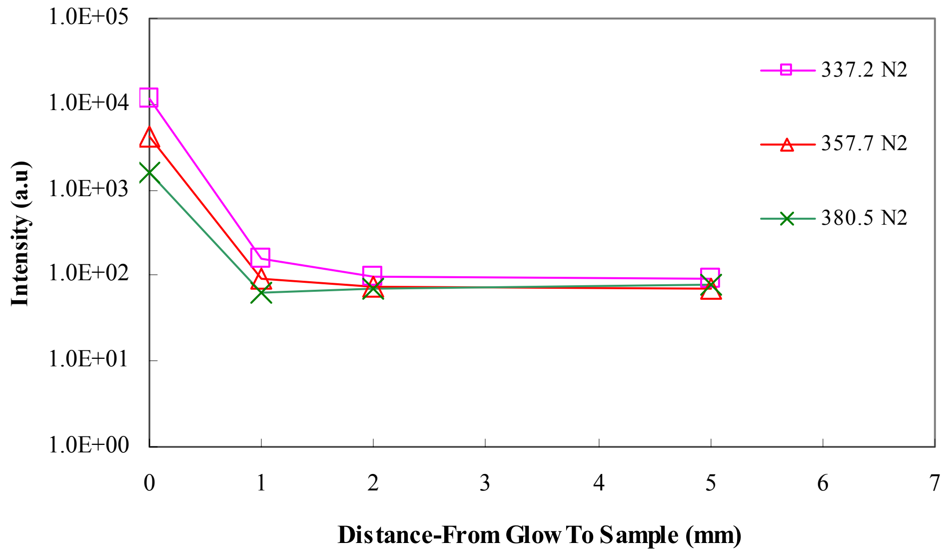

(a)

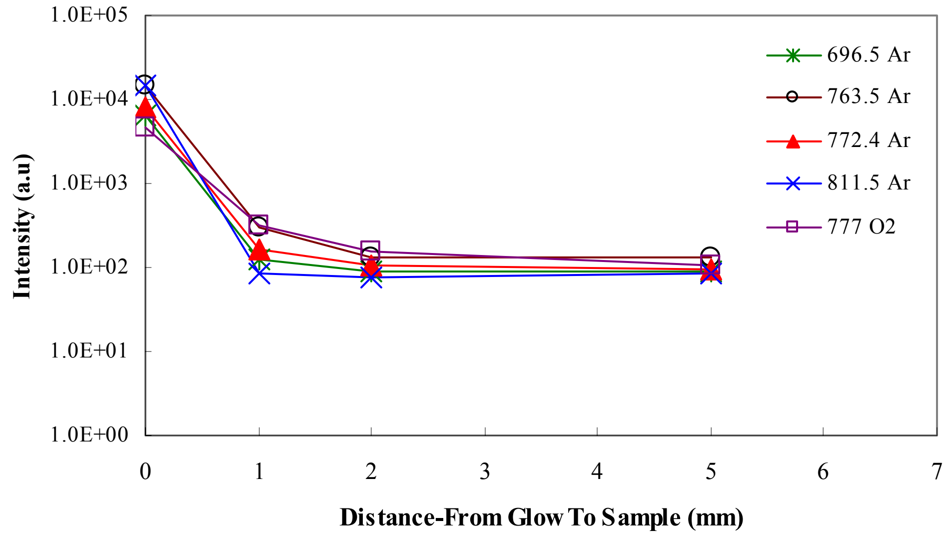

(b)

Figure 3. 15. Optical emission intensity dependence of (a) nitrogen 2nd positive band (b) argon and oxygen lines on remote distance Conditions are DC 15 Watt, 1500 sccm Ar 14.2% oxygen addition 150g/mm, at 180sec.

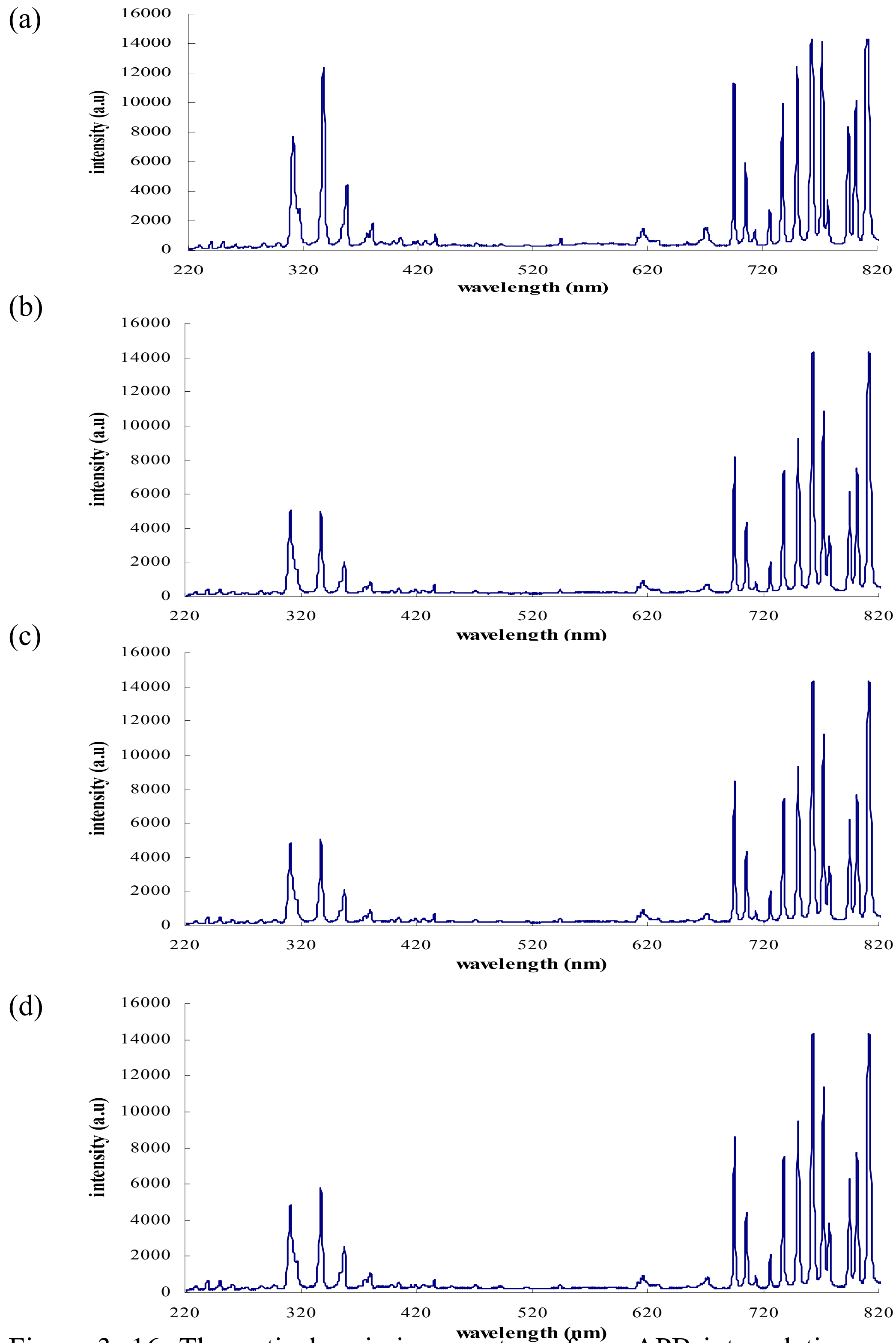

Figure 3. 16. The optical emission spectrum from APB intercalations with filter paper (a) pure argon (b) 7.6% oxygen (c) 14.2% oxygen (d) 18.9% oxygen Conditions are 1500 sccm Ar, DC 15Watt, 150g/mm, at 180sec.

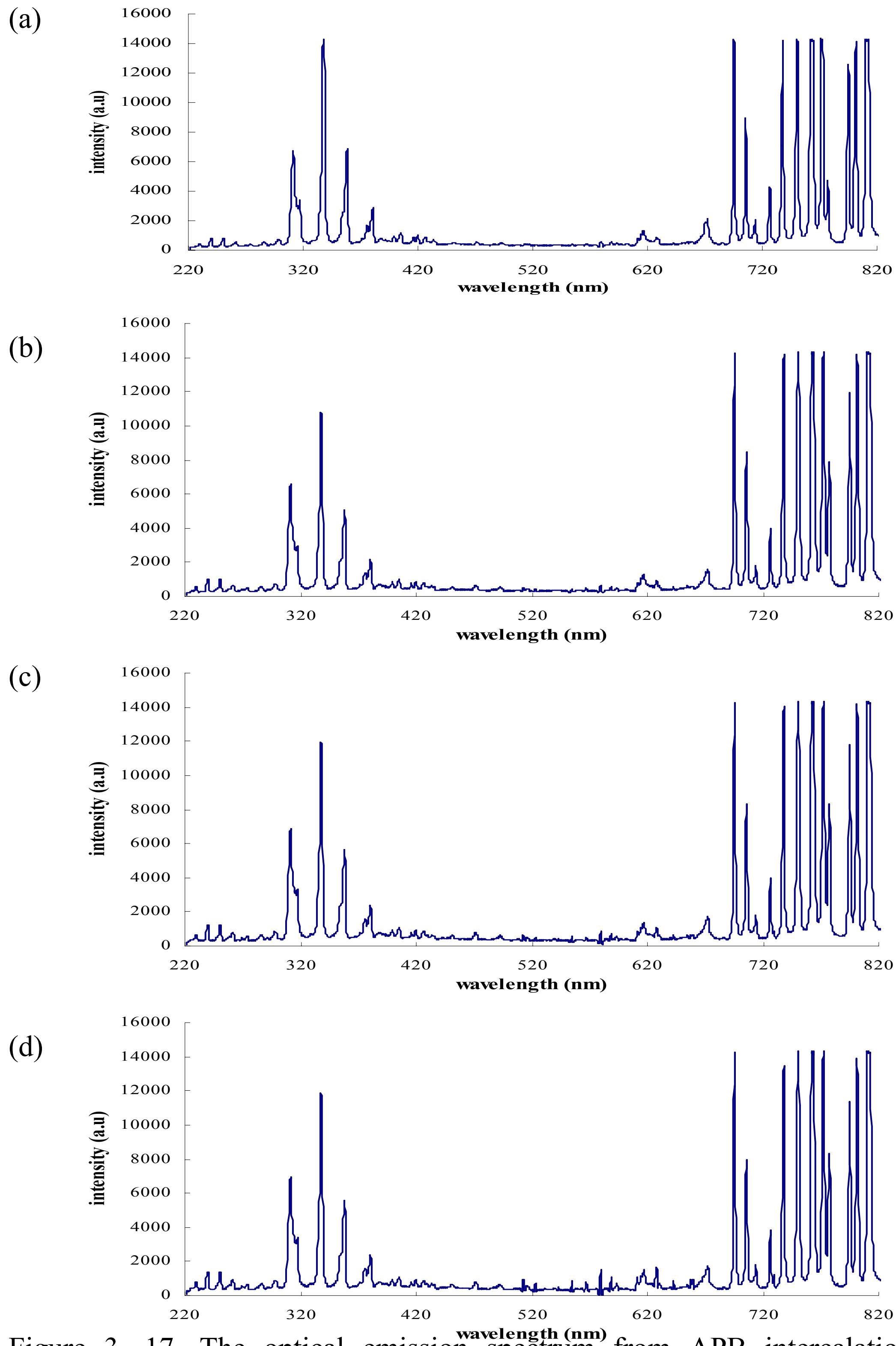

Figure 3. 17. The optical emission spectrum from APB intercalations with aluminum panel (a) pure argon (b) 7.6% oxygen (c) 14.2% oxygen (d) 18.9% oxygen Conditions are 1500 sccm Ar, DC 15Watt, 150g/mm, at 180sec.

3.4. Summary

The glow characteristics and the optical emission features of brush-shape atmospheric pressure plasma were studied. The low-temperature nature of this atmospheric pressure plasma brush makes the plasma source extremely useful in various applications including surface cleaning, surface modification, and surface sterilization/decontamination. Optical emission spectroscopy (OES) studies of argon brush-shape atmospheric pressure plasma and low oxygen addition in argon-based atmospheric pressure plasma have indicated that the excited argon atoms are the main energy carrier from brush-shape atmospheric pressure plasma to generate reactive species such as nitrogen molecules and atomic oxygen. It was also found that the excitation of reactive species was controlled by electronic energy and gas flow rate. Another important consideration in brush-shape atmospheric pressure plasma processes involves mechanisms governing the ionization of carrier gas and its interactions with reactive gases used. As a result, the suitable reactive gas parameters can be archived in increasing working efficiency of brush-shape atmospheric pressure plasma processes, which may have the definite contribution in either plasma bacterial inactivation or plasma surface modification processes. The present work examines atmospheric pressure plasma

brush type discharge to understand further the reactions occurring between inert gases such as argon and oxygen species within the main glow region of atmospheric pressure plasma brush. Certainly, more investigations and in-depth study of the atmospheric pressure plasma brush are needed to conduct in the future.

3.5. Reference

1. S. Kanazawa, M. Kogoma, T. Moriwaki, S.Okazaki, *"Stable glow plasma at atmospheric pressure."* J. of Phys. D: Appl. Phy. vol. 21, no.5, p. 838-40, 1988
2. S. Kanazawa,. M. Kogoma, T. Moriwaki, S.Okazaki, *"Glow plasma treatment at atmospheric pressure for surface modification and film deposition."* Nucl. Instru.& Meth. B vol. 37-38, p. 842-845, 1989
3. B. Eliasson, U**.** Kogelschatz, ***"****Nonequilibrium volume plasma chemical processing****"*** IEEE Trans. Plasma Sci. vol. 19, no.6, p.1063-1077, 1991
4. E. E. Kunhardt ***"****Generation of large-volume, atmospheric-pressure, nonequilibrium plasmas****"*** IEEE Trans. Plasma Sci. vol. 28, no.1, p.189-200, 2000
5. A. Schutze, J. Y. Jeong, S. E. Babayan, J. Park, G. S. Selwyn and R. F. Hicks ***"****The atmospheric-pressure plasma jet: a review and comparison to other plasma sources****"*** IEEE Trans. Plasma Sci. vol. 26, no.6, p.1685-1694, 1998
6. Y. P. Raizer "*Gas Discharge Physics."* (Berlin: Springer), 1997
7. M. Laroussi, "*Nonthermal decontamination of biological media by atmospheric-pressure plasmas: review, analysis, and prospects*" IEEE Trans. Plasma Sci., vol. 30, no. 4, p. 1409-1415, 2002
8. M. Laroussi, "*Sterilization of contaminated matter with atmospheric pressure plasma*", IEEE Trans. Plasma Sci., vol. 24, no. 3, p. 1188-1191, 1996
9. M. Laroussi, I. Alexeff, W. Kang, "*Biological decontamination by non-thermal plasmas*", IEEE Trans. Plasma Sci., vol. 28, no.1, p.184-188, 2000.
10. J. P. Richardson, F. F. Dyer, F. C. Dobbs, I. Alexeff, and M. Laroussi, " *On the use of the resistive barrier discharge to kill bacteria: recent results*", In Proc. IEEE Int. Conf. Plasma Science, New Orleans, LA, 2000
11. H. W. Herrmann, I. Henins, J. Park, and G. S. Selwyn, "*Decontamination of chemical and biological warfare (CBW) agents using an atmospheric pressure plasma jet (APPJ)*", Phys. Plasma, vol. 6 no. 5, p. 2284-2289, 1999
12. B. J. Park, D. H. lee, J. C. Park, I. S. Lee, K. Y. Lee, S. O. Hyun, M. S. Chun and K. H. Chung, *"Sterilization using a microwave-induced argon plasma system at atmospheric pressure*", Phys. Plasma, vol.10, no. 11, p. 4539-4544, 2003
13. Y. Duan, C. Huang, Q.S. Yu, ***"****Low-temperature direct current glow discharges at atmospheric pressure* ***"*** IEEE Trans. Plasma Sci., vol. 33, p.328-329, 2005.

14. Y. Duan, C. Huang, and Q.S. Yu, Appl. Phys. Lett. 2005, submitted

CHAPTER 4

STERILIZATION USING A LOW-TEMPERATURE ATMOSPHERIC PLASMA BRUSH

4.1. Introduction

Sterilization is a physical or chemical process to destroy or eliminate unfavorable microorganisms. Common sterilization methods include heat sterilization (saturated or pressurized steam autoclaving or dry heat oven), gaseous chemical sterilization (ethylene oxide (EtO), ozone (O_3), formaldehyde), irradiation sterilization (EM irradiation, Particle irradiation, UV irradiation), and filtration sterilization [1, 2]. These conventional sterilization methods have been well-studied, well-documented, and are being extensively used. It has been recognized, however, that each of these conventional sterilization methods has their limitations or disadvantages. Heat sterilization methods are usually used to kill bacteria, viable spores, and viruses in heat resistant materials. But heat sterilization is an extremely time-consuming process and is not suitable for articles made of heat sensitive materials such as plastics and fabrics. Gaseous chemical sterilizations are capable to sterilize at low temperature but limited by its use of highly toxic gases. Irradiation sterilization may cause undesirable changes of the materials and must be used with caution to avoid dispersing problem. Both

chemical sterilization and irradiation sterilization require professionally well-trained personnel to operate and the cost of operation is high. Filtration sterilization is often used in pharmaceutical industry. Filtration is not strictly a sterilization process because it cannot destroy or remove all microorganisms. For these reasons, there is a need to develop a safe, rapid less damaging sterilization method in order to eliminate these drawbacks imposed by the conventional sterilization processes [3].

Sterilization by low-temperature plasmas, which are partially ionized gases, is an alternative to conventional and/or traditional sterilization methods. Low-temperature plasmas, which can be easily created at low-pressure (e.g., less than 10 torr) by applying electrical field, contains a huge amount of reactive species including various atoms, ions, energetic electrons, UV irradiation. Because of the existence of these reactive plasma species, low-temperature plasma technique has proven to be an effective alternative to existing sterilization methods. Since early 1990s, several types of plasma sterilizers, are now commercially available in the market and are being used in biomedical areas [4]. In spite of their excellent sterilization efficiency, the currently available plasma sterilization processes with regard to medical uses have several major limitations, such as the

restricted volume of the plasma reactor and one or more vacuum and chemical cycles required.

To eliminate the limitations imposed by low-pressure plasmas, various nonthermal atmospheric pressure plasma sources have been developed since late 1980s. Since it is operated at one atmospheric pressure, atmospheric plasma eliminates the use of vacuum equipment and thus significantly reduces the cost as well as the operation complexity. These nonthermal or low-temperature atmospheric plasmas do possess some of the reactive characteristics of low-pressure plasmas. Therefore, these atmospheric pressure plasmas can be used for sterilization purpose and considered as a potential and promising alternative to conventional sterilization techniques [5]. These atmospheric pressure plasmas can be created in different forms including dielectric barrier discharge [5-7], corona discharge [8], resistive barrier discharge [9, 10], and atmospheric pressure plasma jets sustained by radio frequency (RF) or microwave [11, 12].

Recent study by Stoffels has shown that nonthermal atmospheric pressure plasmas operated at room temperature do not cause pain or bulk destruction of living tissues [13]. Because of its low-temperature nature, the nonthemal atmospheric pressure plasma sterilization does not cause damages on

heat-sensitive materials such as plastics [14] and it is safe to use as compared with low-temperature gaseous chemical sterilization (EtO sterilization) [15]. To date, the currently available atmospheric plasma sources have commonly suffered from their miniature plasma volumes or sizes, and consequently limited their sterilization applications. For example, the size and the shape of the items to be sterilized are restricted by the electrode spacing of the corona discharge, dielectric barrier discharge, and the resistive barrier discharge. The atmospheric pressure plasma jets [11] have potential for large surface sterilization when a scanning operation is used. But their high power consumption may not only make the sterilization process expensive, but may also cause undesirable changes or even damages on various materials due to the resulted high power density and thus high heat flux carried by the plasmas.

Moreover, the interactions of atmospheric pressure plasma with biological agents in sterilization processing are not fully understood. Most of atmospheric pressure plasma researches recognized the reactive species in gas composition of atmospheric pressure plasma to be the dominant part in plasma sterilization process. Richardson et al [9] and Herrmann et al [11] determined that the atmospheric pressure plasma containing oxygen produced a profound

antimicrobial influence on bacterial spores. Kelly-Wintenberg et al [6] have proposed that germicidal effect observed on various microorganisms was related to the concentration of oxygen-based active species diffusing through the cell surface. Despite of its crucial necessity for cellular respiration; any oxygen in excessive can become lethal to them with the presence of highly reactive free radicals (super oxide, O_2^-, hydroxyl, OH^-) and hydrogen peroxide produced from the partial reduction of diatomic oxygen [7].

In this study, we present a new plasma source, i.e., a low-temperature atmospheric plasma brush of argon dc glow discharge, which is ignited and sustained at very low power consumption of tens of watts or even a few watts. The temperature measurement indicated that the gas phase temperature is very close to room temperature. The sterilization effects of such a low-temperature atmospheric plasma brush of argon were investigated on two selected bacteria of *Escherichia coli* and *Micrococcus luteus* in various supporting media. This study also determines the bacterial deactivation of oxygen-based reactive species in a DC atmospheric pressure plasma brush for sterilization effects of *Escherichia coli* and *Micrococcus luteu*s. The sterilization effectiveness of DC plasma mixture of argon and oxygen (Ar + O_2) conditions including the different amount oxygen

addition, the different types of support media, and dc power input were examined and compared to those of pure argon atmospheric pressure plasma brush. This paper reported the experimental results obtained through such investigations.

4.2. Experimental procedures

4.2.1. Materials and organisms

Argon (99.997% purity) and oxygen (99.994% purity) gases used to create atmospheric plasma were purchased from General Store of University of Missouri-Columbia. The bacteria of *Escherichia coli* and *Micrococcus luteus* used for plasma treatment were obtained from the Department of Food Science, University of Missouri-Columbia. The qualitative P5 filter paper (11.0 centimeters in diameter) used as the porous solid medium for the bacteria was obtained from Fisher Scientific. The nutrient broth (pH=6.8 at 25°C) was obtained from Difco Bacto (Detroit, MI, USA), and the standard methods agar was obtained from Becton Dickson (Cockeysville, MD, USA).

4.2.2. Low-temperature atmospheric plasma brush

This plasma source contains discharge chamber with a proprietary design. The argon gas passes through the discharge chamber at a flow rate controlled by a MKS mass flow controller. An electrical field was applied to the two electrodes

located inside the chamber to ignite a DC glow discharge by a DC power supply (Pd 1556C-Power Design Inc.). Fig. 4.1 shows the pictorial view of the low-temperature atmospheric plasma brush that touches a paper surface.

This plasma source can be operated under very low electrical power (as low as a few watts), and as a result very low plasma temperature can be achieved. Fig. 4.2 shows the gas phase temperature of such an argon atmospheric plasma measured using a thermocouple at various operating conditions. It can be seen that a low plasma temperature approaching room temperature are obtained at high argon flow rate.

4.2.3. Experimental procedures

The *Escherichia coli* or *Micrococcus luteus* organisms in stock nutrient broth solution were kept at 35℃ in an incubator. Prior to plasma treatment, *the bacteria* were transferred into 10 ml nutrient broth allowed to grow for 24 hours. All experiments were repeated with two samples and the plating was done in duplicate for each of the samples unless otherwise noted. The values reported in cell reduction were an average value of two samples.

Figure 4. 1. Photographs of an argon atmospheric plasma brush touching a paper surface. Plasma conditions are 1500 sccm argon, 15 w DC power input.

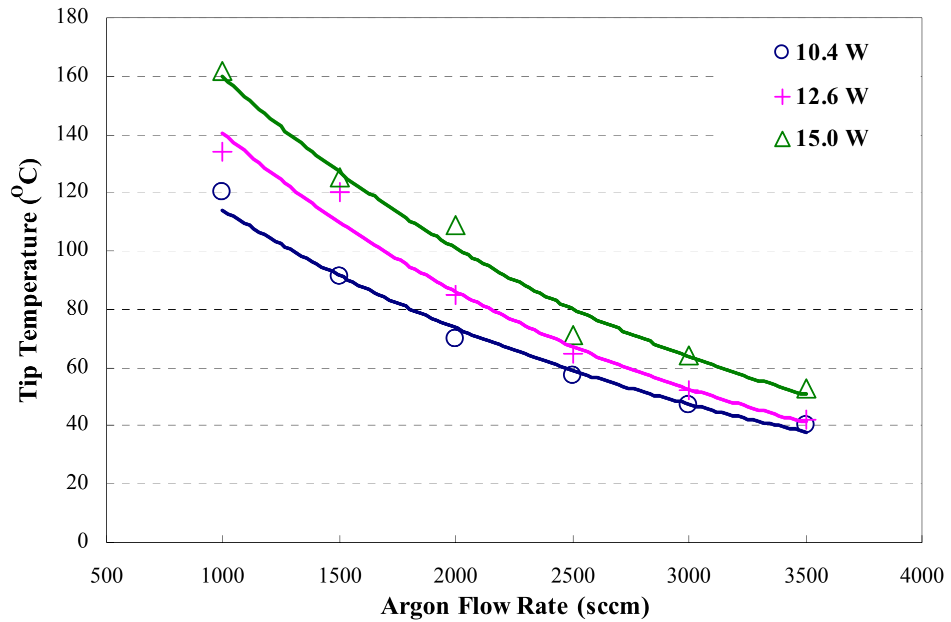

Figure 4. 2. Temperature change of argon atmospheric plasmas with argon flow rate at different DC power input.

4.2.3.1 Bacteria on filter papers (porous solid medium)

With filter paper as the media, 5 μl nutrient broth containing the bacteria were dispensed onto sterilized filter paper discs (4 mm diameter), and then allowed them to dry in a desiccator for 1 hour. The filter paper discs containing bacteria were treated with the low-temperature atmospheric plasma brush with a preset exposure time from 1.0 to 5.0 minutes. After plasma treatment, the plasma treated filter paper discs were transferred into test tubes containing 10 ml peptone water and mixed by vortex mixer for 2 minutes. The bacterial strains were serially diluted and dispersed into the agar in petri dishes. The number of the living bacteria cells was counted after 48 hours incubation at 35℃.

4.2.3.2 Bacteria in nutrient broth (liquid medium)

A volume of 5 μl nutrient broth containing the bacteria was dispensed on a sterilized aluminum dish (15 mm in diameter) to form a liquid droplet of ~1.0 mm in diameter. The droplet was then placed under atmospheric plasma brush for plasma treatment. After plasma treatment, the aluminum dish was repeatedly washed with peptone water and transferred the remaining bacteria strains into test tubes that contain 10 ml peptone water. The solution was then mixed by vortex mixer for 2 minutes and serially diluted and dispersed into the agar in petri dishes.

The number of the living bacteria cells was counted after 48 hours incubation at 35 ℃.

4.2.3.3 Bacteria in standard methods agar (colloid medium)

A volume of 5 μl nutrient broth containing the bacteria was mixed with 30 μl standard methods agar in a sterilized aluminum dish (15 mm in diameter) and allowed to harden to form agar plug (~3 mm in thickness and ~ 5 mm in diameter). The agar plug on sterilized aluminum dishes was then placed under the atmospheric plasma brush for plasma treatment. After plasma treatment, the aluminum dishes were repeatedly macerated and washed with peptone water. The solution was then mixed by vortex mixer for 2 minutes and serially diluted and dispersed into the agar in petri dishes. The number of the living bacteria cells was counted after 48 hours incubation at 35℃.

4.2.4. Scanning electron microscopy

The plasma treatment effects on the cell structures of *Escherichia coli* and *Micrococcus luteus* were examined by SEM measurements. The bacteria solution of the original and plasma treated samples, were placed in the fixation and then coated with a thin layer of plasma sputtered Pt. The SEM measurements were performed using an Hitachi S4700 scanning electron microscopy at Electron

Microscopy Core of University of Missouri-Columbia.

4.3. Results and Discussion

4.3.1. Plasma sterilization effects on *Escherichia coli* and *Micrococcus luteus*

With filter papers as supporting media, bacteria of *Escherichia coli* and *Micrococcus luteus* were subjected to the low-temperature atmospheric plasmas of argon. The plasma conditions were controlled at 1500 sccm of argon flow and 15 W of DC power input, which give the gas phase temperature of 125 ^{o}C. Fig 4.3 shows the survival curves of the two bacteria as a function of plasma exposure time. As can be seen in Fig. 4.3, 90% of *Escherichia coli* were killed within 2 minutes of plasma exposure; and only 1% *Escherichia coli* colony was detected after 5 minute plasma exposure. In the case of *Micrococcus luteus*, 90% of the cells were killed after a 15 seconds exposure, while no colonies grew on the agar plate after a 3 minute plasma exposure.

It was noticed that longer plasma treatment time is required for sterilizing *Escherichia coli* than killing *Micrococcus luteus*. This difference is of course mainly resulted from the cell structure difference of *Escherichia coli* from *Micrococcus luteus*. Another possible reason of this difference is that, upon plasma exposure, there remained a few *Escherichia coli* survivors, which could start much

faster proliferation in the culture medium before bacterial counting.

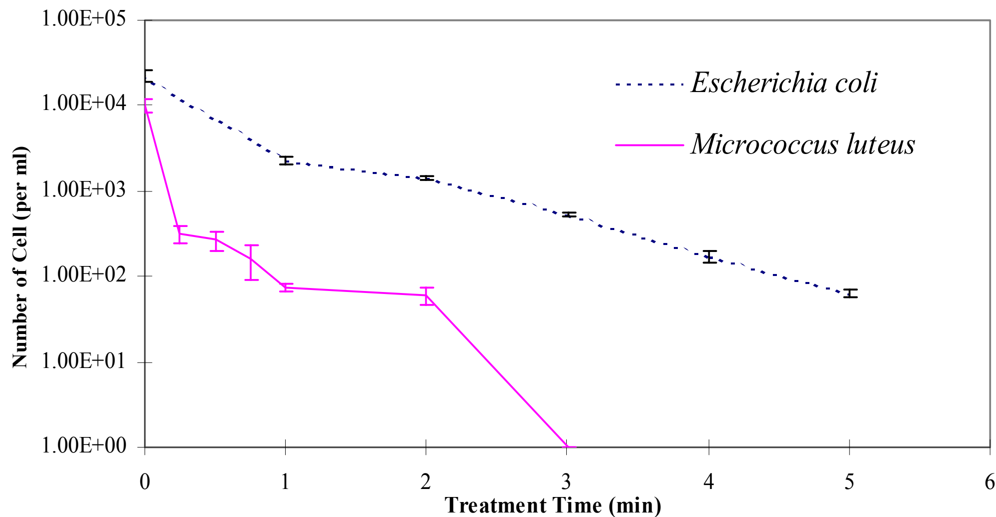

Figure 4. 3. Survival curves of *Escherichia coli* and *Micrococcus luteus* on filter paper medium after argon atmospheric plasma treatment with argon flow rate of 1500 sccm and DC power input of 15 W.

4.3.2. Effects of supporting medium

The plasma sterilization effects on *Escherichia coli* and *Micrococcus luteus* were investigated with different supporting media, including nutrient broth, standard methods agar, and the filter paper. Fig. 4.4 shows the survival curves of two bacteria on these supporting media upon argon plasma exposure. As shown in Fig. 4.4, among the three media, plasma treatment enables the fastest cell reduction of 6 orders of magnitude on nutrient broth. When seeded in nutrient broth, a 6 orders of magnitude *Escherichia coli* cell reduction requires 3-minute plasma treatment; and *Micrococcus luteus* needs 2-minute plasma exposure.

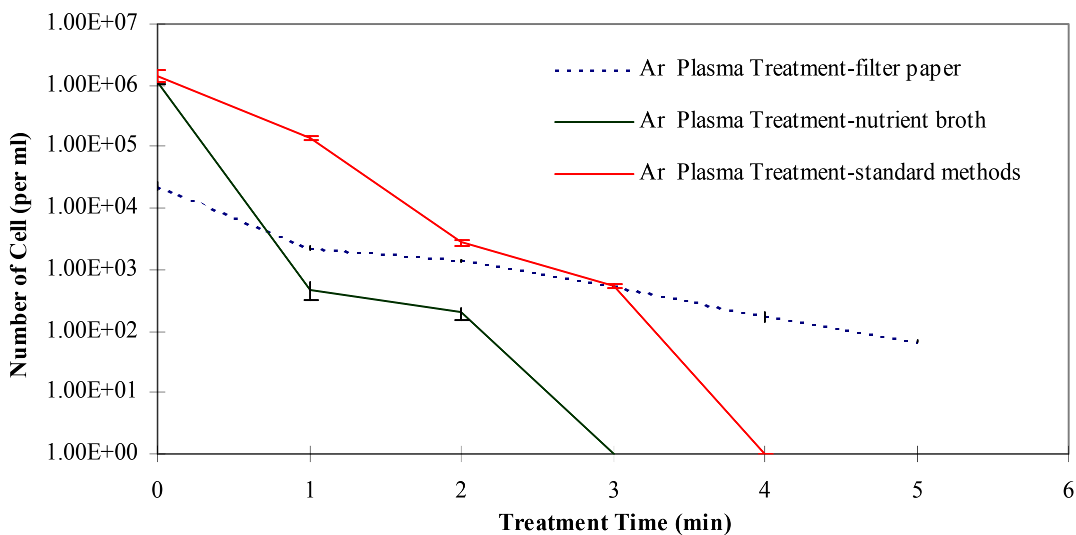

(a) *Escherichia coli*

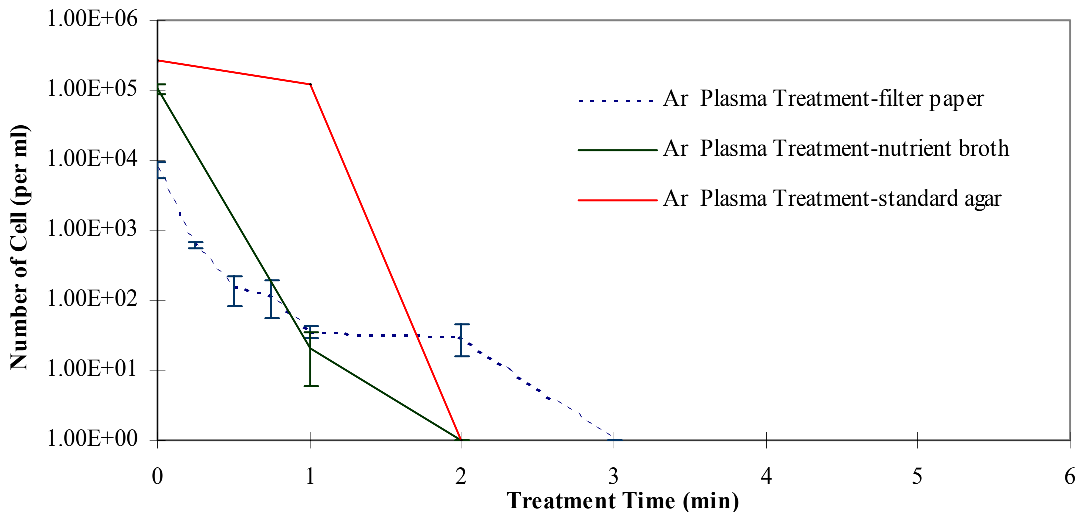

(b) *Micrococcus luteus*

Figure 4. 4. Survival curves of (a) *Escherichia coli* and (b) *Micrococcus luteus* in various supporting media after argon atmospheric plasma treatment with argon flow rate of 1500 sccm and DC power input of 15 W.

With standard methods agar, one more minute plasma treatment is required for *Escherichia coli* when compared with nutrient broth media. While seeded in filter paper, both two bacteria needs the longer exposure times in order to achieve the similar level of cell reduction.

The fast plasma killing of the two bacteria on nutrient broth is mainly because of the direct attack of plasma species on the bacteria cells. It was observed that the droplets of the nutrient broth dried out within one minute plasma exposure. This enables direct contact of the plasmas to the bacteria cells. With nutrient broth as supporting medium, no stain of *Escherichia coli* and *Micrococcus luteus* was observed after 4-minute plasma treatment. A possible reason for the very different plasma sterilization time is the plasma penetrating efficiency with different culture mediums. The filter paper used in this study is a porous solid and requires plasma penetration to kill the bacteria cells resided inside the pores. The colloid state of agar could slow down the plasma penetration but was eventually destroyed through evaporation of water with longer plasma treatment time.

4.3.3. Effects of heat and gas blowing on cell reduction

In order to distinguish the plasma sterilization effects from the possible heat effect of the plasmas, a sterilization test to elucidate the dry heat effect was

performed using a temperature controllable oven (Fisher Scientific Isotemp Vacuum Oven Model 282 A). Under the operating condition studied, the gas phase temperature of the argon plasmas was 125 ^{o}C. Therefore, *Escherichia coli* and *Micrococcus luteus* on filter papers was kept inside the oven with temperature set at 125 ^{o}C. The cell survival curves of the two bacteria subjected to the dry heat were shown in Fig 4.5(a). It was confirmed that the 125 ^{o}C dry-heat treatment did not show any killing effect on both bacteria within 5-minute exposure. These data indicated the heat carried by the argon atmospheric plasmas did not contribute to the sterilization effects shown in Figs. 4.3 and 4.4.

A high follow rate of argon higher than 500 sccm is necessary in order to blow the argon glow discharge out of the discharge chamber and form a free brush-shaped plasma jet. To determine if the high flowing plasma gas could blow the bacteria cell off the supporting media, the blowing effect of argon gas on the two bacteria was examined by flowing the argon gas at the same flow rate (1500sccm) without igniting electrical discharge. Fig. 4.5 (b) shows the cell survival curves of *Escherichia coli* and *Micrococcus luteus* on different supporting media with argon gas blowing on the surface. From Fig. 4.5 (b), it can be seen that the high flow argon gas did not reduce the cell number of both bacteria

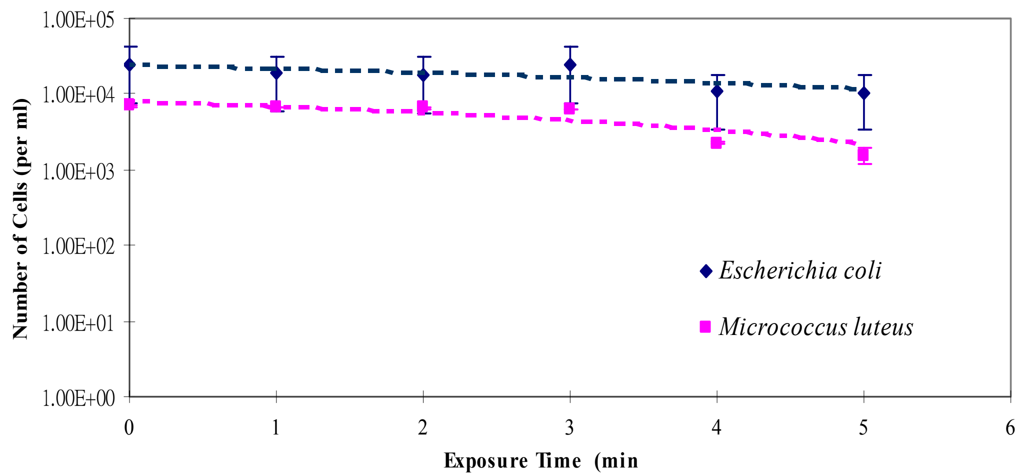

(a) dry heat effect

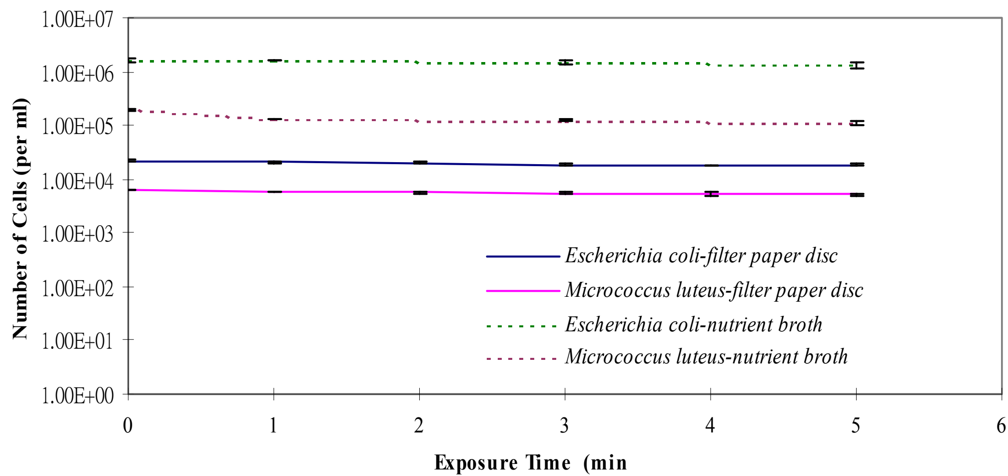

(b) Gas blowing effects

Figure 4. 5. Sterilization effects of (a) dry heat at 125℃ and (b) gas blowing at a 1500 sccm on *Escherichia coli* and *Micrococcus luteus* seeded on filter paper and nutrient broth.

on all three supporting media. The results shown in Fig. 4.5 indicate that the sterilization effects of argon plasmas are due to the presence of reactive plasma species, but not the heat or the high flowing gas it carries.

4.3.4. Effects of argon plasma conditions

In creation of atmospheric plasmas, the power input and gas flow not only affect the plasma density, but also the plasma temperature s shown in Fig. 4.2. Consequently, it is expected that these plasma operating parameters should have a certain degree of influence on the plasma sterilization results. Therefore, the effects of power input and argon flow rate of the plasma on the sterilization of the two bacteria were also examined. Fig. 4.6 (a) shows the cell survival number changes of both *Escherichia coli* and *Micrococcus luteus* on filter paper medium with DC power input of the plasma under a fixed argon flow at 1500 sccm and plasma treatment time of 1minute. It can be seen that higher DC power input did result in fast killing of both bacteria. Fig. 4.6 (b) shows cell survival number changes of the two bacteria with argon flow rate of the plasmas under a fixed DC power of 15 W and plasma treatment time of 1 minute. Since it doesn't affect plasma density, the change of argon flow rate in the plasmas did not affect the bacteria killing rate.

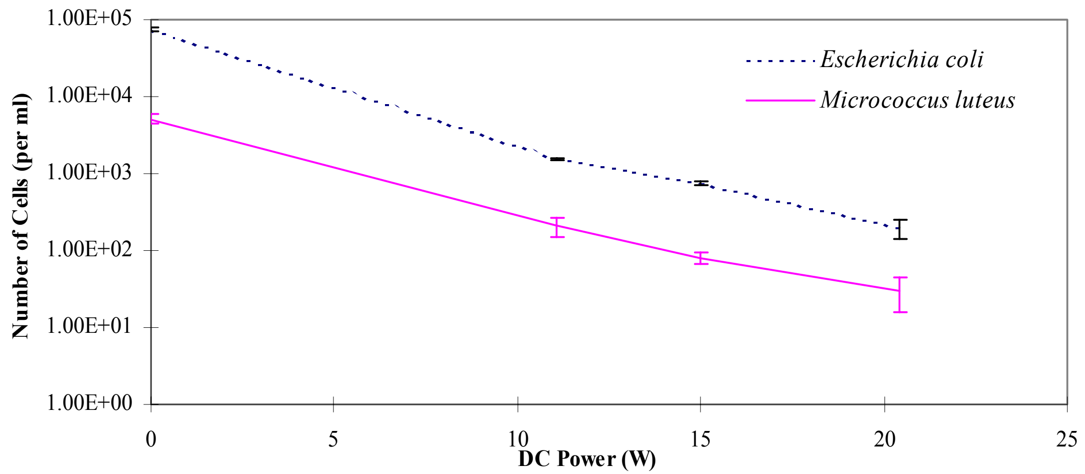

(a) Effects of plasma power

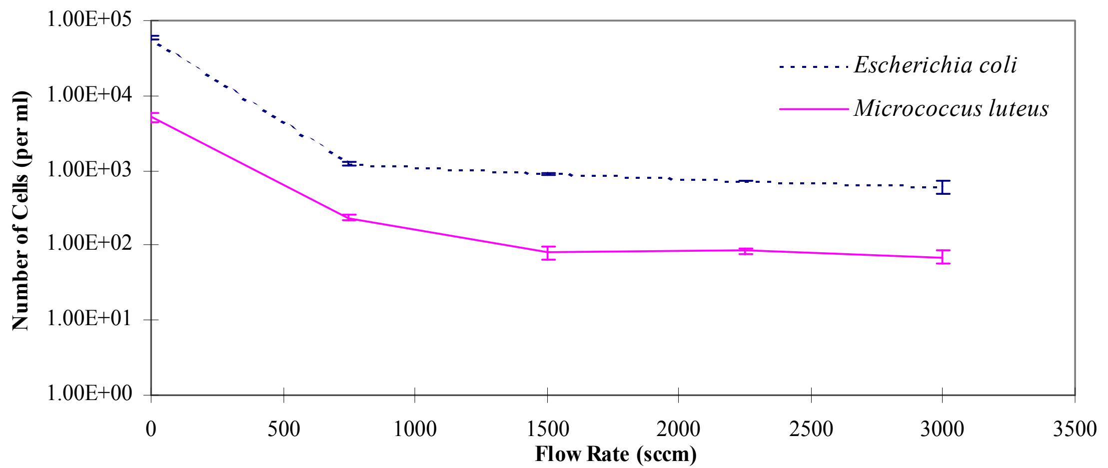

(b) Effects of argon flow rate

Figure 4. 6. The surviving cell numbers of *Escherichia coli* and *Micrococcus luteus* on filter papers as a function of plasma parameters: (a) plasma power and (b) argon flow rate after 1 minute plasma treatment under condition, if not specified in the plots, of 1500 sccm argon and 15 W DC power input.

4.3.5. Effects of remote argon plasma exposure

In atmospheric plasmas, the plasma species could lose its energy or reactivity in a very short time due to the much higher collision frequency among the plasma particles. The life time of the reactive plasma species is much shorter when compared to that in low-pressure plasmas. As a result, the plasmas could lose their reactivity dramatically in a remote position (away from the glow). To examine the sterilization effects of a remote plasma, the bacteria seeded in filter papers were subjected to plasma exposure in the down stream at a position 2 mm away from the glow. The long-life plasma species from the plasmas were allowed to diffuse and get in contact with the bacteria cells resided on the supporting media. Fig. 4.7 shows a comparison of the cell survival curves of the two bacteria upon a remote plasma exposure and direct plasma exposure. It was observed that the remote plasma exposure causes much slower cell reduction on *Micrococcus luteus* than the direct plasma exposure.

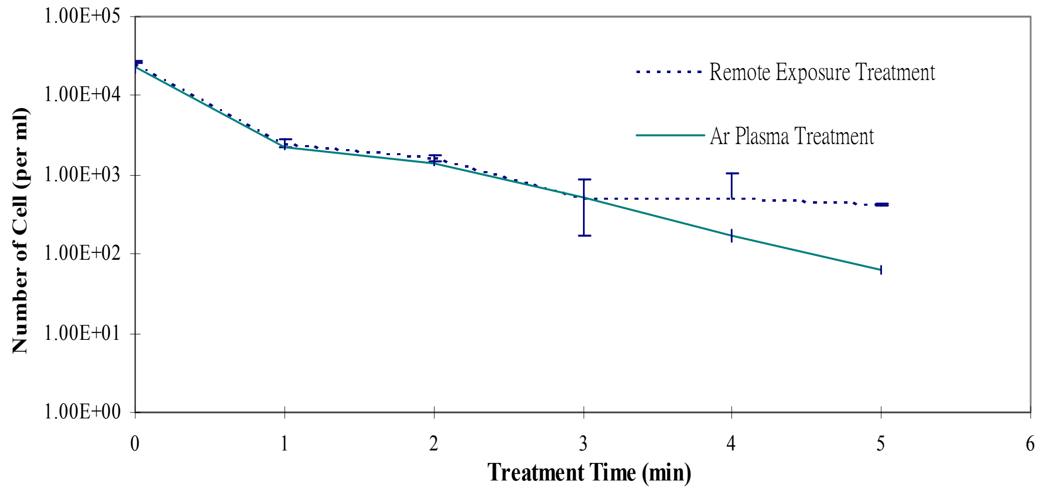

(a) *Escherichia coli*

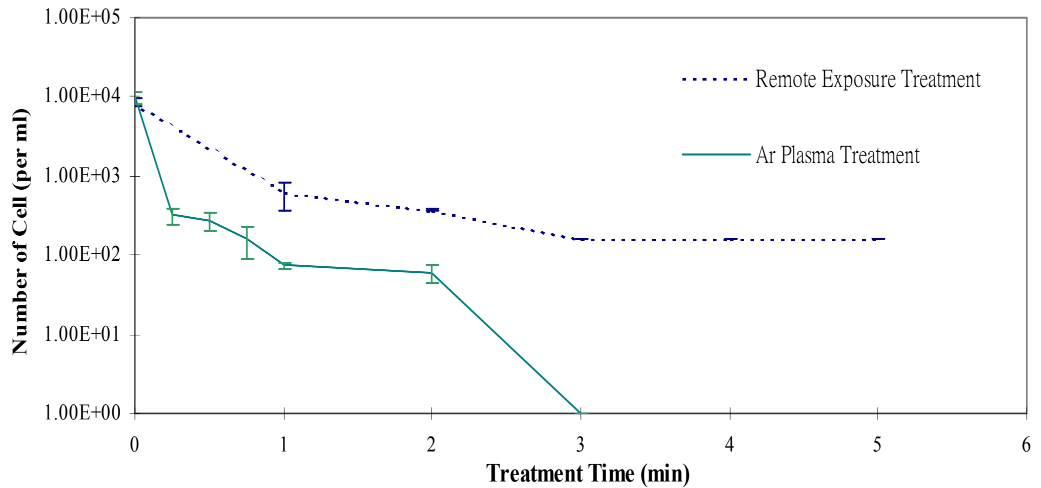

(b) *Micrococcus luteus*

Figure 4. 7. Comparison of the survival curves of *Escherichia coli* and *Micrococcus luteus* on filter papers under direct plasma exposure and remote plasma exposure (2 mm away from the plasma glow). Argon atmospheric plasma conditions are 1500 sccm argon and 15 W DC power input.

4.3.6 Oxygen addition effects of *Escherichia coli* and *Micrococcus luteus*

To determine if the oxygen-based reactive species could interact with *Escherichia coli* and *Micrococcus luteus*, oxygen gas of different amount (125 sccm (7.6 % O_2), 250 sccm (14.2 % O_2), 350 sccm (18.9 % O_2)) were added into DC argon atmospheric pressure plasma brush. Fig. 4.8 comprises the bacterial-killing efficiency of *Escherichia coli* and *Micrococcus luteus* with filter papers as supporting media exposed to Ar plasma and to the $Ar+O_2$ mixture plasma. In the pure argon plasma case, we suppose that argon ions and electronically excited neutrals are the only species to destroy *Escherichia coli* and *Micrococcus luteus*. The characteristic energies of the argon ions and neutrals are in the level of ~ 15 eV and >11 eV, which are much higher than the bonding energy of the organic molecules constituting microorganisms. The results in Fig 4.8 (A) showed that *Escherichia coli* cell reduction of 3 orders of magnitude required 30 seconds in $Ar+O_2$ (14.2 % addition) mixture plasma exposure while it required 5 minutes in the Ar plasma. Identical experiments were performed with *Micrococcus luteus* in Fig 4.8 (B), and no colonies grew on the agar plate after a 1-minute $Ar+O_2$ (7.6 %, 14.2 %, 18.9 % addition) mixture plasma exposure, while it needed 3 minutes in Ar plasma. The shortest sterilization time in the $Ar+O_2$

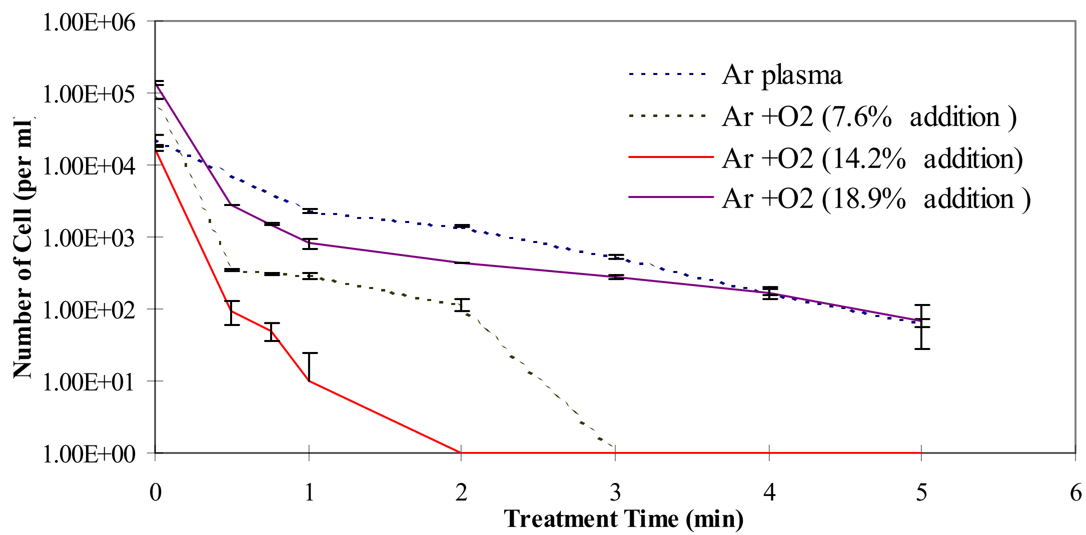

(A)*Escherichia coli*

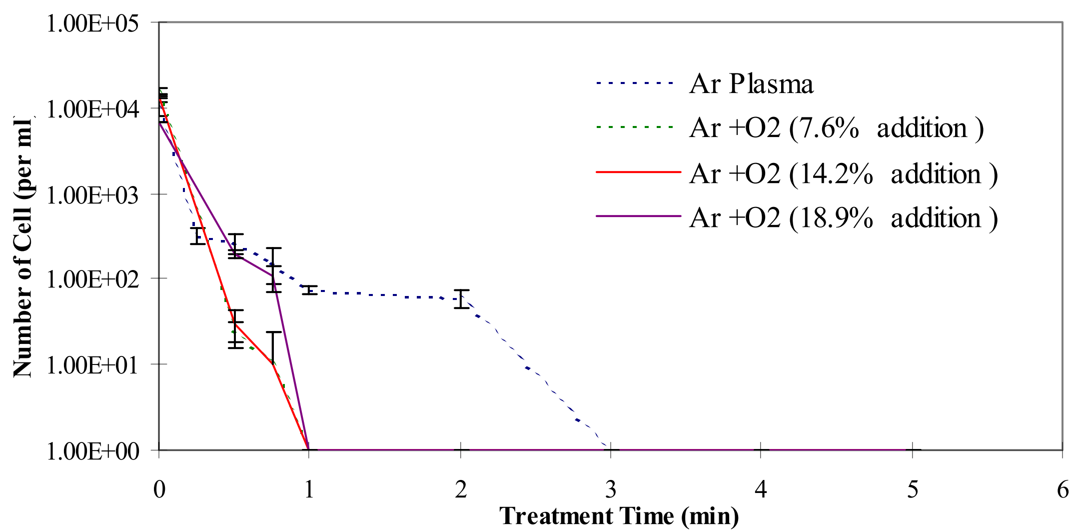

(B)*Micrococcus luteus*

Figure 4. 8. Survival curves of (A) *Escherichia coli* and (B) *Micrococcus luteus* on filter papers with different amount oxygen addition into argon atmospheric plasma treatment with argon flow rate of 1500 sccm and DC power input of 15 W.

mixture plasma is supposed the interaction of cell structure with oxygen-based reactive species. The oxygen-based reactive species such as O and O_3 could penetrate and destroy the microorganism surface by oxidation.

Fig 4.8 depicts the increasing sterilization efficiency of oxygen-based reactive species into DC argon atmospheric pressure plasma brush. However, at higher oxygen addition (18.9%) into atmospheric pressure plasma brush, little or no improvement sterilization effectiveness was obtained. It is hypothesized that the production of oxygen-based reactive species saturates at some level of DC power. N. Philps et al [15] detected the increasing oxygen percentage in the mixture beyond the individual level (the maximum UV emission intensity) caused the increasing sterilization time.

4.3.7 Culture medium effects of *Escherichia coli* and *Micrococcus luteus*

Previous experiments examined the swift bacterial deactivation effects of DC Ar+O_2 atmospheric pressure plasma brush exposure on filter paper seeded with *Escherichia coli* and *Micrococcus luteus*. These data suggested that the oxygen-based reactive species plays a significant role of DC argon atmospheric pressure plasma sterilization. To further resolve the sterilization effects on different culture medium (nutrient broth and standard methods agar) seeded with

Escherichia coli and *Micrococcus luteus*, the controlled Ar+O_2 mixture plasma containing 14.2% O_2 was used in the serial treatments and compared to pure argon plasma. Fig. 4.9 shows the survival curves of *Escherichia coli* on nutrient broth and standard methods agar upon Ar plasma and Ar+O_2 mixture plasma exposure. When seeded in nutrient broth, a 6 orders of magnitude *Escherichia coli* cell reduction required 3-minute Ar plasma treatment; with standard methods agar 4-minute Ar plasma exposure time was needed. Under Ar+O_2 mixture plasma exposure, the extended treatment time was required for *Escherichia coli* both on nutrient broth and standard methods agar. The 5 orders of magnitude *Micrococcus luteus* cell reduction was archived in 2 minutes with Ar plasma treatment in Fig. 4.10. In contrast, it takes 3-5 minutes to reach the same sterility with Ar+O_2 mixture plasma. As shown in Fig. 4.9-10, between the two media, pure argon plasma treatment enables the faster *Escherichia coli* and *Micrococcus luteus* reduction of 5-6 orders of magnitude on nutrient broth and standard methods agar. It exhibits the different interaction between the oxygen containing plasma and supporting media. The possible explanation is due to the slower incisive rate of oxygen-based reactive species to the cell on the nutrient broth and standard methods agar.

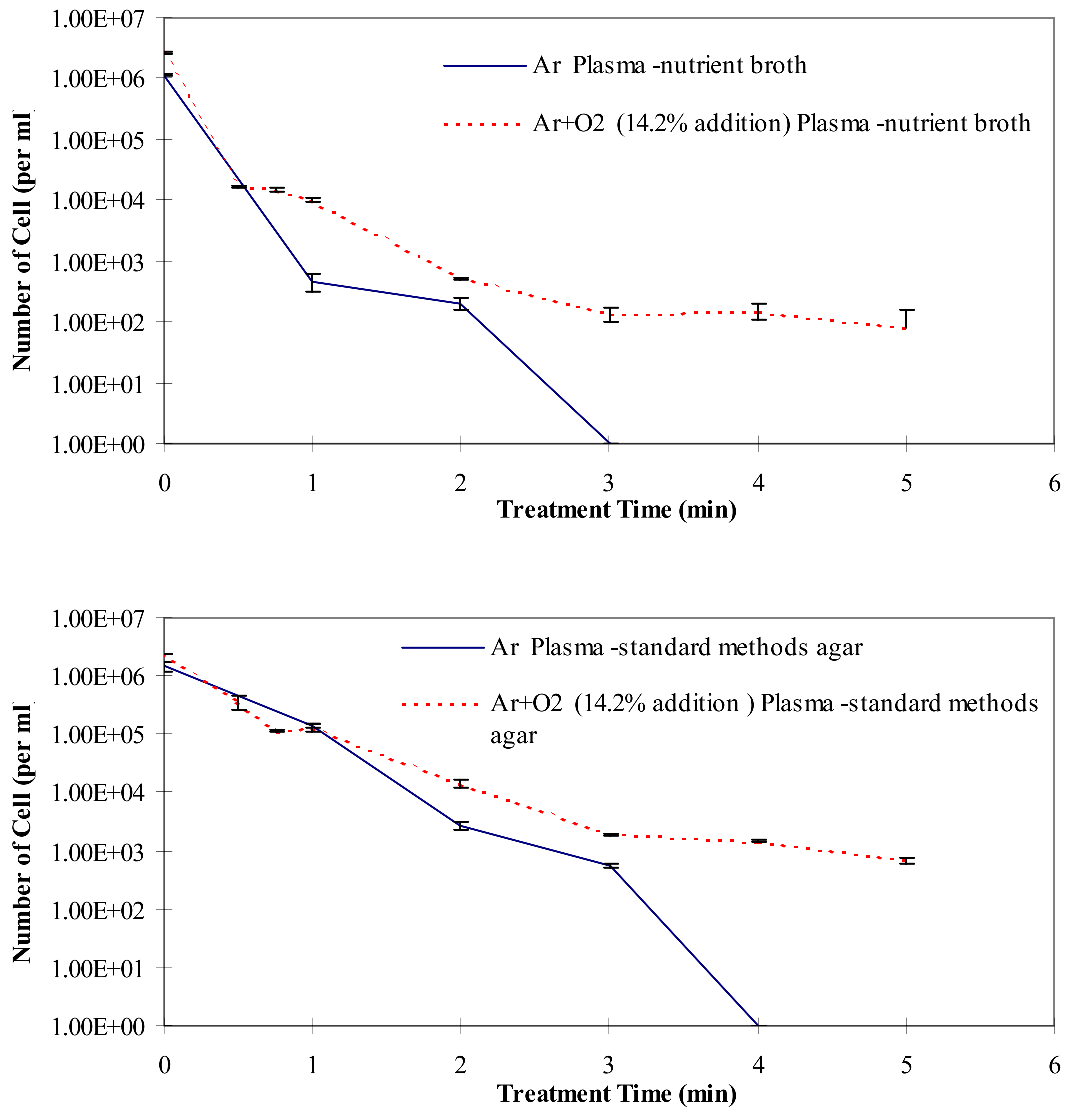

Figure 4. 9. Comparison of survival numbers of *Escherichia coli* in various supporting media after argon atmospheric plasma and argon atmospheric plasma with oxygen addition (14.2 %) treatment. Atmospheric plasma condition: argon flow rate of 1500 sccm, oxygen flow rate of 250 sccm, and DC power input of 15 W.

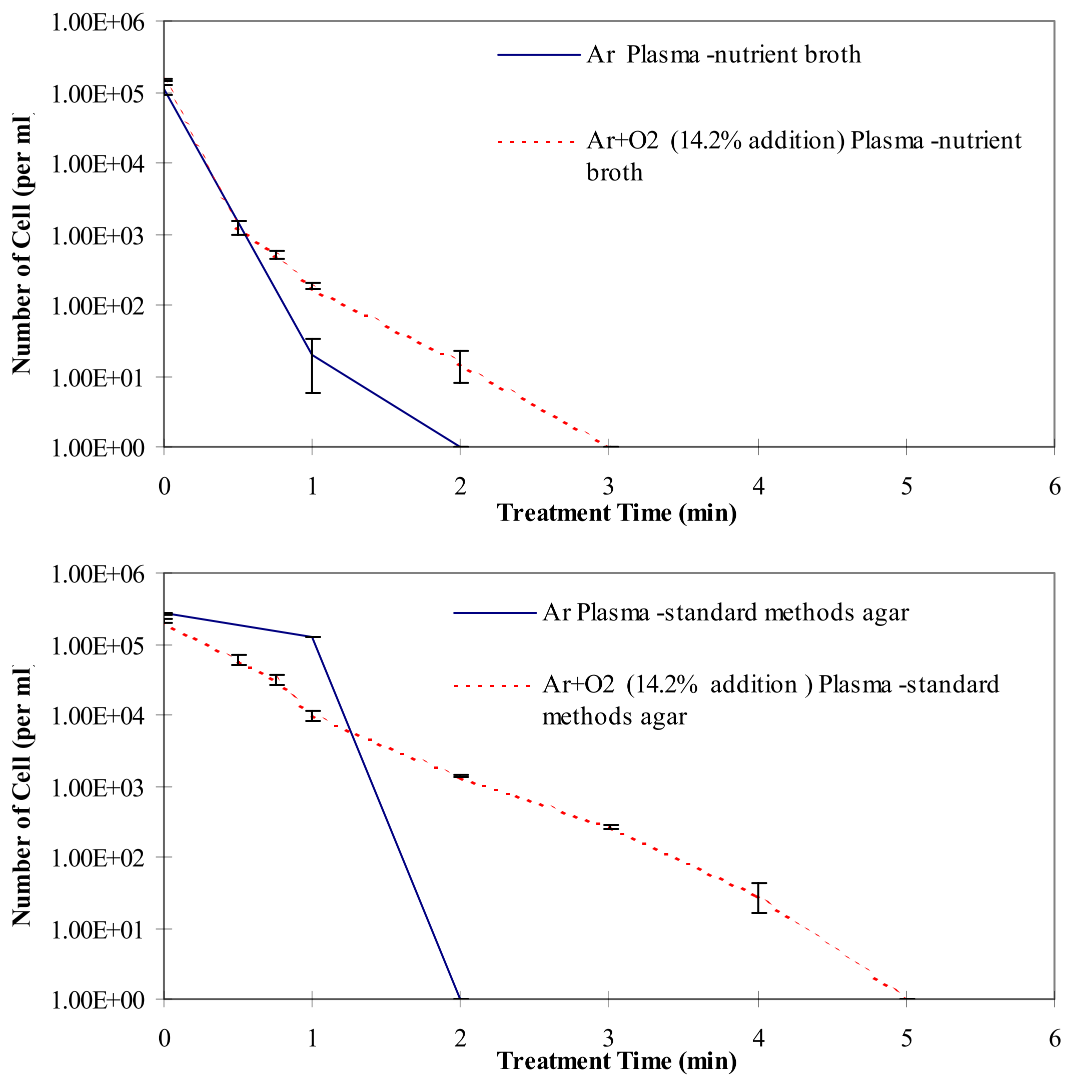

Figure 4. 10. Comparison of survival numbers of *Micrococcus luteus* in various supporting media after argon atmospheric plasma and argon atmospheric plasma with oxygen addition (14.2 %) treatment. Atmospheric plasma condition: argon flow rate of 1500 sccm, oxygen flow rate of 250 sccm, and DC power input of 15 W.

4.3.8 DC power input effects of *Escherichia coli* and *Micrococcus luteus*

It is anticipated that power input affects the sterilization possessions during plasma process. Therefore, the effects of power input of the plasma on the sterilization of the two bacteria were also examined. Fig. 4.11 shows the cell survival number changes of both *Escherichia coli* and *Micrococcus luteus* on filter paper medium with DC power input of the controlled Ar+O_2 mixture plasma containing 14.2% O_2 and Ar plasma under plasma treatment time of 1 minute. It can be seen that higher DC power input did cause in fast killing of both bacteria. In comparison with pure argon atmospheric pressure plasma torch, the Ar+O_2 (14.2% addition) mixture plasma has more capable bacterial decontamination ability than Ar atmospheric pressure plasma does. It was also confirmed that the oxygen-based species in Ar+O_2 (14.2% addition) mixture plasma has the fast bacterial deactivation capability on filter papers with different DC power input.

4.3.9 Remote Ar+O_2 mixture plasma exposure effects of *Escherichia coli* and *Micrococcus luteus*

In atmospheric plasmas, the plasma species could lose its energy or reactivity in a very short time as a result of the much higher collision frequency among the plasma particles. The lifetime of the reactive plasma species is much shorter

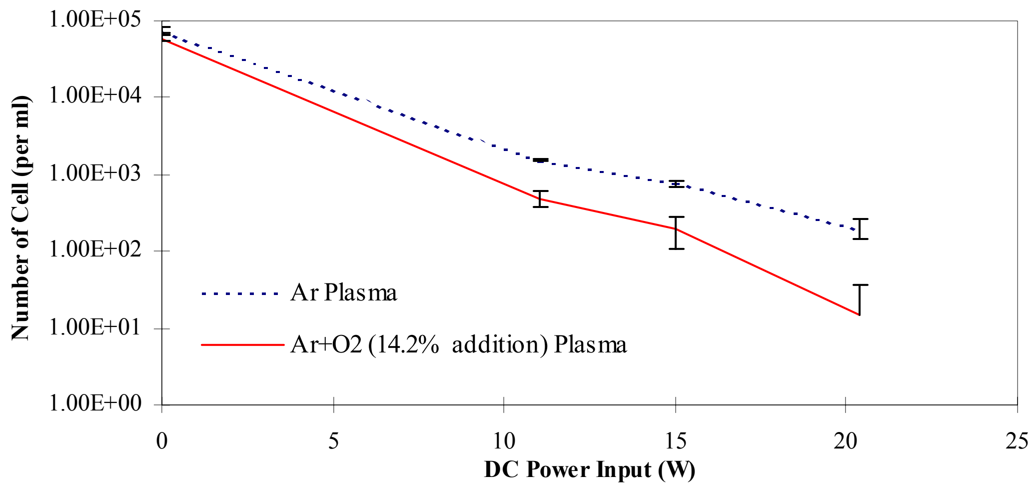

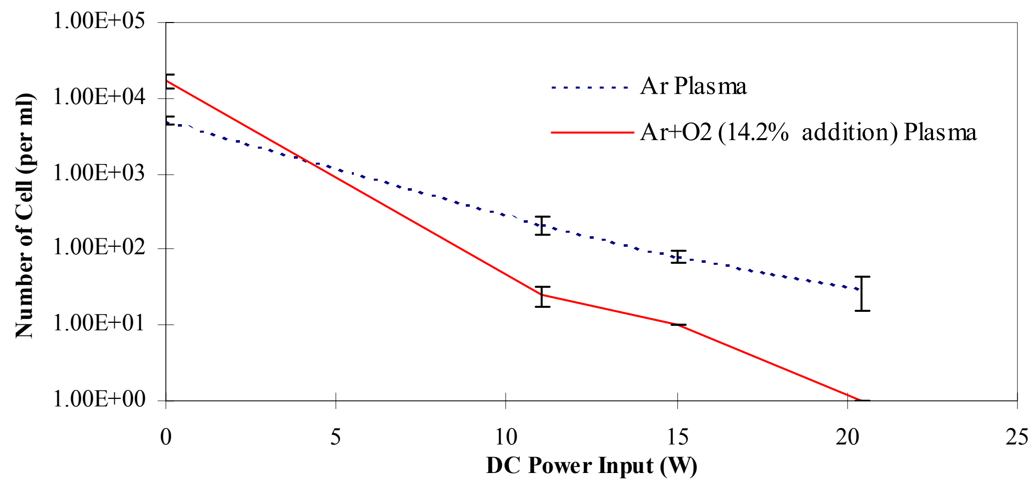

(A) *Escherichia coli*

(B) *Micrococcus luteus*

Figure 4. 11. Comparison of survival curves of (A) *Escherichia coli* and (B) *Micrococcus luteus* on filter papers with different DC plasma power input under 1 minute argon atmospheric plasma and argon atmospheric plasma with oxygen addition (14.2 %) treatment with argon flow rate of 1500 sccm oxygen flow rate of 250 sccm and DC power input of 15 W.

when compared to that in low-pressure plasmas. As a result, the plasmas could lose their reactivity dramatically in a remote position (away from the glow). To examine the sterilization effects of remote plasma, the bacteria seeded in filter papers were subjected to plasma exposure in the down stream at a position 2 mm away from the glow. The long-life plasma species from the plasmas were allowed to diffuse and get in contact with the bacteria cells resided on the supporting media. Fig. 4.12 shows a comparison of the cell survival curves of the two bacteria upon a remote plasma exposure and direct plasma exposure. It was observed that the remote plasma exposure causes much slower cell reduction on *Escherichia coli and Micrococcus luteus* than the direct plasma exposure.

4.3.10 Heat effects of *Escherichia coli* and *Micrococcus luteus*

In order to identify the plasma sterilization effects from the possible heat effect of the plasmas, a sterilization test to explicate the dry heat effect was performed using a temperature controllable oven (Fisher Scientific Isotemp Vacuum Oven Model 282 A). Under the operating condition studied, the gas phase temperature of the $Ar+O_2$ mixture plasmas was 100-165 ^{o}C. Therefore, *Escherichia coli* and *Micrococcus luteus* on filter papers was kept inside the oven with temperature set at 125 ^{o}C and 165 ^{o}C. The cell survival curves of the two

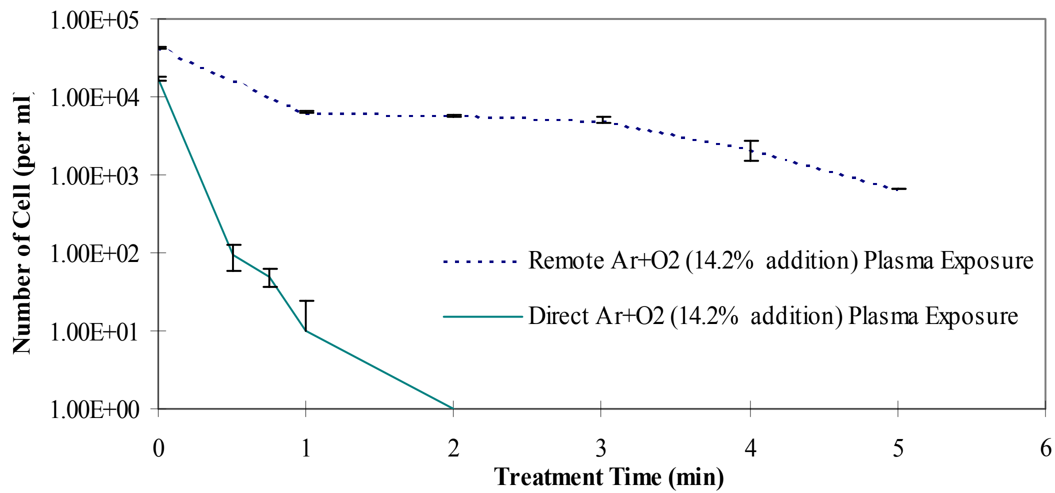

(A) *Escherichia coli*

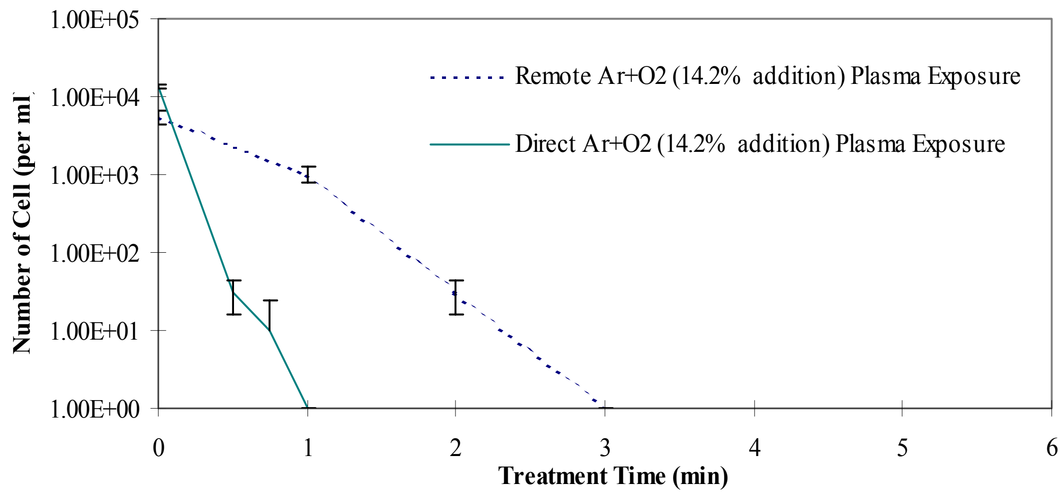

(B) *Micrococcus luteus*

Figure 4. 12. Comparison of the survival curves of (A) *Escherichia coli* and (B) *Micrococcus luteus* on filter papers under direct plasma exposure and remote plasma exposure (2 mm away from the plasma glow). Argon atmospheric plasma and argon atmospheric plasma with oxygen addition (14.2 %) conditions: 1500 sccm argon, 250 sccm oxygen, and 15 W DC power input

bacteria subjected to the dry heat were shown in Fig 4.13. It was confirmed that the 100-165 °C dry-heat treatment did not show any antimicrobiological effect on both bacteria within 5-minute exposure. These data designated the heat carried by the argon atmospheric plasmas did not contribute to the sterilization effects.

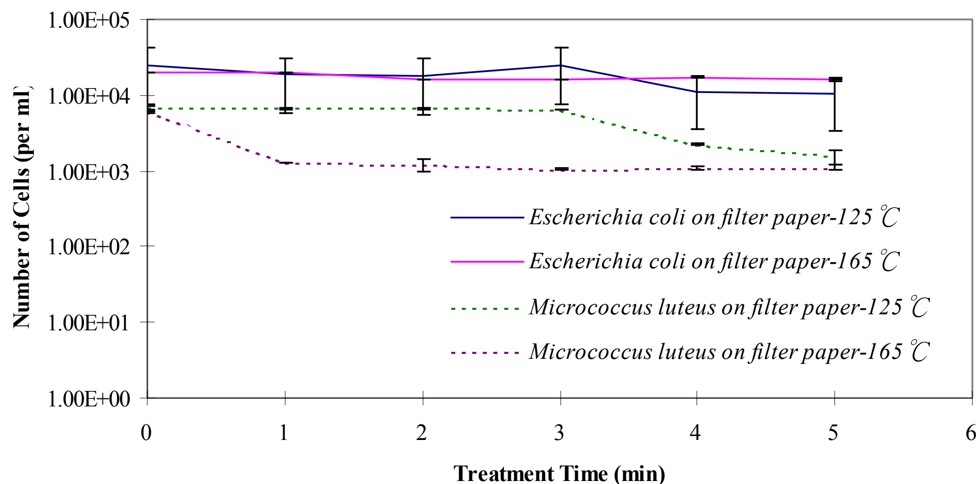

Figure 4. 13. Sterilization effects of dry heat at 125℃ and 165℃ on *Escherichia coli* and *Micrococcus luteus* seeded on filter paper.

4.3.11 SEM images of *Escherichia coli* and *Micrococcus luteus* under DC atmospheric pressure plasma brush treatment

SEM measurements were used to examine the cell structure changes of the two bacteria upon plasma treatments. Figs. 4.14 and 4.15 show the SEM images of untreated and plasma treated *Escherichia coli* and *Micrococcus luteus* respectively. From Fig. 4.14, it was observed that the *Escherichia coli* cells were severely

damaged and only some cell debris was detected by SEM with the argon plasma sterilized samples. The SEM measurements on *Micrococcus luteus* shown in Fig. 4.15 provided the similar information, i.e. the bacteria cells were damaged by argon plasma treatment. After the plasma treatment, the size of *Micrococcus luteus* cells was significantly reduced and the shape of the dead cells was distorted. The distorted cell shape shown in Fig. 4.15 indicated that the lipid moieties have been lost after the plasma treatment.

A possible sterilization mechanism of pure argon atmospheric plasma is the continuous impact on the bacterial cells by energetic plasma species such as argon ions, electronically excited neutrals. The characteristic energies of the argon ions and neutrals is in the level of $\sim$ 15 eV and $>$11 eV, which are much higher than the bonding energy of the organic molecules constituting microorganisms. Thus, even simple argon plasmas should have sterilization ability to destroy various microorganisms. D.A. Mendis et al. suggested charged particles might cause the rupture of the outer membrane of the bacterial cell [16, 17]. Therefore, the plasma exposure of the bacteria cells could eventually damages the cell structure or the cell membrane, and consequently destroys the viability of the cells.

To examine the oxygen-based reactive species effects of DC atmospheric

pressure plasma brush on the morphology of *Escherichia coli* and *Micrococcus luteus*, micrographs obtained with scanning electron microscopy were produced. These SEM images show a significant alteration in size, and present transformed and amorphous morphologies in Fig. 4.14-15. After 5 minute Ar plasma exposure, the majority of the remaining viable *Escherichia coli* colonies had distinct cell structure damage in morphology and grew more slowly than non-exposed cells. The fragments of *Micrococcus luteus* colonies were also found in 5 minute Ar plasma treatment. These observations suggested that the surviving cells were injured by high-energy ions of DC argon atmospheric pressure plasma. On the other hand, *Escherichia coli* and *Micrococcus luteus* were reduced to the smaller structures and microscopic debris after 1 minute $Ar+O_2$ mixture plasma exposure. These SEM results demonstrated that strong oxidation of Ar plasma with oxygen addition caused the rapid sterilizing effect on microorganisms, when the microorganisms were exposure to $Ar+O_2$ mixture plasma brush.

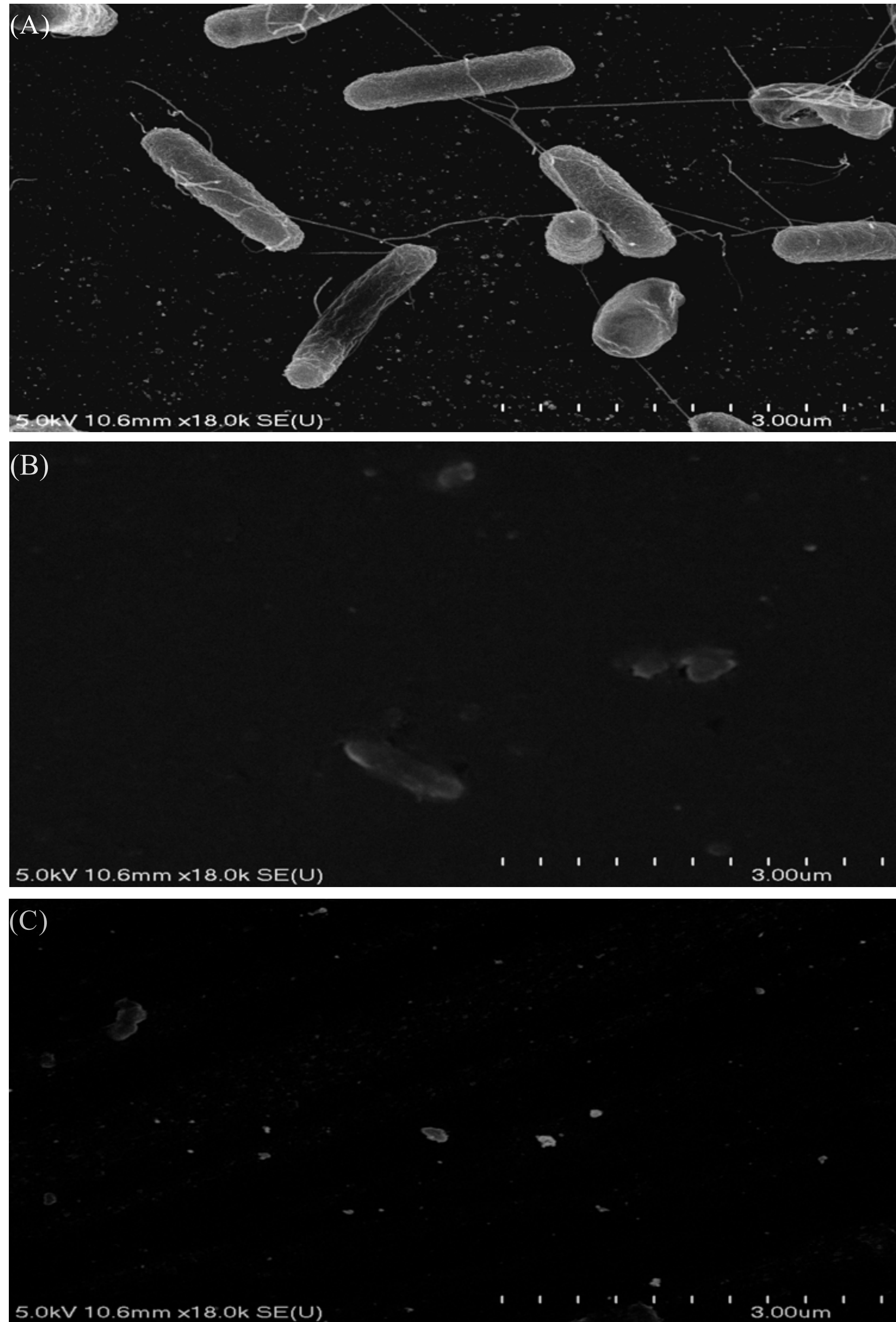

Figure 4. 14. Scanning electron micrographs of (A) Untreated *Escherichia coli* control (B) 5 min argon plasma treated *Escherichia coli* (C) 1 min argon plasma with 14.2% oxygen addition treated *Escherichia coli* under plasma condition 1500 sccm argon, 250 sccm, and 15 W DC power input

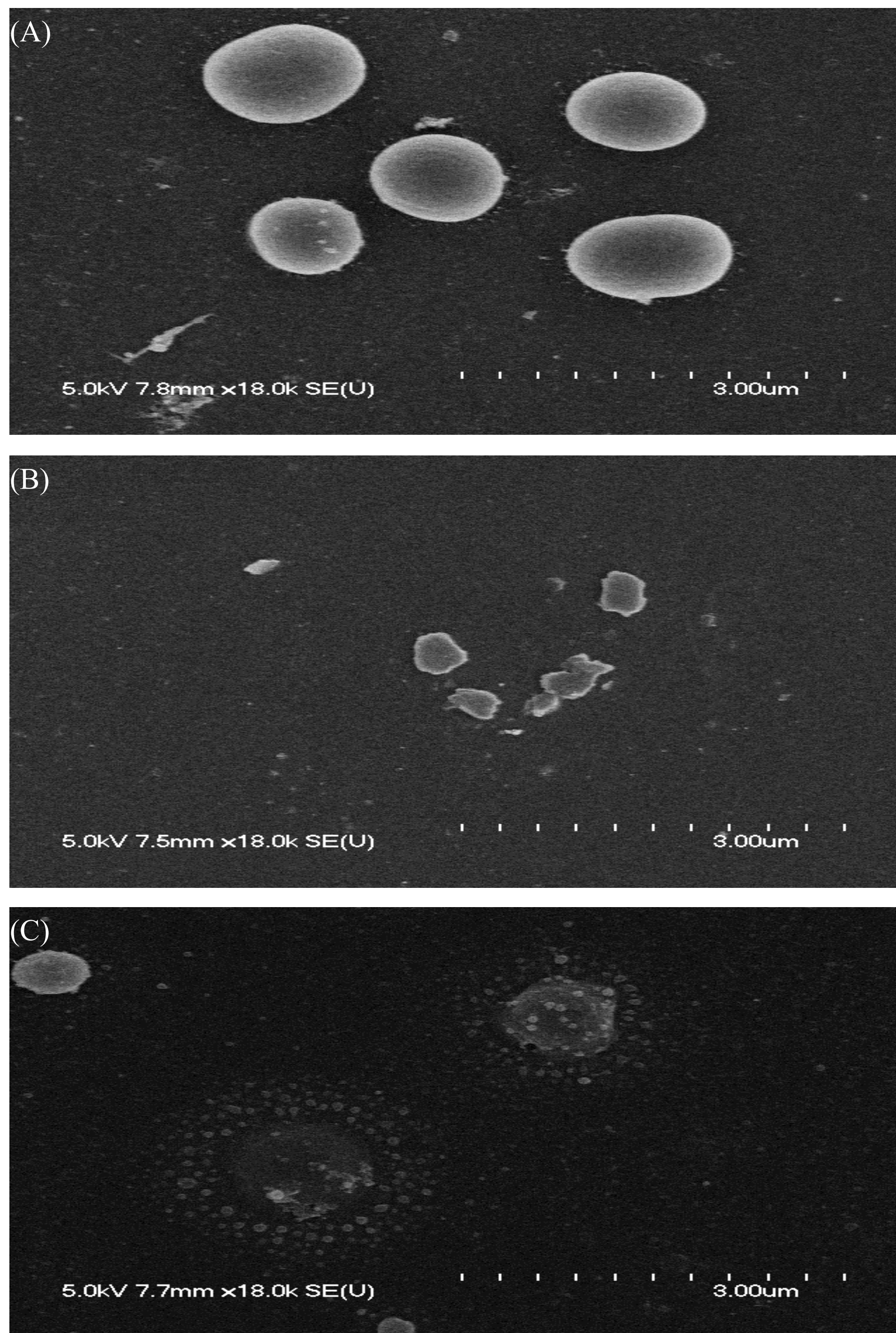

Figure 4. 15. Scanning electron micrographs of (A) Untreated *Micrococcus luteus* control (B) 5 min argon plasma treated *Micrococcus luteus* (C) 1 min argon plasma with 14.2% oxygen addition treated *Micrococcus luteus* under plasma condition 1500 sccm argon, 250 sccm, and 15 W DC power input

4.4. Conclusion

This study demonstrated the rapid sterilization capability of low-temperature argon plasmas created under one atmospheric pressure with a very low DC power input in the level 15 watts, which ensures the low-temperature nature of the gas discharges. The sterilization test results have shown that both *Escherichia coli* and *Micrococcus luteus* bacteria seeded on various supporting media (including filter paper, nutrient broth, and standard methods agar) were completely sterilized within 2 to 4 minutes after exposed to such low-temperature atmospheric argon plasmas. The only exception is the *Escherichia coli* seeded on filter paper required longer exposure time to be fully sterilized. The sterilization effects of argon plasmas were confirmed and distinguished from the possible synergetic effects of heat and fast gas blowing, which did not cause any cell reduction as observed from separate sterilization tests.

The experimental results presented in this paper also confirmed that the oxygen-based reactive species has an important role in the case of low-temperature $Ar+O_2$ plasmas created under one atmospheric pressure with a very low DC power input. The sterilization test results have shown that both *Escherichia coli* and *Micrococcus luteus* bacteria seeded on filter paper had the

fast bacterial cell reduction with oxygen addition. The conceivable explanation would be that the oxygen-based reactive species penetrate cell surface and destroy the microorganism by oxidation. In contrast, both bacteria seeded on nutrient broth and standard methods agar required extended treatment time after exposed to atmospheric Ar+O_2 plasmas. It represented the bacterial killing efficiencies of oxygen-based reactive species varied among the different types of supporting media owing to the penetrating rate of oxygen-based reactive species. The possible heat effect of Ar+O_2 plasmas was isolated from separate sterilization tests.

SEM investigation of the plasma treated samples showed that cell structure damages of both *Escherichia coli* and *Micrococcus luteus* bacteria. Because only pure argon gas was used, the sterilization capability of the argon atmospheric plasmas was mainly ascribed to the high energy argon ions and electronically excited argon neutrals presented in the plasmas. The SEM analysis of the Ar+O_2 plasma treated samples showed that cell structure damages of both *Escherichia coli* and *Micrococcus luteus* bacteria. It confirmed that prospective oxidation of Ar+O_2 plasma contributed to the rapid germicidal effect on microorganisms.

The plasma sterilization capability demonstrated through this study

indicated the tremendous potential of this low-power driven atmospheric plasmas as a promising alternative sterilization technique. Such a low-power atmospheric plasma source is cost effective in both fabrication and operation, simple and safe to use, requires much less treatment time as compared with traditional sterilization methods. The low-power feature of such an atmospheric plasma source makes it not only applicable to various heat-sensitive materials or device, but is also practical to assemble an array of individual plasma brushes for sterilizing large surface or object. This study is our first step to demonstrate the applicability of low-power atmospheric plasma source in sterilization application.

4.5. Reference

1. L.J. Joslyn, J.M. Hansen, H.L. Shaffer, P.T. Jacobs, S.-M. Lin, J. Dunn, R.V. Levy, E.R. Blatchley III, M.M. Peel, D. Knorr, and V. Heinz, *"Part IV: Physical Sterilization and Disinfection", in "Disinfection, Sterilization and Preservation",* 5th, edition, SS. Block Ed., Philadelphia, Lippincortt Willams & Wilkins, p.695-877, 2001
2. A. D. Russell, W. B. Hugo, and G. A. J. Ayliffe, *"Principles and Practice of Disinfect ion, Preservation and Sterilization"*, Oxford, Blackwell Scientific publications, 1992
3. P. T. Jacobs and S. M. Lin, "Gas-Plasma Sterilization", in *"Plasma Deposition Treatment, and Etching of Polymers"*, R. d'Agostino ed., San Diego, Academic Press, p.217-245, 1996
4. P. T. Jacobs and S. M. Lin, *"Sterilization Processes Utilizing Low-Temperature Plasma", in "Disinfection, Sterilization and Preservation"*, 5th, edition, SS. Block Ed., Philadelphia, Lippincortt Willams & Wilkins, p.747-763, 2001
5. M. Laroussi, *"Sterilization of contaminated matter with atmospheric pressure plasma"*, IEEE Trans. Plasma Sci., vol. 24, no. 3, p. 1188-1191, 1996
6. K. Kelly-Wintenberg, A. Hodge, T. C. Monite, L. Deleanu, D. Sherman, J. R. Roth, P. T. Tsai, and L. C. Wadsworth, *"Use of a one atmosphere uniform glow discharge plasma to kill a broad spectrum of microorganisms "* , J. Vac. Sci. Technol. A, vol.17, no. 4 , p. 1539-1544, 1999
7. K. Kelly-Wintenberg, T. C. Monite, C. Brickman, J. R. Roth, A. K. Carr, K. Sorge, L. C. Wadsworth, and P. T. Tsai , *" Room temperature sterilization of surfaces and fabrics with a One Atmosphere Uniform Glow Discharge Plasma."*, J. Industrial Microbiol. Biotechnol., vol. 20, no. 1, p. 69-74, 1998
8. M. Laroussi, I. Alexeff, W. Kang, *"Biological decontamination by non-thermal plasmas"*, IEEE Trans. Plasma Sci., vol. 28, no.1, p.184-188, 2000.
9. J. P. Richardson, F. F. Dyer, F. C. Dobbs, I. Alexeff, and M. Laroussi, *" On the use of the resistive barrier discharge to kill bacteria: recent results"*, In Proc. IEEE Int. Conf. Plasma Science, New Orleans, LA, 2000
10. M. Laroussi, *"Nonthermal decontamination of biological media by atmospheric-pressure plasmas: review, analysis, and prospects"* IEEE Trans. Plasma Sci., vol. 30, no. 4, p. 1409-1415, 2002
11. H. W. Herrmann, I. Henins, J. Park, and G. S. Selwyn, *"Decontamination of chemical and biological warfare (CBW) agents using an atmospheric pressure*

plasma jet (APPJ)", Phys. Plasma, vol. 6 no. 5, p. 2284-2289, 1999

12. B. J. Park, D. H. lee, J. C. Park, I. S. Lee, K. Y. Lee, S. O. Hyun, M. S. Chun and K. H. Chung, *"Sterilization using a microwave-induced argon plasma system at atmospheric pressure"*, Phys. Plasma, vol.10, no. 11, p. 4539-4544, 2003
13. E. Stoffels, *"Biomedical applications of electric gas discharges"*, High Temp. Material Process., vol. 6, p.191-202, 2002
14. T. C. Monite, K. Kelly-Wintenberg, and, J. R. Roth, *"An overview of research using a one atmosphere uniform glow discharge plasma (OAUGDP) for sterilization of surfaces and materials",* IEEE Trans. Plasma Sci., vol. 28, no. 1, , p. 41-50, 2000
15. N. Philps, B. Saoudi, M. C. Crevier, M. Moison, J. Barbeau, and J. Pelletier, *"The respective roles of UV photons and oxygen atoms in plasma sterilization at reduced gas pressure : the case of N_2-O_2 mixtures"*, IEEE Trans. Plasma Sci., vol. 30, no. 4, p. 1429-1436, 2002
16. D.A. Mendis, M. Rosenberg, and F. Azam, *"A note on the possible electrostatic disruption of bacteria"*, IEEE Trans. Plasma Sci., vol. 28, no. 4, p. 1304, 2000
17. M. Laroussi, D.A. Mendis, and M. Rosenberg. *"Plasma Interaction with Microbes"* New Journal of Physics, vol. 5, p. 41.1-41.10, 2003

CHAPTER 5

POLYMER SURFACE EFFECTS OF A COLD ATMOSPHERIC PLASMA BRUSH

5.1. Introduction

Polymers have been generally used in the advancement of biomaterials for biological and medical applications because of their lightweight, low cost, and flexibility features. The polymeric materials including poly (ethylene terephthalate) (PET), nylon 6,6 (PA 6,6), silicon rubber (elastomer) (SR), polypropylene (PP), and low-density polyethylene (LDPE) are anticipated adapting to the complex situations in the biological system but their less effective wettability and low surface energy may not be suitable for the requirement of biocompatibility [1]. Poly (ethylene terephthalate) (PET), which has the excellent stretch strength, is used as cardiovascular implant for medical applications. However, there is an argument about the long-term thrombogenic stability of PET for in vivo applications and demand for improving its blood compatibility [2]. Nylon 6,6 is a semicrystalline polymer with high tensile strength, low friction coefficient, and great resistance to heat and solvents. It is often used for catheter and reverse osmosis membrane [3-4]. Silicon rubber (elastomer), which has a backbone of

silicon oxygen linkage, is a synthetic polymer. It plays a vital role in many long-term medical implantations, yet it comes under rising controversies because of potential illnesses associated with silicone breast implant aging [5]. Polypropylene (PP) is noted for its lightweight and admirable resistance to solvents. It is frequently used to construct the artificial heart valve structures [6-7]. Low-density polyethylene (LDPE) is one of relevant cardiovascular biomaterials in biomedical applications [8]. Since these polymer surfaces are in direct contact with the biological system, the optimal performance to controlled surface properties of polymers plays a key role in both academic and industrial areas. The hydrophilic surface means a stable significant increase of the polarity, which is reached by a radical interference in the nature of surface layer of the polymer. To provide polymeric materials with the better surface properties, a process that can efficiently modify polymer surface is needed.

Low-temperature plasma technique has exhibited the great potential for promoting surface properties of polymeric materials [9-15]. It is well known that the hydrophilicity of polymer surfaces can be significantly improved by low temperature plasma treatment with reactive gases. The formation of the free radicals in plasma environment improves the surface cross-linking,

functionalization, and degradation of polymers [9]. The advantage of low temperature plasma surface modification is the fact that plasma usually changes the surface properties of the polymer without interfering with the bulk properties [9,14]. This is of the particular significance from the viewpoint of preserving the mechanical and physicochemical properties of modified polymeric materials. In general, the low temperature plasma modification process has usually been performed under the low pressure or vacuum environments to sustain the plasma state. The polymers have been modified by low-pressure plasma processes including poly (ethylene terephthalate) (PET) [16], nylon 6,6 (PA 6,6) [17], silicon rubber (elastomer) (SR) [18], polypropylene (PP) [19], and low-density polyethylene (LDPE) [20]. The objective of these investigations was generally to improve the wetting and surface properties of these polymers. Table 5.1 shows the change of hydrophilic surface property on the polymer surfaces before and after the plasma treatments from literature references [16-20]. For all studies, the improved hydrophilic surface properties of low-pressure plasma treated polymer surfaces were observed. In addition, a much smaller increase of the hydrophilicity of only 3–7° was observed for low-pressure plasma modified PET and nylon 6,6. The long-term plasma treatment time (1-10 min) to modify polymers corresponds

Table 5.1. Low-pressure plasma modification of conventional polymers

Polymer	Low pressure plasma treatment	Change of hydrophilic surface property		Reference
PET	NH_3+Ar, MW plasma, 500 W	Initial C.A: ~72°	Treated C.A: ~65° (10 sec)	[21]
Nylon6,6	Ar, RF plasma, 3.36 W	Initial C.A: 77°	Treated C.A: 74° (1 min)	[22]
SR	Ar, sputter coater, 5 W	Initial C.A: ~110°	Treated C.A: ~84° (5 min)	[23]
PP	Acrylic acid, RF plasma, 5 W	Initial C.A: 108°	Treated C.A: 69° (10 min)	[24]
LDPE	Ar, RF plasma, 8 W	Initial C.A: 100°	Treated C.A: 40° (1 min)	[25]

C.A: water static contact angle

well with all low-pressure plasma processes in Table 5.1. However, the costly vacuum system and the complex maintaining procedure limit the use of low-pressure plasma in surface modification of polymers.

To eliminate the restrictions imposed by low-pressure plasmas, different low temperature atmospheric pressure plasma sources have been developed since last two decades [21,22]. The atmospheric plasma process offers unique advantages over existing low-pressure plasma modification techniques since it does not require any vacuum systems and provides treatment of different substrates at low temperatures while operating open to the atmosphere. The atmospheric pressure plasma can be used for modification purpose and considered as a promising alternative to low-pressure plasma modification techniques. Since the dielectric barrier discharge is nowadays the common atmospheric pressure plasma system, the studies of dielectric barrier discharge become the mainstream in atmospheric

pressure plasma surface modification processes [21-26]. To date, the currently available atmospheric plasma surface modification techniques have commonly suffered from their miniature plasma volumes or sizes, and consequently limited their modification applications. For instance, the electrode spacing of the dielectric barrier discharge restricts the size and the shape of the polymeric items to be modified. In addition, dielectric barrier discharge may cause to non-uniform treatment and can even induce local damage on the treated polymer surface.

As a rule, the improvement of atmospheric plasma surface modification technique is due not only to the reactor setup limitations but also to the rapid and reliable modification capabilities. In this study, we present a novel atmospheric plasma modification method. The atmospheric cold plasma brush (ACPB) consists of a gas compartment and two metallic electrodes placed certain distance apart inside the gas compartment. The very low power consumption in generating and sustaining atmospheric cold plasma brush is in the level of several watts or tens of watts and it provides many unique advantages in practical applications including possibilities powered by batteries and for large-scale applications. In addition, the low power consumption also ensures the plasma of low-temperature features. The low-temperature nature of the atmospheric cold plasma brush makes the plasma

source tremendously useful in various applications including surface cleaning, modification, and treatment, material processing, and surface sterilization and decontamination. The purpose of this study is to characterize the surface properties of conventional polymers subjected to the argon atmospheric pressure plasma brush.

5.2. Experimental procedures

5.2.1. Experimental materials

Argon gas used to create atmospheric plasma was an industrial grade with 99.997% purity and purchased from General Store of University of Missouri-Columbia. The different conventional polymer samples were supplied by Goodfellow Corporation: poly (ethylene terephthalate) (PET) (0.05 mm thick), nylon 6,6 (PA 6,6) (0.05 mm thick), silicon rubber (elastomer) (SR) (1 mm thick), polypropylene (PP) (0.013 mm thick), and low-density polyethylene (LDPE) (0.125 mm thick). The polymer films were cut into strips and were used as samples for atmospheric plasma surface modification experiments. Prior to use in experiment, each polymer sample was cleaned in an ultrasonic soap water bath for 30 minutes, thoroughly rinsed with DI water for 60 minutes, and dried completely in air.

5.2.2. Low-temperature atmospheric plasma brush

This plasma source contains discharge chamber with a proprietary design. The argon gas passes through the discharge chamber at a flow rate controlled by a MKS mass flow controller (MKS Instruments Inc. Andover, MA, USA). An electrical field was applied to the two electrodes located inside the chamber to ignite a DC glow discharge by a DC power supply (Pd 1556C, Power Design Inc. New York, NY, USA). This plasma source can be operated under very low electrical power (as low as a few watts), and as a result very low plasma temperature can be achieved. The gas phase temperatures of an argon atmospheric plasma measured using a thermocouple thermometer (Fisherbrand Traceable Dual Channel Thermometer, Fisher Scientific, Houston, TX, USA) are in a range from 40 to 160 ^{o}C with argon flow rate changing from 3500 sccm to 1000 sccm correspondently (see chapter 2). It is obvious that a low plasma temperature close to room temperature were obtained at high argon flow rate.

5.2.3. Experimental procedures

The polymer samples were put on the sample stage under the discharge chamber for atmospheric plasma modification treatment. After argon gas at a certain flow rate (1500 sccm) was fed into the discharge chamber through the gas

line, DC power (15 Watt) was applied to create a plasma brush for the plasma modification treatment. During the atmospheric plasma modification treatment, the polymer samples were kept in the predetermined exposure position as the target of the plasma brush, which was adjusted by rotating the sample stage. The exposure position from the plasma brush to the polymer sample was adjusted by changing the vertical position of the sample stage from the top of the discharge chamber.

5.2.4. Static Contact Angle Measurement

The static contact angles of polymer samples were measured by projecting an image of an automatic sessile droplet resting on a membrane surface with a VCA-2500XE Video Contact Angle System (AST Products, Inc.). After the atmospheric plasma modification treatments, the untreated polymer samples and the plasma modified polymer samples were placed on a vertically and horizontally adjustable sample stage. The microsyringe can be set to automatically dispense a predetermined amount of water by the computer. After the 0.3 μL water droplet has made contact with the polymer surface, a snapshot of the image was taken. The captured image was saved and contact angle measurements were commenced at leisure. After placing markers around the perimeter of the water droplet, the

VCA-2500 Dynamic/Windows software calculated right and left contact angles.

5.2.5. Optical Emission Analysis

The major plasma diagnostic apparatus of brush-shape atmospheric pressure plasma is an optical emission spectroscopy. This equipment consists of both the instrumentation and spectrum analysis software, which was supplied by Princeton Instruments, Inc. The observable spectral range was 200-1050 nm. A 2m long fiber optic cable, coupled to a variable width (10–2000 μm) slit (typical width: 15 mm, with resolution: 0.3 nm), was mounted on a Jarrell–Ash Monospec 27 monochromator/spectrograph (crossed Czerny–Turner, 275 mm focal length, f/3.8) with a triple (150, 600, and 1200 grooves/mm) grating holder. A Princeton Instruments RY-1024 unintensified diode array detector is mounted at the Monospec 27 exit port, and is controlled by a Princeton Instruments ST120 OSMA detector controller that interfaces with a Dell computer.

5.3. Results and Discussion

The polymers including PET, nylon 6,6,SR, PP, and LDPE were treated by the atmospheric pressure plasma brush. The primary operational parameter of atmospheric pressure plasma modification is the plasma treatment time. The static water contact angle measurements determined the surface tension of the

atmospheric plasma treated polymers. Fig. 5.1 shows the surface tension changes of atmospheric pressure plasma treated polymers. The blue lines in Fig 5.1 represent the static water contact angle measurements directly after the modification treatment, whereas the pink lines in Fig. 5.1 represent the contact angles of the samples washed in a deionized water ultrasonic bath for 3 minutes, then blowing dried with compressed air and left in the air for 10 minutes. For untreated PET nylon 6,6, and SR samples with initial static water contact angle of approximately around 80°-120°, the static water contact angles of atmospheric plasma treated samples extremely decreased after 2 second treatment time as shown in Fig. 5.1 (a), (b), and (c). As a result, Fig. 5.1 (a) (b) and (c) show that the atmospheric plasma brush can efficiently modifies PET, nylon 6,6, and SR samples with the shorter treatment time compared to low-pressure plasma modification processes. In addition, the similar rapid atmospheric plasma modified results of PP and LDPE samples are also shown in Fig. 5.1 (d) and (e) respectively. The after washing results of the atmospheric plasma treatments as shown in Fig.5.1 (a), (b), and (e) for PET, Nylon 6,6, and LDPE showed

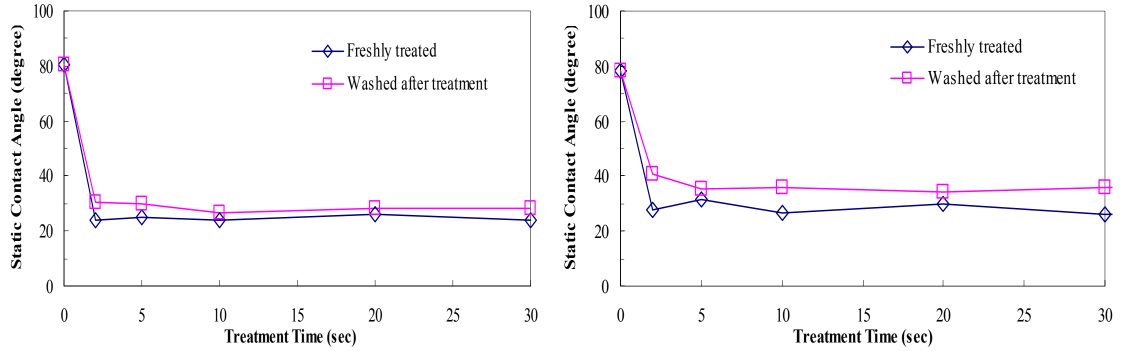

(a) (b)

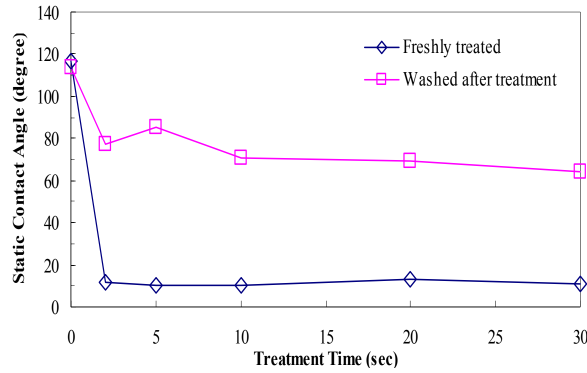

(c)

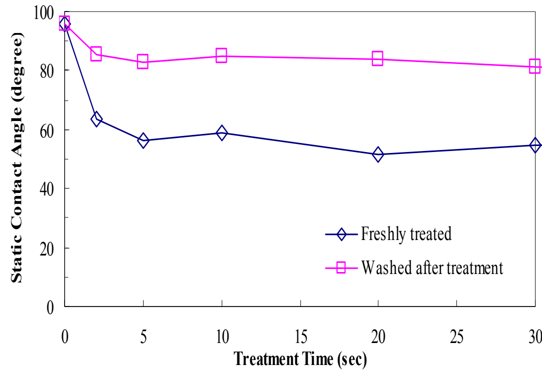

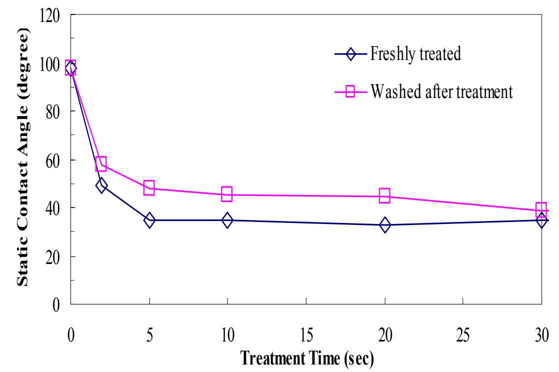

(d) (e)

Figure 5. 1. Argon atmospheric plasma modification with argon flow rate of 1500 sccm and DC power input of 15 W. (a) polyethylene terephthalate (PET) (b) Nylon 6, 6 (PA 6,6) (c) silicon elastomer (SE) (d) polypropylene (PP) (e) low-density polyethylene (LDPE)

a slight increase, (< 15°) hydrophobicity recovery in static water contact angle. The after washing results of the atmospheric plasma treated SR and PP samples as shown in Fig. 5.1 (c) and (d) showed the significant increase as high as 68° for SR and ~ 40° for PP in static water contact angle. The hydrophobicity recovery after washing samples is an obvious evidence of the washing away of surface oligomers that were formed from the polymer surface degradation or damages during the atmospheric plasma treatments [25]. The coincident hydrophobicity recovery results were also acquired from these atmospheric plasma treated polymer surfaces after washing processes. Consequently, the atmospheric pressure plasma brush obtains the relatively rapid and consistent polymer surface modification effects as traditional low-pressure plasma processes.

Optical emission spectroscopy was used to monitor the excited plasma reactive species generated by atmospheric pressure plasma brush. The optical emission analysis is expected to explicate the reactions of plasma reactive species that may contribute to plasma surface modification process. The optical emission spectrum of atmospheric pressure plasma brush is presented in Fig. 5.2. From optical emission spectrum of atmospheric pressure plasma brush, the strong excited argon emission lines are observed at about 700-800 nm.

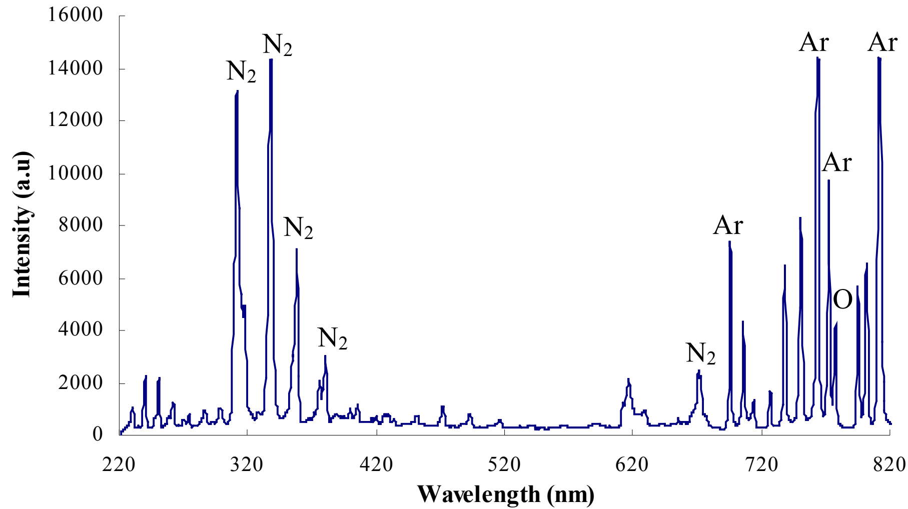

Figure 5. 2. The optical emission spectrum from an argon atmospheric plasma brush. Conditions are 1500 sccm Ar, DC 15Watt, 150g/mm, at 180sec.

The obvious emission line of the molecular nitrogen bands between 300-400 nm are also exhibited in optical emission spectra, as well as the emission line of the oxygen atom at 777 nm from the ambient air. From optical spectra of atmospheric pressure plasma brush, it is corresponded to the possible modification mechanism of Ar^+, $N2^+$, and O^+ plasma species.

In atmospheric pressure plasma state, the reactive species could lose its energy or reactivity in a very short time due to the much higher collision frequency among the plasma particles. The lifetime of the reactive plasma species is much shorter when compared to that in low-pressure plasmas. Therefore, the atmospheric pressure plasma could lose its reactivity dramatically in a remote position (away from the glow region). To examine the modification effects of

remote atmospheric pressure plasma, the polymer films were subjected to plasma exposure in the down stream at different positions away from the glow. When the atmospheric pressure plasma conditions were fixed at 1500 sccm of argon flow rate and 15 W of DC power, the luminous atmospheric pressure plasma brush length was about 1.3 cm from the output of the discharge chamber. Only the long-life reactive species from the atmospheric pressure plasma brush were allowed to diffuse and get in contact with the polymer surface.

Fig. 5.3 (a) shows the remote exposure atmospheric plasma surface modification effects on PET at different positions away from the glow. The modification effects of a remote atmospheric pressure plasma shows that the 1 mm from the tip of glow to PET surface produced the lowest contact angle (22°). It should be noted that, as is shown in Fig. 5.3 (a), the increasing distances from the atmospheric pressure plasma glow to PET surface gave decreasing surface hydrophilicity of PET surfaces as compared with the direct remote exposure treatment. Fig. 5.3 (b) shows optical emission trend of major reactive atmospheric pressure plasma species with different vertical positions away from atmospheric pressure plasma. At remote atmospheric pressure plasma brush, the intensity of

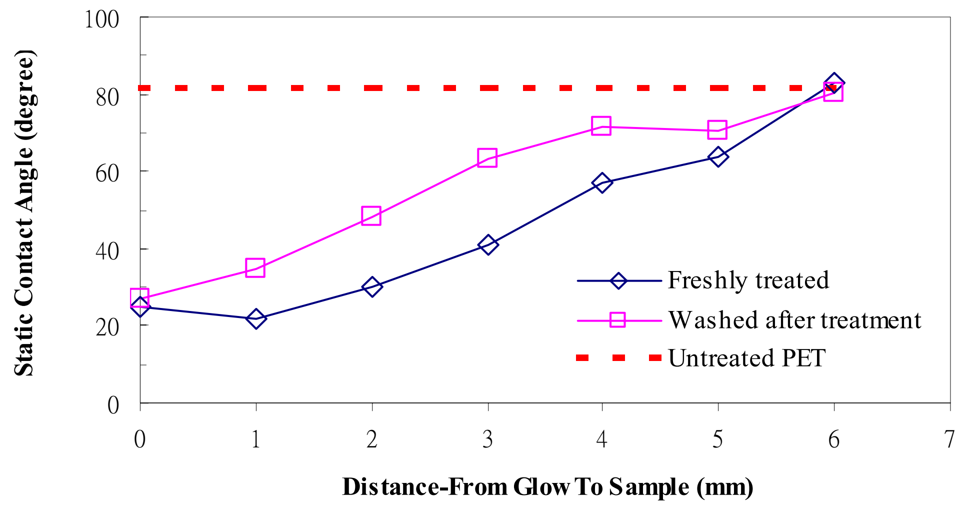

(a)

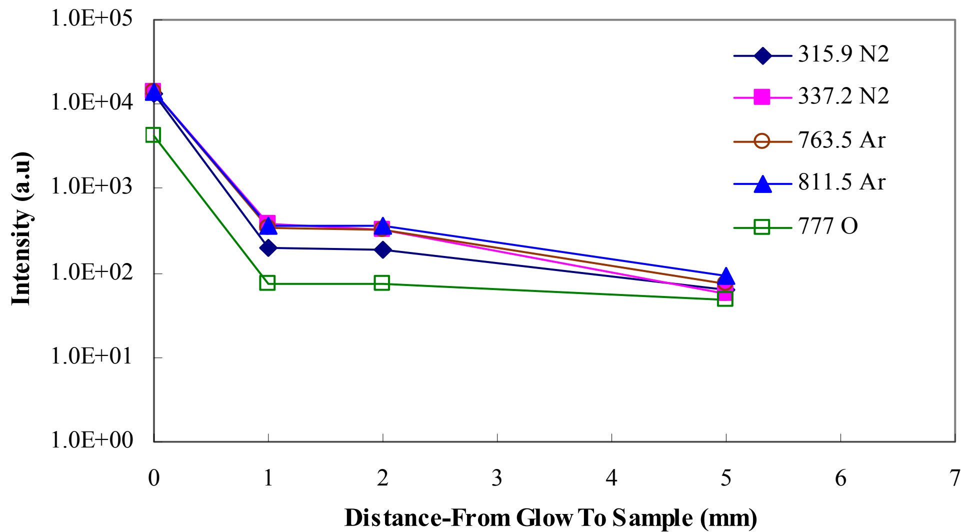

(b)

Figure 5. 3 Argon atmospheric plasma modification on polyethylene terephthalate (PET) with argon flow rate of 1500 sccm and DC power input of 15 W, Treatment Time: 10sec Distance: 0-6 mm (a) remote modification effect with distance (b) optical emission trend of major plasma species with remote distance

major emission lines significantly decreased away from atmospheric pressure plasma brush as shown in Fig. 5.3 (b). This can be easily understood due to the quicker consumption of reactive plasma species at relatively longer remote distance. As discussed above, it can be concluded that, under the present operation conditions, the short lifetime of reactive plasma species are primarily responsible for the decreasing modification efficiency in the remote atmospheric pressure plasmas.

The effects of remote exposure on atmospheric pressure plasma modified polymer surfaces are shown in Fig. 5.4. The atmospheric pressure plasma modification of polymers conducted beyond the atmospheric pressure plasma brush also had the obvious effect on the surface hydrophilicity improvement of the most polymers. For an instance, the short treatment of 2 seconds significantly decreased the static water contact angle of PET from 82° to less than 20° as seen from Fig. 5.4 (a). The after washing results show that the surface hydrophilicity of polymer samples indirectly exposed to atmospheric pressure plasma was more hydrophobic than the direct plasma exposure polymer samples. The possible explanation could be the long-life reactive species from the atmospheric pressure plasma brush cause the surface damage of PET. However, the after washing

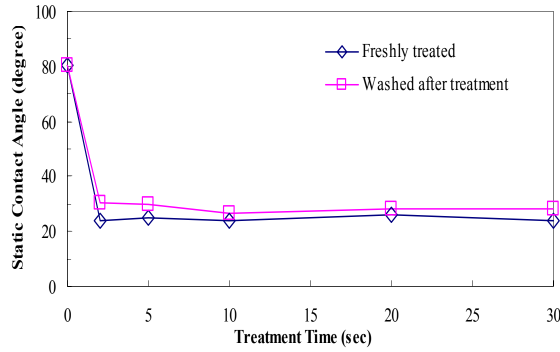

(a)

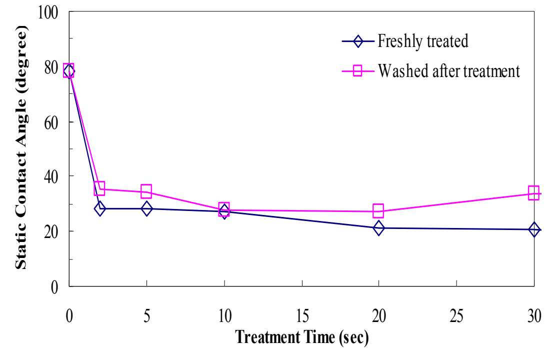

(b)

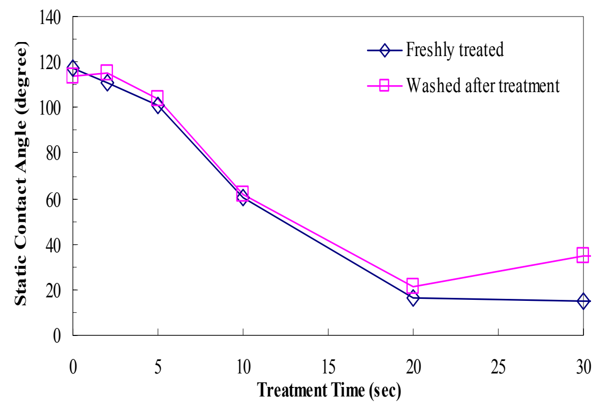

(c)

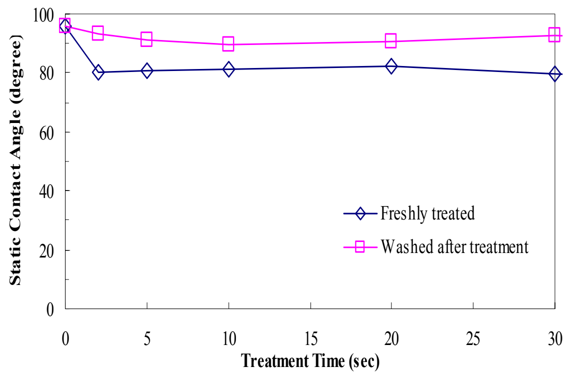

(d)

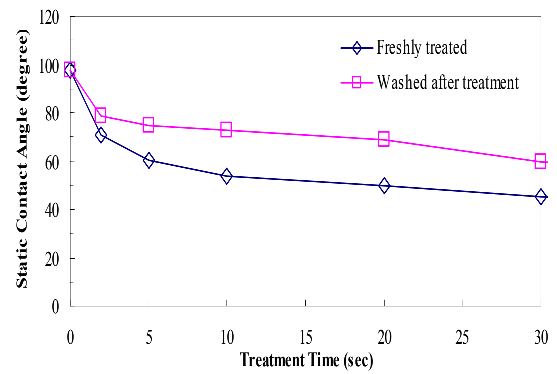

(e)

Figure 5. 4. Remote argon atmospheric plasma modification with argon flow rate of 1500 sccm and DC power input of 15 W. Remote Distance: 1mm (a) polyethylene terephthalate (PET) (b) Nylon 6, 6 (PA 6,6) (c) silicon elastomer (SE) (d) polypropylene (PP) (e) low-density polyethylene (LDPE)

results from the other polymers show the less increase in static water contact angle measurements as compared with those from the direct remote exposure treatments.

It is expected that the atmospheric pressure plasma operating conditions such as power input and inert gas flow rate may have a certain degree of influences on the atmospheric pressure plasma brush modification results. Thus, the surface modification of PET and Nylon 6, 6 by atmospheric pressure plasma brush was carried out at different DC power inputs and argon flow rates and the contact angle data is shown in Fig. 5.5-5.6. Fig. 5.5 shows the static contact angle changes of PET and Nylon 6,6 films with different DC power inputs of the plasma under a fixed argon flow at 1500 sccm and the treatment time of 10 seconds. It can be seen that the higher DC power input did result in lower static contact angles on both PET and Nylon 6,6 surfaces. In addition, it was clearly observed that the after washing results of the atmospheric plasma treated Nylon 6,6 under the higher DC power input showed a great increase (> 20°) hydrophobicity recovery in static water contact angle in Fig. 5.5b. It elucidate that the different surface modification effects base on the various chemical structures of polymers from Fig. 5.5b. The experimental result in Fig. 5.5 indicates that the higher DC power input more efficiently improves the free surface energy of PET and Nylon6, 6. From Fig. 5.6,

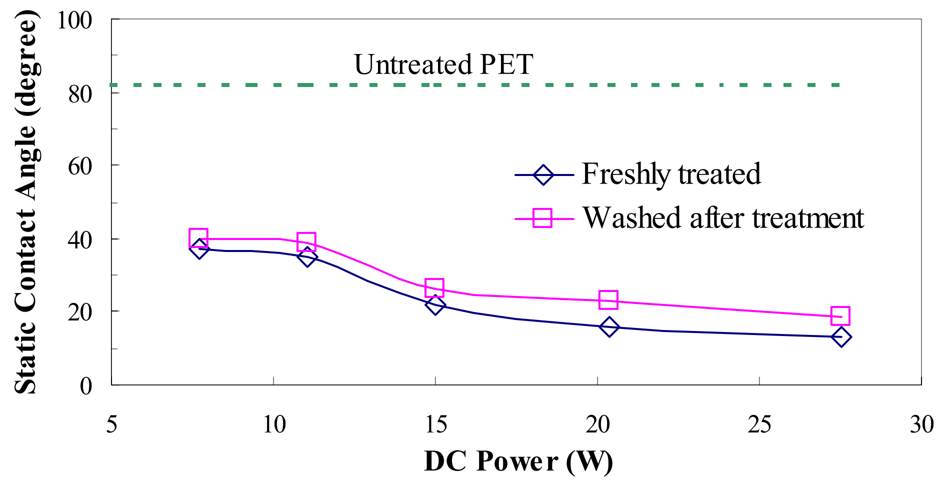

(a)

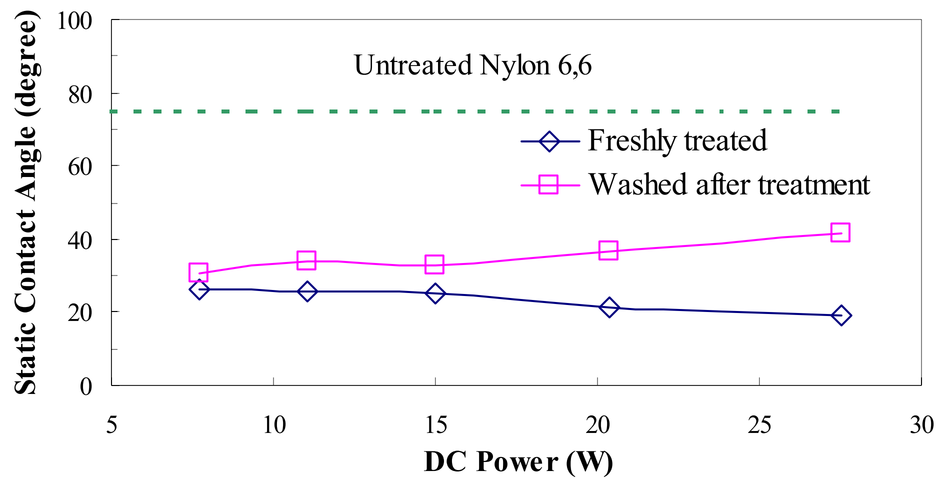

(b)

Figure 5. 5. The static contact angles of argon atmospheric plasma treated polymers as a function of plasma power: (a) polyethylene terephthalate (PET) and (b) Nylon 6, 6 (PA 6,6) after 10 seconds plasma treatment time

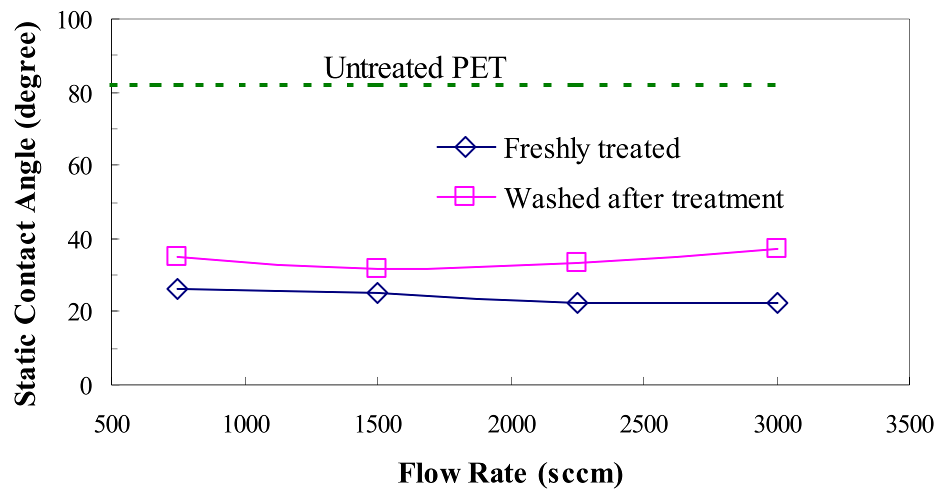

(a)

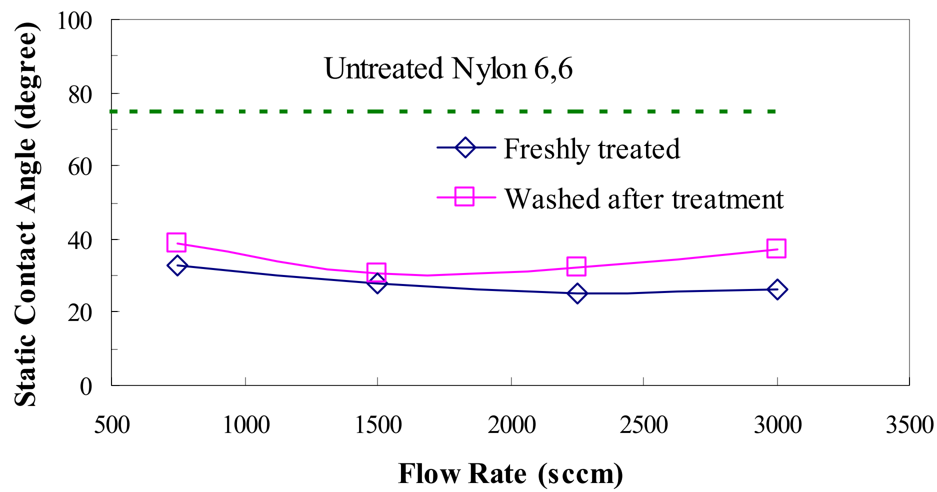

(b)

Figure 5. 6 The static contact angles of argon atmospheric plasma treated polymers as a function of argon flow rate: (a) polyethylene terephthalate (PET) and (b) Nylon 6, 6 (PA 6,6) after 10 seconds plasma treatment time

the high argon flow rate over 700 sccm of atmospheric pressure plasma brush is essential to create the stable ACPB. However, the change of the argon flow rates did not show a significant effect on the surface contact-angle change of PET and Nylon6, 6 samples.

The atmospheric plasma treated polymers were also monitored and tested to investigate the aging effect of the atmospheric plasma modification process. The aging effect of treated polymers would limit the usefulness of atmospheric plasma modified polymeric materials. The effects of aging on atmospheric plasma treated polymers were investigated by storing the samples in ambient air for more than 100 hours as shown in Fig 5.7. After a 120 hours aging, atmospheric plasma treated PET nylon6, 6 and LDPE showed the good surface hydrophilicity, whereas atmospheric plasma treated SR and PP showed the significant hydrophobic recovery.

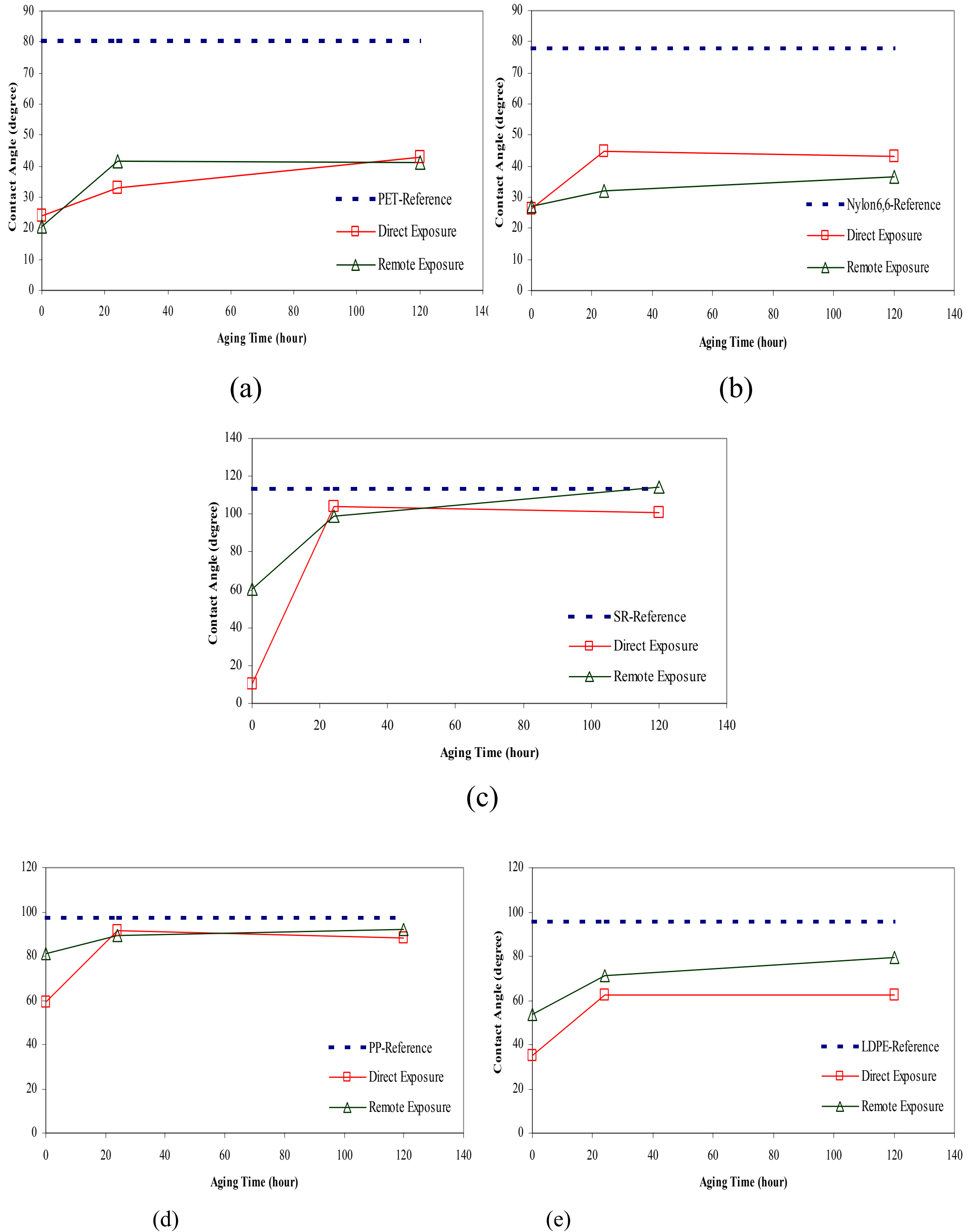

Figure 5. 7 .Aging effects with Direct Plasma Exposure and Remote Plasma Exposure. argon flow rate of 1500 sccm and DC power input of 15 W. 10sec (a) polyethylene terephthalate (PET) (b) Nylon 6, 6 (PA 6,6) (c) silicon elastomer (SE) (d) polypropylene (PP) (e) low-density polyethylene (LDPE)

5.4. Summary

The present study demonstrates the capability of the atmospheric pressure plasma brush in surface modification of polymers Static contact angle measurement results indicate that the atmospheric pressure plasma rapidly improves the surface energy of conventional polymers. In the study, both remote exposure and direct exposure of polymers to atmospheric pressure plasma the was used to modify the polymer surfaces. Plasma operational conditions including plasma power levels and gas flow rates were manipulated to enhance the atmospheric pressure plasma modification efficiency. In contrast to the improved modification efficiency by increasing DC plasma power inputs, the effect of argon gas flow rate showed the less influence on modification. We also examine the aging results when using atmospheric plasma brush with conventional polymers. In most cases, the surface hydrophilicity of atmospheric pressure plasma treated polymers increased.

The plasma modification capability investigated through this study indicated that an atmospheric pressure plasma brush is relatively effective in both fabrication and operation as compared with traditional low-pressure plasma modification methods. The low-temperature feature of such an atmospheric

plasma source makes it applicable to various heat-sensitive polymer films. This preliminary study demonstrates the applicability of atmospheric pressure plasma brush in polymeric surface modification applications.

5.5. Reference

1. Gil'man, A.B. *"Low-Temperature Plasma Treatment as an Effective Method for Surface Modification of Polymeric Materials"* High Energy Chemistry, (2003) 37(1), 17-23.
2. Murayama, Yuichi; Suzuki, Yoshiaki; Vinuela, Fernando; Massoud, Tarik F.; Do, Huy M.; Guglielmi, Guido; Iwaki, Masaya; Kamio, Masami; Abe, Toshiaki. *"A new surface modification technique of platinum coils by ion implantation and protein coating: Use in intravascular treatment of brain aneurysms."* Nuclear Instruments & Methods in Physics Research, Section B: Beam Interactions with Materials and Atoms (1997), 127/128 1015-1018.
3. Hamilton, Murray G.; Lundy, Paul M. *"HI-6 therapy of soman and tabun poisoning in primates and rodents."* Archives of Toxicology (1989), 63(2), 144-9.
4. Wildermuth S; Dumoulin C L; Pfammatter T; Maier S E; Hofmann E; Debatin J F *"MR-guided percutaneous angioplasty: assessment of tracking safety, catheter handling and functionality."* Cardiovascular and interventional radiology (1998), 21(5), 404-10.
5. Adams W P Jr; Robinson J B Jr; Rohrich R J *"Lipid infiltration as a possible biologic cause of silicone gel breast implant aging."* Plastic and reconstructive surgery (1998), 101(1), 64-8; discussion 69-71.
6. Steinhoff G; Stock U; Karim N; Mertsching H; Timke A; Meliss R R; Pethig K; Haverich A; Bader A *"Tissue engineering of pulmonary heart valves on allogenic acellular matrix conduits: in vivo restoration of valve tissue."* Circulation (2000), 102(19 Suppl 3), III50-5.
7. Thornton M A; Howard I C; Patterson E A *"Three-dimensional stress analysis of polypropylene leaflets for prosthetic heart valves."* Medical engineering & physics (1997), 19(6), 588-97.
8. Gorbet, M. B.; Yeo, E. L.; Sefton, M. V. *"Flow cytometric study of in vitro neutrophil activation by biomaterials."* Journal of Biomedical Materials Research (1999), 44(3), 289-297.
9. Yasuda, H. K.. *"Modification of polymer surfaces by plasma treatment and plasma polymerization."* Polymeric Materials Science and Engineering (1984), 50 135-8.
10. Yasuda, H. *"Surface state of polymers investigated by low-temperature plasmas."* Makromolekulare Chemie, Macromolecular Symposia (1993), 0-71

(34th International Symposium on Macromolecules, 1992), 29-36.
11. Weikart, Christopher M.; Miyama, Masayo; Yasuda, Hirotsugu K. *"Surface modification of conventional polymers by depositing plasma polymers of trimethylsilane and of trimethylsilane + O2. I. Static wetting properties."* Journal of Colloid and Interface Science (1999), 211(1), 18-27.
12. Lamendola, R.; Favia, P.; Palumbo, F.; D'Agostino, R. *"Plasma-modification of polymers: process control in PE-CVD of gas-barrier films and plasma-processes for immobilizing antithrombotic molecules."* European Physical Journal: Applied Physics (1998), 4(1), 65-71.
13. d'Agostino,Riccardo. *"Process control and plasma modification of polymers."* Journal of Photopolymer Science and Technology (2005), 18(2), 245-249.
14. Yasuda, H. K., *Luminous Chemical Vapor Deposition & Interface Engineering*, Marcel Dekker, New York, 2004.
15. Shenton, M. J.; Stevens, G. C. *"Surface modification of polymer surfaces: atmospheric plasma versus vacuum plasma treatments."* Journal of Physics D: Applied Physics (2001), 34(18), 2761-2768.
16. Ohl, A.; Schroder, K.; Keller, D.; Meyer-Plath, A.; Bienert, H.; Husen, B.; Rune, G. M. *"Chemical micropatterning of polymeric cell culture substrates using low-pressure hydrogen gas discharge plasmas."* Journal of Materials Science: Materials in Medicine (1999), 10(12), 747-754.
17. Wade, G. A.; Cantwell, W. J.; Pond, R. C. *"Plasma surface modification of glass fibre -reinforced nylon-6,6 thermoplastic composites for improved adhesive bonding."* Interface Science (2000), 8(4), 363-373.
18. Price, C.; Waters, M. G. J.; Williams, D. W.; Lewis, M. A. O.; Stickler, D. *"Surface modification of an experimental silicone rubber aimed at reducing initial candidal adhesion."* Journal of Biomedical Materials Research (2002), 63(2), 122-128.
19. Kang, Min Soo; Chun, Baehyuck; Kim, Sung Soo. *"Surface modification of polypropylene membrane by low-temperature plasma treatment."* Journal of Applied Polymer Science (2001), 81(6), 1555-1566.
20. Gilliam, M. A.; Yu, Q. S. *"Surface characterization of low-temperature cascade arc plasma-treated low-density polyethylene using contact angle measurements."* Journal of Applied Polymer Science (2006), 99(5), 2528-2541.
21. Kanazawa, S.; Kogoma, M.; Moriwaki, T.; Okazaki, S. *"Stable glow plasma at atmospheric pressure."* Journal of Physics D: Applied Physics (1988), 21(5), 838-40.

22. Kanazawa, S.; Kogoma, M.; Okazaki, S.; Moriwaki, T. *"Glow plasma treatment at atmospheric pressure for surface modification and film deposition."* Nuclear Instruments & Methods in Physics Research, Section B: Beam Interactions with Materials and Atoms (1989), B37-B38 842-5.
23. Massines, F.; Gouda, G. *"A comparison of polypropylene-surface treatment by filamentary, homogeneous and glow discharges in helium at atmospheric pressure."* Journal of Physics D: Applied Physics (1998), 31(24), 3411-3420.
24. Zhang, Qing; Wang, Chunren; Babukutty, Yohannan; Ohyama, Toshie; Kogoma, Masuhiro; Kodama, Makoto. *"Biocompatibility evaluation of ePTFE membrane modified with PEG in atmospheric pressure glow discharge."* Journal of Biomedical Materials Research (2002), 60(3), 502-509.
25. Seebock, R.; Esrom, H.; Charbonnier, M.; Romand, M. *"Modification of polyimide in barrier discharge air-plasmas: chemical and morphological effects."* Plasmas and Polymers (2000), 5(2), 103-118.
26. Massines, F.; Gouda, G.; Gherardi, N.; Duran, M.; Croquesel, E. *"The role of dielectric barrier discharge atmosphere and physics on polypropylene surface treatment."* Plasmas and Polymers (2001), 6(1/2), 35-49.

CHAPTER 6

A STUDY ON LUMINOUS GAS PHASES OF HYDROCARBON PLASMA POLYMERIZATION SYSTEMS

6.1. Introduction

It is well known that plasma polymerization of organic molecules has the extensive applications in progressive technology. For these applications, to understand the reaction mechanism is critical in achieving a thriving plasma polymerization process. However, the reaction mechanism in plasma polymerization has not been well understood to date. The recent investigations on plasma polymerization of DC trimethylsilane (TMS) glow discharge indicate that the glow characteristic of DC TMS plasma is entirely different from that of DC argon plasma [1-5]. In DC plasma of an inert gas such as argon, the negative glow where ionization mainly occurs developed at a distinctive distance away from the cathode, whereas the cathode remained in the dark space [6]. On the contrary to DC argon plasma, the primary glow, which created at the cathode surface, is the cathode glow in DC TMS plasma polymerization system. The existence of cathode glow in DC TMS plasma polymerization system indicates that the major chemical reactions occur at the cathode surface, but not in the negative glow. The cathode

glow can be designated as dissociation glow since the dissociation of TMS molecules was recognized the major contribution to cause the cathode glow in DC TMS plasma polymerization system. This implies that the chemically reactive species are not created by electron impact ionization of TMS molecules, which should occur at the fringe of the negative glow, but by the low energy electron dissociation at cathode in DC TMS plasma polymerization system [1-3].

The discovery of dissociation glow in DC TMS plasma polymerization system determines that the glow formation and glow characteristics in plasma polymerization system are different from those observed in inert gas glow discharges, which do not polymerize. This finding of dissociation glow also infers that the low energy electron dissociation could precede the ionization in DC TMS plasma polymerization system. In this term, the prevailing ionization concept from inert gas glow discharges, which has been acknowledged that plasma polymerization is an effect on the ionization of the gas molecule in plasma state, cannot be applied to plasma polymerization systems. In plasma polymerization systems, the glow region is where most plasma chemical reactions occurred; for this reason, it is essential to investigate the nature of luminous gas phase e.g., the origination of luminous gas phase in plasma polymerization system, and the

creation of chemically polymeriable species in the luminous gas phase.

The novel investigation of the dissociation glow characteristic in DC trimethylsilane (TMS) plasma polymerization system is redefined the role of the dissociation process in plasma polymerization system. Because of this new aspect, some important fundamental factors to investigate the luminous gas phase in DC plasma polymerization system are further required to examine this hypothesis. The objective of this study is to characterize the glow formation, optical emission feature, the deposition distribution on both cathode and anode substrates, and electrical breakdown in various DC hydrocarbon plasma polymerization systems. The present study reports the systematic investigation in DC plasma polymerization of a series of hydrocarbon monomers.

6.2. Experimental procedures

6.2.1. Materials

The cathode electrodes used in this study were unpolished cold roll steel (CRS) panels (10.2 cm × 15.2 cm × 0.08 cm), which were procured from Q-Panel (Q-Panel Lab Products, Cleveland, OH). Inert gas argon (Ar, 99.997%) procured from General Store of University of Missouri-Columbia. The monomers used for the DC plasma polymerization processes were methane (CH_4, 99% purity), ethane

(C_2H_6, >99% purity), and n-butane (99.5% purity) purchased from Matheson Gas Products Inc. Ethylene (C_2H_4, 99.995% purity) and acetylene (C_2H_2, 99.6% purity) were purchased from Praxair Inc.

6.2.2. Plasma polymerization system

6.2.2.1. DC plasma polymerization reactor for deposition and electrical breakdown studies

A low temperature DC plasma technique was used in this study to perform plasma polymerization of various hydrocarbons monomers. The DC plasma reactor system used in this study was a bell jar-type reactor, with dimension of 46 cm in height and 44.5 cm in diameter. The CRS panel was used as the center electrode, which is also the cathode in DC plasma chemical vapor deposition. The two counter electrodes consisting of a pair of titanium (Ti) plates (17.9. cm × 17.9 cm × 0.08 cm) were placed 10 cm apart. While a new cathode panel was used in each trial, the two anode electrodes remained the same for the entire series of this study. The DC power was supplied by MDX-1K magnetron drive (Advanced Energy Industries, Inc.). In the breakdown voltage study, the electrodes were fabricated from titanium disks 0.2cm thick and 13.3 cm diameter. One of two titanium disks was used as cathode and another as anode. The inter-electrode

distance was 4.5 cm. The power supply used in this study was Pd 1556C (Power Design Inc.) for the breakdown voltage treatment. The HP digital 3435A multimeter was used for measuring the breakdown voltage.

Before each plasma polymerization process, the reactor system was first evacuated to less than 1 mTorr using a vacuum system consisting of a mechanical and booster pump work in series. The flow rates of various monomers were then allowed to flow into the reactor, at which the system pressure was varied by adjusting the pressure controller. The reactor was once again evacuated to its background pressure after each process; the cathode and anodes were carefully removed from the chamber. The silicon wafer strips were detached from the electrodes and the thickness was subsequently measured on different spots at 1-cm increment away from the center.

6.2.2.2. Optical Emission Spectroscopy (OES) Detection in Pyrex cross reactor

The OES spectroscopic investigation of DC polymerization system was conducted in a Pyrex cross reactor. The main chamber consists of following Pyrex glassware: a. 6 inch (152.4 mm) I.D. glass cross, a 6 inch (152.4 mm) to 4 inch (101.6 mm) I.D. reducer, and a 4 inch (101.6 mm) I.D. y-section. The glass cross

is 18 inches (457 mm) from port to port and the reducer is 9 inches (229 mm). The y-section is 14 inches (356 mm) along the straight run and the branch of the y-section serves as the gas exhaust port. The electrical feedthroughs in the flange, mounted on the bottom port of the cross, are used to connect a power generator with discharge electrodes inside the reactor. Vacuum is produced by an Edwards High Vacuum EH500A/E2M80 combination pump.

Gas flow rates are controlled with MKS 2259B and 1259C mass flow controllers in conjunction with MKS 247B readout controller. Pressure readings are obtained with an MKS 220 Baratron capacitor manometer. The power supply used in this study is MDX-1K magnetron drive for DC plasma chemical vapor deposition process.

The optical emission spectroscopy (OES) is the major diagnostic device of this reactor. The OES system includes both apparatus and spectral analysis software, which supplied by ACTON Research Corporation. The observable spectral range is 0 to 1400 nm. A 2 m long fiber optical cable is coupled to a variable width (10 μm-3 mm) slit that is mounted on SpctroPro-300i monochromator (crossed Czerny-Turner, 14 mm high by 27 mm wide focal plane) with a triple grating turret. The gratings are 300, 600, 1200 grooves/mm. The

charge-coupled detector (Model 256HB) is mounted at exit port of a 0.300 m monochromator (Model SpctroPro-300i) and controlled by Roper Scientific WinSpecd/32 v.2.5 software. Light is detected from the plasma to optical emission spectroscopy by optical fiber cable with one end connected to the entrance slit of monochromator and another end mounted on the top plate of the Pyrex cross reactor chamber by means of a Cajon ultra-torr fitting. The light detection head of the optical fiber cable mounted on the top plate pointed to the space between the two electrodes. Since the optical fiber cable was off the top plate center by 3 cm, the position to the light detection was adjusted simply by rotating the top plate so that OES spectra from different luminous regions between the cathode and anode could be measured.

6.2.2.3. DC plasma polymerization process in flow / closed reactor system

The reactor system pressure achieved below 10 mTorr before each treatment in flow / closed system. Hydrocarbon monomers including methane (CH_4), ethane (C_2H_6), butane (C_4H_{10}), ethylene (C_2H_4), acetylene (C_2H_2) were started with the desired flow rate and were maintained by mass flow controllers. The flow system treatments except optical emission detection were conducted in bell jar-type reactor. In flow system, the system pressure was continuously adjusted by

controlling the opening of a throttle valve connected to the pumping system and the steady state flow of a consistent gas phase composition was established at a predetermined system pressure. The closed system treatments including system pressure detection, OES analysis, and thickness/refractive index of plasma polymer coatings were conducted in pyrex cross reactor. For the closed system treatments, the main valve of the reactor was closed to accede the reactor to fill with the monomer gas. When the reactor has reached the desired pressure, the valve on the monomer inlet flow would be closed. Power was produced to form plasma for a certain period. After treatments, the reactor system pressure was evacuated to 9-10 mTorr then the vacuum was released and panels were taken out from the reactor.

6.2.3. Deposition Rate Measurement

The surface of cathode and anode was wiped with Kimwipes® tissue paper imbued with acetone. The silicon wafer strips used as substrates were also cleaned with acetone wipe and attached to the electrode surfaces by using conductive silver paint. For the purpose of thickness and refractive index measurement, a null-seeking type AutoEL-II Automatic Ellipsometer (Rudolph Research Corporation, Flanders, NJ) with a 632.8 nm helium-neon laser light source was

utilized. The deposition rate of plasma polymers was calculated from the average film thickness by integral method divided by the deposition time.

6.2.4 Electrical Breakdown Measurement

The breakdown voltage is a function of the product of the gas pressure and the electrode distance. The breakdown curve of DC plasma polymerization system would be measured by varying the gas pressure, and the distance between the electrodes being fixed. In the attempt to understand the electrical breakdown voltage in DC plasma polymerization system, the measurements were taken using diverse hydrocarbons, including methane (CH4), ethane (C2H6), butane (C4H10) and ethylene (C2H4) that relate the minimum voltage required to spark across a gap between the electrodes. The minimum voltage was plotted versus the pressure value in different hydrocarbon monomers.

6.3. Results and Discussion

6.3.1. Glow characteristics of DC hydrocarbon plasma polymerization systems

The pictorial views of the DC hydrocarbon plasma polymerization systems are as shown in Fig. 6.1. The obvious cathode glow on the cathode surface forms

the primary glow in all DC hydrocarbon plasma polymerization systems as shown in Fig. 6.1. In DC hydrocarbon plasma polymerization systems, the cathode glow where was attached to the cathode surface indicated that cathode glow is a low energy glow owing to its intimate position from the cathode. Since the low-energy electron in the cathode fall region could become energetic enough to dissociate an organic molecule far before it acquires enough energy to ionize the vapor, the dissociation should occur much more preferably than ionization in plasma-polymerization system [1-3]. For this reason, the primary cathode glow in DC hydrocarbon plasma polymerization systems should be defined as low energy dissociation glow due to the dissociation of hydrocarbon gas molecules caused by low energy electron impactions. Besides, the secondary glow, which exists away from the cathode in DC hydrocarbon plasma polymerization systems, can be designated as negative glow because of the same location where the negative glow was observed in DC argon glow discharge [1]. The negative glow is reasonable to recognize as an high-energy ionization glow [1-3]. It can be also observed in Figure 1; the relative intensity of both cathode glow and negative glow varies with hydrocarbon monomer molecular structures. In DC hydrocarbon plasma

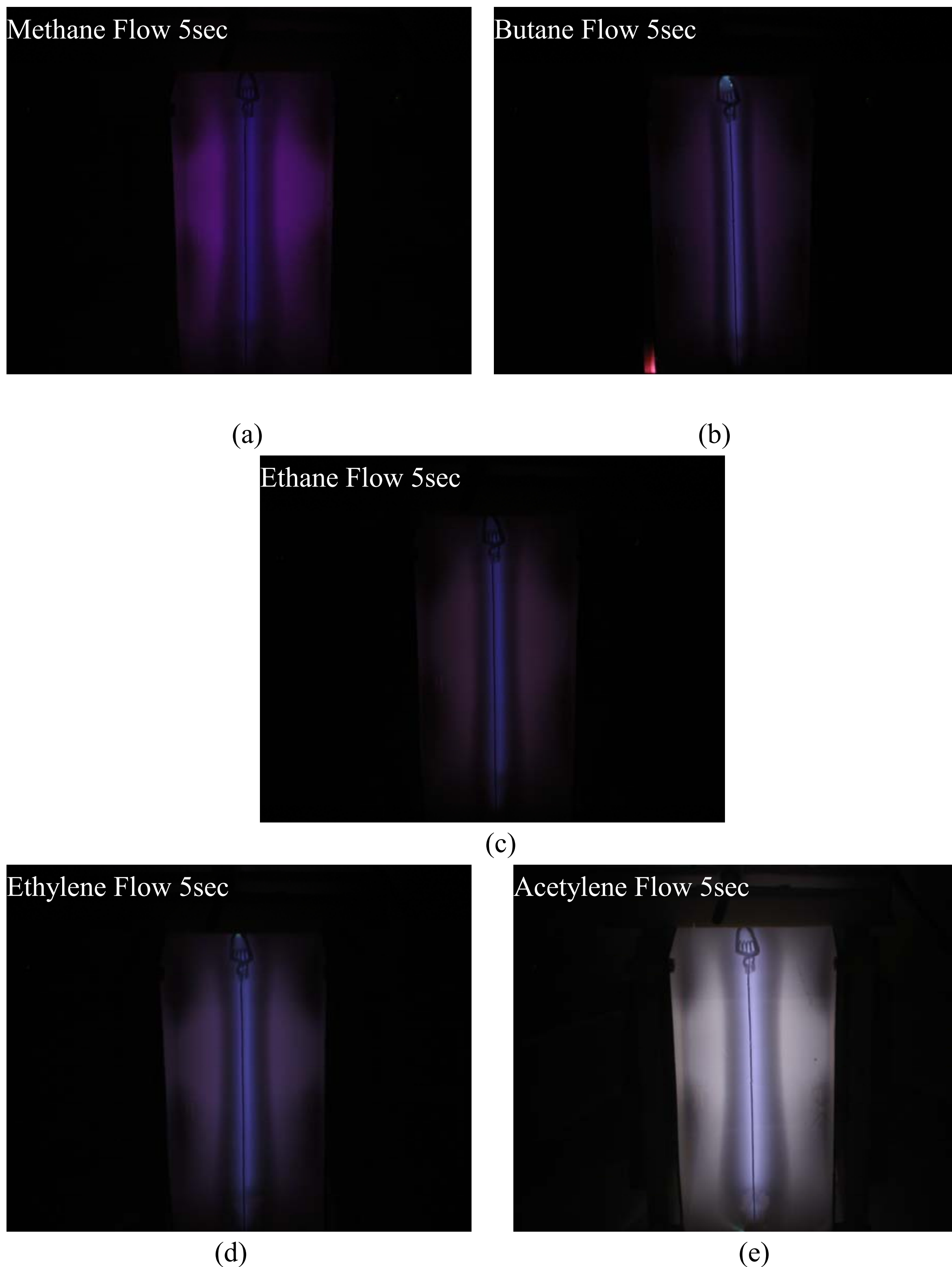

Figure 6. 1. Pictorial view of DC glow discharge with different hydrocarbon monomers (a) methane (b)butane (c) ethane (d) ethylene (e) acetylene. Conditions are 1 sccm Flow System 50 mT, DC 5 Watt.

polymerization systems, both cathode glow and negative glow intensified with hydrocarbon monomer molecular structures change, acetylene (triple bond) > ethylene (double bond)> ethane (single bond). On the contrary, the cathode glows exhibited the similar intensity while the H/C ratio of saturated hydrocarbon monomers decreased from CH_4 (H/C = 4) to C_4H_{10} (H/C = 2.5). The significant glow characteristics of DC hydrocarbon plasma polymerization systems have the insightful inference that elucidates the glow discharge formation from the organic molecules and the dissociation process to form the plasma polymer deposition in plasma polymerization system.

6.3.2. Optical emission features of DC hydrocarbon plasma polymerization systems

The luminous gas phase has been mostly described in terms such as low-pressure plasma, non-equilibrium plasma, glow discharge plasma, and so forth [7]. However, the influence of the luminous gas phase to plasma deposition features has not been fully understood. The photo-emitting species are vitally important in luminous gas phase, and the location of the luminous gas phase indicates where the chemically reactive species reaction occurs with the

inter-electrode space [3]. To distinguish the photo-emitting species, and thus indirectly measure the chemical composition of the cathode glow and negative glow in the DC plasma polymerization system, an optical emission spectrometry (OES) was used as plasma diagnostic. The OES spectra measured from cathode glow and negative glow in DC hydrocarbon plasma polymerization systems are as shown in Figs. 6.2-6.3. The optical emission spectra of DC hydrocarbon plasmas were investigated in the wavelength range from 200 nm to 1000 nm. The typical emission spectra of DC hydrocarbon glow discharges are from 300-700 nm, with no significant emission outside of this region examined. From Figs. 6.2-6.3, it can be noted that the feature of optical emission in cathode glow is entirely different from that in negative glow. From the OES spectra as shown in Fig. 6.2, the photoemission of CH free radicals that can contribute to plasma polymerization mainly appeared in the cathode glow region of the plasma systems [3]. It is supported the assumption that cathode glow is primary glow in DC hydrocarbon plasma polymerization systems owing to the electron-impact-dissociation of hydrocarbon molecules. The dissociation of molecules produces photo-emitting and chemically reactive species such as CH radicals in the cathode glow. In contrast, the foremost photoemission from the negative glow region of the plasma

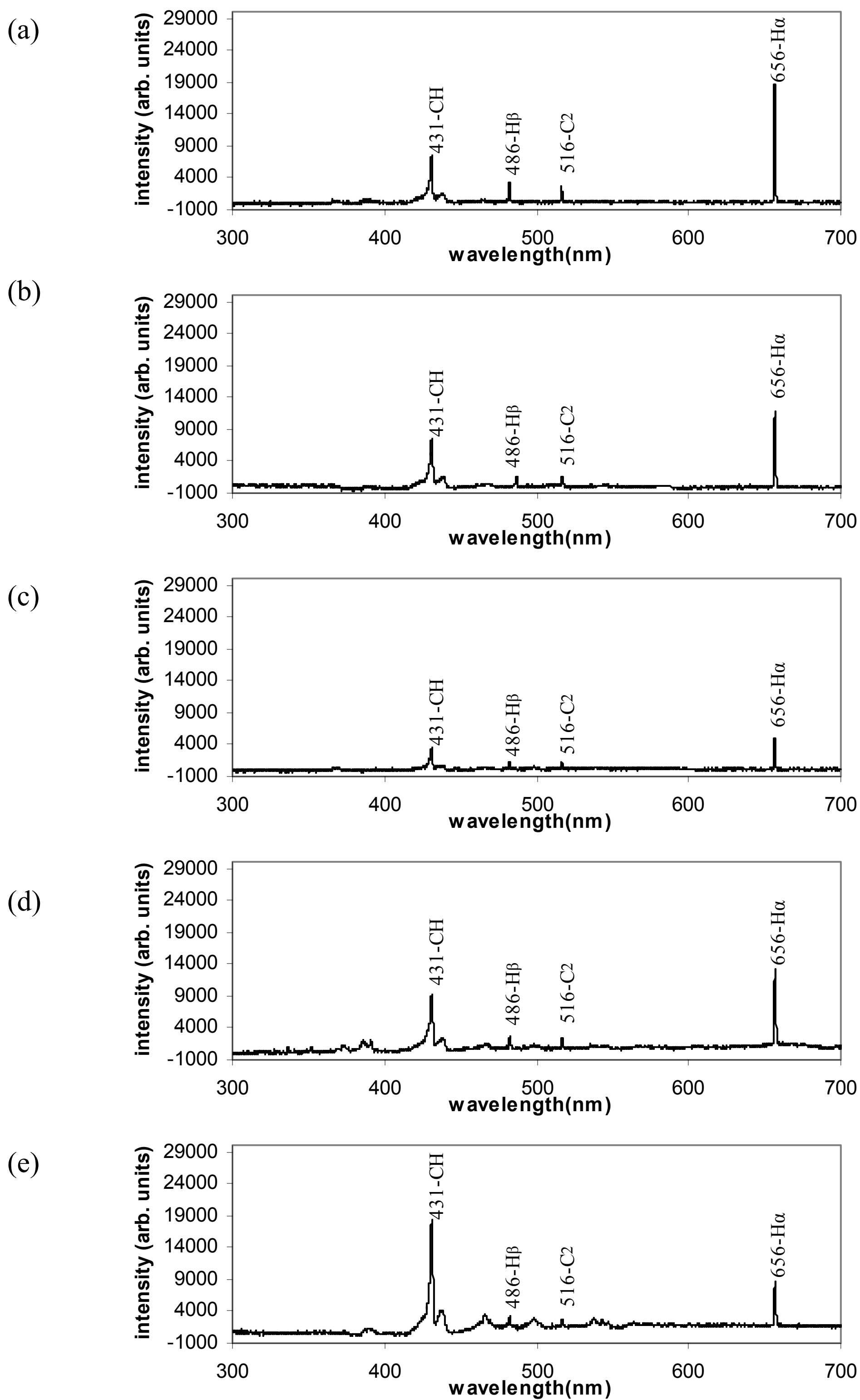

Figure 6. 2. The optical emission spectrum from cathode glow with different monomers (a) methane (b) ethane (c) n-butane (d) ethylene (e) acetylene Plasma Conditions are 1.48 sccm Flow System 69mT, DC 5Watt, 600g/mm, at 30sec.

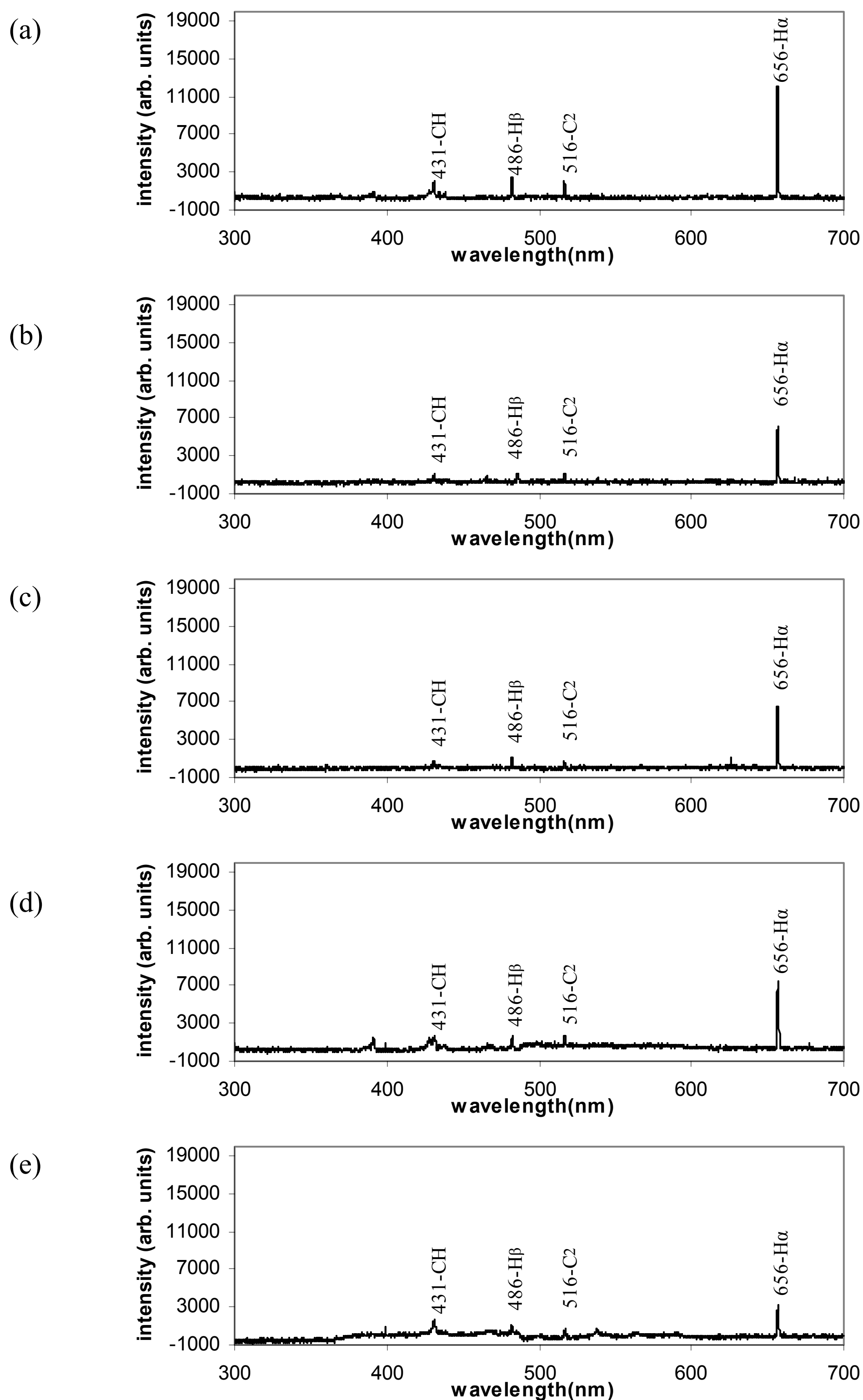

Figure 6. 3. The optical emission spectrum from negative glow with different monomers (a) methane (b) ethane (c) n-butane (d) ethylene (e) acetylene Plasma Conditions are 1.48 sccm Flow System 69mT, DC 5Watt, 600g/mm, at 30sec.

systems in Fig. 6.3 is Hα species, which is non-polymerizable. The differences between cathode glow and negative glow indicate that the major plasma polymer deposition process of DC plasma polymerization system is mainly occurred at the cathode surface, but not in the negative glow. From the optical emission spectra, the intensities of chemically reactive species such as CH A-X bands are stronger in cathode glow than those in negative glow. This further implies that, in DC hydrocarbon plasma polymerization systems, the chemically reactive species are not created by ionization, which should occurred at the edge of the negative glow, but the electron impact dissociation of molecules with low-energy electrons.

Since the cathode glow is attached to cathode surface, the electron energy level in cathode glow region is much less that in the negative glow region [1-3]. The low-energy electrons in the cathode glow are considered are primarily responsible for the dissociation of the monomer molecules and particularly these hydrocarbons. It can be also observed in Figs. 6.2-6.3, that as the distinctive glow in plasma polymerization systems, the strong cathode glow was observed in DC glow discharges of all hydrocarbon monomers examined. To further distinguish relative emission intensity change of plasma photon-emitting species in cathode glow, and thus understand the influence of H/C ratio in saturated hydrocarbon and

hydrocarbon monomer structures, the CH/H emission intensity ratio of cathode glow in various DC hydrocarbon plasma polymerizations are shown in Fig. 6.4.

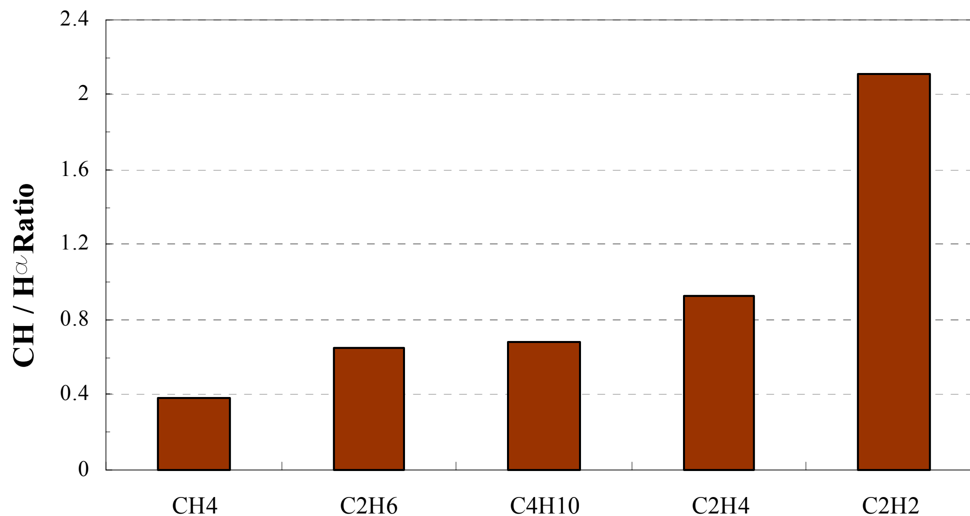

Figure 6. 4. The CH /Hα emission intensity ratio in cathode glow from DC plasma polymerization of hydrocarbon monomers including methane (CH4), ethane (C2H6), n-butane (C4H10), ethylene (C2H4), and acetylene (C2H2). Plasma Conditions are 1.48 sccm Flow System 69mT, DC 5Watt, 600g/mm, at 30sec.

From H/C ratio of saturated hydrocarbon examination, the CH/H emission intensity ratio of cathode glow decreased with the increase in the H/C ratio of saturated hydrocarbon monomers, CH_4 (H/C = 4) > C_2H_6 (H/C = 3) > C_4H_{10} (H/C = 2.5) as shown in Figure 6.4. Moreover, it was noted that the highest H/C ratio of the hydrocarbon monomers-CH_4 (H/C = 4) exhibited in DC hydrocarbon plasma polymerizations as shown in Fig. 6.1 (a) contributes the strongest H emission line in cathode glow as compared to the other DC hydrocarbon plasma polymerizations

as shown in Fig. 6.2 (a). According to OES analysis, hydrogen detachment (H/C ratio) seems to plays a key role in the glow formation of plasma polymerization system. The hydrogen detachment expresses as the hydrogen production decreases the plasma polymer deposition since stable C-H bonding of saturated hydrocarbon requires the higher electron dissociation energy (4.30 eV) to break up in plasma polymerization system [7]. In contrast, via comparison of hydrocarbon monomer structures, it can be observed that the CH/H emission intensity ratio decreases in order of acetylene (triple bond) > ethylene (double bond) > ethane (single bond) as shown in Fig. 6.4. It implies that the low energy dissociation of monomer molecules greatly occurred in cathode glow, especially the unsaturated hydrocarbons such as ethylene and acetylene since unstable π bonds (2.74 eV) in double bond/triple bond chemical structures of unsaturated hydrocarbons are much more preferably to be dissociated than stable C-C bond (3.61 eV) or C-H bond (4.30 eV) of saturated hydrocarbons in DC plasma polymerization system [7].

6.3.3. Deposition features of DC hydrocarbon plasma polymerization systems

The examination of plasma polymer deposition rate and its distribution is essential to elucidate the luminous gas phase effects on forming polymeric deposition in plasma polymerization system. The contribution of the cathode glow

(dissociation glow) and negative glow in DC plasma polymerization system can be estimated by measuring the deposition rate on both cathode and anode substrates in a series of hydrocarbon monomers. The plasma polymer deposition rate profiles of DC plasma polymerization in a series of hydrocarbon monomers are as shown in Table 6.1.

Table 6.1 Deposition rates and the ratio of relevant deposition over total deposition on cathode and anode surfaces in DC plasma polymerization of hydrocarbon monomers including methane (CH_4), ethane (C_2H_6), n-butane (C_4H_{10}), ethylene (C_2H_4), acetylene (C_2H_2). Plasma Conditions are 1 sccm Flow System 50 mT, DC 10mA voltage: 500-900 V.

Hydrocarbon monomers	Cathode Deposition Rate (nm/min)	Anode Deposition Rate (nm/min)	Total Average Deposition/ Total Area.Time (nm/ cm^2. min)	The Ratio of Relevant Deposition on Cathode (%)	The Ratio of Relevant Deposition on Anode (%)
CH_4	6.56	2.88	4.01	0.55	0.45
C_2H_6	14.29	4.52	6.94	0.67	0.33
C_4H_{10}	22.42	5.66	11.42	0.66	0.34
C_2H_4	23.60	6.75	12.31	0.64	0.36
C_2H_2	46.75	15.03	12.59	0.63	0.37

It is noted that, regardless of the kinds of hydrocarbon monomers, the deposition of plasma polymer preceded at the cathode substrate in all DC hydrocarbon plasma polymerization systems. Moreover, the deposition rates

increased the reduction in the H/C ratio of the monomers, C_4H_{10} (H/C = 2.5) > C_2H_6 (H/C = 3) > CH4 (H/C = 4). For hydrocarbon monomer structures, the deposition rates decreased in order of acetylene (triple bond) > ethylene (double bond)> ethane (single bond). These deposition rate data of DC plasma polymerization in a series of hydrocarbon monomers correlate with OES analysis in DC hydrocarbon plasma polymerization systems. It elucidates the significant relationship between the luminous gas phase and plasma polymer deposition in DC plasma polymerization system.

In DC hydrocarbon plasma polymerization systems, the relatively smaller amount of deposition occurs on the anode substrate than occurs onto the cathode as shown in Table 6.1. The ratio of relevant deposition over total deposition implies that the major deposition at cathode surface is referred to the dominant dissociation process with hydrocarbon molecules in the plasma polymerization system. Consequently, the deposition rate and relevant deposition distribution of DC hydrocarbon plasma polymerization systems are well constant with the OES examination of hydrocarbon monomers under similar operational conditions as seen in section 6.3.2.

6.3.4. System characteristics of closed DC hydrocarbon plasma polymerization reactor

In a closed system plasma polymerization, the fixed amount of monomers is contained in the reactor then glow discharge is initiated with electrical power. The system characteristics with discharge time in closed plasma polymerization system indicate the change in the overall balance between the plasma fragmentation/ablation and the plasma polymer deposition [4]. DC hydrocarbon plasma polymerizations were performed in closed reactor system in order to investigate the luminous gas phase dependence with plasma chemical species. Fig. 6.5 shows the luminous gas phase change of DC ethane plasma polymerization with discharge time. It was found that, in the initial plasma polymerization period, the cathode glow formed the primary glow of the closed reactor system. However, the cathode glow became weaker with increasing discharge time in closed reactor system. Eventually, the secondary negative glow became the dominant glow of the closed plasma polymerization system. As a result, the weaker cathode glow with increasing discharge time can be referred to the nearly consumed polymeribale species by low energy dissociation in closed reactor system. The similar luminous gas phase dependences were also acquired from the other closed

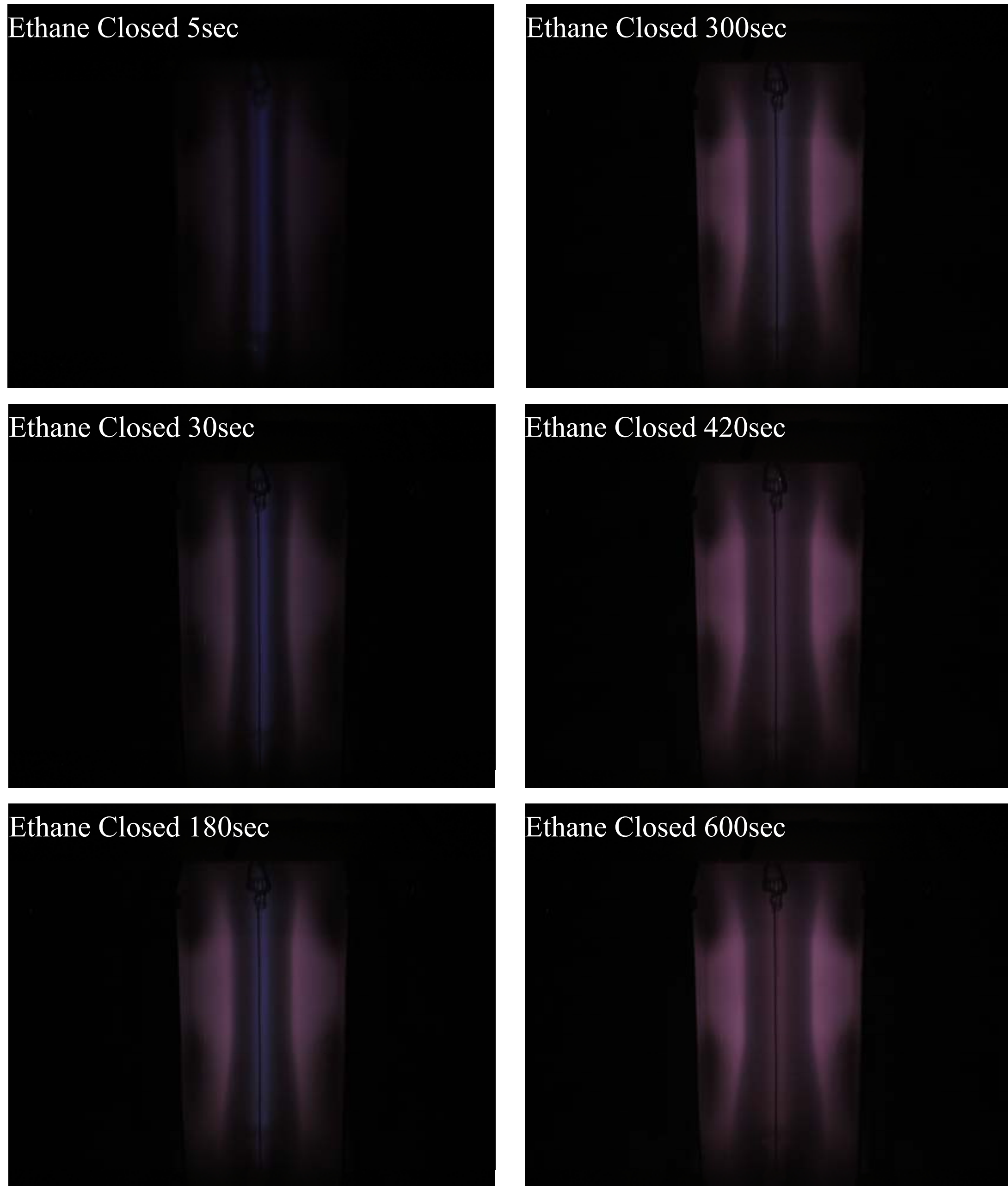

Figure 6. 5. Change of the luminous gas phase of DC ethane plasma polymerization with discharge time in the closed reactor system. Plasma Conditions: DC power 5W, 50mT ethane, Closed System.

DC hydrocarbon plasma polymerization systems including methane, butane, and ethylene.

In contrast to DC ethane plasma polymerization in closed reactor system, the luminous gas phase of DC acetylene plasma polymerization mostly extinguishes a few minutes in closed reactor system in Fig. 6.6. This is for the reason that acetylene rapidly forms plasma polymers and deposits on the wall of the reactor. When the system pressure decreases beyond a certain threshold value owing to quick consuming acetylene gas molecules, the glow discharge cannot be maintained. The noteworthy aspect that can be concluded from Fig. 6.5-6.6 is that the composition of luminous gas changes with discharge time in a plasma polymerization environment. This luminous gas phase composition change is reflected by the relative intensity change between cathode glow and negative glow with discharge time in closed DC hydrocarbon plasma polymerization systems.

Fig. 6.7 illustrates the system pressure change with discharge time in the closed reactor system of DC hydrocarbon plasma polymerizations. The system pressure increased continuously with discharge time in most of DC hydrocarbon plasma polymerizations in the closed reactor system. The increase of the system pressure with the discharge time implies the number of increased gaseous species

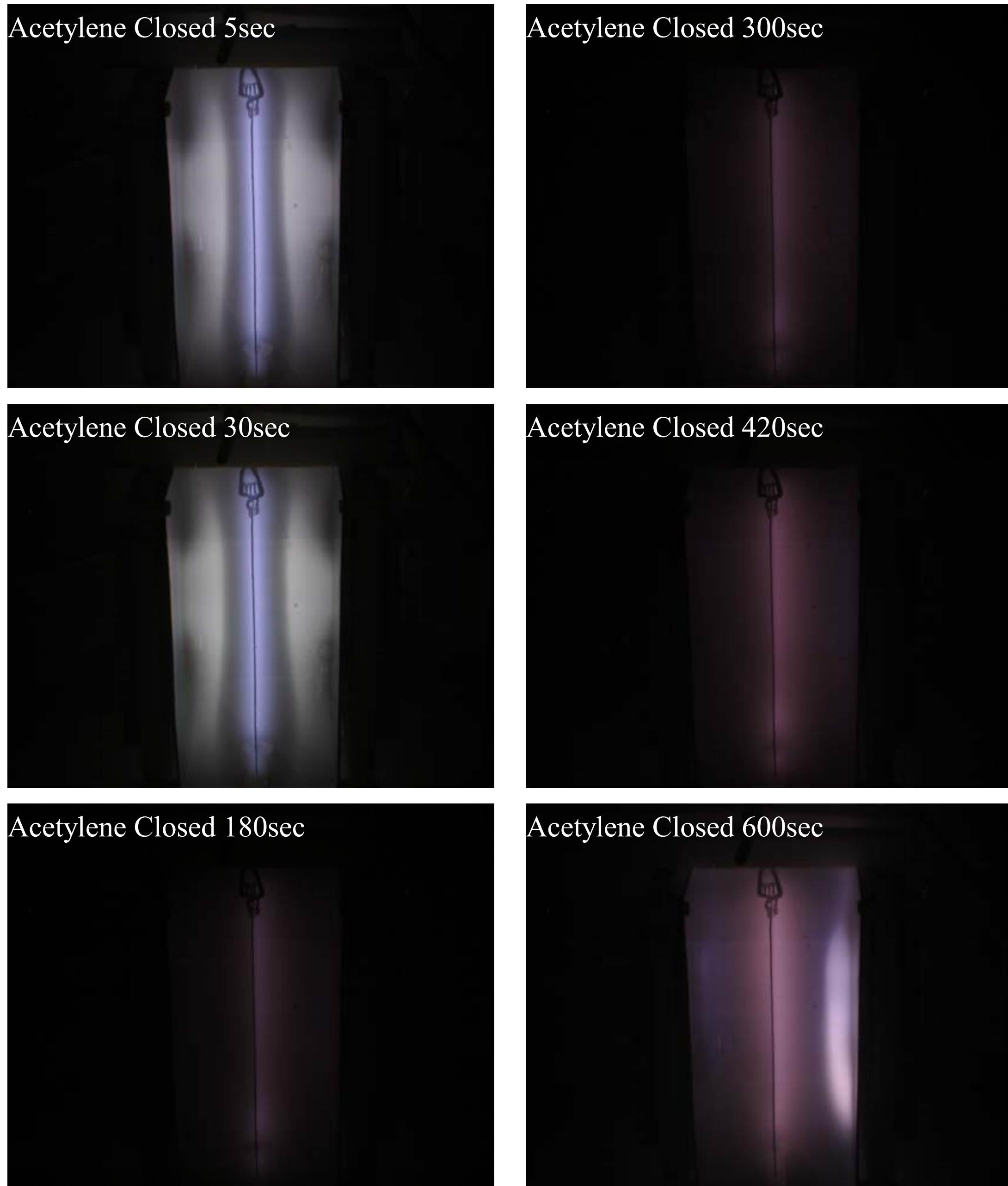

Figure 6. 6. Change of the luminous gas phase of DC acetylene plasma polymerization with discharge time in the closed reactor system. Plasma Conditions: DC power 5W, 50mT acetylene Closed System.

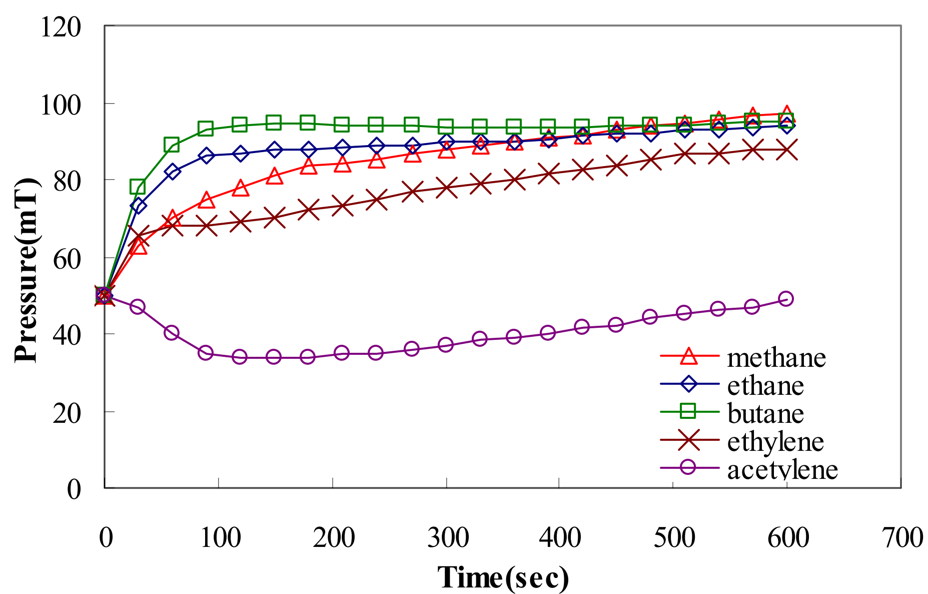

Figure 6. 7. Time dependence of system pressure of hydrocarbon monomers including methane (CH_4), ethane (C_2H_6), n-butane (C_4H_{10}), ethylene (C_2H_4), and acetylene (C_2H_2) changed with discharge time in the closed DC plasma polymerization reactor system. Plasma Conditions are Closed System 50mT, DC 5Watt.

because of the fragmentation of hydrocarbon molecules by low energy electron impact dissociation. However, the system pressure change in a closed DC acetylene plasma polymerization system is different from the other closed DC hydrocarbon plasma polymerization systems. But it is coincident to the time dependence of the luminous gas phase change in a closed reactor system. In other words, the system pressure decreases and the glow discharge diminishes in DC acetylene plasma polymerization system owing to its specific deposition feature.

Fig. 6.8 depicts the time dependence of the thickness and refractive index of DC hydrocarbon plasma polymer coatings in the closed reactor system. It is conformed to the change of luminous gas phase, the increase of plasma polymer film thickness stopped after the cathode glow, which can be referred the major cause of plasma polymer formation in DC plasma polymerization system, were becoming weaker in a closed reactor system. The high refractive index values as shown in Fig. 6.8 (b) implies the high density of DC plasma polymer films. As supported by the luminous gas phase change in the closed DC hydrocarbon plasma polymerization system, the time dependence of the thickness and refractive index of DC hydrocarbon plasma polymer coatings in Fig. 6.8 indicates that, in DC hydrocarbon plasma polymerization system, the cathode glow was mainly

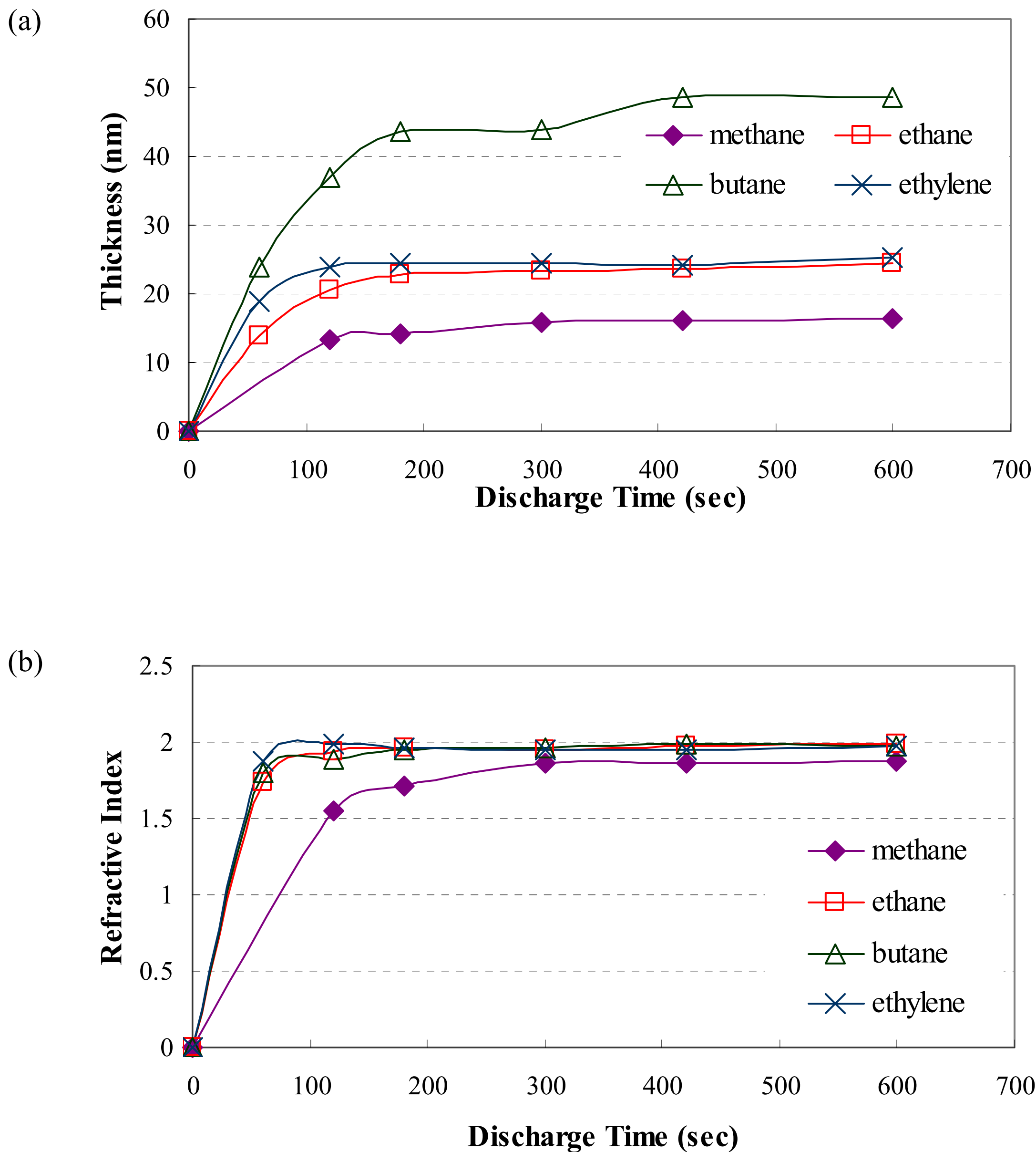

Figure 6. 8. Time dependence of (a) thickness and refractive index (b) of hydrocarbon monomers including methane (CH_4), ethane (C_2H_6), n-butane (C_4H_{10}), and ethylene (C_2H_4) changed with discharge time in the closed DC plasma polymerization reactor system. Plasma Conditions are Closed System 50mT, DC 5Watt.

associated with chemically reactive species responsible for plasma polymerization, whereas the negative glow was related to the hydrogen species that would not polymerize.

OES was used to monitor the emission intensity change of the major photo-emitting species in both glow regions of DC hydrocarbon plasma polymerizations including methane, ethane, and butane (H/C ratio in saturated hydrocarbon) in the closed reactor system. Fig. 6.9 shows the time dependence of emission intensity of CH and H species from both cathode glow and negative glow. Fig. 6.9 (a) shows the time dependence of CH emission intensity in a closed reactor system. It was found that the emission intensity from polymer-forming species such as CH radicals dramatically increased during the first 60 sec, then reached a maximum value, and weakened after 150-250 sec of discharge time in a closed reactor system. Because of the rapid deposition feature of polymer-forming species, CH radicals were consumed fast. In accordance with the change of the thickness and refractive index of DC hydrocarbon plasma polymer coatings in Fig. 6.8, CH species disappeared after a certain period of plasma polymerization due to polymeric material deposition to solid phase as indicated from the luminous gas phase change in a closed reactor system shown in Fig. 6.5.

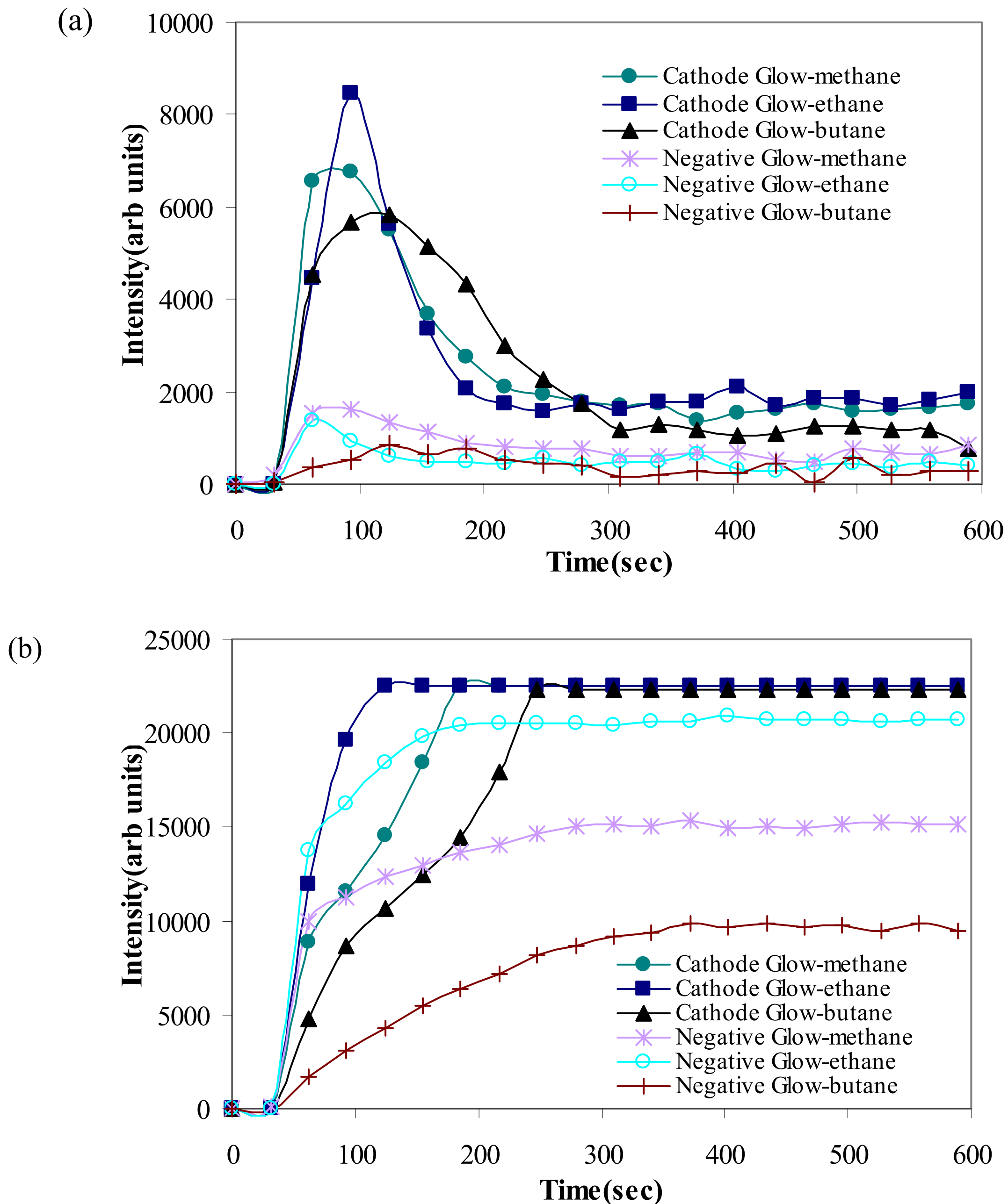

Figure 6. 9. (a) The intensity of CH species (431nm) (b) The intensity of species H_α of the different H/C ratio in saturated hydrocarbon monomers changed with discharge time. including methane (CH_4), ethane (C_2H_6), and n-butane (C_4H_{10}) changed with discharge time in the closed DC plasma polymerization reactor system. Plasma Conditions are Closed System 50mT, DC 5Watt.

From Fig. 6.9 (b), it is found that the Hα emission intensity increased abruptly and remained at the plateau after 3-5minutes. After the plateau was reached, the emission intensity of Hα line in both cathode and negative glow showed no further changes with increasing time since all hydrocarbon molecules have been consumed by plasma polymerization in a closed reactor system. It was found that Hα emission intensity in cathode glow showed sharper increase and reached its plateau earlier than that in negative glow did. Owing to Hα line is the only photo-emitting line in both glow regions, the faster intensity increase of Hα in cathode glow than that in negative glow, could also be explained by the phenomena that dissociation in cathode glow occurs prior to ionization in negative glow as discussed in previous section. It also supports the implication that dissociation in cathode glow precedes ionization in negative glow as discussed in previous section.

Fig. 6.10 shows the time dependence of the emission intensity of CH radical and Hα species in DC hydrocarbon plasma polymerizations with different hydrocarbon monomer structures (ethane, ethylene, and acetylene) in the closed reactor system. From Fig. 6.10 (a), it was clearly observed that the emission intensity of CH radical (at 431 nm) in cathode glow from acetylene has reached its

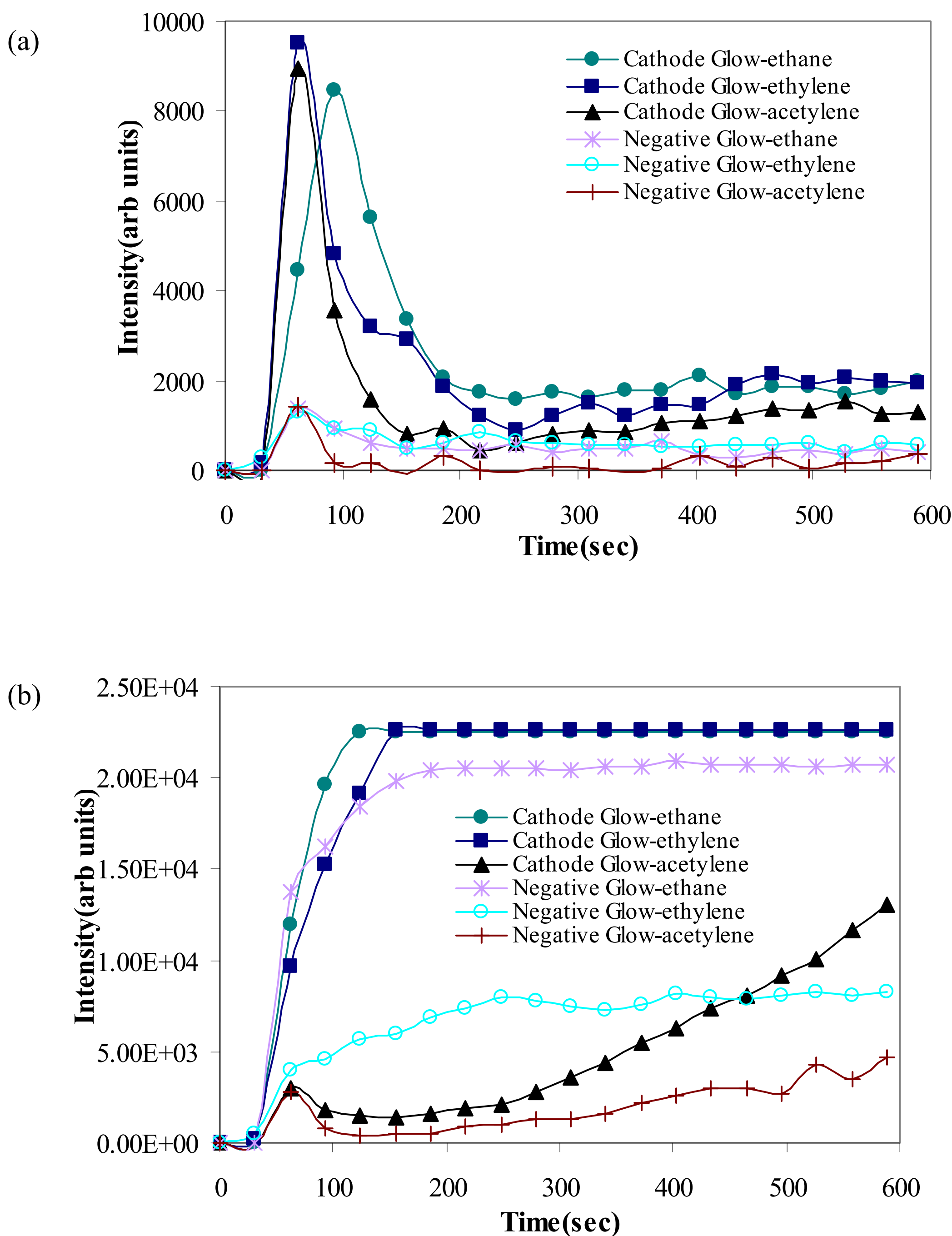

Figure 6. 10. (a) The intensity of CH species (431nm) (b) The intensity of species H_α of the different chemical structures hydrocarbon monomers including ethane (C_2H_6), ethylene (C_2H_4), and acetylene (C_2H_2) changed with time in the closed DC plasma polymerization reactor system. Plasma Conditions are Closed System 50mT, DC 5Watt.

maximum value and went down earlier than those from the others did. It could be also observed that the CH emission trend decreases in order of acetylene (triple bond) > ethylene (double bond)> ethane (single bond) as shown in Fig. 6.10 (a). From Fig. 6.10 (b), the emission intensity of Hα line in cathode glow of ethane increased sharper and reached its plateau earlier than that of ethylene. It was also noticed that the trend of Hα emission intensity was different in a closed DC acetylene glow discharge system as shown in Fig. 6.10 (b). It is suspected that the glow discharge nearly extinguished because acetylene swiftly forms plasma polymers and deposits on the wall of the reactor as described above section. Therefore, the emission intensity change results obtained in the closed plasma polymerization system further confirmed that the photo-emitting CH species are mainly responsible for the creation of polymerizable species, while the photo-emitting Hα species are related to non-polymerizable species.

6.3.5. Electrical breakdown in DC plasma polymerization system

Electrical breakdown of DC plasma system is the transition from the electrodes to a conductive state and the minimum electrical voltage at this transition is defined the breakdown voltage. The physics of the electrical breakdown has a great significance because of its application for understanding

the properties of glow discharges used for plasma processing [8]. However, the measurements of the breakdown curves of a glow discharge are mostly carried in inert gases including in helium, neon, and argon. The breakdown curves of plasma polymerization from organic molecules are still not well studied. For this reason, electrical breakdown study is carried out to gain some insights to the ionization aspects of DC hydrocarbon plasma polymerization systems.

Fig. 6.11 depicts the breakdown voltage dependence on the system pressure of DC hydrocarbon plasma polymerizations and the fixed electrode distance. The rise from the breakdown voltages at high gas system pressure occurs because the electron energy was too low to produce ionization. It can occur at high gas system pressures, because the electron collisions with gas molecules become so frequent that the electrons cannot accumulate the sufficient energy to overcome the ionization potential [9]. It is also found that the breakdown characteristics of DC hydrocarbon glow discharges are dependent on the H/C ratio of the saturated hydrocarbons and the chemical structure changes. It is clear that the minimum breakdown voltage of methane is lower than those of ethane and n-butane. The breakdown voltages with increasing gas system pressure intensified with the reduction in the H/C ratio of saturated hydrocarbons, C_4H_{10} (H/C = 2.5) > C_2H_6

(H/C = 3) > CH_4 (H/C = 4).

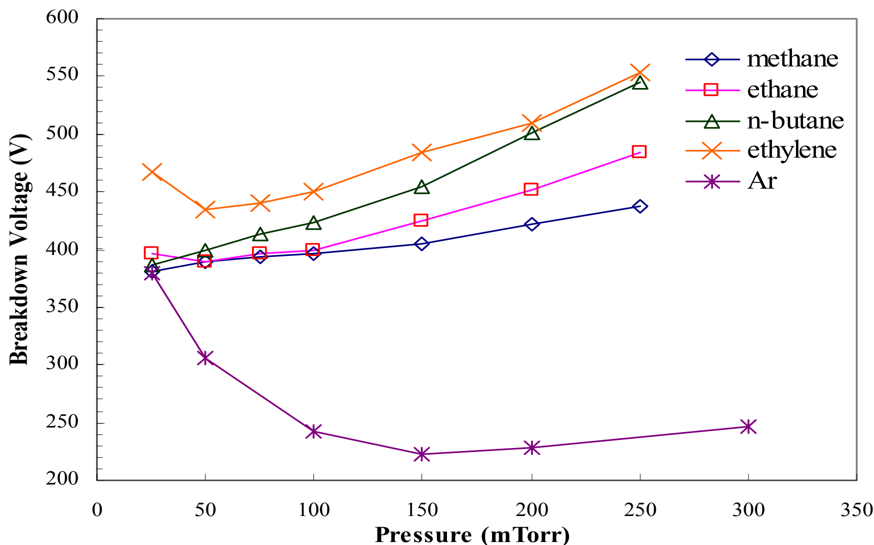

Figure 6. 11. Electrical breakdown voltage in DC plasma polymerization of hydrocarbon monomers

This can be attributed to the higher energy of the secondary ionization processes in DC plasma polymerization of ethane and n-butane as compared to that of methane. In addition, the breakdown voltages also increased while the chemical structure changes from saturated ethane to unsaturated ethylene. This is due to the different ionization potential of the various chemical structure hydrocarbon monomers. The rise from the breakdown voltages of ethane and ethylene at the lowest gas system pressure occurs because the electrodes were so small, or the gas density so low, that electrons were lost to the walls without colliding with gas atoms and producing ionization.

Based on electrical breakdown curves of DC hydrocarbon plasma polymerizations, the breakdown voltages of DC ethylene and n-butane plasma polymerizations were higher than those of DC methane and ethane plasma polymerizations. In this sense, to break down ethylene and n-butane gas molecules need more ionization energy than methane and ethane gas molecules. Therefore, the monomers that have higher electrical breakdown voltage are expected to demonstrate the slower deposition rates or less deposition referred to the ionization concept of plasma polymerization. However, Table 6.1. shows that the monomers, which have higher electrical breakdown voltage, have higher deposition rate in DC hydrocarbon plasma polymerization systems. These electrical breakdown and deposition data demonstrate that polymeric material formation reactions could be created more easily by low-energy electron-impact dissociation of organic molecules rather than by ionization in DC plasma polymerization system.

6.4. Conclusion

The DC plasma polymerization process was studied with a serious of hydrocarbon monomers including methane (CH_4), ethane (C_2H_6), n-butane (C_4H_{10}), ethylene (C_2H_4) and acetylene (C_2H_2). The study of luminous gas phase in DC

plasma polymerization systems showed that the glow discharges of organic molecules are significantly different from corresponding discharges of inert gases such as argon. The cathode glow where the low-energy electron impact dissociation occurs at cathode surface is the foremost glow in DC hydrocarbon plasma polymerization systems. In addition, the negative glow that occurred by ionization as secondary glow formed away from the cathode in DC hydrocarbon plasma polymerization systems.

OES examination on DC hydrocarbon plasma polymerization systems demonstrated that the cathode glow, which is designated as dissociation glow, is the primary glow where the main polymerizable species such as CH free radicals are formed. On the other hand, the negative glow (ionization) is where the non-polymerizable species such as H atoms were determined. The plasma polymer deposition rates obtained from cathode and anode substrates with different hydrocarbon monomers evidently indicated the cathodic dissociation glow is mainly associated with the plasma polymer deposition. The OES data obtained in this study also showed that luminous gas phase in hydrocarbon plasma polymerization system was dependent on the H/C ratio in saturated hydrocarbons and monomer molecular structures. Within a series of hydrocarbons, CH/Hα

emission intensity ratio of cathode glow decreases with molecular structures in order of triple bond> double bond > single bond, and CH/Hα emission intensity ratio increases with decreasing H/C ratio in saturated hydrocarbon monomers. The plasma polymer deposition study clearly showed the dominating effects of luminous gas phases on the polymerizable tendency in plasma polymerization system.

The luminous gas phase composition, system pressure change, deposition data, and OES analysis data acquired from the closed hydrocarbon plasma polymerization reactor evidently illustrated that the dissociation glow mainly contains polymerizable species, whereas the negative glow is related to gaseous species that would not produce plasma polymer. The electrical breakdown curves of these DC plasma polymerization processes were also investigated and correlated to the role of ionization in DC plasma polymerization of hydrocarbon monomers.

On the basis of the experimental results presented in this paper, the luminous gas phase in glow discharge reflects the major plasma chemical occurrences and has a critical influence on hydrocarbon plasma polymerization characteristics. The dissociation reaction of hydrocarbon monomers occurred in the primary cathode

glow precedes the ionization in the secondary negative glow region in hydrocarbon plasma polymerization system.

Acknowledgement

This study was supported by the University of Missouri Research Board. The authors express their appreciation to Professor Hirotsugu Yasuda at the University of Missouri–Columbia for his helpful discussions of this work.

6.6. Reference

1.Yasuda, H.; Yu, Q.S. J Vac Sci Technol A 2004, 22, 472-476.

2.Yasuda, H.; Yu, Q.S. Plasma Chem and Plasma Processing 2004, 24, 325-351.

3.Yu, Q. S.; Huang, C.; Yasuda, H. K. J Polym Sci, Part A: Polym Chem 2004, 42, 1042-1052.

4.Yu, Q.S.; Moffitt, C. E.; Wieliczka, D. M.; Yasuda, H. J Vac Sci Technol A 2001, 19, 2163-2167.

5.Yasuda, H. K.; Yu, Q. S. J Vac Sci Technol A 2001, 19, 773-781.

6.Tao, W.H.; Prelas, M. A.; Yasuda, H.K. J Vac Sci Technol A 1996, 14, 2113-2121.

7.Yasuda, H. Luminous Chemical Vapor Deposition and Interface Engineering; Marcel Dekker: New York, 2005; pp 1-28.

8.Madou, M. Fundamentals of Microfabrication; Imperial Coll. Sci. Technol. Med: London, 1998; pp 81-86.

9. Tao, W.H.; Yasuda, H. Plasma Chem and Plasma Processing 2002, 22, 313-333.

CHAPTER 7

THE ANALYSIS AGING PHENOMENA IN GAS DECTORS FROM DIRECT CURRENT PLASMA POLYMERIZATION INVESTIGATIONS

7.1. Introduction

Gas detectors have been used for a long time in modern particle physics researches [1]. The aging effects occurred in the gas detector system were the performance degradations since the detection wire would be coated by the deposition in gas discharge. The common aging phenomena in the gas detectors led to the relevance of this issue to the existing coating layers on the electrodes, possibly induced by the plasma polymerization in the gas system. The deposition on electrodes observed in gas detector system appears to have similar properties to those created in plasma polymerization system. It designates that a qualitative approach to the aging effects based on plasma polymerization could be used to realize the origin of aging phenomena [1,2]. Although high frequency plasma polymerizations have numerous attentions on plasma processing researches, a direct current plasma polymerization would be much suitable candidate to investigate phenomena drawn in the aging effects of gas detectors. The direct current plasma at low-pressure could be used for understanding plasma

polymerization system while the surroundings of the anode detection wire in gas detectors might be considered as a direct current plasma at 1 atmosphere [1]. Although many operational parameters such as electric field, electron density, and current density are greatly diverse in two plasma systems, the free radicals that contribute in plasma polymer formation are mainly active species involved in both plasma systems.

The recent investigations on plasma polymerization of DC trimethylsilane (TMS) glow discharge indicate that roughly 80% of materials deposition is cathode deposition because the dissociate glow is the main glow that touches the cathode. The anode is a passive surface so far as the deposition is concerned [3]. Although anode deposition is less important in practical use of DC plasma polymerization, it is believed to be the major factor in the aging phenomenon encountered in the expensive multiwire gas detectors, which takes years to build and prevailingly used in nuclear science and high energy physics research to investigate collision processes in the interior of matter [2,4]. In a multiwire gas detector, electron avalanche occurs near the anode wire leads to the degradation of detectors, such as the appearance of local and permanent damages, excessive currents, gradually loss of energy resolution, and decrease and non-uniformity of

the gas gain. The classical aging effects could be recognized the consequence of chemical reactions occurring in gas discharge in wire chambers conducting to the deposition on anode surfaces [5]. Lack of knowledge about anode deposition, particularly as a function of the molecular structure of gases used, is the main hurdle in solving the aging phenomena of gas detectors.

In gas detector system, hydrocarbons were added into noble gases such as argon in order to obtain high gas gains and frequently observed the aging phenomena. There are various researches that clearly determine early aging in Ar/CH4 mixtures and the aging rate of Ar/CH4 mixtures is a function of current density [6-8]. This observation indicates that methane polymerizes itself in plasma state and there is a great tendency to polymerize for all hydrocarbon gases. CF4 that obtains high primary ionization and excellent aging resistance was expected to be the aging effect preventing agent. However, the polymeric formation on the cathode and anode surfaces was observed in CF4/CH4 and Ar/CF4/CO2 mixture in the high rate HERA-B [9-10]. For that reason, the plasma polymerization study of hydrocarbons and perfluorocarbons becomes essential to be acquainted with the complicated processes of aging phenomena in gas detector system.

Understanding of the extensive effects of DC plasma polymerization such as

luminous gas phases, electrical breakdown, and plasma polymer deposition distribution is believed to provide new perceptibility into the aging effects. From this aspect, we are attempting to clarify this situation in the research reported in this paper by taking a novel approach to direct current plasma polymerization.

7.2. Experimental setup

7.2.1 Materials

The cathode electrodes used in this study were unpolished cold roll steel (CRS) panels (10.2 cm × 15.2 cm × 0.08 cm), which were procured from Q-Panel (Q-Panel Lab Products, Cleveland, OH). Inert gas argon (Ar, 99.9%) procured from Airgas Inc.and monomers used for the DC plasma polymerization processes were methane (CH_4, 99% purity), butane (99.5% purity), and ethane (C_2H_6, >99% purity), purchased from Matheson Inc. and ethylene (C_2H_4, 99.995% purity) purchased from Praxair Inc. Hexafluoropropene (C_3F_6 98% purity) and hexafluoropropene oxide (C_3F_6O 97% purity), which were obtained from Lancaster Synthesis Inc. . All the gases were used as received without any further purification.

7.2.2. DC plasma polymerization reactor for deposition and electrical breakdown studies

A low temperature DC plasma technique was used in this study to perform

plasma polymerization of various hydrocarbons monomers. The DC plasma reactor system used in this study was a bell jar-type reactor, with dimension of 46 cm in height and 44.5 cm in diameter. The CRS panel was used as the center electrode, which is also the cathode in DC plasma chemical vapor deposition. The two counter electrodes consisting of a pair of titanium (Ti) plates (17.9. cm × 17.9 cm × 0.08 cm) were placed 10 cm apart. While a new cathode panel was used in each trial, the two anode electrodes remained the same for the entire series of this study. The DC power was supplied by MDX-1K magnetron drive (Advanced Energy Industries, Inc.). In the breakdown voltage study, the electrodes were fabricated from titanium disks 0.2 cm thick and 13.3 cm diameter. One of two titanium disks was used as cathode and another as anode. The inter-electrode distance was 4.5 cm. The power supply used in this study was Pd 1556C (Power Design Inc.) for the breakdown voltage treatment. The HP digital 3435A multimeter was used for measuring the breakdown voltage.

Before each plasma polymerization process, the reactor system was first evacuated to less than 1 mTorr using a vacuum system consisting of a mechanical and booster pump work in series. The flow rates of various monomers were then allowed to flow into the reactor, at which the system pressure was varied by

adjusting the pressure controller. The reactor was once again evacuated to its background pressure after each process; the cathode and anodes were carefully removed from the chamber. The silicon wafer strips were detached from the electrodes and the thickness was subsequently measured on different spots at 1-cm increment away from the center.

7.2.3 Electrical Breakdown Measurement

The breakdown voltage is a function of the product of the gas pressure and the electrode distance. The breakdown curve of DC plasma polymerization system would be measured by varying the gas pressure, and the distance between the electrodes being fixed. In the attempt to understand the electrical breakdown voltage in DC plasma polymerization system, the measurements were taken using diverse hydrocarbons and perfluorocarbons, including methane (CH_4), ethane (C_2H_6), n-butane (C_4H_{10}), ethylene (C_2H_4), hexafluoropropylene (C_3F_6), and hexafluoropropylene oxide (C_3F_6O) that relate the minimum voltage required to spark across a gap between the electrodes. The minimum voltage was plotted versus the pressure value in different hydrocarbon monomers.

7.2.4 Deposition Rate Measurements

The surface of cathode and anode was wiped with Kimwipes® tissue paper

imbued with acetone. The silicon wafer strips used as substrates were also cleaned with acetone wipe and attached to the electrode surfaces by using conductive silver paint. For the purpose of thickness and refractive index measurement, a null-seeking type AutoEL-II Automatic Ellipsometer (Rudolph Research Corporation, Flanders, NJ) with a 632.8 nm helium-neon laser light source was utilized. The deposition rate of plasma polymers was calculated from the average film thickness by integral method divided by the deposition time.

7.3. Results and Discussion

7.3.1. Luminous gas phase of DC plasma polymer polymerization systems

In plasma state, the luminous gas phase is where most plasma reactions are involved; for this reason, the examination of the nature of glow becomes important to demonstrate the fundamental aspects of plasma polymerization system. Fig.7.1 represents the luminous gas phase in DC glow discharge of argon with one cathode located in the middle of two enhanced magnetron anodes. It was clearly observed that the center cathode was surrounded by a dark space in DC argon glow discharge (see in Fig.7.1). Meanwhile, a characteristic funnel-shaped negative glow appears away from the cathode on both sides since the two enhanced magnetron anodes are used against one center cathode panel. In DC

argon glow discharge, the secondary electrons are emitted from the cathode surface by the impinging ions created by the ionization of gas that occurs at the fringe of negative glow [11]. In other wards, the negative glow of DC argon glow discharge is reasonable to recognize as a high-energy glow (ionization glow) and its appearance can be explained well by the mechanisms of ionization of Ar [11-12].

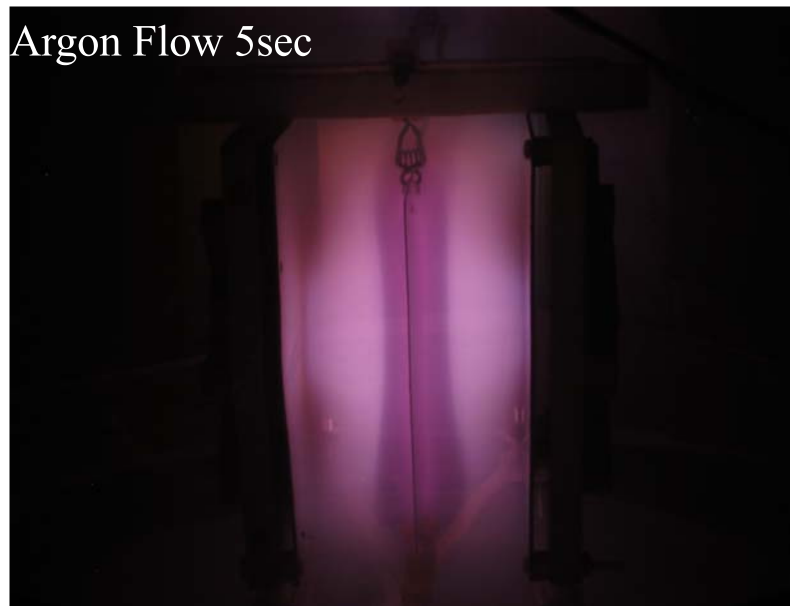

Figure 7. 1. Pictorial view of DC glow discharge of argon. Plasma Conditions: Input gas: 1 sccm argon, DC power 5 W, 50 mT Flow System

Fig.7.2-7.5 represents the luminous gas phase in a DC plasma hydrocarbon and perfluorocarbon polymerization systems with the additive magnetron

enhancing-electrode arrangement in the same reactor setup as shown in Fig.7.1. The obvious cathode glow on the cathode surface forms the primary glow in all DC homogeneous hydrocarbon and perfluorocarbon plasma polymerization systems as shown in Fig.7.2-7.5. In addition, the secondary glow, which exists away from the cathode in DC homogeneous hydrocarbon and perfluorocarbon plasma polymerization systems, can be designated as negative glow because of the same location where the negative glow was observed in DC argon glow discharge in Fig.7.1. The shutter speed, aperture, and the film speed were all set up on the same condition to result in the comparable photographs. The coincident luminous gas phases were also acquired from DC glow discharge systems of a homogeneous series of hydrocarbon monomers together with ethane and ethylene. Cathode glow can be considered low-energy glow, whose energy is at the level of the dissociation energy of bonds involved in a hydrocarbon and fluorocarbon molecules, and can be designated molecular dissociation glow. Since the low-energy electron in the cathode fall region could become energetic enough to dissociate an organic molecule far before it acquires enough energy to ionize the

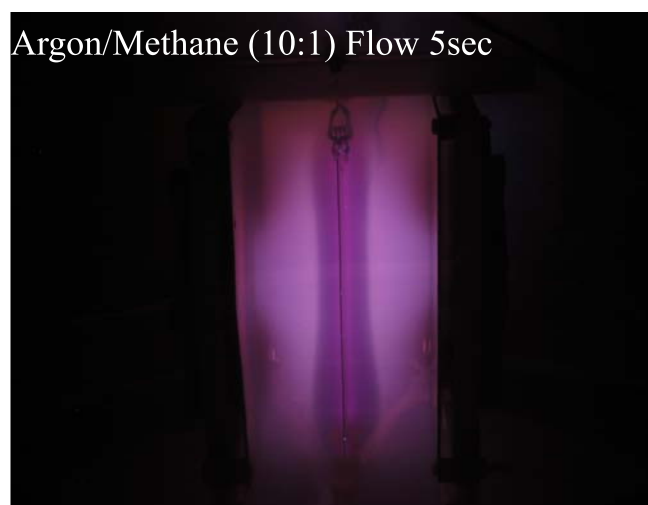

Figure 7. 2. The luminous gas phase of DC plasma polymerization. Plasma Conditions: Input gas: 1sccm methane, 1sccm methane+ 10sccm argon, DC power 5W, 50mT Flow System

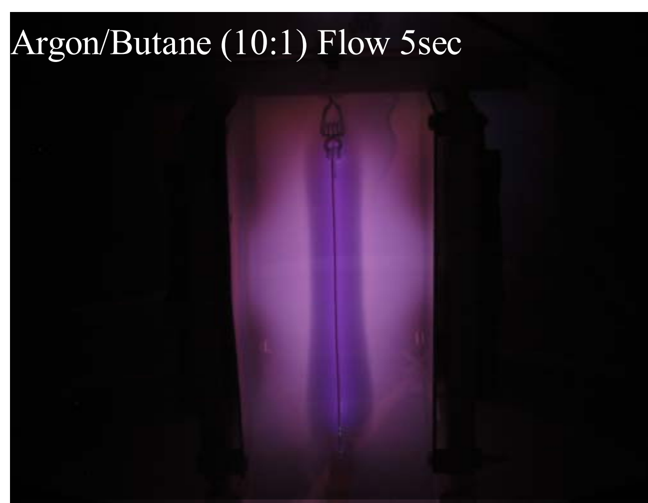

Figure 7. 3. The luminous gas phase of DC plasma polymerization. Plasma Conditions: Input gas: 1sccm butane, 1sccm butane + 10sccm argon, DC power 5W, 50mT Flow System

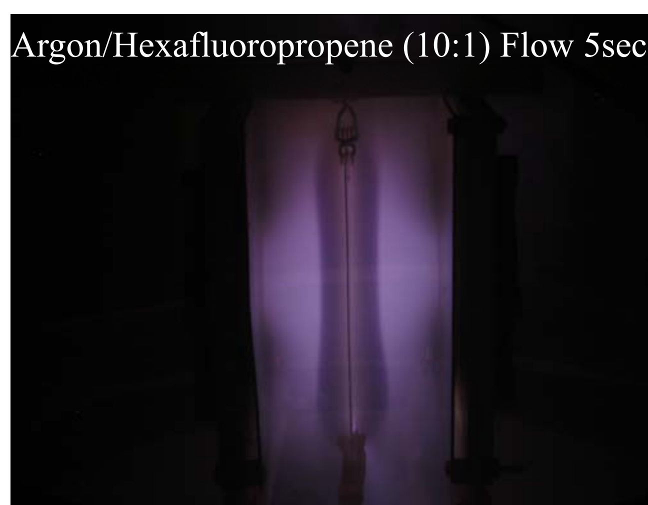

Figure 7. 4. The luminous gas phase of DC plasma polymerization. Plasma Conditions: Input gas: 1sccm hexafluoropropene, 1sccm hexafluoropropene + 10sccm argon, DC power 5W, 50mT Flow System

Figure 7. 5. The luminous gas phase of DC plasma polymerization. Plasma Conditions: Input gas: 1sccm hexafluoropropene oxide, 1sccm hexafluoropropene oxide + 10sccm argon, DC power 5W, 50mT Flow System

vapor, the dissociation should occur much more preferably than ionization in plasma-polymerization system [11-12]. As a result, the significant glowcharacteristics of DC hydrocarbon and perfluorocarbon plasma polymerizations have the discerning implication that elucidates the glow discharge formation from the organic molecules and the dissociation process to form the plasma polymer deposition in plasma polymerization system.

The luminous gas phase in DC plasma polymerization system is related to the nature of monomers and reactive gases. Inert gases such as Ar do not form the molecular dissociate glow; the addition of inert gas to homogeneous hydrocarbon /perfluorocarbon monomers entirely alter the basic glow characteristics in DC plasma polymerization systems. It can be clearly observed that the effect of adding argon to DC glow discharges of homogeneous hydrocarbon/perfluorocarbon monomers such as methane, n-butane, hexafluoropropylene, and hexafluoropropylene oxide, the glow intensity and the glow volume are very different to those of DC homogeneous hydrocarbon/perfluorocarbon and pure argon glow discharges. The secondary negative glow intensity becomes much stronger and glow volume extends in DC Ar+ hydrocarbon/perfluorocarbon plasma polymerization systems since Ar additive gas only forms negative glow.

Moreover, both distinct glow characteristics (cathode glow and negative glow) appeared in the luminous phase of argon additive plasma polymerizations indicates that gaseous mixture occurred dissociation as well as ionization in plasma state.

7.3.2. Electrical breakdown voltage analysis

In a multiwire gas detector, electrons created by the passage of energetic particles must be amplified to be detected. For electron amplification, high DC voltage is applied between the cathode (cylindrical wall of detector) and anodes (numerous small diameter wires) in an inert gas at atmospheric pressure. Organic gas or gases are added to an inert gas in order to increase the electron amplification that results from electron avalanche and improve the stability of the gas by preventing catastrophic break down of the total gas phase. These two objectives seem to contradict each other if we examine this electron amplification at atmospheric pressure from the view point of DC glow discharge at a reduced pressure, we could find important fundamental factors which are often not recognized but help in understanding the detector aging processes and its origins.

The deposition of polymeric coating layer on the electrodes in the gas detector seem to be caused by the molecular dissociation of organic molecules in

the localized break down gas phase. The concept of the rigidity and resistivity of breakdown gas phase for a specific gas mixture could play a vital role for aging phenomena in gas detector system. Therefore, the breakdown voltage measurement using different gas mixture in DC plasma polymerization system was crucial to examine. In the attempt to understand the electrical breakdown voltage in DC plasma polymerization system, the measurements were taken using hydrocarbons and fluorocarbons, including methane (CH_4), ethane (C_2H_6), ethylene (C_2H_4), hexafluoropropylene (C_3F_6), and hexafluoropropylene oxide (C_3F_6O) and their mixture with argon that relate the minimum voltage required to spark across a gap between the electrodes. The minimum voltage was plotted versus the pressure value in different gas compositions.

Figs 7.6 –7.7 shows the minimum voltage required for electrical breakdown of argon inert gas, homogeneous hydrocarbon and perfluorocarbon monomers, and their mixture with argon in DC plasma polymerization systems. First, it is interesting to note that Ar obtains the lowest breakdown voltage among gases list in Figs 7.6 –7.7. In DC glow discharge of argon, the ionization occurs at the edge of negative glow (ionization glow). Where the electron temperature is the highest but electron density is low. The electron density increases sharply near the anode

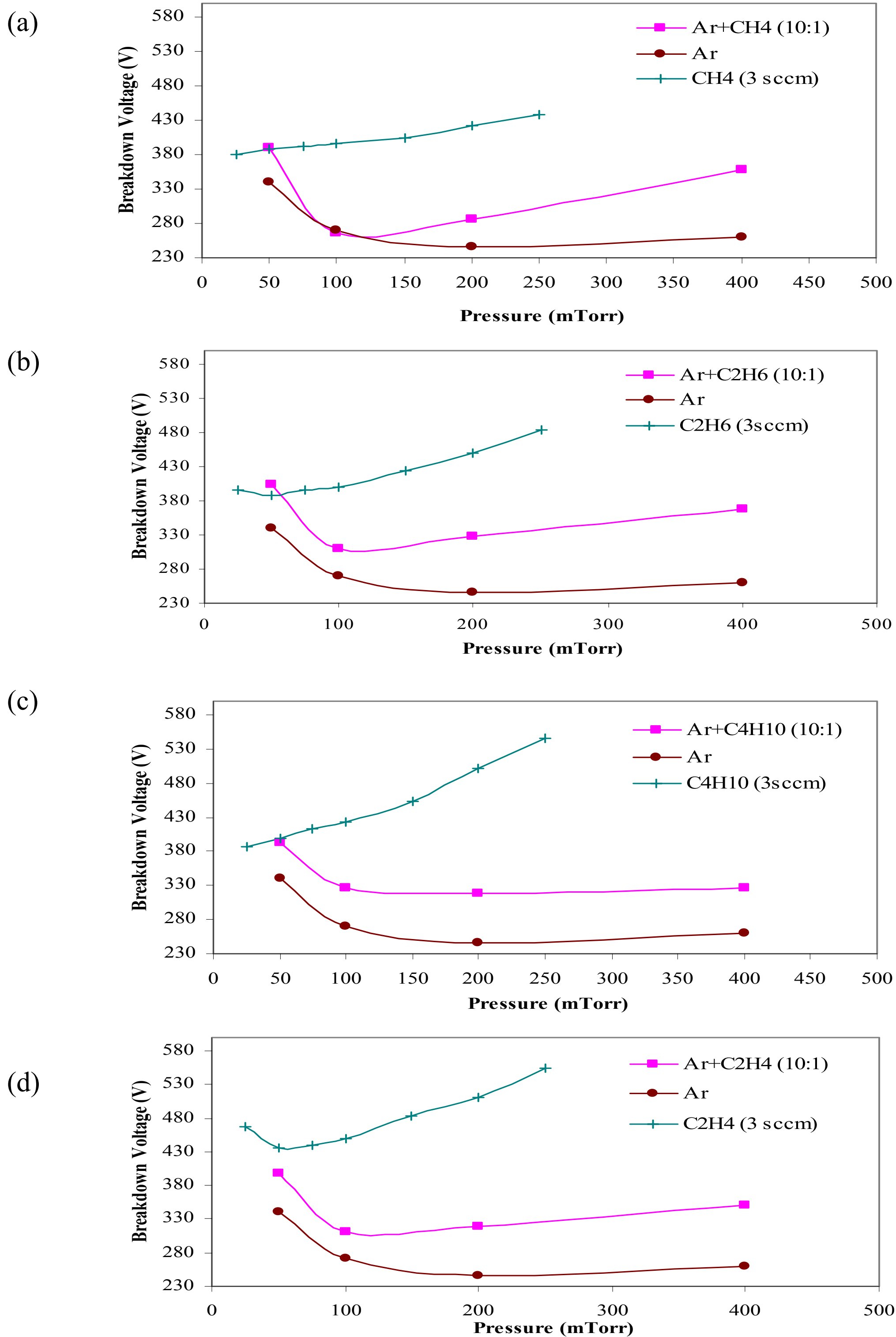

Figure 7. 6. Electrical breakdown voltage measurements for argon and hydrocarbons, and their mixtures (a) methane (b) ethane (c) butane (d) ethylene Plasma Conditions: Input gas: 10sccm argon, 1sccm hydrocarbon monomer, 1sccm hydrocarbon monomer + 10sccm argon, DC power, Flow System

(a)

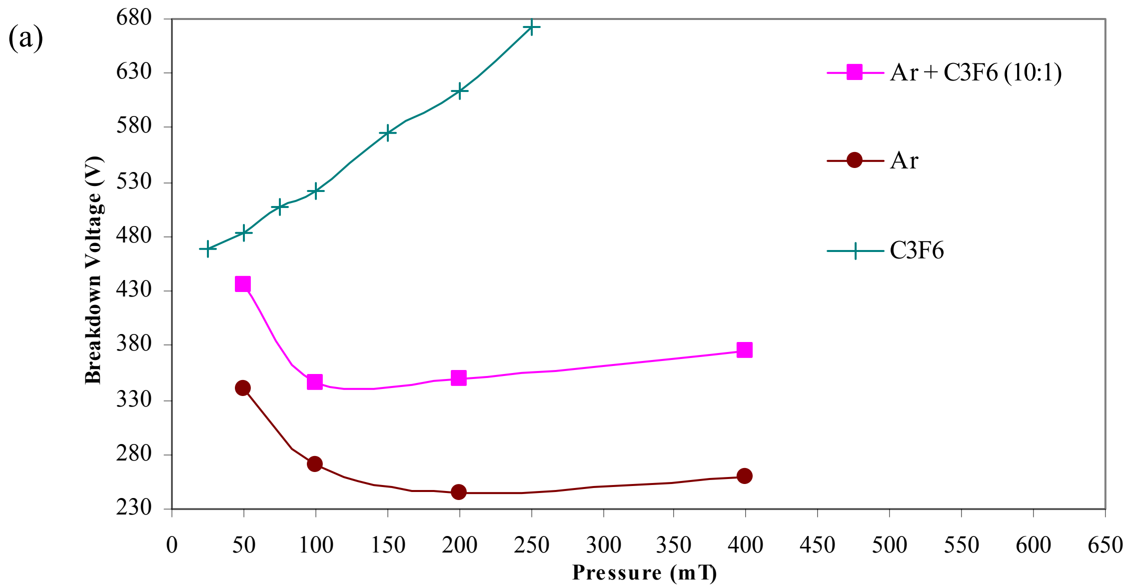

(b)

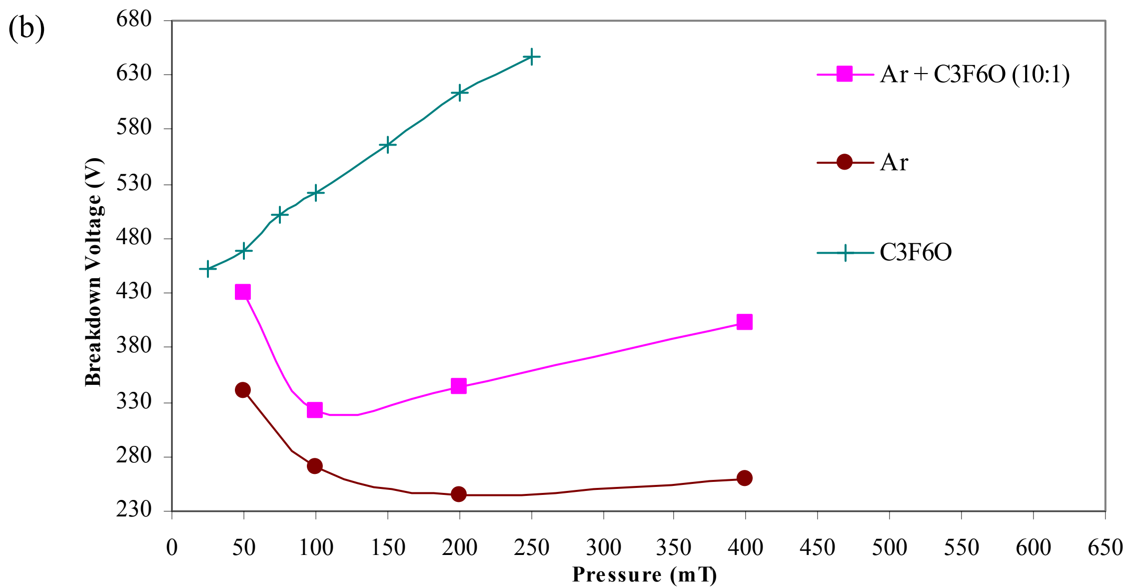

Figure 7. 7. Electrical breakdown voltage measurements for argon and fluorocarbons, and their mixtures (a) hexafluoropropylene (b) hexafluoropropylene oxide Plasma Conditions: Input gas: 10sccm argon, 1sccm fluorocarbon monomer, 1sccm fluorocarbon monomer + 10sccm argon, DC power, Flow System

surface, but electron temperature remains low. Since the electrical field is low beyond the negative glow (ionization glow) in the electrically broken down gas phase, the acceleration of the electrons to increase their energy does not occur. In the electrically broken down gas phase, the main electrical field is in the dark space near the cathode. In this case, the increase in the total number of electrons is caused by the emission of electrons from the cathode surface, and the sharp increase of electron density near anode surface seems to be simply an accumulation of electrons near anode, i.e. electron amplification is achieved by ionization in ionization glow.

It also shows the relevant higher breakdown voltages of homogeneous hydrocarbon and perfluorocarbon monomers compared to breakdown voltages of argon inert gas for pressures ranging between 50 and 400 mTorr in Figs 7.6 –7.7. This is mainly due to the fact that organic monomers required more electrical energy to break down than mono-atomic inert gas such as Ar. Moreover, the breakdown voltages of DC perfluorocarbon plasma polymerizations were higher than those of DC hydrocarbon plasma polymerizations as shown in Figs 7.6 –7.7. In this sense, a larger fluorocarbon gas molecule can absorb more electrical energy than a smaller hydrocarbon gas molecule. Another factor that should be taken into

account that it needs greater electrical energy to break down C-F bond (102 Kcal/mol) of fluorocarbons than C-C bond (80 Kcal/mol) or C-H bond (99 Kcal/mol) of hydrocarbons in plasma polymerization system [13]. Furthermore, its can be clearly observed that the small concentrations of hydrocarbons and prefluorocarbons (1:10) into DC argon glow discharge increased breakdown voltage for pressures ranging between 50 and 400 mTorr in Figs 7.6 –7.7. Clearly, as the content of hydrocarbons and perfluorocarbons rises, higher electrical voltage is required to break down for argon mixture with hydrocarbons and fluorocarbons. Therefore, the molecules that obtain superior electrical breakdown energy are expected to demonstrate the slower plasma polymerization rates and the use of higher molecular weight monomer gas might reduce the deposition growth on the electrodes of the gas detector.

In order to elucidate the influence of organic gases addition into an inert gas on electron amplification, the electrical resistance of the broken-down gas phase measurement with hydrocarbon and perfluorocarbon monomers and their mixture with argon in DC plasma polymerization systems acquired from the slope of form the shape of I-V curves such as methane monomer shown in Fig**.** 7.8. In opposite

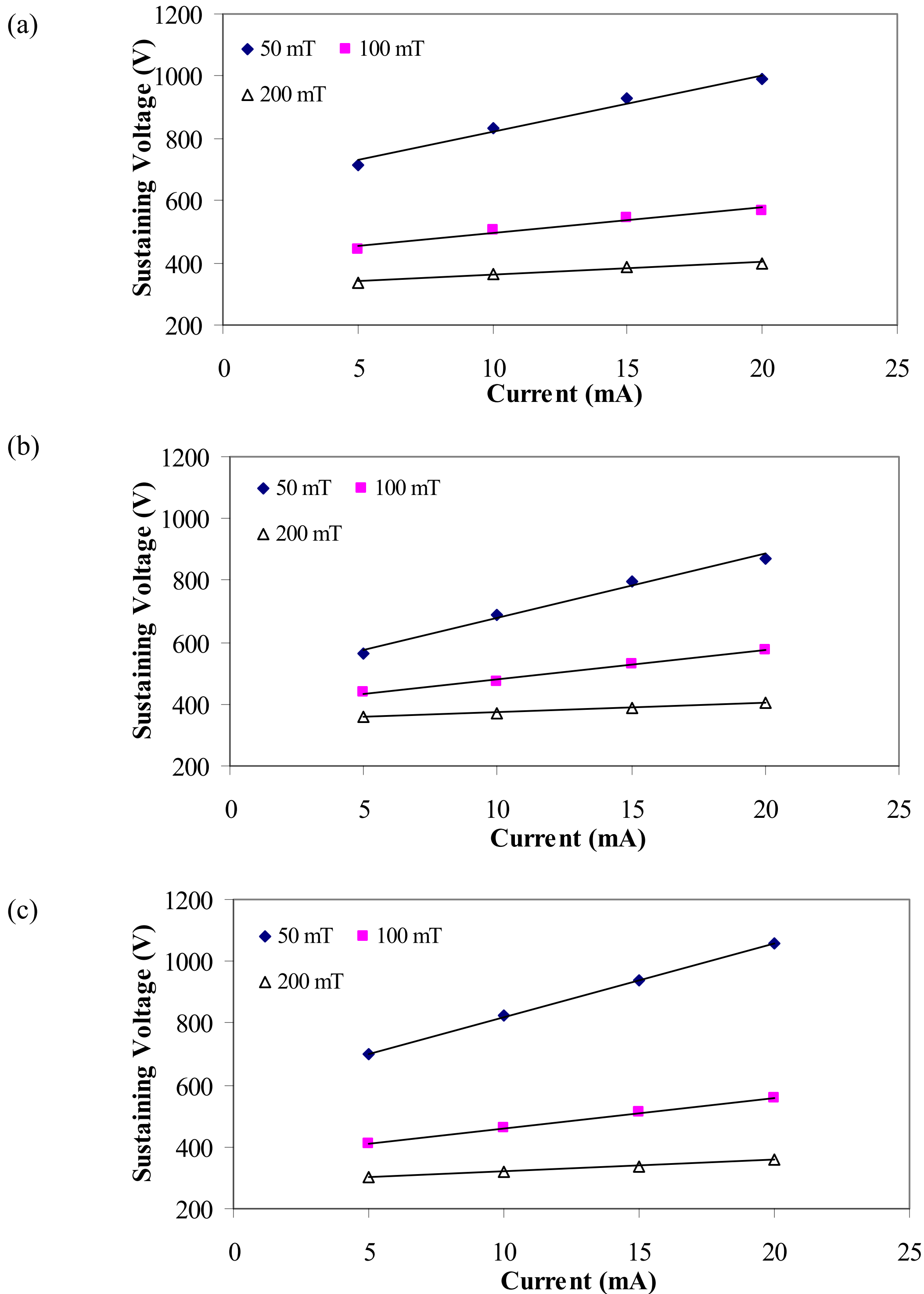

Figure 7. 8. Electrical resistance of the broken-down gas phase measurement for argon methane and their mixtures (a) argon (b) methane (c) argon+ methane (10:1) Plasma Conditions: Input gas: 10sccm argon, 1sccm methane, 1sccm methane+ 10sccm argon, DC power current 5-20 mA, 280-920 V, Flow System

to electrical breakdown voltage analysis, Ar, which obtained the lowest breakdown voltage, has the highest electrical resistance among homogeneous hydrocarbon and perfluorocarbon monomers as shown in Table 7.1. This data seems to provide justification for adding organic gas to Ar in a gas detector. Since organic gases have higher breakdown voltage that prevents the expansion of localized filamentary discharge and lower electrical resistance in the broken down gas phase, these gases provide better electron amplification. In addition, the electrical resistivity of broken-down gas phase shows that homogeneous perfluorocarbons have relatively lower electrical resistance than homogeneous hydrocarbons in Table 7.1. From this observation, it seems that perfluorocarbon monomer can be used to greatly enhance electron amplification in the gas detector. When we compare the value of breakdown voltage under a set of experimental conditions and electrical resistance of the broken-down gas phase that is calculated from the slope of voltage-current plots, we find an important distinction between these two parameters. Within a homogeneous series of hydrocarbons, breakdown voltage increases with molecular weight, and gas phase electrical resistance decreases with the molecular weight. In contrast, a homogeneous series of perfluorocarbons exhibited the contrary tendencies to breakdown voltage and electrical resistance

Table 7.1. Electrical resistance measurements for argon, hydrocarbons, fluorocarbons, and their mixtures Plasma Conditions: Input gas: 10sccm argon, 1sccm methane, ethylene hexafluoropropylene, and hexafluoropropylene oxide, 1sccm monomer (methane, ethylene hexafluoropropylene, and hexafluoropropylene oxide)+ 10sccm argon, DC power: 5-20 mA, 150-1160 V, Flow System

		Resistance (kΩ)			
Pressure (Torr)	**CH_4**	Ar	Ar + CH_4 (10:0.5)	Ar + CH_4 (10:1)	Ar + CH_4 (10:4)
0.05	20.74	24.64	26.56	23.80	25.64
0.1	9.40	13.08	10.52	9.84	9.88
0.2	5.12	5.12	4.72	3.72	3.52

		Resistance (kΩ)			
Pressure (Torr)	**C_2H_6**	Ar	Ar + C_2H_6 (10:0.5)	Ar + C_2H_6 (10:1)	Ar + C_2H_6 (10:4)
0.05	15.00	24.64	20.48	22.32	23.28
0.1	6.48	13.08	8.52	8.88	9.04
0.2	2.06	5.12	3.76	3.44	3.32

		Resistance (kΩ)			
Pressure (Torr)	**C_3F_6**	Ar	Ar + C_3F_6 (10:0.5)	Ar + C_3F_6 (10:1)	Ar + C_3F_6 (10:4)
0.05	2.96	24.64	33.60	28.96	3.72
0.1	2.50	13.08	18.00	4.60	5.72
0.2	1.24	5.12	7.24	5.24	13.16

		Resistance (kΩ)			
Pressure (Torr)	**C_3F_6O**	Ar	Ar + C_3F_6O (10:0.5)	Ar + C_3F_6O (10:1)	Ar + C_3F_6O (10:4)
0.05	6.32	24.64	29.96	47.84	40.48
0.1	4.78	13.08	18.68	11.48	6.40
0.2	1.72	5.12	7.92	5.32	4.88

compared as hydrocarbons. Therefore, the breakdown voltage and electrical resistance data indicate that anode plasma deposition could be more difficultly created with perfluorocarbons mixed with argon and perfluorocarbon monomer would be the better candidate to increase electron amplification in the gas detector.

However, Ar + perfluorocarbons mixture have much greater electrical resistance than Ar + hydrocarbon mixture in contrast to the data of homogeneous hydrocarbon and perfluorocarbon monomers in Table 7.1. Since the limitation of experimental data set in this present study, the wider range set of operational parameters such as monomer kinds, Ar/monomer ratios, and system pressure are needed to complete the data in the future that could gain more clear picture of the influence of organic gases addition into an inert gas on electron amplification in the gas detector.

7.3.3. DC plasma polymer deposition examination

The use of hydrocarbons or perfluorocarbons as quenching gas in proportional counters in the gas detector has been a rather well known preference since it gives an excellent energy resolution and small variations in gain [5]. These advantages work against their inherent tendencies to polymerize [2,14]. It is only a demand of time when enough thickness polymers would deposit on the electrodes

to perturb detection sensitivity or efficiency in the gas detector. The quenching gas that no deposit is ideal but is impractical. From this point of view, it is imperative to use the gases, which hardly polymerize in the glow discharge environment.

In light of the coexistence of dissociate glow and ionization glow in the initial stage of glow discharge of some monomers, the investigation of cathode deposition and anode deposition seems to be warranted in order to elucidate whole schemes of glow discharge of dissociate gases. A comparison of cathode deposition to anode deposition for some organic compounds is shown in Table 7.2. In a DC plasma polymerization system, the deposition of plasma polymer mainly occurs in the cathode region and a minor amount of deposition occurs on the anode surface than what occurs on the cathode. It was also confirmed from Table 7.2, the more rapid deposition forms on the cathode than that forms on the anode. The recent discovery of the electrical impact dissociation glow (cathode glow) in DC plasma polymerization has a significant influence in interpretation of the mechanism of polymeric deposition by organic gas molecules [11-12]. According to this finding of molecular dissociation of organic molecules, it is not necessary to ionize gas, which causes the break down of gas phase, to deposit polymeric films on the surface of cathode in DC plasma polymerization system.

Table 7.2 Deposition rate on cathode and anode in DC plasma of hydrocarbon monomers, fluorocarbon monomers, and their mixtures with argon Plasma Conditions: Input gas: 10sccm argon, 1sccm methane, ethane, butane, ethylene hexafluoropropylene, and hexafluoropropylene oxide, 1sccm monomer (methane, ethane, butane, ethylene, hexafluoropropylene, and hexafluoropropylene oxide)+ 10sccm argon, DC power current 10 mA, 50 mT, Flow System

Monomers	Cathode Deposition Rate (nm/min)	Anode Deposition Rate (nm/min)	Total Average Deposition/ Total Area.Time (nm/ cm^2. min)	The Ratio of Relevant Deposition on Cathode (%)	The Ratio of Relevant Deposition on Anode (%)
CH_4	6.56	2.88	4.01	0.55	0.45
C_2H_6	14.29	4.52	6.94	0.67	0.33
C_4H_{10}	22.42	5.66	11.42	0.66	0.34
C_2H_4	23.60	6.75	12.31	0.64	0.36
C_3F_6	41.20	17.98	23.32	0.57	0.43
C_3F_6O	16.95	9.22	11.04	0.50	0.50
Ar+CH_4 (10:1)	2.58	1.51	1.76	0.50	0.50
Ar+C_2H_6 (10:1)	3.07	2.33	2.48	0.42	0.58
Ar+C_4H_{10} (10:1)	8.1 6	4.8 2	4.51	0.57	0.43
Ar+C_2H_4 (10:1)	7.80	3.11	6.01	0.44	0.56
Ar+C_3F_6 (10:1)	13.35	6.47	8.12	0.53	0.47
Ar+C_3F_6O (10:1)	4.70	3.06	3.48	0.42	0.58

It might be the major cause of Malter effect during the gating operation in an early period [3].

Via comparison of DC homogeneous hydrocarbon and perfluorocarbon plasma polymerizations, it can be seen that the average deposition rates of DC hydrocarbon plasma polymerizations decrease in order of ethylene > butane > ethane> methane. For DC perfluorocarbon plasma polymerizations, average deposition rates decrease in order of hexafluoropropylene > hexafluoropropylene oxide. Hexafluoropropylene oxide was expected to obtain the less plasma deposition in plasma polymerization system because both fluorine containing and oxygen containing molecules are hesitant to form polymeric deposition [14]. It is important to recognize that anode deposition is greater than cathode deposition for perfluorocarbon monomers compared to hydrocarbon monomers as shown in Table 7.2. It is likely that negative ions are formed by electron attachment to F and then pulled towards the anode. This finding opens up a relatively simple avenue for examining the influence of negative ions on plasma polymerization processes.

Many plasma diagnostic methods have very limited utility in studying glow discharge that causes deposition of materials because of plasma deposits formed on the diagnostic probes. The prevention of the deposition, e.g., by raising the

temperature of probes, often introduces so great a perturbation as to call the validity of the data into questions. From the perspective of plasma polymerization system, fluorine containing and oxygen containing molecules delay the deposition of plasma polymers, and hence the inclusion of these compounds might be helpful to degrade the aging effect. However, the lower deposition rate for these molecules could due to the tendency to form negative ions. If this was the case, the deposition to the anode wire of gas detector might be enhanced because the formation of polymerizable species takes place in the vicinity of anode under strong electrical field.

In addition, it can be noted that both cathode and anode deposition rate decreased with high flow rate ratio (10:1) argon adding into the hydrocarbon and fluorocarbon monomers as shown in Table 7.2. The average deposition rates of argon additive plasma polymerizations are slower compared to the rate of the homogeneous hydrocarbons and perfluorocarbons, and consequently, the addition of argon into DC hydrocarbon or fluorocarbon glow discharges can be considered as similar polymeric formation in gas discharge of argon mixture of gas detector. The ratio of relevant deposition over total deposition with different monomers and their mixtures are shown in Table 7.2**.** From Table 7.2 the ratios of relevant anode

deposition over total deposition of most hydrocarbon monomers except for methane are lower than those of perfluorocarbon monomers. It indicates that the large amounts of negative ions with high electro- negativity pass to anode and collide with gas molecule to cause more deposition on anode surface in DC perfluorocarbon plasma polymerization systems. In other wards, in the case of gas detector, chemically reactive species are created in the vicinity of the anode, and if negative ions were generated, they would be pulled to the anode enhancing the deposition of material on the anode. In this sense, the role of fluorine containing compound in reducing the aging effect is somewhat questionable. Moreover, the ratio of relevant deposition over total deposition in argon mixture was confirmed the assumption described above.

The ratio of relevant anode deposition over total deposition of Ar + perfluorocarbons mixture greatly rise comparing to those of homogeneous perfluorocarbon monomers. The cause of this phenomenon may be the enhancement from negative argon ions from high flow rate argon addition. The certain additive enhances polymeric deposition on the anode in both DC hydrocarbon and perfluorocarbon plasma polymerization systems. Consequently, the ratio of cathode deposition to anode deposition is high in DC plasma

polymerization systems of hydrocarbon and perfluorocarbon monomers; however, this ratio seems to be dependent on the existence and relative intensity of dissociate glow and ionization glow, which in turn are highly dependent on the chemical nature of the monomers.

7.4 Conclusion

In this study, luminous gas phases in DC glow discharges, electrical breakdown voltage, electrical resistance, and plasma polymer deposition were examined from argon mixed with various hydrocarbons and fluorocarbons, including methane (CH_4), ethane (C_2H_6), ethylene (C_2H_4), hexafluoropropylene (C_3F_6), and hexafluoropropylene oxide (C_3F_6O). The influences of non-polymerizable argon gas added up to a ratio of 10:1 to direct current plasma polymerization of hydrocarbon and fluorocarbon monomers were investigated by evaluating the deposition features on the cathode and anode surfaces. This investigation is intended to understand the aging phenomena in which deposition occurs on anode wires due to polymeric formation in gas detectors.

Based on the experimental results of plasma polymer deposition rate and the ratio of relevant anode deposition over total deposition, a large amount of plasma polymers of hydrocarbon and perfluorocarbon was found on the anode in DC

plasma polymerization systems although the lower anode deposition rates of DC hydrocarbon and fluorocarbon glow discharges. This finding seemed opening a completely new perception in the aging study. Partition of molecular dissociation glow / ionization glow features and the possibility of negative ions contributing the plasma polymer deposition of F containing monomers on the anode seem to be the most interesting and important topics applicable to the aging phenomena of gas detectors. While the use of highly polymerizable gas should be avoided, the selection of fluorocarbon mixture based on the existed plasma polymerization concept might not be a right approach. To eliminate the variations of indefinite phenomena and provide an authentic inference for understanding aging effects in gas detectors, more in-depth perfluorocarbon plasma chemistry researches should be carried out with specific conditions.

7.5. Reference

1. M. Capeans, Nucl. Instr. and Meth. A 515 (2003) 73.
2. H. Yasuda, Nucl. Instr. and Meth. A 515 (2003) 15.
3. H. K Yasuda, et al., J.of Vac.Sci. & Technol. A 19 (3) (2001) 773.
4. J. Va'vra, Nucl. Instr. and Meth. A 515 (2003) 1.
5. M. Hohlmann, et al., Nucl. Instr. and Meth. A 494 (2002) 179.
6. M. Titov, et al., IEEE Trans. Nucl. Sci. 49 (2002) 1609.
7. K. Silander, et al., Nucl. Instr. and Meth. A 367 (1995) 298.
8. K. Kurvinen, et al., Nucl. Instr. and Meth. A 515 (2003) 118.
9. M. Titov, Science and Culture Series--Physics 25(Innovative Detectors for Supercolliders), (2004), 199.
10. M. Danilov, et al., Los Alamos National Laboratory, Preprint Archive, High Energy Physics--Experiment (2001), No pp.given, arXiv: hep-ex/0111078.
11. H. Yasuda, et al., Plasma Chem. Plasma Process 24 (2004) 325.
12. Q. S. Yu, et al., J.of Polym. Sci., Part A: Polym. Chem. Ed 42 (2004) 1042.
13. H. Yasuda, Plasma Polymerization, Academic Press, Inc., 1985.
14. H. Yasuda, Luminous Chemical Vapor Deposition and Interface Engineering, Marcel Dekker Inc., 2005.

CHAPTER 8

Deposition of Protective Coatings on Polycarbonate and Polymethylmethacrylate Substrates by Low Temperature Radio Frequency Plasma Process

8.1. Introduction

Plastic substrates such as polycarbonate (PC) and polymethylmethacrylate (PMMA) are progressively substituting glass substrates owing to their lightweight, low cost, and similar light transmission characteristics to glass in recent years. Many commercial products such as optical lenses, digital electronic panels, and automotive headlamp lenses are widely used plastic substrates. Moreover, the miniaturation of the next generation display panel has naturally required the more skinny and flexible panel substrates such as plastic materials. The rapid motivation of commercial plastic use leads to a relative raise in the strong demand for the advanced plastic development. However, the components of plastic substrates are intrinsically soft, and thus the usage of plastic is limited to moderately mild applications. To refine the inherent restrictions of plastic substrates, a variety of the protective coating fabrication methods are performed during the last decade [1-5]. The wet chemistry, which consists of curing by UV radiation or oven

heating, is easily accessible and most commonly used. Nevertheless, it is hard to obtain ultra-thin protective coatings and to control the thickness uniformity from wet chemistry process [17]. These coating techniques are also considered as uneconomical and some processes require that toxic materials be used.

For most protective coatings for modern technologies, the film materials are desired to be ultra-thin, uniform, adhesive, and with anti-scratch strength. Plasma chemical vapor deposition process seems to be a very promising technique for protective coating applications [6-10]. It overcomes many of these problems to provide an ultra-thin, extremely hard, non-cracking coating using a simple process method. In addition, plasma protective coating on plastic substrates demonstrates a capable means for modification of the substrate surface without altering the substrate bulk property. Among many investigations to the successful development of plasma protective coating on plastic substrates, there is a need for large-scale substrate in plasma chemical vapor deposition system. Importantly, the reactor setup of plasma chemical vapor deposition system must be widely available, easily cleaning, and simple to operate.

To address these demands, we develop the novel reactor setup for plasma protective coating process. In this study, we have deposited uniform protective

coatings on PC and PMMA substrates by RF plasma chemical vapor deposition using tetramethyldisiloxane (TMDSO) and oxygen mixture. The plasma protective coatings properties were determined by FTIR-ATR analysis. The transparent and hard silicon oxide (SiOx) films were deposited from RF TMDSO mixed with oxygen plasma chemical vapor deposition. An argon plasma pretreatment before plasma chemical vapor deposition was conducted to eliminate the contaminants on the PMMA surfaces. The effects of process parameters including, TMDSO-O2 ratio, plasma pre-treatment, RF plasma power, and interlayer effects on silicon oxide coating qualities were examined.

8.2. Experimental Procedures

8.2.1. Materials

Reactive gases used for plasma pre-treatments were an industrial grade argon (99.997% purity) an industrial grade oxygen (99.9% purity) purchased from General Store of University of Missouri-Columbia. Monomers used for plasma polymerization were ethane (C_2H_6), trimethylsilane (TMS) and tetramethyldisiloxane (TMDSO). Ethane (>99% purity) was purchased from Matheson Gas Products, Inc and trimethylsilane (TMS) was purchased from Gelest Inc. with 98% purity. Tetramethyldisiloxane (TMDSO, 97% purity)

purchased from PFALTZ & BAUER Inc. The tetramethyldisiloxane (TMDSO) was degassed by freezing-thawing process and used as vapor in RF plasma process.

8.2.2. RF Plasma Chemical Vapor Deposition

Polycarbonate (PC 4.0x4.0 inch) and polymethylmethacrylate (PMMA 4.0x4.0 inch) were used as substrates and cleaned ultrasonically in deionized water for 15 minutes to remove surface contamination before loading into the plasma reactor. These substrates were individually placed in the plasma reactor. The plasma reactor system used in this study was a bell jar-type reactor, with dimension of 46 cm in height and 44.5 cm in diameter. An electrode assembly has a proprietary design was connected with the RF power source. Tetramethyldisiloxane (TMDSO) and oxygen gas mixture were used as major monomer gas input in plasma chemical vapor deposition process. After the system was under vacuum to a base pressure of 1 mTorr or below, TMDSO and oxygen mixture was introduced into the chamber and adjusted to a stable working pressure (30 mTorr) in flow reactor system mode. The plasma power source was applied 13.56 MHz with a required match network unit (RFX-600 generator Advanced Energy Industries Inc. Fort Collins, CO, USA). Plasma power was initiated at a

power of 40 Watt for 25 minutes. The silicon wafer samples were also cleaned with acetone wipe and attached to the substrate surfaces by using double-layer tape.

8.2.3. SiOx film Thickness Measurement

For the purpose of thickness and refractive index measurement, a null-seeking type AutoEL-II Automatic Ellipsometer (Rudolph Research Corporation, Flanders, NJ) with a 632.8 nm helium-neon laser light source was utilized.

8.2.4. FTIR-ATR Measurement

In this study, FTIR-ATR spectra were recorded on a Nicolet FTIR 460 spectrometer from Thermo Electron Corporation (Waltham, MA, USA) to determine functional groups of chemical compounds on plasma protective coatings. The instrument was purged with dry nitrogen to prevent the interference of atmospheric moisture with the spectra. The Nicolet FTIR 460 spectrophotometer connected to the computer running standard OMNIC software from Thermo Electron Corporation. In total, 256 scans were accumulated to obtain high signal-noise levels for the final spectra in the spectral range of 4000–400 cm^{-1}.

8.2.5. UV-VIS transmission detection

UV-VIS transmission detection was carried out using a Varian Cary 50 UV spectrophotometer with 80Hz Flash Lamp (Varian, Inc. Palo Alto, USA). UV–VIS spectra of plasma protective coating plastic samples, RF plasma deposited silicon oxide coatings obtained in absorption mode with a Varian Cary 50 UV spectrophotometer in the wavelength range 300–800 nm at room temperature. The optical absorption was measured in the above wavelength region for the RF plasma deposited silicon oxide coatings on polycarbonate substrates against a blank uncoated polycarbonate substrate as the reference.

8.2.6. Pencil Hardness Test Method

The surface hardness of both untreated and plasma treated plastic substrates was examined by the pencil hardness method according to ASTM D3363-05. The pencils, which were obtained from Derwent Inc., had hardness from 6H to 6B (hard to soft). In this method, the flat pencil head was placed against the polymeric substrates at a 45° angle and was pushed away to make a scratch on the substrate. The tested pencils that harness levels are from hard to soft were used until one pencil was found that could not make a scratch on the substrate. The harness level of the final test pencil defined the hardness of the polymeric substrate.

8.2.7. Tape Adhesion Test

The adhesion of SiOx coating was tested by the ASTM 3359-93B-tape adhesion test. This testing method provides semi-quantitative results given in levels of 0-5. The level of adhesion is graded by the pattern of coating lifting; 0 for greater than 65% lift-off to 5 for no lift off along with the level described in the standard method. The method was applied to the dry surface. Wet tape test is a modification of the tape adhesion test. In this process, test samples are prepared consistent with the standard procedure described above. Instead of undergoing the tape test directly, samples are placed in hot water (65 ^{o}C) for a prearranged period of time. In this study, 1, 2, 4, 8, 24, 72 hours were used.

2.8 Static Contact Angle Measurement

The static contact angles of plastic samples were measured by projecting an image of an automatic sessile droplet resting on a plastic surface with a VCA-2500XE Video Contact Angle System (AST Products, Inc. Billerica, MA, USA). After RF plasma modification treatments, the untreated plastic samples and the plasma modified plastic samples were placed on a vertically and horizontally adjustable sample stage. The microsyringe above the sample stage can be set to automatically dispense a predetermined amount of water by the computer. After

the 0.3 μL water droplet has made contact with the plastic surface, a snapshot of the image was taken. The captured image was saved and contact angle measurements were commenced at leisure. After placing markers around the perimeter of the water droplet, the VCA-2500 Dynamic/Windows software calculated right and left contact angles.

8.3. Results and Discussion

8.3.1. Uniformity of SiOx coating with different substrate sizes and plasma power inputs in RF plasma chemical vapor deposition

During plasma chemical vapor deposition process, the uniformity of the plasma deposited film on the substrate is important for the formation of protective coating on plastic substrate. Fig. 8.1. shows the deposition profiles of silicon oxide coating on different size power electrodes as substrates. The refractive index of silicon oxide coating in all plasma treatments were maintained around 1.4. It can be noticed that the deposition profile of silicon oxide coatings are relatively more uniform on large size substrates than those on the small size substrate as shown in Fig. 8.1. The major cause of uniformity change of plasma chemical vapor deposition on different size substrates could be the electrode geometry in

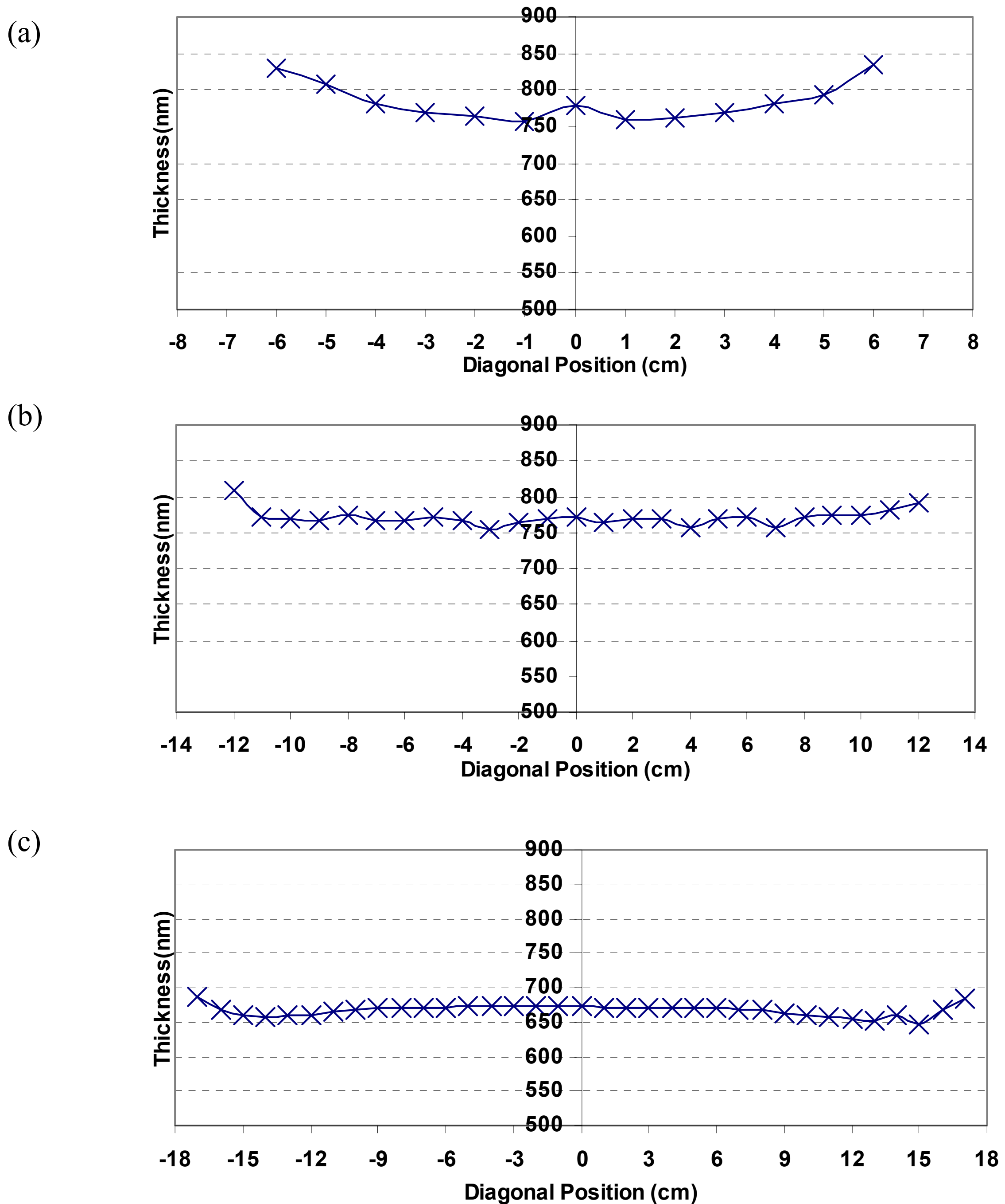

Figure 8. 1. The thickness profile of plasma deposited SiOx with different diagonal distances on different size substrates. The size of substrate: (a) 3x3 inch, (b) 7x7 inch, (c) 10x10 inch. Plasma Conditions: 1 sccm TMDSO, 10 sccm O_2, 30 mT, RF 40 W, 25 min.

plasma reactor. The average deposition rate of the silicon oxide coatings on different size substrates, as measured by ellipsometry, does not show a significant dependence on power density as shown in Fig 8.2. From Fig. 8.2, it determines that non-linear relationship between the substrate size and plasma deposition rate since the major parameter of power density is the electrode size as substrate size. Fig. 8.3. shows the deposition and refractive index profiles of silicon oxide coating with different RF plasma power inputs. The refractive index of silicon oxide coating in all plasma treatments were also maintained around 1.4. It can be noticed that the uniformity of silicon oxide coating improved with increasing RF plasma power input from Fig. 8.3. Fig. 8.3. also shows that, under increasing RF plasma power, the deposition rate increased substantially, indicating a substantial change in the reaction behavior. The average deposition rate of silicon oxide coating exhibits a strong linear dependence on RF plasma power input as shown in Fig. 8.4. Also shown in Fig. 8.4. is the similar dependence of the refractive index on RF plasma power input. From Fig. 8.1-4, it determines that a steady state deposition process was achieved at well-controlled operational parameters of RF plasma

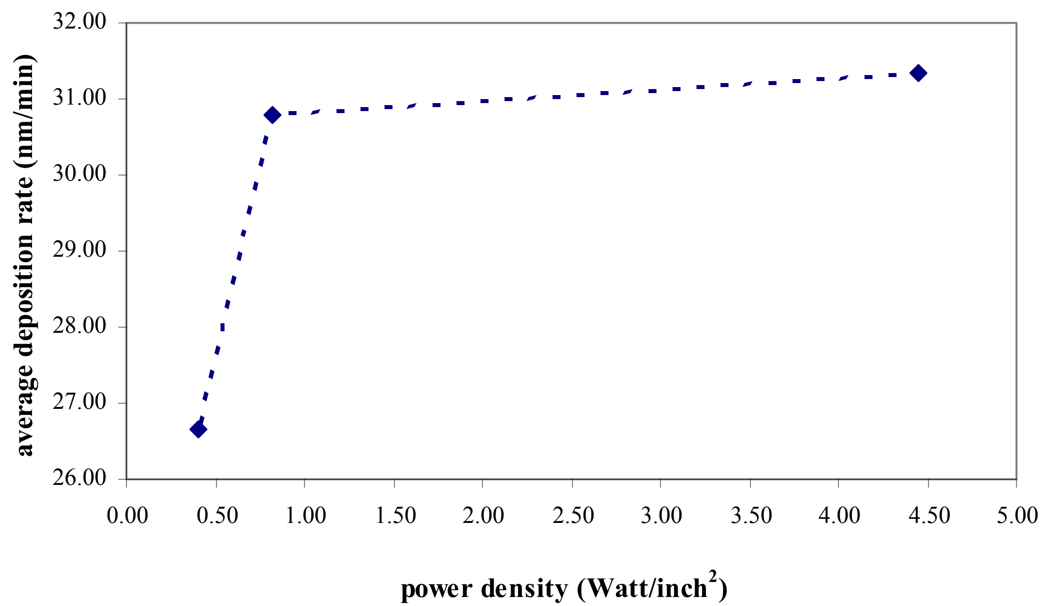

Figure 8. 2. The dependence of power density with deposition rate and refractive index Conditions: 1 sccm TMDSO, 10 sccm O_2, 30 mT, 25 min, the size of substrate: 3x3 inch, 7x7 inch, 10x10 inch

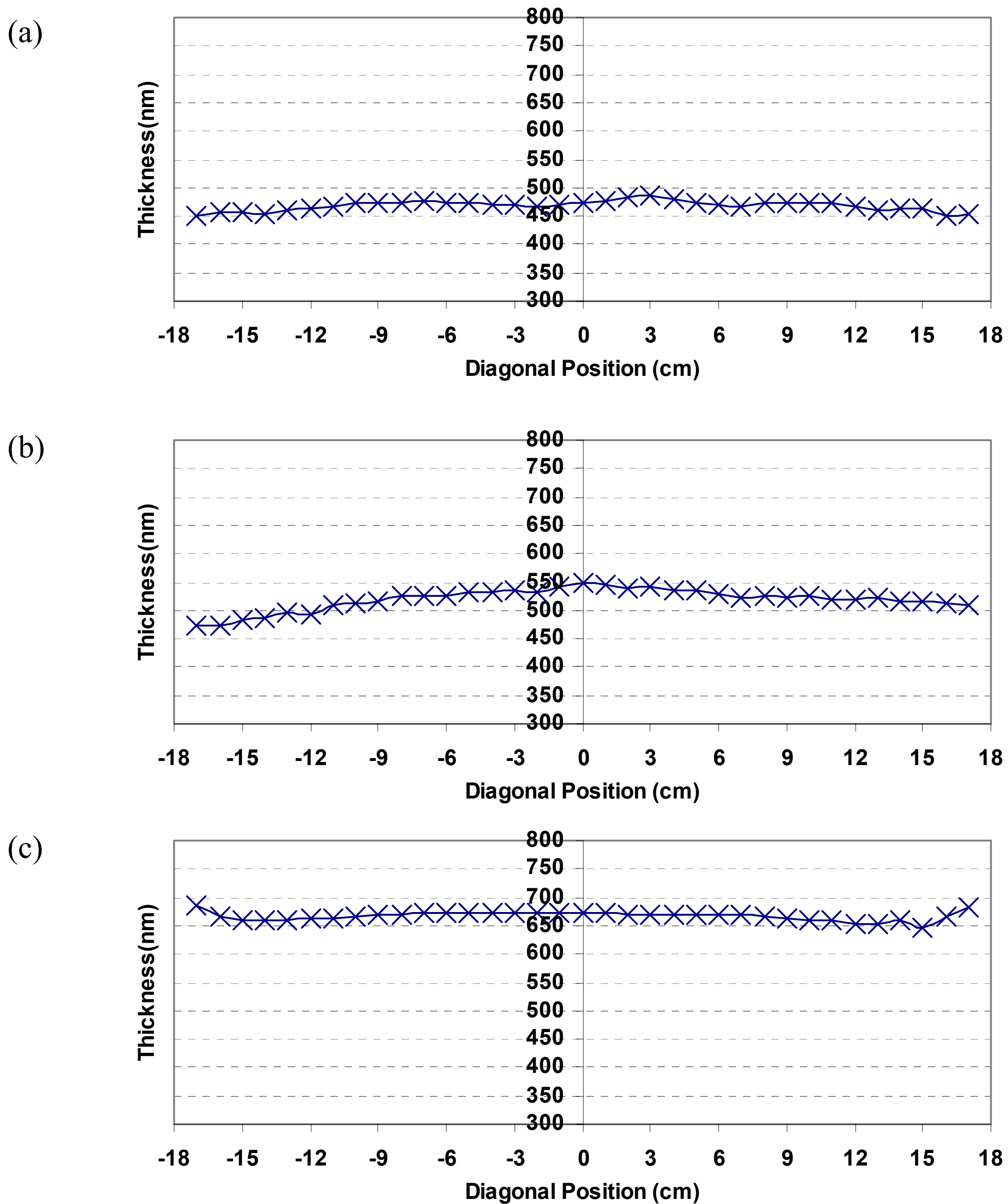

Figure 8. 3. The thickness profile of plasma deposited SiOx with different diagonal distances under different RF plasma power inputs. RF plasma power: (a) 10 W, (b) 20 W, (c) 40 W. Plasma Conditions: 1 sccm TMDSO, 10 sccm O2, 30 mT, 25 min, 10x10 inch substrate.

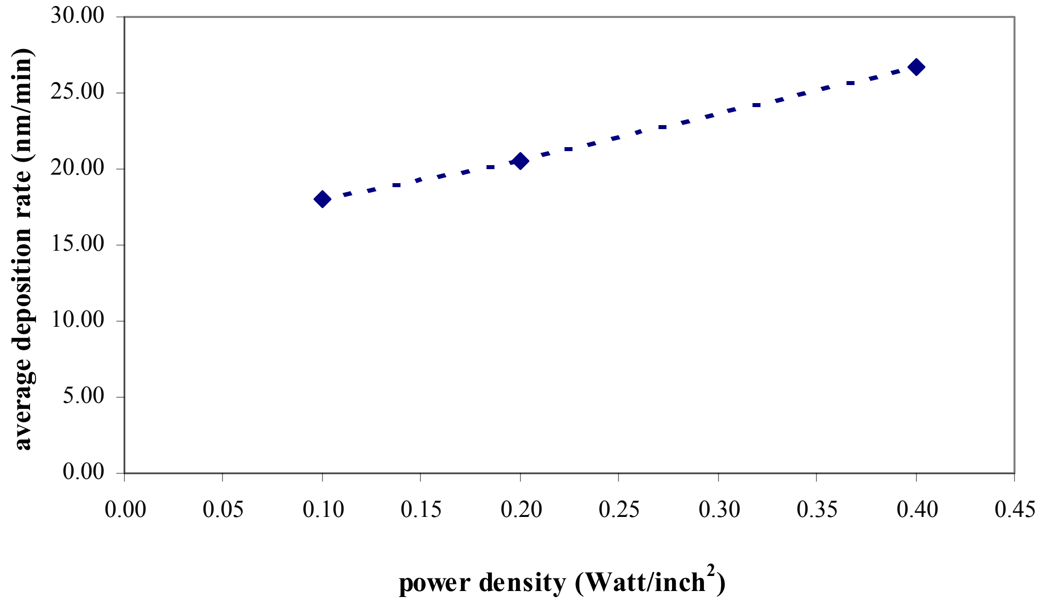

(a) the dependence of average deposition rate with power density

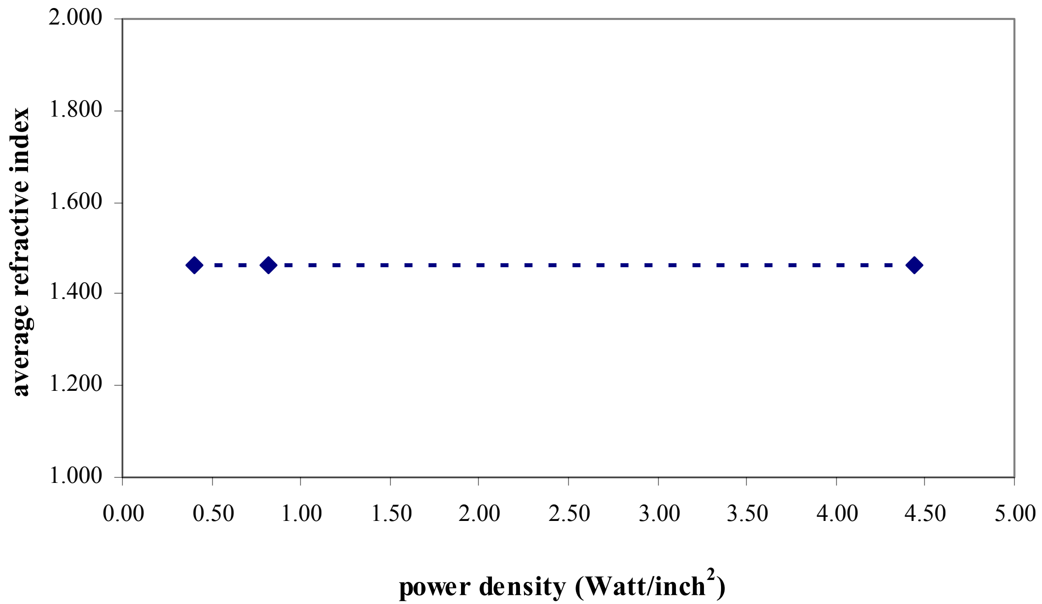

(b) the dependence of average refractive index with power density

Figure 8. 4. The dependence of power density with deposition rate and refractive index Conditions: 1 sccm TMDSO, 10 sccm O_2, 30 mT, 25 min, RF plasma power:10 W, 20 W, 40 W

chemical vapor deposition system. As a result, this study indicates that this plasma chemical vapor deposition system has the potential application to attain the uniform silicon oxide coating on large scale plastic substrates without any magnetron enhancement assembly in traditional plasma chemical vapor deposition process.

8.3.2. FTIR-ATR analysis of TMDSO plasma polymerized interlayer and SiOx coating properties

The FTIR-ATR analysis results of the plasma polymerized TMDSO interlayer and plasma deposited silicon oxide coatings with different plasma powers /TMDSO:O_2 ratios are shown in Fig. 8.5. (a) (b) and (c). It is obvious that plasma polymerized TMDSO films deposited without oxygen addition retained the structure of the starting silicon carbon monomers. However, new absorption peaks appeared which are not in the TMDSO monomers (Si-OH stretching at 930 cm^{-1} and Si- $(CH_3)_3$ stretching at 800 cm^{-1}). The Si-OH peaks of plasma deposited silicon oxide coating FTIR-ATR spectra could be owing to OH groups formed from H_2O that was created during the plasma interaction between TMDSO and oxygen and was taken up in the film [11]. It should be noted that no peaks are detected at 2900 cm^{-1} and 1730 cm^{-1} due to C–H and C=O stretching vibrations.

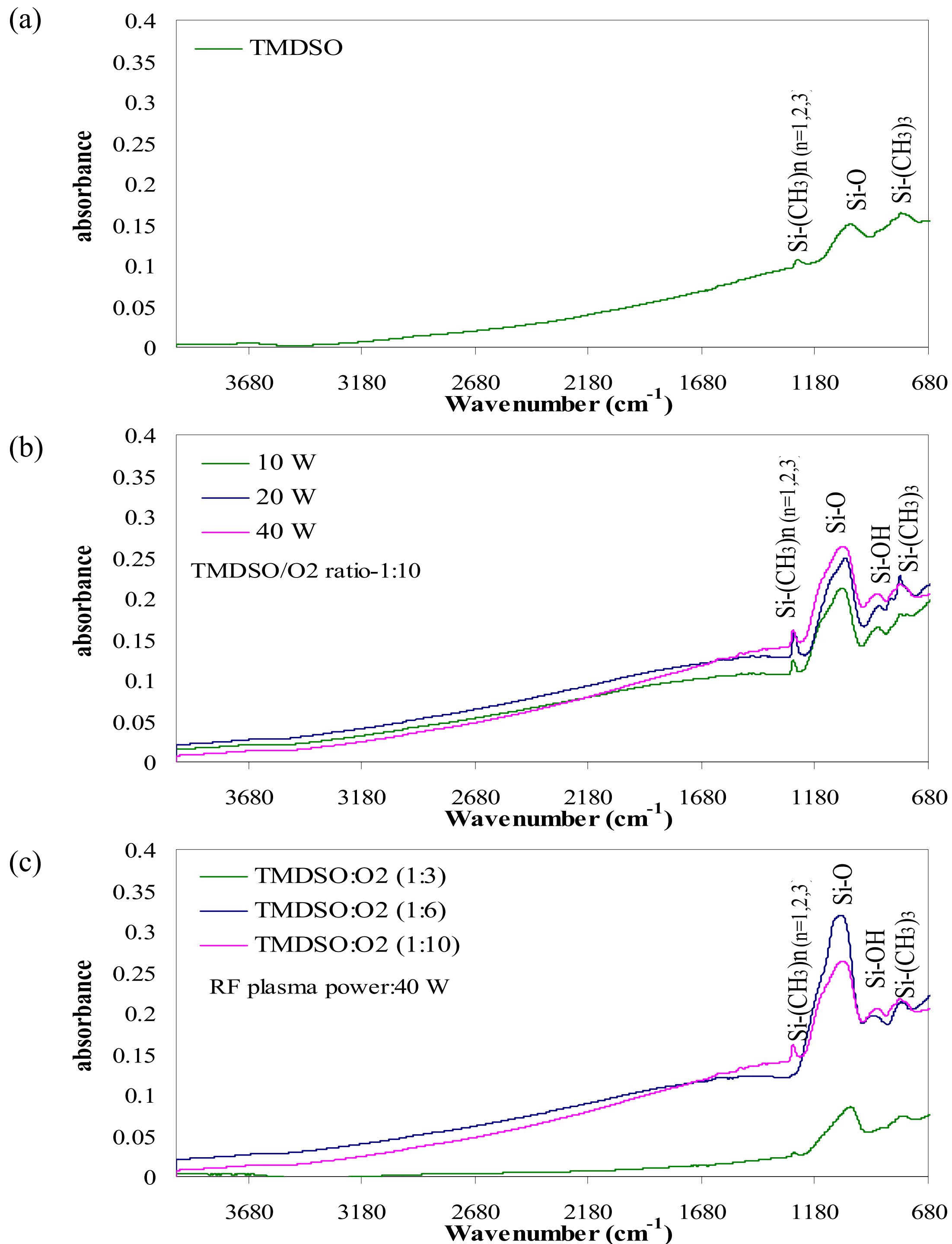

Figure 8. 5. FTIR-ATR spectra for plasma deposited coating (a) Plasma polymerized TMDSO coating (b) RF plasma deposited SiOx coating with different power input (c) RF plasma deposited SiOx coating with different TMDSO:O_2 ratio Plasma Conditions: 1 sccm TMDSO, 3,6,10 sccm O_2, 30 mT, 25 min, 10x10 inch substrate, RF plasma power:10 W, 20 W, 40 W. Thickness: 0.45 µm-0.8 µm.

Therefore, the plasma deposited silicon oxide coatings obtain inorganic characteristics at the low substrate temperature of 35~40^{0}C, and the Si-O absorption peaks at 1078 cm-' were more pronounced with increasing RF plasma powers. Furthermore, the strongest intensity of Si-O absorption peak obtained at TMDSO:O2 ratio (1:6) FTIR-ATR spectrum implies that reasonably more Si-O groups occurred in RF TMDSO and O2 mixture (1:6) plasma chemical vapor deposition system. Consequently, Si-O groups are indicated as the major groups in the decomposition of TMDSO and O_2 mixture in RF plasma chemical vapor deposition process, and a relatively high inorganic characteristic was detected by FTIR-ATR analysis and compared to the literature [12].

8.3.3. Plasma deposited protective coatings with different oxygen-TMDSO ratios on PC and PMMA substrates

The dependence of deposition rate and refractive index with different oxygen - TMDSO ratios on PC and PMMA substrates were investigated as shown in Fig. 8.6. The typical plasma deposition rate is about 21-32 nm/min. Ar plasma pre-treatment was only used in PMMA trials to clean surface of PMMA substrate. The plasma deposited silicon oxide coating was characterized as a hard and transparent film on both PC and PMMA substrates. With rising oxygen of PMMA

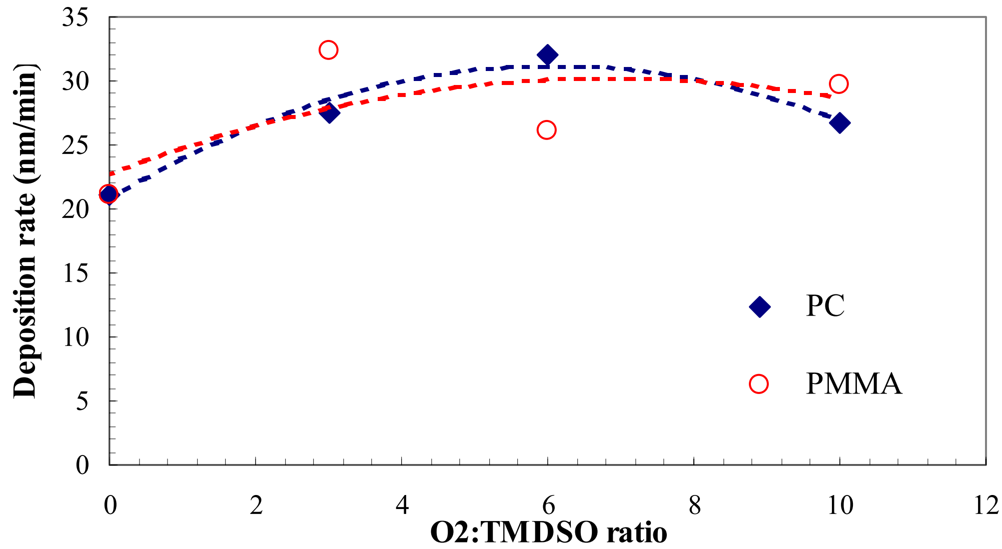

(a) The dependence of average deposition rate with O_2/TMDSO ratio

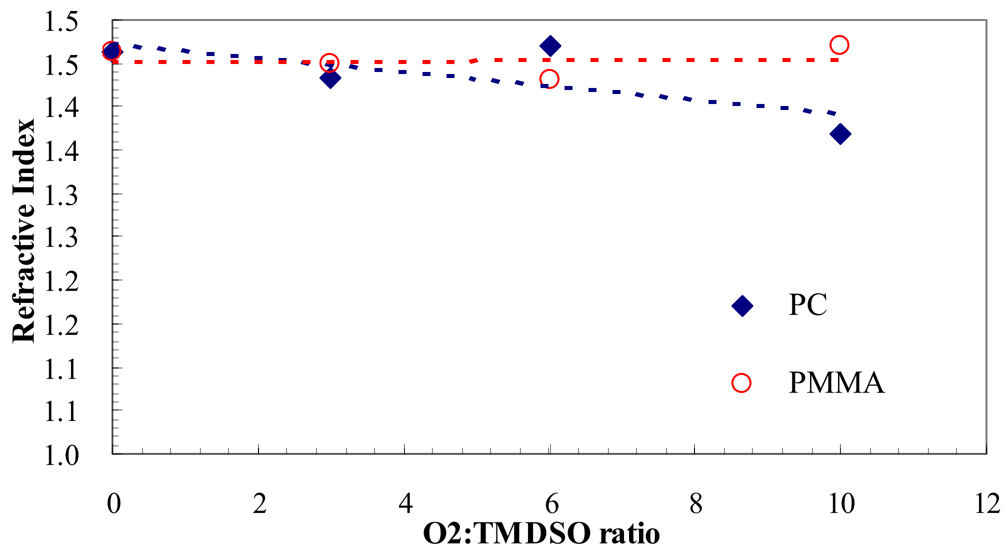

(b) The dependence of average refractive index with O_2/ TMDSO ratio

Figure 8. 6. The average deposition rate and refractive index of SiOx coatings with different O_2: TMDSO ratio monomer inputs on PC and PMMA substrates. Conditions: 1 sccm TMDSO, 10 sccm O_2, 30 mT, 25 min, 40 W

substrate. The plasma deposited silicon oxide coating was characterized concentration of RF TMDSO +O_2 mixture plasma chemical vapor deposition, the trend of deposition rate increased initially and then leveled off on both PC and PMMA substrates. The refractive index of plasma deposited silicon oxide on both PC and PMMA substrates were maintained around 1.4-1.5 with increasing oxygen concentration. Thus, the deposition rate was increased with increasing oxygen concentration, however the excessive amount oxygen dilute the TMDSO monomer concentration thus reduce the deposition rate of RF plasma chemical vapor deposition process.

Since the transparency of protective coating is essential to the advanced plastic development for optical applications, UV-VIS transmission analysis of plasma deposited silicon oxide on PC substrates was conducted in this study. Fig 8.7 presents the UV-VIS transmission spectra of plasma deposited silicon oxide coatings with different oxygen - TMDSO ratios; they are colorless and have a transmission of above 80% in the visible region measured on PC substrates. As the results, UV-VIS transmission analysis evidently confirmed that the plasma deposited silicon oxide coatings have an excellent transparency on plastic substrates. In addition, the hardness of plasma deposited silicon oxide on PC

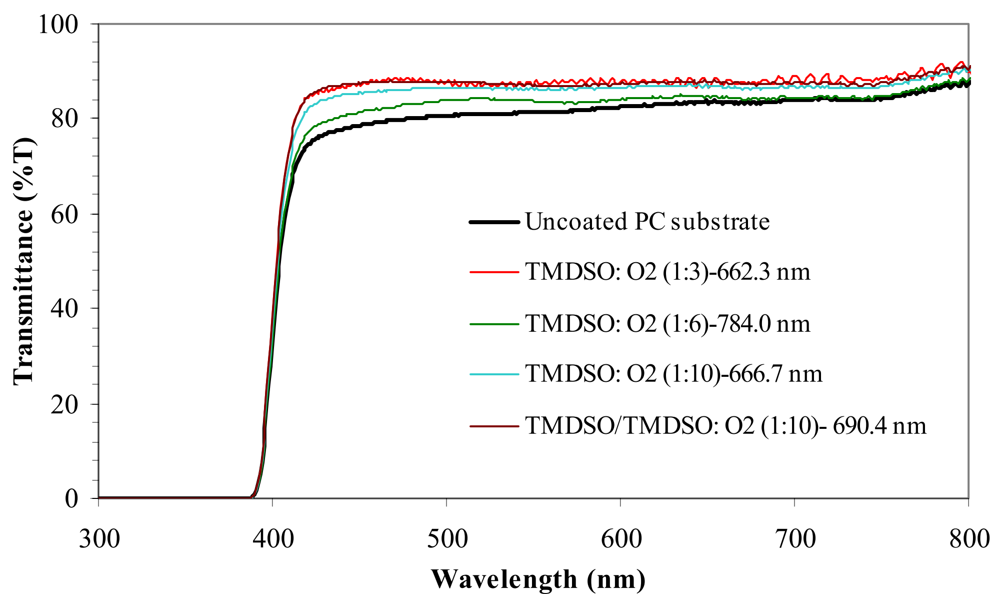

Figure 8. 7. UV-VIS transmission spectra of plasma deposited SiOx coatings with different O_2:TMDSO ratio monomer inputs on PC substrates. Plasma Conditions: 1 sccm TMDSO, 3,6,10 sccm O_2, 30 mT, 25 min, RF 40 W. Thickness: 0.66 μm-0.79 μm.

substrate improved above 1 H from pencil hardness method as shown in Table 8.1. Moreover, 1:6 (TMDSO:O2) ratio was found to further enhance the hardness to 4 H; it is corresponded to the highest intensity of Si-O absorption peak observed from FTIR-ATR spectra (as mention in section 8.3.2). It shows that the relevance between Si-O groups and hardness of plasma protective coating on plastic substrates.

Table 8.1
Pencil hardness test for RF plasma deposited SiOx coatings on polycarbonate substrate
Plasma Conditions: 1sccm TMDSO, 3,6, 10 sccm O_2 30 mT, RF 40 W, 25min

TMDSO : O_2 ratio	reference	1 : 3	1 : 6	1:10	1:10 (with interlayer)
PC substrate	6B <	H	4H	H	H

Table 8.2
Dry tape test for RF plasma deposited SiOx coatings on PC & PMMA substrates
Plasma Conditions: 1sccm TMDSO, 3,6, 10 sccm O_2 30 mT, RF 40 W, 25min

	Adhesion levels measured for TMDSO : O_2 ratio			
TMDSO : O_2 ratio	1 : 3	1 : 6	1:10	1:10 (with interlayer)
PC substrate	4B	5B	5B	5B
PMMA substrate	5B	5B	5B	5B

Further depositing an interfacial layer between plastic substrate (PC and PMMA) and silicon oxide coating layer was in order to improve the adhesion of silicon oxide coating to PC and PMMA surfaces. The monomer used for the formation of the plasma polymerized interfacial layer was tetramethyldisiloxane (TMDSO), and the typical operational condition was: 1 sccm TMDSO, 30 mTorr, 40 Watt, 1minute. From Table 8.2, the dry tape test adhesion results of plasma deposited silicon oxide coating on both PC and PMMA surfaces are excellent. However, the wet tape test adhesion results of plasma deposited silicon oxide coatings on PMMA surfaces compared to those on PC surfaces are less durable as shown in Fig. 8.8. One potential cause is that PMMA, which is thermoplastic polymer, could be caused a little phase change by itself in the hot water bath (65° C) of wet tape test. Another possible reason is that the surface free energy of PMMA surface is lower than that of PC surface. The plasma deposited silicon oxide coating is difficult to adhere on PMMA because of the lower surface free energy of PMMA surface. The other possible explanation is owing to PMMA, which consists of the mobile side ester group, has a negative effect for the adhesion of plasma deposited silicon oxide coating.

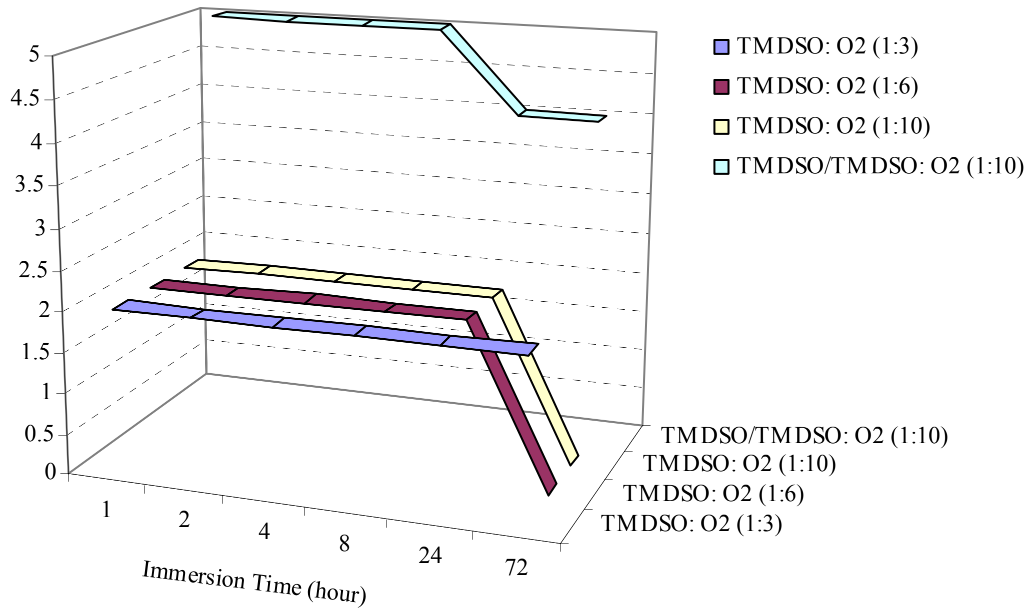

(a) PC substrate

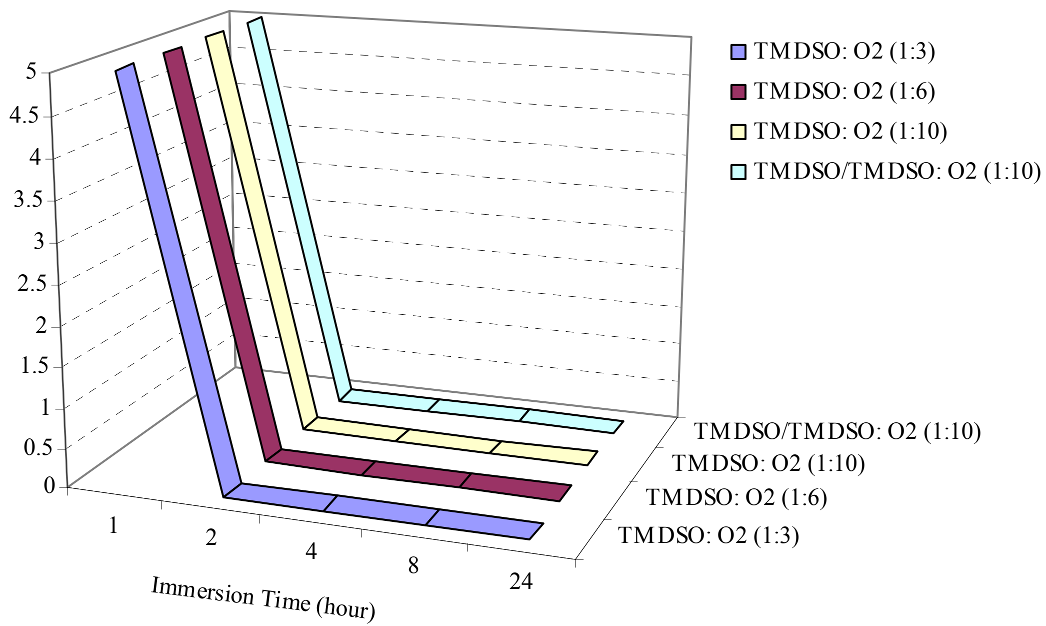

(b) PMMA substrate

Figure 8. 8. The adhesion levels of wet tape tests from of SiOx coatings with different TMDSO:O_2 ratio monomer inputs on PC and PMMA substrates. Conditions: 1 sccm TMDSO, 10 sccm O_2, 30 mT, 25 min, 40 W

8.3.4. Adhesion enhancement of plasma coated PMMA substrates

Polymethylmethacrylate (PMMA) is well-known by its low density, flexibility, ease of production, and cost-effectiveness. However, the surface free energy of PMMA is too low to satisfy the demands regarding scratch-resistance and adhesion [14]. Hence, an additional plasma surface treatment before plasma chemical vapor deposition process is required to attain the desired surface property of PMMA with maintaining its bulk property [15-16]. It has been found that noble gas plasmas such as Ar or He plasmas are effective in creating free radicals, but do not add new chemical functionalities from gas phase. Typically, reactive plasma such as O2 and H2O is used to add a polar functional group to increase the surface free energy of polymer.

Fig. 8.9 shows the static contact angle changes of RF argon and oxygen plasma modified PMMA surfaces. The blue lines demonstrate the static water contact angle measurements directly after the modification treatment, whereas the pink lines demonstrate the contact angles of the samples washed in a deionized water ultrasonic bath for 3 minutes, then blowing dried with compressed air and left in the air for 10 minutes. For untreated PMMA samples with initial static water contact angle of approximately around 80°, the static water contact angles of

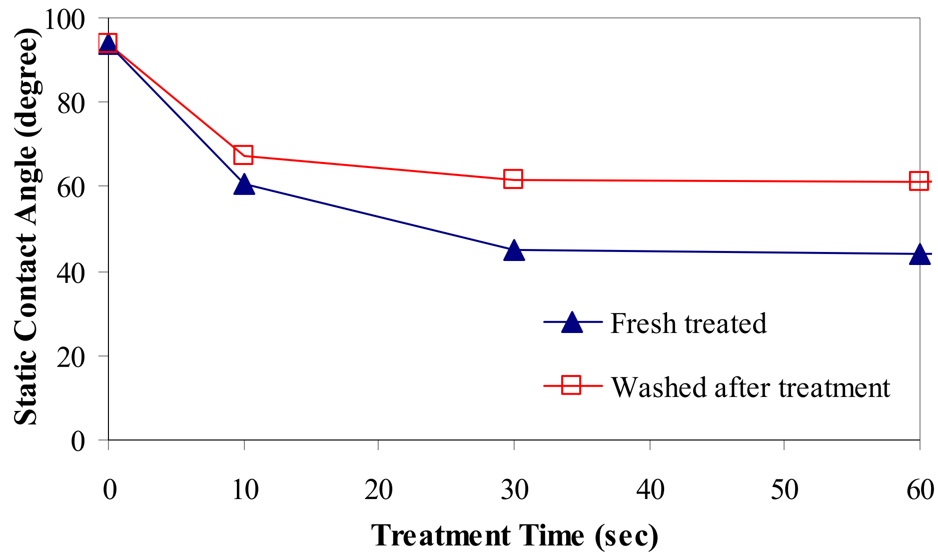

(a) RF Ar plasma treated PMMA

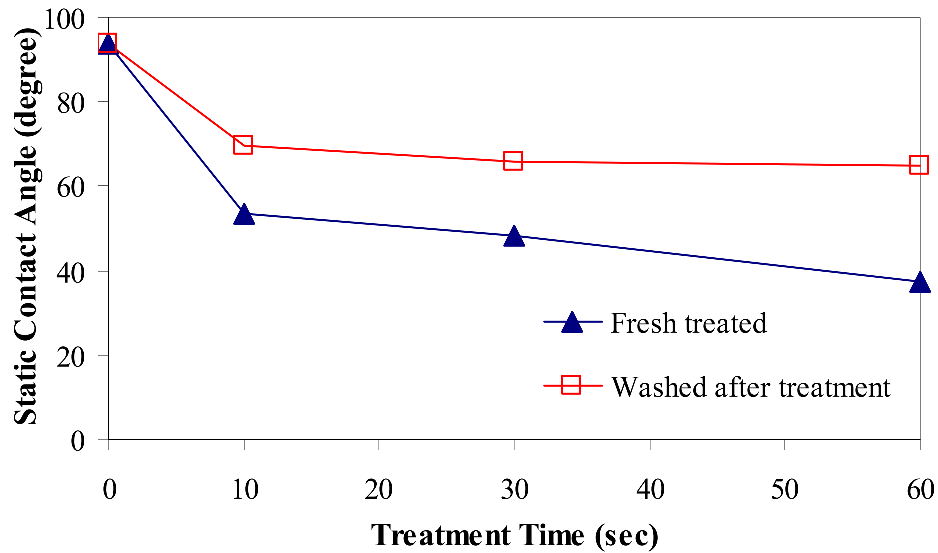

(b) RF O_2 plasma treated PMMA

Figure 8. 9. The surface modification effects of PMMA from RF plasma pre-treatment with 1 sccm argon, 1sccm oxygen, 30mT, RF power input of 10 W, Treatment time: 10sec, 30sec, 60 sec

RF argon and oxygen plasmas modified samples decreased after 10 second treatment time as shown in Fig. 8.9. The after washing results of the RF argon and oxygen plasmas treatments as shown in Fig. 8.9, however, showed a significant increase, from 40° to 60° in static water contact angle. The hydrophobicity recovery after washing samples indicates the damage of polymer surface during the plasma treatments. From this examination, RF plasma modification can be recognized as an effective method to activate PMMA surface before coating.

In the further test, we study the effect of Ar, O_2, and Ar+O_2 RF plasma pre-treatment on the surface energy of PMMA surfaces, in the context of improving the adhesion of silicon oxide coating layer on PMMA substrates. Table 8.3 shows the plasma pre-treatment effects on the adhesion of silicon oxide coating layer on PMMA surfaces. Nevertheless, there is no obvious adhesion improvement of plasma pre-treatments to silicon oxide coating layers as shown in Table 8.3.

Several researches determined that the adhesion strengths of interfacial layers and plasma coatings were dependent on plasma power density during plasma chemical vapor deposition process [17]. From this aspect, different RF plasma powers were used in this study to examine the plasma power effects on the

Table 8.3.

Adhesion test results for RF plasma deposited SiOx coatings with various operational parameters of plasma chemical vapor deposition system Plasma Conditions:, 1 sccm TMDSO +10 sccm O_2, 30 mT, 25 min, RF 40W. Plasma pre-treatment effect: 1 sccm Ar & O_2, 30 mT, 30-60 sec RF 40W. RF power effect: 40 W, 60 W. Plasma polymerized interlayer effect:1 sccm TMDSO,TMS, C_2H_6 30 mT, 1min, RF 40W.

Operational Parameter		Tape test					
		Dry	After in hot H_2O (65°C) for 1, 2, 4, and 8 h				
Plasma pretreatment	Ar plasma	5	5	0	0	0	0
Plasma pretreatment	O_2 plasma	5	0	0	0	0	0
Plasma pretreatment	Ar+O_2 plasma	5	0	0	0	0	0
Plasma power level	RF 40 Watt	5	5	0	0	0	0
Plasma power level	RF 60 Watt	5	0	0	0	0	0
Plasma polymerized Interlayer	TMDSO interlayer	5	5	0	0	0	0
Plasma polymerized Interlayer	TMDSO-O2 interlayer	0	0	0	0	0	0
Plasma polymerized Interlayer	TMS interlayer	0	0	0	0	0	0
Plasma polymerized Interlayer	TMS+ethane (1:1) interlayer	5	0	0	0	0	0
Plasma polymerized Interlayer	ethane interlayer	0	0	0	0	0	0
Plasma polymerized Interlayer	ethane-TMDSO interlayer	0	0	0	0	0	0
Plasma polymerized Interlayer	ethane+TMDSO (1:0.5) interlayer	0	0	0	0	0	0
Plasma polymerized Interlayer	ethane+TMDSO (1:1) interlayer	5	5	0	0	0	0
Plasma polymerized Interlayer	ethane+TMDSO (1:2) interlayer	0	0	0	0	0	0
Plasma polymerized Interlayer	ethane-TMDSO+O2 interlayer	0	0	0	0	0	0

The thickness and refractive index of all RF plasma deposited SiOx coatings were controlled ~ 0.7 µm & 1.45

adhesion strengths. The RF plasma power was also recognized as an important factor in plasma chemical vapor deposition system to influence the property of SiOx film deposition during plasma coating process. Table 8.3 shows the RF plasma power effects on the adhesion of silicon oxide coating on PMMA surface from both dry and wet tape tests. However, there are no significant enhanced adhesion level differences between 40 watts RF plasma power and 60 watts RF plasma power as shown Table 3. The possible cause could be that the higher RF plasma power may enhance the sputtering effect and damage the surface of PMMA.

In this section, an organic interlayer deposited next to the PMMA surface was used in promoting adhesion approach. The plasma polymerized organic interlayer was anticipated as the improving adhesion function for plasma protective coatings on polymeric surface since the excellent adhesive characteristics of plasma polymerized interface-engineering system was investigated by Yu and Yasuda et al [18-20]. As mentioned in the section 8.3.3, a thin interfacial layer was used to grow on the top of the clean PMMA surface first before depositing a continuous, hard, silicon oxide coating layer. This was performed by plasma chemical vapor deposition of TMDSO or TMDSO-O_2 by 40W RF plasma power. The reactive gas

used for the adhesion enhancement after interfacial layer deposition was oxygen (O_2), and the operational conditions for O_2 plasma modification was 1 sccm and 10W RF power. The typical interfacial layer thickness is about 20 nm and typical deposition time is 1 minute. As can be seen in Table 8.3, there is no noticeable upgrading on the adhesion of silicon oxide coating layer on PMMA surfaces. In order to amend the improved adhesion, the further studies with different organic interfacial layer deposition conditions were performed as shown in Table 8.3. However, the adhesions of silicon oxide coating layer on PMMA surfaces are still undesired with various interfacial layer deposition conditions. Owing to the failure of improving plasma deposited silicon oxide coating adhesion on the PMMA substrate, the further effort is to develop the exact design of the whole plasma chemical vapor deposition process. It depends on the thickness of plasma deposition, functionality of interfacial layer, and kinds of substrate polymers. modification was 1 sccm and 10W RF power. The typical interfacial layer thickness is about 200 A and typical deposition time is 1 minute. As can be seen in Table 8.3, there is no noticeable upgrading on the adhesion of silicon oxide coating layer on PMMA surfaces. In order to amend the improved adhesion, the further studies with different organic interfacial layer deposition conditions were

performed as shown in Table 8.3. However, the adhesions of silicon oxide coating layer on PMMA surfaces are still undesired with various interfacial layer deposition conditions. The further aspect is to develop the exact design of adhesion promoting organic interlayer. It depends on the thickness, functionality of interfacial layer, and kinds of substrate polymers.

8.4. Summary and Future work

The present study demonstrated the use of plasma deposition in producing protective hard silicon oxide coating on the surface of PC and PMMA substrates. FTIR-ATR analysis determined both plasma polymerized interlayer and plasma deposited silicon oxide film properties. The major Si-O absorbance observed in the FTIR-ATR spectra showed that plasma deposited silicon oxide coatings had relatively more inorganic features compared to those obtained in the literature. The improved hardness of plasma coated PC substrates was examined by ASTM pencil hardness test method. Regarding the uniformity and the qualities of the plasma protective silicon oxide coatings, this RF plasma deposition technique is comparable to the traditional techniques. Therefore, we conclude that this RF plasma deposition method is a promising technique for coating protective silicon oxide layer on plastic materials, especially when taking into account its simplicity

and suitability to coat large-scale substrate size for industrial needs.

However, the silicon oxide coatings deposited on PMMA substrates often encountered the worse wet adhesion than those on PC substrates in this process. Using different plasma pre-treatments, power levels, and interfacial layers could not be able to gain an improved adhesion to PMMA surfaces. Thus, the improvement the adhesion of SiOx coating on PMMA surface will be the major attempt in the further work.

ACKNOWLEDGEMENT

The authors would thank the personnel of Professor Shubhra Gangopadhyay from Department of Electrical engineering at University of Missouri-Columbia for supporting the FTIR-ATR analysis and Professor Joseph Turner from Department of Chemistry for supporting the UV-VIS detection.

8.5. Reference

1. Yoshikawa, Atsuo; Igari, Tokuo. "*Photocurable acrylic coating compositions for protection of plastics.*" Jpn. Kokai Tokkyo Koho (1991)
2. Yamamoto, Naoki; Hatakeyama, Hiroki; Watanabe, Hiroyuki. "*UV-curable coating compositions and coated articles.*" Jpn. Kokai Tokkyo Koho (1993)
3. Bilkadi, Zayn; Rambosek, Thomas W. "*Making acid- and abrasion-resistant protective coating, for thermoplastic transparencies.*" U.S. Patent (1997)
4. Motonaga, Akira; Takeuchi, Hiroshi; Inoue, Hiroshi. *"Radiation-curable coating compositions and method for forming protecting film layers with good scratch resistance."* Jpn. Kokai Tokkyo Koho (2005)
5. Mahltig, B.; Boettcher, H.; Rauch, K.; Dieckmann, U.; Nitsche, R.; Fritz, T. "*Optimized UV protecting coatings by combination of organic and inorganic UV absorbers.*" Thin Solid Films (2005), 485(1-2), 108-114.

6Yasuda, H. *"Plasma polymerization for protective coatings and composite membranes ."* Journal of membrane Science (1984), 18, 273-284.

7. Morita, Shinzo; Hattori, Shuzo; Takigawa, Akio; Yoshida, Motoaki. *"Formation of protective coating by plasma polymerization."* Jpn. Kokai Tokkyo Koho (1987),
8. Gauthier, Jean Marie; Bonet, Claude; Coeuret, Francois. *"Protective multilayer coating for a substrate and its plasma deposition."* Fr. Demande (1989)
9. Yang, M.-R.; Chen, K.-S.; Hsu, S.-T.; Wu, T.-Z. *"Fabrication and characteristics of SiOx films by plasma chemical vapor deposition of tetramethylorthosilicate. "* Surface and Coatings Technology (2000), 123(2-3), 204-209.
10. Kuhr, M.; Bauer, S.; Rothhaar, U.; Wolff, D. *"Coatings on plastics with the PICVD technology".* Thin Solid Films (2003), 442(1,2), 107-116.
11. Yasuda, Hirotsugu."*Luminous Chemical Vapor Deposition and Interface Engineering.*" Marcel Dekker, New York (2005)
12. Sawada, Yasushi; Ogawa, Satoru; Kogoma, Masuhiro. "*Synthesis of plasma-polymerized tetraethoxysilane and hexamethyldisiloxane films prepd. by atmospheric pressure glow discharge.*" Journal of Physics D: Applied Physics (1995), 28(8), 1661-9.
13. Babayan, S. E.; Jeong, J. Y.; Schutze, A.; Tu, V. J.; Moravej, Maryam; Selwyn, G. S.; Hicks, R. F. *"Deposition of silicon dioxide films with a non-equilibrium*

atmospheric -pressure plasma jet." Plasma Sources Science & Technology (2001), 10(4), 573-578.

14. Liston, E. M.; Martinu, L.; Wertheimer, M. R. *"Plasma surface modification of polymers for improved adhesion: a critical review."* Journal of Adhesion Science and Technology (1993), 7(10), 1091-127.
15. Schulz, U.; Munzert, P.; Kaiser, N. *"Surface modification of PMMA by DC glow discharge and microwave plasma treatment for the improvement of coating adhesion."* Surface and Coatings Technology (2001), 142-144, 507-511.
16. Groning, P.; Collaud, M.; Dietler, G.; Schlapbach, L. *"Plasma modification of polymethylmethacrylate and polyethyleneterephthalate surfaces."* Journal of Applied Physics (1994), 76(2), 887-92.
17. Guo,Yoou-Bin; Hong, Franklin Chau-Nan. *"Adhesion improvements for diamond-like carbon films on polycarbonate and polymethylmethacrylate substrates by ion plating with inductively coupled plasma."* Diamond and Related Materials (2003), 12(3-7), 946-952.
18. Yu, Qingsong; Deffeyes, Joan; Yasuda, Hirotsugu. "*Corrosion protection of ion vapor deposition (IVD) Al-coated Al alloys by low-temperature plasma interface engineering Part I. DC cathodic polymerization with anode magnetron enhancement."* Progress in Organic Coatings (2001), 43(4), 100-109.
19. Yu, Qingsong; Deffeyes, Joan; Yasuda, Hirotsugu. "*Corrosion protection of ion vapor deposition (IVD) Al-coated Al alloys by low-temperature plasma interface engineering Part II. DC cathodic polymerization under conditions of IVD (without using anode assembly)."* Progress in Organic Coatings (2001), 43(4), 243-250.
20. Yu, Qingsong; Moffitt, C. E.; Wieliczka, D. M.; Deffeyes, Joan; Yasuda, Hirotsugu. "*Corrosion protection of ion vapor deposition (IVD) Al-coated Al alloys by low-temperature plasma interface engineering Part III-DC cathodic polymerization in a closed reactor system."* Progress in Organic Coatings (2002), 44(1), 37-47.

VITA

Chun Huang was born on December 15, 1978 in Taipei, Taiwan. In June 2001, he has received a Bachelor of Science degree in Chemical Engineering from Chung-Yuan Christian University in Chung-Li, Taiwan. He has been enrolled in the Graduate School at University of Missouri-Columbia, in Chemical Engineering Department since January 2002 and received Master's degree in Chemical Engineering in December 2003. From January 2003 to the present, he has been a graduate research assistant at the Surface Science and Plasma Technology Center in University of Missouri-Columbia.